Recombinant expression and characterization of *Plasmodium falciparum* copper-binding proteins: Glutaredoxin 1 and S-adenosylhomocysteine hydrolase

by

Mwenya C. Kwangu

Bachelor of Veterinary Medicine (BVM), MSc. Biochemistry (UNZA)

Submitted in fulfillment of the academic requirements for the degree of

Doctor of Philosophy

in

Biochemistry

School of Life Sciences

University of KwaZulu-Natal

Pietermaritzburg

2024

Preface

The experimental work described in this dissertation was carried out in the School of Life Science, University of KwaZulu-Natal, Pietermaritzburg, from January 2021 to December 2023, under the supervision of Professor J.P.D Goldring. The studies represent original work by the author and have not otherwise been submitted in any other form to another University. Where use has been made of the work of others, it has been duly acknowledged in the text.

_____

Mwenya C. Kwangu

2024

As the candidate's Supervisor, I agree to the submission of this dissertation.

_____

Prof. J.P.D. Goldring

2024

Declaration – plagiarism

I, Mwenya C. Kwangu, declare that,

1. The research reported in this dissertation, except where otherwise indicated, is my original research.

2. This dissertation has not been submitted for any degree or examination at any other university.

3. This dissertation does not contain other persons' data, pictures, graphs, or other information unless specifically acknowledged as being sourced from other persons.

4. This dissertation does not contain other persons' writing unless specifically acknowledged as being sourced from other researchers. Where other written sources have been quoted, then:

> a. Their words have been rewritten, but the general information attributed to them has been referenced.
>
> b. Where their exact words have been used, then their writing has been placed in italics and inside quotation marks and referenced.

5. This dissertation does not contain text, graphics, or tables copied and pasted from the Internet, unless specifically acknowledged, and the source is detailed in the dissertation and the reference section.

_____

Mwenya C. Kwangu

2024

Abstract

Plasmodium falciparum (*Pf)* is responsible for most malaria deaths in humans, however, but most *Pf* infections do not lead to death of the infected individual. Elimination strategies have not worked well due to the emergence of drug resistance from parasites, creating a need for further research on novel drug targets against malaria. Copper is a cofactor for enzymes like the cytochrome *c* oxidase in various organisms. If not tightly regulated, its redox activity may lead to a free radical generation that may be destructive to the cellular structure. In infected red blood cells, excess or absence of copper leads to the growth inhibition of malaria parasites. This is because copper is an essential mineral to the parasite. Therefore, acquisition, distribution both in the cytosol and mitochondria, and efflux of this metal must be understood. The current study aimed to identify and determine the copper-binding abilities of *Pf*Grx1 and *Pf*SAHH, proteins that could have a role in the cytosolic distribution of copper and secretory pathway, thereby maintaining optimum copper levels in *P. falciparum*.

The *in-silico* analysis revealed copper binding CXXC and GXGXXGXG motifs in the amino acid sequences for *Pf*Grx1 and *Pf*SAHH proteins, respectively. These binding motifs which are present in the two proteins, have been found to bind copper in other organisms. *Pf*Grx1 and *Pf*SAHH were cloned, expressed as His-tag proteins, purified, and resolved on SDS-PAGE gel, then detected as ~12 and ~53 kDa proteins respectively, using mouse anti-His-tag antibodies on a western blot. Just like proteins in other systems, the purified r*Pf*Grx1 and r*Pf*SAHH bound copper *in-vitro* and *in-vivo* using ascorbic acid oxidation, and Bicinchoninic acid (BCA) copper release assays. When the growth of *E. coli* cells with or without the plasmid expressing the recombinant proteins was monitored in the presence or absence of 8 mM copper, *E. coli* cells with expressed recombinant proteins were able to grow suggesting that copper was bound to the recombinant proteins *in-vivo,* thus enabling growth of the bacteria. Protein-to-protein interaction modeling studies showed a possibility of *Pf*Grx1 and *Pf*SAHH interacting with each other and other copper proteins, suggesting a possible transfer of copper from protein to protein, and potential copper pathways in *P. falciparum*. The binding of copper was supported by docking studies that established copper binding sites for *Pf*Ctr1, *Pf*Grx1, *Pf*SAHH, *Pf*Cox17, *Pf*Cox11, *Pf*Cox19, and *Pf*Sco1. Characterization of Plasmodial copper-binding proteins can provide an understanding of Plasmodia copper homeostasis with potential novel drug target determination using bioinformatic tools. More interaction studies may provide novel and likely offer the basis for understanding of mechanisms for drug deliveries to the parasite, though further studies are needed to elucidate the existing channels.

Graphical abstract

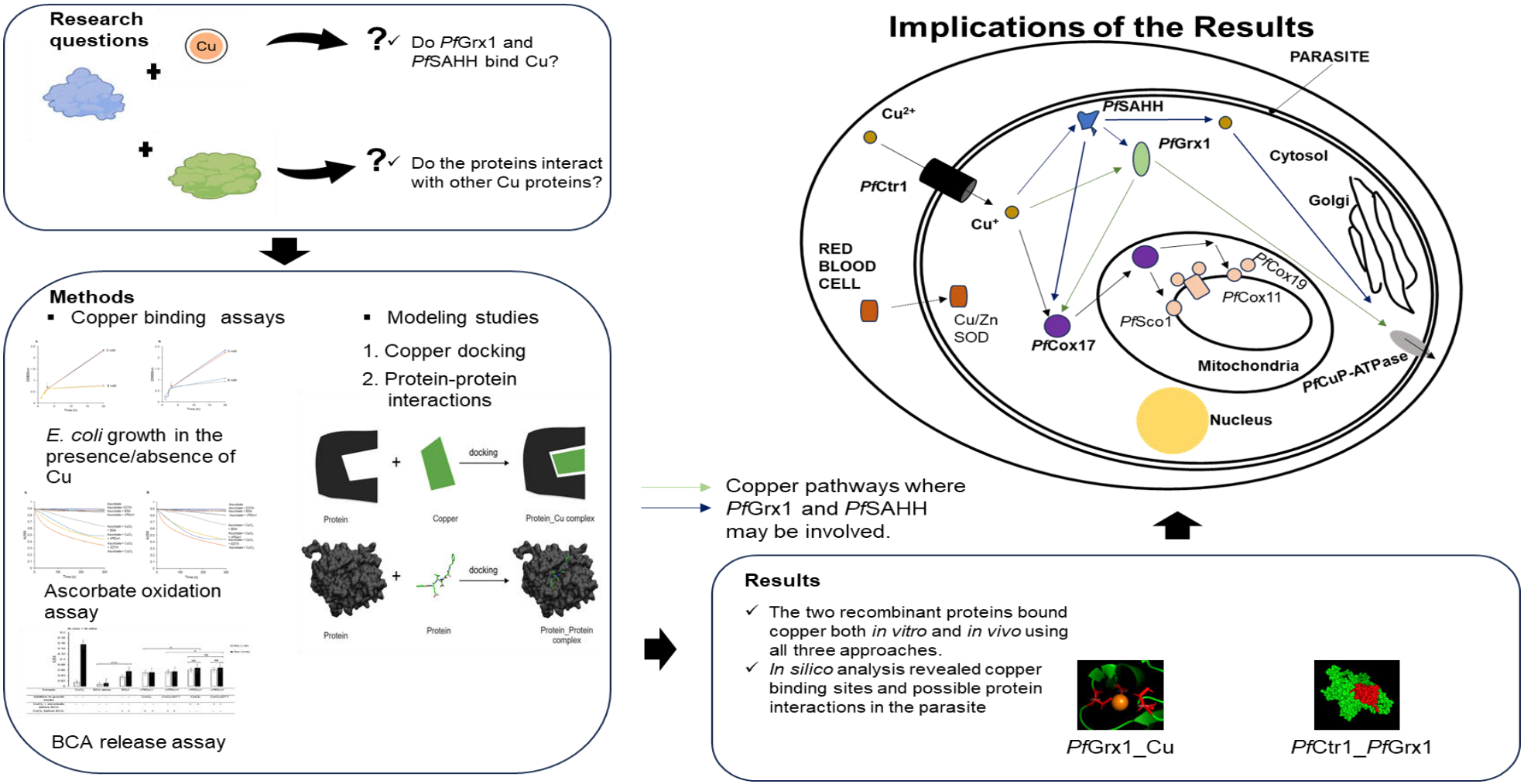

Table of Contents

List of Figures

List of Tables

Acknowledgments

I want to express my appreciation toward the following people and organizations for their invaluable contribution to this study:

My supervisor, Professor J.P. Dean Goldring for his expert advice, guidance, patience throughout my training, and funding of my Research. I will always be grateful for allowing me to be part of your great laboratory team.

I would also like to thank Professor Theresa H.T. Coetzer for her kindness, and allowance to access her laboratory throughout this study.

Sthokozile Mtshatsha, I am grateful for your help whenever I needed it. You are dedicated to your administrative duties. I appreciate.

My laboratory colleagues and fellow students, Timothy Kirkman, Javen Munsami, Joseph Fulakeza, and Brooklyn Goosen, to you I say thank you. I am grateful to the late Dr Lucky Marufu who I wish was around to see this come to pass, till we meet again.

The Copperbelt University for funding my stay in South Africa. I am grateful and honored to be one of the Research fellows in the Staff Development program.

My wife Chalwe, thank you for your sacrifices and support throughout my PhD journey, without you, I wouldn't have reached this far. To you, my beautiful daughters, Sibongile and Mapalo, your love and existence motivated me to do more and achieve this for you.

To my parents, you have been supportive from the time I was an infant to this day. May God bless you always and give you more time with me and my family. Thank you, Mum, and Dad.

My sister Bwalya, and my brothers, Mwamba and Mulenga thank you for being there for me and checking on my family while I was away for studies.

I am grateful to Dr. Mkhize P, Dr. Sichande, Dr. Siamupa, Barnabas, Zack, Sarah, and Hilder for being there for me. My special gratitude goes to the families of Dr. Akiri Saphan, Dr. and Mrs. Mangundu, Mr. and Mrs. Mazibuko, and Joyful Sthembile Msomi.

Abbreviations

ACTs	Artemisinin-based Combination Therapies
AQAS	Amodiaquine artesunate
ART	Artemisinin and its derivatives
ATOX1	Antioxidant 1
ATP7A	ATPase copper transporter alpha
ATP7B	ATPase copper transporter beta
BCA	Bicinchoninic acid
BSA	Bovine serum albumin
BSA-TBS	Bovine Serum Albumin-Tris-Buffered Saline
CcO	Cytochrome *c* oxidase
CCS	Copper chaperone for superoxide dismutase
CDC	Centers for Disease Control and Prevention
Cox11	Cytochrome *c* oxidase assembly protein 11
Cox17	Cytochrome *c* oxidase assembly protein 17
Cox19	Cytochrome *c* oxidase assembly protein 19
Cox2	Cytochrome *c* oxidase assembly protein 2
Cox23	Cytochrome *c* oxidase assembly protein 23
CoxI	Cytochrome oxidase I
CoxIII	Cytochrome oxidase III
CQ	Chloroquine
CREBBP	CREB-binding protein
Crs5	Metallothionein-like protein Crs5
CSP	Circumsporozoite protein
C-terminal or Ct	Carboxy-terminal
Ctr1	Copper transport protein 1
Ctr2	Copper transport protein 2
CuL	Copper-binding ligand
Cup1	Copper metallothionein 1
Cyt b	Cytochrome b

Cyt c	Cytochrome *c*
DDC	Diethyldithiocarbamate
DDT	Dichloro-diphenyl-trichloroethane
DMT1	Divalent metal transporter 1
DNA	Deoxyribonucleic acid
dNTPs	Deoxynucleotide triphosphates
DTT	Dithiothreitol
ECL	Enhanced chemiluminescence
EtBr	Ethidium bromide
exo-E415G	exonuclease gene polymorphism on chromosome 13
Fet3	Ferroxidase
GAPDH	Glyceraldehyde-3-Phosphate Dehydrogenase
GLP1	Glutaredoxin-Like-Protein 1
GLP2	Glutaredoxin-Like-Protein 2
GLP3	Glutaredoxin-Like-Protein 3
GMP	Global Malaria Programme
GMS	Greater Mekong subregion
GSH	Reduced Glutathione
H_2Asc	Ascorbic acid
HEPES	4-(2-hydroxyethyl)-1-piperazineethanesulfonic acid
*h*Grx1	Human Glutaredoxin 1
HMMTOP	Hidden-Markov Model Topology
HRP-2	Histidine-rich protein-2
HRP-3	Histidine-rich protein-3
HRPO	Horseradish peroxidase
HSA	Human serum albumin
IPTG	Isopropyl-beta-D-thiogalactopyranoside
IPTp	Preventive Treatment of Pregnant Women
IRS	Indoor residual spray
ITNs	Insecticide-treated nets

K13	*Kelch 13*
KA1407	Cipargamin
kb	kilobase
kDa	Kilo Daltons
LAMP	Loop-mediated isothermal amplification
LDH	Lactate dehydrogenase
LUM	Lumefantrine
MBDs	Metal Binding Domains
MDA	Malondialdehyde
MIB2	Metal-Ion Binding (MIB2) site prediction and modeling server
MQ	Mefloquine
Mrs3	Iron transporter
MT	Metallothioneins
mtDNA	Mitochondrial DNA
mtETC	Mitochondrial electron transport chain
NADH	Reduced nicotinamide adenine dinucleotide
NMR	Nuclear magnetic resonance
PDB	Protein data bank
PlasmoDB	*Plasmodium* database
PMT	Phosphoethanolamine-N-methyltransferase
PPQ	Piperaquine
PrPC	Prion Protein
PTMs	Post-Translational Modifications
PYR	Pyrimethamine
QN	Quinine
QZ439	Artefenomel
R21/MM	R21 in adjuvant Matrix-M
RAN1	Copper transporter in plants
RDTs	Rapid diagnostic tests
RMSD	Root mean square deviation

RNA	Ribonucleic acid
RPM	Revolutions per minute
SABLE	Sequence-based prediction of relative Solvent AccessiBiLitiEs
SDS-PAGE	Sodium dodecyl-sulfate- polyacrylamide gel electrophoresis
SLC25A	Phosphate carrier protein
SNPs	Single nucleotide polymorphisms
Sod1	Cu/Zn superoxide dismutase
SPPIDER	Solvent accessibility-based Protein-Protein Interface iDEntification and Recognition
SSU RNA	Small Subunit RNA
STEAP	Six transmembrane epithelial antigen of the prostate
TAE	Tris-acetate-EDTA
TBS	Tris-buffered saline
TCA	Trichloroacetic acid
TEMED	Tetremethylethylenediamine
TMHMM	Transmembrane Helices-hidden Markov Model
	transporter
WD	Menkes and Wilson disease

Chapter 1

Introduction and Literature Review

1.1 Overview of Malaria

Malaria is a public health problem affecting millions of people around the globe (WHO., 2023). It is a mosquito-borne infectious disease caused by a protozoan of the *Plasmodium* genus (Sigh *et al.,* 2013). Approximately, 200 *Plasmodium* species that are known to infect mammals, birds, and reptiles have been described (Sato., 2021). *Plasmodium* species are responsible for human malaria and are carried by *Anopheles* female mosquitoes (Tuteja, 2007). *Anopheles* mosquitoes transmit five *Plasmodium* species: *P. falciparum, P. vivax, P. ovale*, *P. malariae,* and *P. knowlesi*, which cause human malaria (Mayxay *et al.,* 2004, Collins *et al.,* 2009). Mixed infections have been noted to occur in places where more than one species is present. Infections from *P. knowlesi* were known previously to be rare until a report was made in 2004 from Sarawak, Malaysian Borneo (Singh *et al.,* 2004). According to White., 2008, *P. knowlesi* is now recognized as the fifth species of *Plasmodium* causing malaria in humans (White., 2008). *P. falciparum* and *P. vivax* account for the most malaria morbidity around the world, however, *P. falciparum* has the highest prevalence and is the parasite often associated with severe illness and death, mostly among children under the age of five (WHO, 2023). According to the 2023 World Malaria Report, the number of malaria cases increased compared to pre-COVID era. However, countries in the Greater Mekong subregion (GMS)-Cambodia, recorded a 55.5 % reduction in total indigenous cases of malaria (WHO, 2023). Due to many asymptomatic cases, *P. vivax and P. ovale* complicate malaria diagnosis and treatment efforts (Haiyambo *et al.,* 2019, Robinson *et al.,* 2015). Malaria caused by these two species tends to relapse due to hypnozoites (dormant form of *Plasmodium* parasites) in the liver and extravascular merozoites in the bone marrow (Markus, 2018, 2023). On the other hand, *P. malariae* parasites are prevalent throughout the tropics and subtropics and cause minimal infections because they mature slowly in both human and mosquito hosts; however, the infections might go on for a lifetime (Warrell *et al.,* 2017 Bruce *et al.,* 2006, Sutherland *et al.,* 2016).

1.2 Global Trends of Malaria

According to the World Malaria Report released in 2023, 249 million cases of Malaria were reported in 2022. There have been fluctuations in the cases between 2000 and 2014 ranging from 243 million to 230 million cases. After 2016, an increase in malaria cases was observed with 11 million more cases being recorded between 2019 and 2020, while in 2020 and 2021, there was an increase of 2 million malaria cases (WHO., 2023). Most affected countries are from Africa with Nigeria topping the list, mainly due to population growth. Another country that recorded a high increase in malaria cases, is Pakistan, which had a five-fold increase in malaria incidence

(WHO, 2023). Malaria deaths have been declining since 2000, from 864,000 to 576,000 in 2019, however, 2020 recorded an increase in mortality by 55,000. This increase in deaths was attributed to the COVID pandemic which caused disturbances in the prevention and treatment of malaria (WHO., 2023). In 2021, a marginal reduction from 631,000 to 610,000 was observed followed by a further decline to 608,000 in 2022 (WHO., 2023, Venkatesan., 2024). These numbers suggest that malaria is still a threat to human life. More work remains to be done to achieve a malaria-free World.

1.3 Regional Trends of Malaria

African countries have not been spared from the falling standards in the eradication of Malaria. Of the estimated cases from the 2023 WHO malaria report, 93.6% of them are from the African region. This proposes that there was no reduction between 2020 and 2022 with 7 countries from Africa having high malaria prevalence rates (WHO., 2023). Interestingly, Tanzania and Mozambique are part of these countries that contribute to Africa's malaria burden. The Republic of Tanzania shares borders with Zambia and Malawi while the latter shares boarders with South Africa, Zambia, Zimbabwe, and Malawi. Therefore, the risk of transborder transmission to South Africa is very high, and more effort is needed towards the prevention and treatment of malaria.

1.4 Malaria Trends in South Africa

In most settings, environmental and ecological factors play a role in the transmission of malaria (Ryan *et al.,* 2020). A large part of South Africa is malaria-free, however, Northeastern regions namely KwaZulu-Natal, Mpumalanga, and Limpopo have low malaria endemicity (Morris *et al.,* 2013, Maharaj *et al.,* 2013). The areas bordering Mozambique, Botswana, and Zimbabwe are known for seasonal malaria transmission and *P. falciparum* is the main causative agent for malaria in South Africa (Balmith *et al.,* 2024). According to a study conducted in the Agincourt community, malaria has been prevalent for two decades without decreasing (Byass *et al*., 2017). The cases in South Africa have been maintained below 10, 000 over the last 2 decades from 60, 000 in 2000 (Maharaj *et al.,* 2013). This is due to the adoption of elimination methods and treatment therapies based on WHO recommendations. Nevertheless, the country is still at risk of a resurgence of the disease because of its borders, implementing control strategies around these areas has led to a decline in the cases and deaths (Coetzee *et al.,* 2013, Abiodun *et al.,* 2020, Lamola *et al.,* 2024). Despite all these efforts, malaria remains a challenge, and more studies are necessary, especially in drug development to eliminate malaria (Balmith *et al.,* 2024). Additionally, intensive inter-country cooperation in the Southern African region will be needed to completely eradicate malaria in South Africa and the surrounding areas (Sikaala *et al.,* 2024).

1.5 Malaria Trends in Zambia

Malaria transmission in Zambia occurs throughout the year and is endemic (Kyomuhangi *et al.,* 2023). The prevalence rate is lowest in cold and dry seasons

and highest in the rainy season (Reiner *et al.,* 2015, Kipruto *et al.,* 2017). It is highest in provinces that receive more rainfall. Zambia is divided into ten provinces that have variations in rainfall patterns and vegetation. Muchinga, Northern, and Luapula provinces receive the highest rainfall and account for the highest (Appx 20%) malaria prevalence in under-five children. Copperbelt, Eastern, North-Western, and Central provinces usually have malaria prevalence that ranges between 10 to 20%. The rest of the provinces (Lusaka, Southern, and Western) have less than 10% of malaria prevalence among under-five children. Previous studies have shown incidence rates of the disease have been increasing especially between 2010 and 2015 (WHO., 2017), though the World Malaria Report recorded a reduction in the incidence cases in 2020 (WHO., 2020). However, Zambia remains one of the highly endemic countries and showed a 29.3% malaria prevalence in under-five children in 2021, indicating a 1.4% of all global cases (Kapiya *et al.,* 2024, Malaria Indicator Survey., 2021, Severe Malaria Observatory., 2022).

1.6 Life cycle of *Plasmodium*

All Plasmodium species have a similar life cycle divided into two mini-cycles (vertebrate host and insect vector cycles). In the vertebrate host cycle, the parasite affects the host which can be a human or any other vertebrate. The second cycle involves transmission between the infected and uninfected host through an insect vector (Votýpka *et al.,* 2016). Mosquitoes belonging to the genus *Anopheles* cause the transmission of *Plasmodium* species among humans and other mammals. In contrast, transmission among birds and reptiles occurs by other mosquitoes belonging to a different genus (Perkins *et al.,* 2014).

1.7 *Plasmodium* cycle in the vertebrate host

The *Plasmodium* host infections begin when sporozoites from an infected female *Anopheles* mosquito are introduced to the blood system through a bite. The sporozoites invade the dermis and then move to the liver hepatocytes (Frischknecht *et al.,* 2017; Amino *et al.,* 2006; Prudêncio *et al.,* 2006). They then undergo a process known as schizogony which results in the development of merozoites which egress from the liver cells and later infect the erythrocytes (Sturm *et al.,* 2006). The merozoites undergo asexual multiplication through the process known as schizogony, developing from ring, early and late trophozoite to schizont producing approximately 8 to 64 merozoites depending on the species of *Plasmodium* involved (Gerald *et al.,* 2011). The erythrocytes rupture, allowing the new merozoites then to invade naïve red blood cells to multiply and repeat the cycle (Dvorin *et al.,* 2022). This happens every 24 hours in the case of *P. knowlesi*. *Plasmodium falciparum*, *P. ovale*, and *P. vivax* undergo this process every 48 hours while *Plasmodium malariae* takes 72 hours (Galinski *et al.,* 2005). Most species undergo several cycles of intraerythrocytic proliferation before differentiating into gametocytes. However, *P. vivax* continuously produces gametocytes in the early cycles of their intraerythrocytic division. Gametocytes are taken up by a mosquito vector through feeding to start

sexual reproduction to complete the life cycle of the parasite (Josling *et al.,* 2015; Bancells *et al.,* 2019).

1.8 *Plasmodium* cycle in the insect vector

Female *Anopheles* mosquitoes take up male and female gametocytes that later differentiate into micro and macrogametes before fusing to form a zygote (Bennink *et al.,* 2016). The resulting zygote later transforms into an ookinete. An ookinete is a motile form of the parasite formed after meiosis (Sinden *et al.,* 1985). It traverses through the midgut epithelium and transforms into an oocyst which undergoes mitosis to produce several sporozoites in a process called sporogony (Araki *et al.,* 2020, Vaughan *et al.,* 2007, Varadi *et al.,* 2007). After the maturation of the oocyst, the sporozoites are released to the hemolymph after the rupture of the oocyst (van Schaijk *et al.,* 2014). The sporozoites migrate to the salivary glands of the mosquito and are passed on to the next host through a bite (human or a different vertebrate) during a blood meal (Kanatani *et al.,* 2024). The process of sporozoites moving to the salivary glands of the mosquitoes ensures infection of the host (Smith *et al.,* 2010, Siciliano *et al.,* 2020). Fig 1.1 shows the summary of the life cycle of Plasmodium.

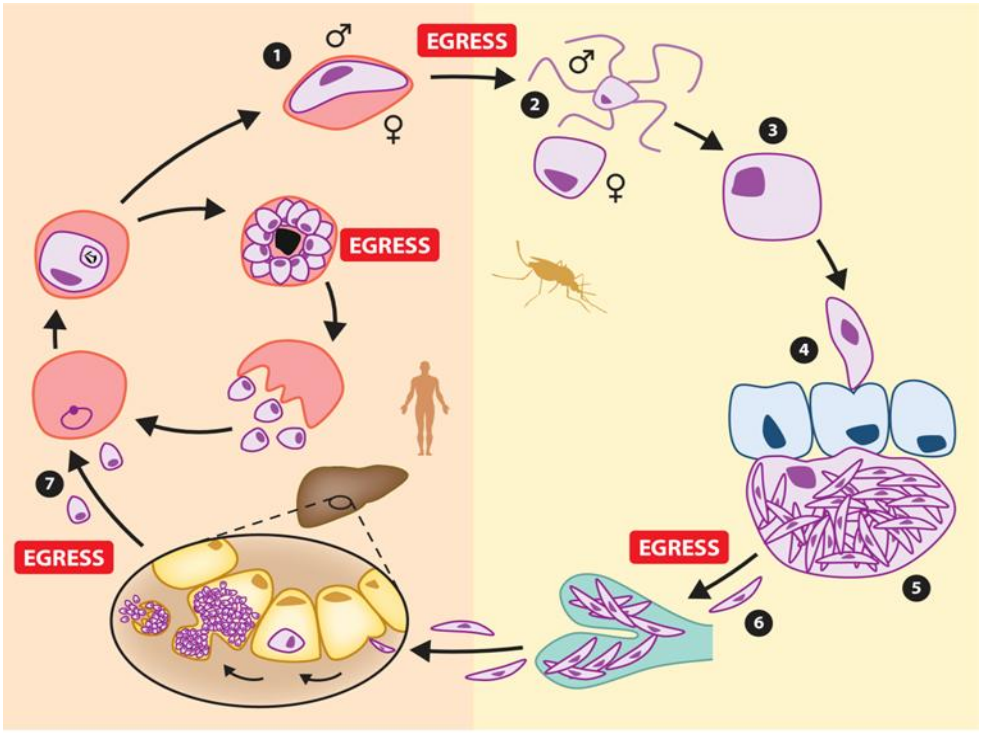

Fig 1.1 Life cycle of *Plasmodium*. Malaria parasite life cycle in the human host (on the left of the cycle) and within the mosquito vector (on the right side of the cycle). Some merozoites differentiate into gametocytes (❶) which are taken up during a blood meal after the next mosquito bite. Gametes in (❷) differentiate into micro- and macrogametes before fusing (syngamy) to form a zygote (❸) that later develops into a motile ookinete (❹) which penetrates the midgut wall, forming an oocyst (❺) at the midgut-hemolymph interface. Sporozoites (❻) leave the oocyst and reach the salivary glands. They are passed to the host through a mosquito bite and traverse through the skin to the bloodstream and liver. They evolve into infectious merozoites (❼) that come out from hepatocytes into the bloodstream, invade erythrocytes, and repeat this intraerythrocytic cycle. The cycle starts with sporozoites leaving the oocyst to reach the mosquito salivary glands. Source: Dvorin *et al.,* 2022

1.9 Malaria prevention

Various methods are used in the prevention of malaria. These include the use and nonuse of drugs. Drugs may be used for prophylactic treatment, especially in travelers (Centre for Disease Control and Prevention (CDCP)., 2023, Markus., 2021). Other documented preventive methods may involve wearing clothes that cover the whole body (Croft., 2014) and avoiding going out at dusk (Lalloo *et al.,* 2008). These methods are not supposed to replace the drugs but be used in addition to them. Insecticide Treated Nets (ITNs) with pyrethroids, while Indoor Residue Spraying (IRS) with carbamates, organophosphates, or DDT have been known to be effective in reducing malaria transmission (Birkholtz *et al.,* 2012, Namuganga *et al*., 2021). For people exposed to biting mosquitoes during outdoor activities, repellents work well (Croft., 2014). The WHO 2023 malaria report recommends the prevention of malaria transmission in pregnant women by using what is called Intermittent Preventive Treatment of Pregnant Women (IPTp) with sulfadoxine-pyrimethamine (WHO., 2012, WHO., 2014). Additionally, in 2021, WHO announced the recommendation of a vaccine aimed at contributing prevention and possible elimination of malaria (WHO., 2021). Despite all these methods of prevention, vector resistance to the insecticides has been observed coupled with low coverage in the distribution of ITNs (Njumkeng *et al.,* 2019, Mboma *et al.,* 2021).

1.10 Malaria Diagnosis

Effective malaria elimination is impossible to achieve without early and accurate diagnosis (Mbafeno *et al.,* 2020). A definitive diagnosis allows for targeted treatment, which ultimately prevents further complications and reduces mortality. There are times when the clinical diagnosis is made using the travel history, symptoms, and clinical signs, this has proved to be non-specific and can result in misdiagnosis due to other diseases with a similar presentation like malaria (Rosenthal *et al.,* 2012). Guidelines for malaria treatment by the WHO state that malaria diagnosis which is solely based on clinical features is likely to result in overtreatment and incorrect use of antimalarials (WHO, 2015). The current recommended diagnostic methods for all malaria cases are microscopy for direct detection of the parasite and immune-chromatographic rapid diagnostic tests (RDT) that are based on the detection of malarial proteins (WHO, 2015). Coleman *et al.,* 2006, reported that parasitic infections may be missed by Microscopy and RDTs; however, polymerase chain reaction (PCR) and Loop-mediated isothermal amplification (LAMP) assays can be employed as they are more sensitive and specific (Coleman *et al.,* 2006). However, these are expensive and need highly trained human capital (Picot *et al.,* 2020).

1.10.1 Malaria Diagnosis with Microscopy

Microscopy has been a gold standard for detecting malaria parasites for over a century (Alam *et al.,* 2011). In this method, thin and thick blood slides are prepared using peripheral blood which is stained with Giemsa (Alam *et al.,* 2011). When the slides are prepared and examined by a skilled microscopist, this method is highly

sensitive and specific (Ameri *et al.,* 2001, Iqbal *et al.,* 2001). The method quantifies malaria parasitemia and classifies species. Co-infections with other parasites can be detected i.e., Babesia, filaria, *Trypanosoma,* and *Leishmania* species. Other organisms detected with the method are bacteria like *Borrelia* species, and fungi (Pillay *et al.,* 2019). Microscopy is still very much in use in providing reliable diagnosis. Challenges include the lack of specialists and costs attached to the procurement of microscopes and the availability of electricity in many rural areas.

1.10.2 Rapid Diagnostic Tests (RDTs)

Another method that has been developed to reduce delays in generating results and improve clinical outcomes is a Lateral flow immunochromatographic-based diagnostic test (RDT) that has been useful in rural endemic places that have no microscopes and specialists to conduct microscopy examinations (Alam *et al*., 2011, Boyce *et al.,* 2015). However, RDTs are not as sensitive as other methods of diagnosis like PCR (Plucinski *et al.,* 2019), but they have proven to be cost-effective and contributed to the reduction of referrals and antibiotic prescriptions both in urban and rural areas (Boyce *et al.,* 2015, Hansen *et al.,* 2015). The RDTs are based on the reaction of proteins that are released upon lysis of the red blood cells using a buffer that is added to blood during the test (Obeagu *et al.,* 2019, Plucinski *et al.,* 2019). *P. falciparum* Histidine-rich protein-2 (HRP-2) has been utilized, though there is selection for HRP-2 deletions due to repetitive use of RTDs leading to diagnosis evasion (Diallo *et al.,* 2023). The protein is a histidine-rich protein that is produced by asexual *P. falciparum* parasites within the red blood cells (Singh *et al.,* 2021). Other proteins produced by the asexual parasites are HRP-1 and HRP-3 (Kilejian., 1979), whose true functions are not well established (Palani *et al.,* 2018). The *Pf*HRP-2 amino acid sequence contains 34% histidine, 37% alanine, and 10% aspartic acid (Howard *et al.,* 1986), and it has many tandem repeats of the sequences AHH and AHHAAD (Stahl *et al.,* 1985). In other cases, detection occurs using *Plasmodium* lactate dehydrogenase (pLDH) which is a cytosolic homotetrameric enzyme (Barney *et al.,* 2022, Jang *et al.,* 2020). Aldolase, an enzyme in glycolysis may be diagnostic and contribute to early detection and treatment of malaria (Alarm *et al.,* 2011). However, LDH-based RDTs show less sensitivity compared to the HRP2-based ones (Hopkins *et al.,* 2007). Therefore, Glyceraldehyde-3-Phosphate Dehydrogenase (GAPDH) and Phosphoethanolamine-N-methyltransferase (PMT) that have roles in glycolysis and lipid malarial biosynthesis respectively, have been identified as potential biomarkers for detecting and differentiating *Plasmodium* species (Krause *et al.,* 2017, Krause *et al.,* 2018).

1.10.3 Detection of Malaria Parasites using Polymerase Chain Reaction (PCR)

Polymerase Chain Reaction (PCR) is another method that has been employed in different places to detect *Plasmodium* species and validate or evaluate the performance of RDTs and microscopy. There are different types of PCR namely, single, multiplex, nested, and real-time PCR. Nested PCR targets 18S SSU rRNA genes of the main five human malaria parasites (Kimura *et al.,* 1997, Abdalla *et al.,*

2019, Calderaro *et al.,* 2024). The nested PCR is cumbersome and involves multiple amplification reactions, therefore, attempts have been made to develop a single and simpler multiplex PCR technique that permits the simultaneous detection of parasites in a single reaction tube (Shokoples *et al.,* 2009, Belachew *et al.,* 2022). This gives Multiplex PCR an advantage over the other types as it shortens the time of processing samples thus being useful in the quick treatment of malaria (Padley *et al.,* 2003, Dong *et al.,* 2023). Single nested PCRs have high sensitivity and low risk of contamination, though they are prone to inhibition by inaccurate sample preparation, thus, Real-time PCR reduces contamination and is a cheaper method (Madamet *et al.,* 2022, Montenegro *et al.,* 2004). However, PCR machines are not widely used especially in rural malaria-endemic places due to their cost implications and well-trained human capital.

1.10.4 Detection of Malaria Parasites using Loop-mediated Isothermal Amplification (LAMP) assays

A detection method for malaria parasites that has high sensitivity and specificity like PCR is Loop Isothermal Amplification Assays (LAMP). According to Ljolje *et al.,* 2021, the results were obtained faster than the real-time PCR which was the reference. The test also recorded a 100% sensitivity when compared to the reference assay (Ljolje *et al.,* 2021). LAMP isothermally amplifies DNA directly from blood samples by using a mutant *Taq* DNA polymerase which is resistant to the PCR inhibitors in blood (Kersting *et al.,* 2014). Due to this reason, LAMP has another advantage over all other PCRs of being suited for the field as well as taking less time to process samples, thus, being categorized as less demanding (Cook *et al.,* 2015).

1.11 Treatment of Malaria

The different drugs that are used to treat and prevent malaria include quinine (QN), chloroquine (CQ), amodiaquine, piperaquine (PPQ), mefloquine (MQ), lumefantrine (LUM), pyrimethamine (PYR), proguanil, sulfadoxine, atovaquone, primaquine, and artemisinin and its derivatives (ART) (Gorobets *et al.,* 2017). The choice to administer one of these drugs depends on whether the drug is cheap, accessible, safe, effective, well-tolerated, and easy to give (Kremsner and Krishna, 2004). These drugs are classified according to their structures and the target during the *Plasmodium* life cycle (Cui *et al.,* 2015). Antimalarials targeting various Plasmodium stages include tissue and blood schizontocides, gametocytocides, anti-relapse, and sporontocides (Frederich *et al,* 2002). Those structures are divided into 4-aminoquinolines, arylamino alcohols, 8- 8-aminoquinolines, artemisinin derivatives, antifolates, and naphthoquinone (Cui *et al.,* 2015, Antony *et al.,* 2016).

1.11.1 Artemisinin-based combination therapies (ACTs) to treat malaria

Resistance to antimalarial drugs has led to challenges in the fight against malaria (Amelo *et al.,* 2021). However, resistance can be delayed by combining drugs to treat malaria, similar to a common practice that was employed to fight antibiotic resistance provided the drugs being combined share similar pharmacokinetics, and pharmacodynamics (White *et al.,* 1996). Additionally, the

drugs should not possess any adverse pharmacological interaction or toxicity (White *et al.,* 1996). Arising from this, a second drug was recommended to be added to Artemisinin to reduce the possibility of development of drug resistance. Since the introduction of Artemisinin-based combination therapies (ACTs), they have been instrumental in the elimination of malaria (Aweeka *et al.,* 2008). They have been effective, especially in treating drug-resistant *Plasmodium falciparum* malaria, a situation that has led to a reduction in malaria-related deaths worldwide (Halder *et al.,* 2018). The major advantage of using the drug combinations in the ACT is that the emergence of drug resistance to the different components of the drug is lower. Additionally, there is improved efficacy due to the different mechanisms of action of each drug (Ashley *et al.,* 2018). The WHO recommends six ACTs for use in the treatment of malaria: artesunate + amodiaquine, artemether + lumefantrine, artesunate + sulfadoxine-pyrimethamine, artesunate + mefloquine, artesunate + pyronaridine, and dihydroartemisinin + piperaquine (WHO, 2019). Various countries have adopted different treatment policies regarding the above-mentioned ACTs to curb malaria (Bennett *et al.,* 2017, Recht *et al.,* 2017).

1.11.2 Chemoprophylactic Treatment for Malaria

In Africa, countries with malaria have embraced the constant use of sulfadoxine/pyrimethamine for pregnant women and children below the age of five years (Kajubi *et al.,* 2019). This has been done especially in areas with reduced seasonal malaria transmission. The type of drug to be used varies in areas with increased cases of malaria, thus, amodiaquine+sulfadoxine/pyrimethamine is recommended in such cases (WHO, 2015). Other drugs used for the prevention of malaria, especially for travelers are mefloquine, atovaquone/proguanil, or doxycycline as chemoprophylaxis by travelers from non-endemic to endemic countries (Schlagenhauf and Petersen., 2008, Meltzer *et al.,* 2018, Freedman., 2019). These regimes have proved to be effective and contribute to the overall efforts of malaria elimination even in the face of antimalarial drug resistance (M´enard *et al.,* 2016).

1.12. Resistance to Anti-Malarial Drugs

1.12.1 Drug resistance in *Plasmodium*

According to the 1967 WHO World Malaria Report, ‘drug resistance’ is defined as the ability of a parasite to survive or multiply despite the drug being administered and absorbed in doses equal to or higher than those usually recommended but within the tolerance of the subject. Antimalarial drug resistance is a major factor in the fight against malaria worldwide (WHO., 2018, WHO., 2023). Drug resistance may be due to the failure to clear the parasite or simply an increase in parasite levels despite adequate treatment being administered (White, 2004). A genetic occurrence that is spontaneous as well as rare is known to be the first step in resistance (Hughes *et al.,* 2015). In an average human malaria infection, total parasite numbers during the asexual stage in the bloodstream range between 10^9 and 10^{13} parasites, this gives an estimated 1.0 to 9.7×10^{-9} mutations per base pair for each generation

(Bopp *et al.,* 2013). With these figures, random mutations that lead to antimalarial resistance are more likely to occur within or after a few cycles of replication (White, 2004). High levels of parasitemia, decreased levels of antimalarials and immunity, drugs with a longer half-life, and malaria transmission are factors that influence the development of resistance to antimalarials in host organisms (Kuile *et al.*, 1995, Hastings *et al.,* 2002, Babiker *et al.,* 2013)

1.12.2 Gene markers for *Plasmodium* Antimalarial drug resistance

Resistance to all known antimalarials has emerged and has frequently been detected in the Greater Mekong region of Southeast Asia, as shown by chloroquine, mefloquine, and artemisinin resistance (White, 2004, Cui *et al.,* 2015, Parckard, 2014). The use of molecular resistance markers has been important in the detection of drug-resistant parasites (Djimde *et al.,* 2001, Ariey *et al.,* 2014, Ashley *et al.,* 2014). The spread of resistance mostly occurs from low-transmission areas to high-transmission areas such as sub-Saharan Africa where *P. falciparum* is very efficient in acquiring and spreading resistant genes (Ehrlich *et al.,* 2020, Slater *et al.,* 2016). The acquisition of these genes is brought by genetic modifications that lead to the reduction of drug susceptibility by the malaria parasite (White, 2004). The modifications may arise at any parasitic developmental stage making drug resistance a complicated issue (Menard and Dondorp, 2017, Platon *et al.,* 2024, McConville *et al.,* 2024). In order to reduce drug resistance, strategies may be formulated to target the invasion and erythrocytic development of the parasite (Burns *et al.,* 2019, Verma., 2024). The following gene markers have been identified; *P. falciparum* chloroquine resistance transporter (*Pfcrt*), *P. falciparum* multidrug resistance-1 (*Pfmdr1*), *P. falciparum* multidrug resistance-associated protein-1 (*Pfmrp1*), *P. falciparum* ATPase4 (*PfATPase4*), and *P. falciparum* Sodium/Hydrogen exchanger (*Pfnhe1*). Furthermore, *P. falciparum* multidrug resistance protein 1 (*Pfmrp1*), dihydropteroate synthase (*Pfdhps*), *P. falciparum* dihydrofolate reductase (*Pfdhfr*), *P. falciparum* cytochrome b (*Pfcytb*), the recent, *Kelch* K13 propeller domain (*Kelch13*), *plasmepsin* 2-3 (*Pfpm 2-3*) and an exonuclease gene polymorphism on chromosome 13 (*exo-E415G*) are also among the gene markers (Table 1.1).

1.12.3 Resistance markers in *Plasmodium* and the associated drugs

The changes in amino acids in the active site of proteins in *Plasmodium* due to substitutions result in the development of resistance to antimalarial drugs (Kongsaeree *et al.,* 2005, Rout *et al.,* 2019). Nevertheless, mutations can occur in the allosteric site and cause conformational changes in the active site, either leading to partial or non-binding of the protein to the drug, thereby leading to drug resistance (Bishop *et al.,* 2022). There are various single nucleotide polymorphisms (SNPs) that are associated with different drug resistance-associated genes which include 76T in *Pfcrt* which has been linked with chloroquine and amodiaquine resistance*,* 51I, 59R, and 108N in *Pfdhfr* associated with resistance to pyrimethamine (Zhao *et al.,* 2019). The 437G and 540E in *Pfdhps* confers resistance to sulfadoxine, while 268N/S/C in *Pfcytb* confers to atovaquone, 86Y, 184Y and 1246Y in *Pfmdr1* confers resistance to

chloroquine, lumefantrine, mefloquine, and amodiaquine for *P. falciparum* (Adjekukor, 2018, Korsinczky *et al.,* 2000, Pickard *et al.,* 2003, Sidhu *et al.,* 2002). According to Ariey *et al.,* 2014, a strong association between the single amino acid substitutions Y493H, R539T, 1543T, and C580Y in the *Kelch13* gene and artemisinin were established (Ariey *et al.,* 2014). The resistance by *Kelch13* is due to the point mutations in the beta-propeller domain of the gene encoding the *Kelch* protein 13, which may reduce parasite susceptibility to artemisinin and its derivatives (Ouji *et al.,* 2018, Straimer *et al.,* 2015). A DNNND repeat motif in *Pfnhe1* is associated with Quinine resistance (Tchekounou *et al.,* 2022). Parasitic resistance to primaquine has been associated with the *plasmepsin 2-3* gene together with the mutation in the *exo-E415G* gene (Menard *et al.,* 2017, Amato *et al.,* 2017). Most of the outlined resistance markers have been identified in *P. falciparum*, with only one resistance marker in *P. vivax* (Menard and Dondorp, 2017). A summary of drug resistance markers and the associated drugs have been outlined in Table 1.1.

Various novel drug targets have been identified in the quest to provide alternative malaria treatment options. Those promising antimalarial drug targets include enzymes that have a role in protein synthesis, proteolysis, isoprenoid and DNA and RNA metabolism (Cheuke *et al.,* 2024). *Plasmodium falciparum* acetyl-coenzyme A synthetase, *N*-myristoyltransferase, and the cyclic guanosine monophosphate-dependent protein kinase G are other drug targets that are important in the development of alternatives treatment regimes for the parasite (Cheuke *et al.,* 2024).

Table 1.1 A summary of *Plasmodium* drug resistance markers and the associated drugs.

Resistant Marker and Accession Number	Chromosome location	Codon associated to Drug resistance	Drug Associated with the resistance marker
Pfcrt (PF3D7_0709000)	7	Mutations (76T)	Chloroquine, Amodiaquine
Pfmdr1 (PF3D7_0523000)	5	Mutations (86Y, 124F, 1042D, 1246Y) Mutations (184F) Increased copy number	Chloroquine, Amodiaquine, Lumefantrine, Mefloquine Mefloquine, artesunate Mefloquine
Pfdhfr (PF3D7_0417200)	4	Mutations (51I, 59R, S108N, 164L)	Pyrimethamine, Cycloguanil
Pfdhps (PF3D7_0810800)	8	Mutations (436A, 437G, 540E, 581G, 613S/T)	Sulfonamide, Sulfadoxine, Sulfone, Dapsone
Pfmrp1 (PF3D7_0112200)	1	Mutations (191H, 437S)	Chloroquine, quinine
Pfcytb (mal_mito_3)	Mitochondrial Genome	Mutations (268N/S/C)	Atovaquone

Pfnhe-1 (PF3D7_1303500)	13	Repeat polymorphism (DNNND repeat motif in microsatellite ms470 region)	Quinine
PfATPase4 (PF3D7_1211900)	12	Mutations (398F, 990R, 211T, 415D, 917L)	Spiroindolones, Pyrazoles, Dihydroisoquinolones
PfATPase6 (PF3D7_0106300)	1	Mutations (263E, 431K, 623E, 769N)	Artemisinin and its derivatives
Pfpm2 (PF3D7_1408000)	14	Increased copy number	Piperaquine
Pfk13 (PF3D7_1343700)	13	Mutations (446I, 458Y, 476I, 493H, 539T, 543T, 553L, 561H, 580Y)	Artemisinin, and its derivatives

KEY: ART: Artemisinin; *Pf*: *Plasmodium falciparum*; *Pfatpase6*: *Pf Ca2+-ATPase*: *Pfcrt, Pf* chloroquine resistance transporter*: Pfdhfr, Pf* dihydrofolate reductase: *Pfcytb, Pf* cytochrome B: *Pfdhps, Pf* dihydropteroate synthase; *Pfk13, Pf* Kelch gene; *Pfmdr1, Pf* multidrug resistance protein 1; *Pf* multidrug resistance protein 1 *Pfmrp1*; *Pfnhe-1, Pf* sodium–hydrogen exchanger; *Pfpm 2-3, Pf* Plasmepsin 2-3. Source: Arya *et al.,* 2021.

1.12.4 Geographical distribution of plasmodial Drug resistance markers

Various studies regarding the geographical distribution of Plasmodia drug resistance markers have been conducted to help in the selection of a drug that would contribute to the elimination of malaria. Furthermore, the surveillance permits the early establishment of correlates linked to the emergence and spread of anti-malarial drug resistance. In Africa, the *Pfk13* (A578S) which is associated with artemisinin and its derivatives has the highest geographical distribution compared to other markers (Ocan *et al.,* 2019, Kamau *et al.,* 2015). However, a novel mutation in the *Pfk13* gene (675V) was reported in Uganda (Ikeda *et al.,* 2018). Gene sequence has confirmed mutations in *Pfk13* have also been confirmed to be high in prevalence in the Greater Mekong Subregion (GMS) (WHO., 2018). Studies conducted on resistance markers and the associated drug resistance in some West, Central, and Eastern African countries link *Pfcrt* (associated with Chloroquine and Amodiaquine), *Pfdhfr* (pyrimethamine) *Pfdhps* (Sulfonamide and Sulfadoxine), *Pfmdr1* (Chloroquine and Amodiaquine), and *PfATPase6* (Artemisinin and its derivatives) with antimalarial drug resistance (Djimde *et al*., 2008, Happi *et al*., 2009, Karema *et al*., 2010, Baliraine and Rosenthal, 2011, Baraka *et al*., 2018). In addition to the already mentioned resistance markers, *Pfpm2* (Piperaquine), and *Pfcytb* (Atovaquone) have been reported in other parts of Africa that include Tanzania, and Angola (Gadalla *et al.,* 2011, 2013, Ngasala *et al.,* 2011, Kamugisha *et al.,* 2015, Kiaco *et al.,* 2015, Tadele *et al.,* 2023, Kakolwa *et al.,* 2018, and Smith *et al.,* 2018). A study conducted in malaria-endemic Mpumalanga province, South Africa, revealed an increase in *mdr86N* and *Pfcrt76K* markers. However, no artemisinin resistance-associated *kelch 13* mutations nor that of *Pfmdr1* which is associated with lumefantrine were observed (Raman *et al.,* 2019). Additionally, similar resistance markers namely *Pfcrt*, *Pfmdr1*, and *Pfpm2* have been established in neighboring southern Mozambique with *Pfk13* not being observed (Gupta *et al.,* 2020). Though previous reviews have highlighted the geographical distribution of different markers of resistance, *Pfk13* which is

associated with resistance to ART and its derivatives, forms the main threat to malaria control in malaria-endemic countries (Arya *et al.,* 2021).

1.12.5 Potential and Novel Antimalarial Drugs

Phenotypic and parallel screening methods have been used to identify potential and novel antimalarial drugs (Xia., 2017). The parallel screening which is targeted at the multiple life cycle stages of Plasmodia forms the best approach to the establishment of novel compounds because the method is based on selective and predictive assays for hepatic development, gametocytocidal activity, and transmission-blocking (Consalvi *et al.,* 2022, Plouffe *et al.,* 2016, Delves *et al.,* 2012, Appetecchia *et al.,* 2024). The method has identified novel antimalarials such as Artefenomel (QZ439), Ferroquine, and Cipargamin (KA1407). Further, Over-the-counter drugs (OTC), Fosmidomysin, and Artefenomel (QZ439) have been discovered. The QZ439 has been combined with Ferroquine and has the possibility of further combining with piperaquine and DSM 265 (Phyo *et al.,* 2016, Chhonker *et al.,* 2017, Okombo *et al.,* 2018). Ferroquine was also assessed alone and in combination with artesunate and amodiaquine artesunate (AQAS) under phase IIa, open-label, clinical trial in Africa, however, patients treated with Ferroquine presented with heart and liver reactions (Supan *et al.,* 2017, Postema *et al.,* 2014). Cipargamin inhibits *PfATP4* (Hien *et al.,* 2017), while Fosmidomysin and KA1407 affect the non-mevalonate pathway in *P. falciparum* and phosphatidylinositol 4-kinase respectively (McNamara *et al.,* 2013). Further, a new piperaquine drug was developed due to the success of trying triazolopyrimidine and pyrazolopyrimidine against malaria (Feitosa *et al.,* 2024). Another avenue of drug targets is transport which may involve proteins such as copper-binding proteins that have been discovered to be potential therapeutic targets in *P. falciparum* (Maciel-Flores *et al.,* 2024). Thus, copper metabolism studies in *P. falciparum* may identify novel anti-malarial drug targets that may help eliminate malaria (Staines *et al.,* 2010, Martin *et al.,* 2009b).

1.13 The Biological Role of Copper

Copper (Cu) is an essential element that exists in oxidized [Cu (II)] and reduced [Cu (I)] states in all living organisms. Copper plays a major role in the survival of various organisms by performing important functions for development and growth (Linder, 1991). Copper facilitates key redox reactions essential for cellular energy production in the electron transport chain (Okafor *et al.,* 2024, Gupta *et al.,* 2020). Copper is also involved in catalytic processes, and provision of structural support to proteins, Additionally, copper undergoes oxidation-reduction cycles in redox reactions (Okafor *et al.,* 2024). The estimated concentration of free copper in yeast and human blood plasma is between 10^{-18} to 10^{-13} M (Linder *et al.,* 1996). However, Rae *et al.,* 1999 established that less than one copper ion is present in a free ionic state in *Saccharomyces cerevisiae* even though the total copper concentration is 70 µM. (Rae *et al.,* 1999). In one of the malaria study, Rasoloson *et al.,* 2004 reported serum copper to be in the range of 11 to 24 µM, though this was

attributed to the presence of ceruloplasmin because large proportion of the copper in the blood of healthy individuals (95%) is carried by ceruloplasmin. In the same study, uninfected erythrocytes showed copper ranging between 14 and 24 µM though other studies quote 20 µM (Beutler *et al.,* 1995). Rasoloson *et al.,* 2004, found a decreased copper concentration in the infected erythrocytes, data that is not consistent with the findings of Beutler *et al.,* 1995 that suggested that there is no difference in copper content between the uninfected and infected red blood cells.

Normal cellular copper levels play various roles in different processes such as peptide hormone production and iron homeostasis, neurotransmitter synthesis, oxidative respiration, skin pigmentation through the synthesis of melanin, tissue repair, and defense against oxidative damage (Kaplan and Maryon., 2016). Copper plays a role in blood clotting, induction of blood vessel formation, and inactivation of histamine, tyramine, dopamine, and serotonin (Tapiero *et al.,* 2003). However, unchecked copper redox activity has the potential to generate free radicals that increase oxidative stress (Sailer *et al.,* 2024, Kaplan and Lutsenko., 2009). The production of free radicals such as hydroxyl (OH^-) occurs in the Fenton reaction ($Cu^+ + H_2O_2 \rightarrow Cu^{2+} + OH^- + OH$) after the initial reaction in the Haber-Weiss ($Cu^{2+} + O_2 \rightarrow Cu^+ + O_2$) reaction (Halliwell and Gutteridge, 1984). The free radicals contribute to an increase in oxidative stress which causes damage to various biomolecules in different organisms (Kaplan and Lutsenko., 2009, Ramos-Zúñiga *et al.,* 2023). Therefore, copper must tightly be regulated to levels that cannot inhibit biological processes and impinge on the growth and development of organisms (Weiss *et al.,* 2018). Disturbance of copper levels in organisms has adverse effects like Menkes and Wilson Disease (WD) which is an autosomal recessive disorder associated with copper deficiency, arising from mutations in the ATP7B gene (Scheiber *et al.,* 2014).This leads to early deaths of individuals with copper deficiency (Menkes disease) or overload (Wilson disease). Alzheimer's disease is associated with *β*-amyloid protein where copper binds and accumulates generating reactive oxygen species that attack the integrity of the cells.Spongiform encephalopathies (prion diseases), may be caused by misfolding of the Prion Protein (PrPC) and copper deficiency. Other conditions linked to the disturbance of copper concentration are Parkinson's and Huntington's diseases (Dudzik, *et al.,* 2013).

1.14 Copper uptake

There are various mechanisms that organisms possess for copper uptake, intracellular distribution, and export (Nevitt *et al.,* 2012, Lutsenko., 2016). Copper can exist in two forms Cu (II) and Cu (I) in biological systems such as plasma, where Cu (II) is predominantly in the extracellular compartment as opposed to Cu (I) which is present intracellularly but complexed with other proteins to prevent it from oxidizing to Cu (II) (Kirsipuu *et al.,* 2020). In most eukaryotic cells, copper is taken up through the high-affinity membrane copper transporter protein (Ctr1) (Banci *et al.,* 2010, Azucenas *et al.,* 2020, Chen *et al.,* 2024). Ctr1 is comprised of an extra-cytoplasmic N-terminal domain, three transmembrane regions, and a cytosolic C-

terminal tail which plays a role in the process of copper docking to various intracellular copper-binding molecules and chaperones (Wang *et al.,* 2011, Wee *et al.,* 2013). The N-terminal region is characterized by multiple methionine and histidine-rich motifs which have been demonstrated to bind Cu (I) and (II), respectively (Puig *et al.,* 2002, Crider *et al.,* 2010, Pope *et al.,* 2012, Shenberger *et al.,* 2018). The N-terminal region of Ctr1 in humans is suggested to be important for the binding and reduction of copper which is postulated to be due to the distance between the methionine and histidine amino acid residues. Since Histidine residues bind copper (II), and the metalloreductases reduce Cu (II) to Cu (I) which is bound to methionine. Thus, Ctr1 may possibly bind copper (II) and reduce it (Haas *et al.,* 2011, Eisses *et al.,* 2005). This is like what is observed with CopC protein in *Pseudomonas aeroginosa* where copper reduction is followed by its transfer from histidine to methionine amino acid residues (Koay *et al.,* 2005). The copper (II) bound by histidine is reduced from Cu^{2+} to Cu^{+} by metalloreductases (Fre1 and Fre2 in yeast, and STEAP family metalloreductases in mammals) (Georgatsou *et al.,* 1997, Linder *et al.,* 2020), before it is transported into the cells. Another metal-binding motif (MXXM) is found in the second transmembrane segment, which takes up Cu by forming Cu-S linkages (De Feo *et al.,* 2009, Maryon *et al.,* 2013a, Smith *et al.,* 2017). Studies show Ctr1 being assembled into a homotrimer having a membrane pore of 9 Å that allows the passage of Cu through the lipid bilayer (De Feo *et al.,* 2009, Smith *et al.,* 2017). In the bloodstream, approximately 70–95% of total circulating Cu is bound to ceruloplasmin and albumin where Ctr1 imports Cu in the form of Cu (I) (Lee *et al.,* 2001, Ramos *et al.,* 2016). Two types of Ctr exist in *Homo sapiens* i.e. Ctr1 and Ctr2. The Ctr2 protein functions alongside Ctr 1 mainly as a low-affinity copper transporter by regulating micropinocytosis and the position of Ctr1 within the plasma membrane (Lee *et al.,* 2000, Dancis *et al.,* 1994, Ohse *et al.,* 2024). In yeast and mammals, Ctr2 has been documented to be localized in intracellular organelles, lysosomes, and endosomes (Van den Berghe *et al.,* 2007, Tamayo *et al.,* 2018). In humans, copper may use Ctr1 and Ctr2 as a gateway to the intracellular compartment, though Ctr2 is suggested to be useful for copper import only when Ctr1 is downregulated (Lutsenko, 2010). However, there should be a gating mechanism to control the import of Cu (I) (Eisses and Kaplan, 2005). Fig 1.2 shows a schematic diagram of the features of Ctr1.

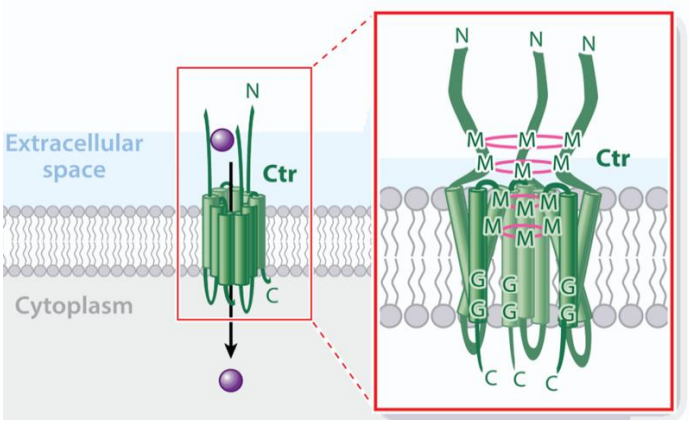

Fig 1.2 Schematic representation of trimeric structure of the yeast copper transport protein depicting copper-binding amino acids. The plasma membrane Ctr transporter protein is organized as a homotrimer and shows how copper moves through it (Ctr1), its N- and C- terminals, and amino acids (methionine and glycine) where copper is thought to bind are shown. Source: Smith *et al.,* 2017.

1.15 Intracellular copper trafficking

Copper is transported from the outside to the inside of the cell through Ctr1 or low-affinity Ctr2 when Ctr1 is downregulated (Cobine *et al.,* 2006). Upon Cu (I) entering the cell, metallochaperones bind and deliver it to different target proteins in various organelles (Rosenzweig, 2002, Prohaska *et al.,* 2004). The mechanism through which Cu (I) passes from Ctr1 to intracellular metallocheperones for delivery is not clear; however, it is suggested that protein-protein interactions are a possible mechanism at play (Rosenzweig, 2002, Banci *et al.,* 2010). In humans, copper chaperones are divided into three functional groups (i) the Atx1-like chaperones, (ii) the copper chaperones for Superoxide Dismutase (SOD1), and (iii) the copper chaperones for cytochrome c oxidase (CcO) (Rae *et al.,* 1999, Huppke *et al.,* 2012). Atx1 is a cytosolic chaperone that binds and delivers Cu (I) to various target organelles in different organisms (Simon *et al.,* 2008, Huffman *et al.,* 2000). In yeast, Atx1 delivers Cu (I) to ATPase Ccc2 copper transporter in the trans-Golgi network (Cankorur-Cetinkaya *et al.,* 2016). Human homolog (Atox1) delivers copper to ATPases for export to the extracellular compartments when copper accumulates above normal levels (Lin *et al.,* 1997, Klomp *et al.,* 1997, Hatori *et al.,* 2016). In Bacteria, an Atx1-like protein, CopZ has been identified to have a similar function to Atx1 (Cobine *et al.,* 2002, Lu *et al.,* 2002, Banci *et al.,* 2003). In this way, copper is regulated within amounts that cannot destroy the cells. In humans, Ctr family proteins play a role in limiting the bioavailability of copper to the intracellular compartment. Additionally, ATP7A and ATP7B (which are both ATPases) function to export copper in cases of an increase in concentration beyond what the cells would require (Wang *et al.,* 2011). Furthermore, findings in *P. falciparum* suggest that Ctr1 may be involved in copper acquisition while *Pf*CuP-ATPase may play a role in copper export to prevent toxicity (Choveaux *et al.,* 2012, Rasoloson *et al.,* 2004). In yeast, Glutathione and Metallothioneins (MT) such as Cup1 and Crs5 have been suggested to bind excess copper or unbound copper to prevent Fenton reactions and the generation that may kill the cell; The proteins protect cells from toxic copper

levels (Cobine *et al.,* 2006). Fig 1.3 shows the copper acquisition and distribution of copper in a human hepatocyte.

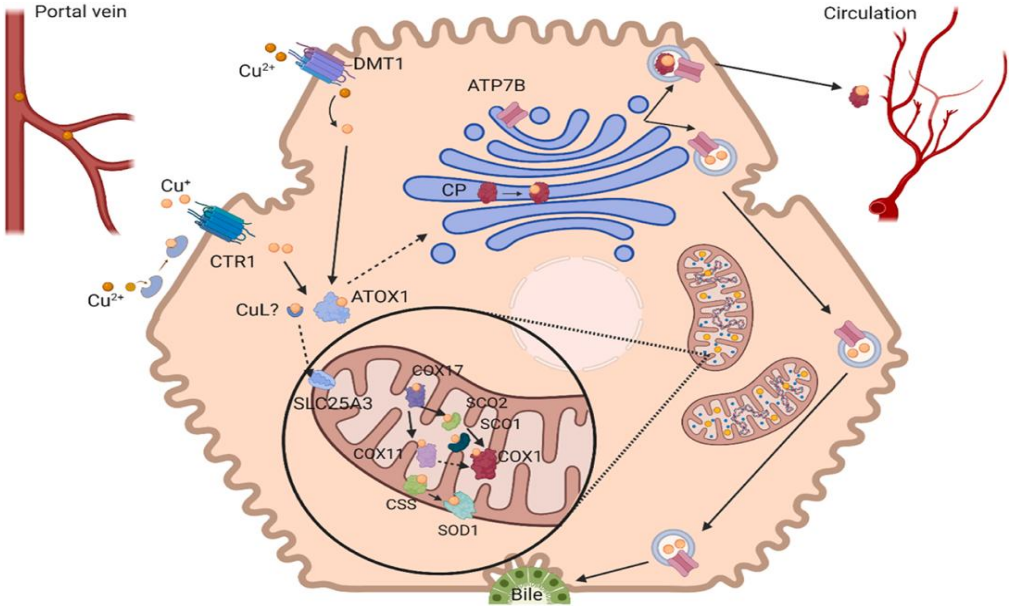

Fig 1.3 Copper pathways in human hepatic cells. Copper is acquired either through Ctr1 or DMT1 after it is reduced by STEAP. Atox1 then binds copper (I) and delivers it to TGN and ATP7B. ATP7B facilitates copper incorporation into ceruloplasmin for distribution to other parts of the body or excretion through bile. Copper is transported to the mitochondria through an unidentified copper ligand (CuL) which passes it on to SLC25A3. Cox17 distributes copper to cytochrome c oxidase where it is incorporated into CuA/B sites via Cox11 and Sco1. Source: Sailer *et al.,* 2024.

1.16 Atx1 Copper delivery to the Golgi and ATPases

Atx1 transports copper from Ctr1 to the copper transporter inside the trans-Golgi apparatus of the efflux pathway (Lin *et al.,* 1997, Pufahl *et al.,* 1997, Valentine *et al.,* 1997, Liu *et al.,* 2003, Xi *et al.,* 2014, Deng *et al.,* 2024). Copper is then moved into the lumen of the Golgi for its addition to the newly synthesized cuproenzymes that are on their way to secretion (Fig 1.4 [arrow in orange]) (Polishchuk *et al.,* 2013, La Fontaine *et al.,* 2007). The main aim of Atx1 is to take copper to P-type copper transporters which belong to a large class of transporting P-ATPases (Xi *et al.,* 2013, Wang *et al.,* 2015) The mechanism of action that P-ATPases use to move copper, and other ions across the membrane is through ATP hydrolysis. P-ATPases are in two forms in humans (ATP7A/B) and are responsible for the regulation and maintenance of copper homeostasis (La Fontaine *et al.,* 2007). Mutations in either P-ATPase led to Menkes or Wilson's disease (Bull and Cox, 1994, Strausak *et al.,* 2003, Dolgova *et al.,* 2014). In yeast, a similar copper transporter (Ccc2) has been discovered. It plays a role in the activation of the Fet3 copper protein in charge of iron uptake (Yuan *et al.,* 1995, Schlecht *et al.,* 2014). RAN1 in plants is a Ccc2 copper transporter version that works together with an Atx1-like molecule in the regulation of development in reacting to ethylene compounds (Binder *et al.,* 2020, Hirayama *et al.,* 1999; Himelblau *et al.,* 1998, Migocka *et al.,* 2018, Gul *et al.,* 2022).

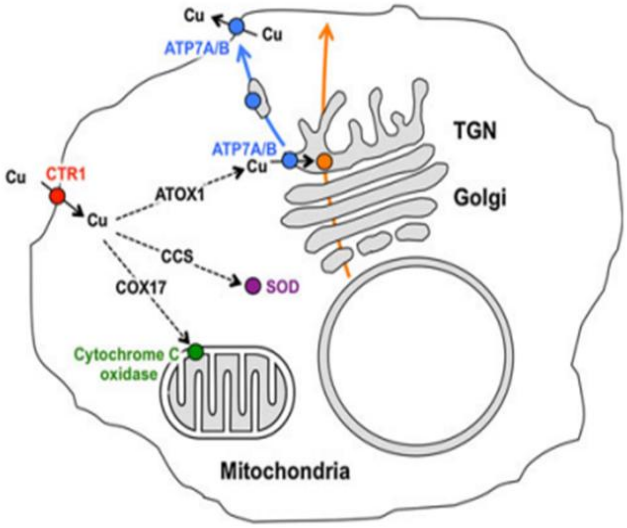

Fig 1.4 Copper movement from Ctr1 to TGN and P-ATPases in a mammalian cell. Atox1 transfers copper to P-ATPases (in blue) and ensures incorporation into cuproenzymes in the secretory pathway (arrow in orange). Source: Polishchuk *et al.,* 2013.

1.17 Copper Delivery to Cytosolic Superoxide Dismutase

Superoxide dismutase is predominantly found in the cytoplasm of most cells. It is in the immature form until Zinc is bound to its binding site, and copper is inserted including the oxidation of disulfide bonds that stabilize the homodimeric conformation (Fetherolf *et al.,* 2017). Copper-dependent and independent mechanisms are responsible for the SOD1 maturation (Boyd *et al.,* 2020, Cobine *et al.,* 2006). As a result, superoxide dismutase (SOD1) is an intracellular chaperone for copper that participates in the alleviation of oxidative stress (Sirangelo *et al.,* 2017, Gale *et al.,* 2024). To have copper inserted in the SOD1, copper chaperone for superoxide dismutase (CCS) interacts with Ctr1 and forms a complex, which leads to the transfer of copper from CCS to SOD1 (Boyd *et al.,* 2020). In yeast, cytoplasm, and mitochondria intermembrane space (IMS), Ccs provides Cu (I) for the activation of SOD1 (O'Halloran *et al.,* 2000), and the catalysis of an important intra-SOD1 disulfide bond (Furukawa *et al.,* 2004). The Ccs-independent pathway occurs because of an amino acid change, largely due to mutations in the Ccs (e.g., proline), especially in mammals and other lower eukaryotes (Carroll *et al.,* 2004, Leitch *et al.,* 2009). Furthermore, other potential copper sources for the activation of SOD1 are reduced glutathione (GSH) and Metallothioneins (MT), though, the GSH and MT mediation of SOD1 activation are not clear and there seems to be little information regarding this pathway (Caroll *et al.,* 2004, Petzoldt *et al.,* 2015, Miyayama *et al.,* 2011). Human SOD1 expressed in Ccs mutant mice only retained 25% activity, a finding that suggests that the CCS protein is essential for the functionality of SOD1 (Wong *et al.,* 2000). In yeast lacking CCS, SOD1 is not activated, and mitochondria IMS SOD1 levels are further reduced, generating an unstable homodimeric conformation unfit for the activities of SOD1 (Field *et al.,* 2003). Interestingly, *Caenorhabditis elegans* lacks CCS but has a fully active SOD1 which is mainly due

to the assortment of post-translational modifications (Jensen *et al.,* 2005). Except for this, most eukaryotes require CCS which interacts directly with Ctr1 and aids copper delivery to SOD1 and thus activates the enzyme (Rae *et al.,* 1999).

1.18 Delivery of Copper to the Mitochondria

The mitochondria harbor the cytochrome *c* oxidase enzyme that plays a role in the energy generation of a cell (Povea-Cabello *et al.,* 2024, Rigby *et al.,* 2007). Copper is essential to the functioning of the cytochrome *c* oxidase (CcO) complex, therefore its delivery to the mitochondria is pivotal and the most complex of the known pathways in biological systems (Thompson *et al.,* 2012, Garg *et al.,* 2021). In mammalian tissues, CcO biogenesis relies on the availability of over 30 other accessory proteins that have individual roles in protein synthesis (Cobine *et al.,* 2006). Cox17 is particularly important in the delivery of copper to CcO through Sco1 and Cox11 whose function is to insert copper into CuA and CuB sites located in the CcO (Cobine *et al.,* 2006). A deletion of human Cox17 has been shown to have negative effects on the assembly and organization of CcO (Oswald *et al.,* 2009, Fontanesi *et al.,* 2013). Furthermore, the absence of Cox17 in mice led to a stoppage of embryogenesis (Takahashi *et al.,* 2002). The deficiency of Cox17 in yeast causes a disruptive effect on respiration due to a complete absence of CcO activity (Glerum *et al.,* 1996, Heaton *et al.,* 2001), therefore, it can be suggested that Cox17 may have a role in the transport of Cu(I) into the IMS for purposes of CcO assembly. However, there is another opposing view that suggests the mitochondria phosphate carrier protein (Pic2) in yeast with the ability to bind copper could have a role in the transportation of copper across the mitochondrial membrane (Vest *et al.*, 2013). Additionally, findings from phylogenetic analyses have demonstrated that Pic2-like ortholog has been observed in all major eukaryotic supergroups arising from gene duplication (Zhu *et al.,* 2021) The depletion of the human homolog SLC25A3 which is identical to Pic2 in human and mouse cells , has been found to cause a deficiency of copper in the mitochondria and led to decreased activity of the CcO (Boulet *et al.,* 2018). Furthermore, Mrs3 in yeast has been demonstrated to complement Pic2 in the import of copper into the mitochondrial copper pool (Vest *et al.,* 2016). Pic2 protein functions provide new insight into the delivery of copper to the mitochondria, which is not in line with earlier suggestions in previous studies that have proposed Cox 17 playing a role in copper trafficking to the mitochondria mainly because of the presence of Cox17 in both the cytoplasm and the Intermembrane Space (IMS) (Choveaux *et al.,* 2015). Therefore, more studies are needed to elucidate Pic2 and its ability to bind copper in most species, especially in *Plasmodium falciparum.* Plasmodia Cox17 was found to bind copper, and it was suggested that it could have a role in copper movement into the mitochondria (Choveaux *et al.,* 2015).

1.19 Role of copper in Malaria parasites

Copper depletion or chelation affects the early erythrocytic stages of *P. falciparum*; therefore, it is critical in the development and function of the malaria

parasite (Asahi *et al.,* 2014). Chelation of Cu (I) with neocuproine [a compound that highly selects Cu (I) (Al-Sa'doni *et al., 1997*)], stops the development from the ring to trophozoite stages of *P. falciparum*, thereby blocking the growth of the parasite (Rasoloson *et al.,* 2004, Ding *et al.,* 2011). Additionally, tetra thiomolybdate a copper chelator, inhibits the erythrocytic development of malaria parasites *in-vitro* (Asahi *et al.,* 2013). However, other copper chelators like cuprizone and bathocuproine disulfonate (BCS) have little effect on the parasites and do not arrest the growth of the parasites because the molecules chelate Cu (II) which is not found inside the cell, the reason being that Cu (I) is preferred (Rasoloson *et al.,* 2004, Asahi *et al.,* 2013). This is because cuprizone is specific for Cu (II) binding, though it crosses the parasitic membrane. Nevertheless, copper (I) is a predominant form of copper inside the parasite, hence the no-effect result that was observed with parasite exposure to cuprizone. On the other hand, the extracellular binding of copper (I) and (II) by BCS which does not penetrate the parasitic membrane did not affect the growth of the parasite (Asahi *et al.,* 2013). In these studies, it is evident that copper (I) is essential for the development and growth of the *Plasmodium* parasite. Copper deprivation in other organisms has been shown to have effects on copper transporters like ATPases, though no evidence exists for *Pf*CuP-ATPase. In yeast, copper deprivation leads to the upregulation of the transcription of ATPase (Dancis *et al.,* 1994, La Fontaine *et al.,* 2007, Scheiber *et al.,* 2013). On the other hand, copper deprivation in bacterial systems leads to a decrease in the ATPase transcription (Gaballa *et al.,* 2003, Argüello *et al.,* 2013). Contrary to these findings, Rasoloson *et al.,* 2004 argue more for a chelator-metal inhibition of specific transcription than the deprivation of copper bioavailability, a factor that leads to a decrease in the need for copper export.

1.20 Copper binding proteins in *Plasmodium falciparum*

In *P. falciparum*, there are several copper proteins have been identified and characterized and suggested to have a role in the copper uptake, cytoplasmic distribution, and its transfer to the mitochondria. Fig 1.5 shows other copper proteins such as CMC1, CutA, GSH, PIC2, Pet191, DMT1, *Pf*Cox23, *Pf*SAHH, and *Pf*Grx1 that have not been characterized in Plasmodia. A summary of the copper proteins that have been identified in *Plasmodium* is shown in Table 1.2. Note that Cox23 and metallothioneins could not be identified using PlasmoDB, a thorough search for these proteins were conducted by using Go-terms like; Cox 23, metallothioneins, Cox23/copper-binding protein, further, BLASTp search was conducted using yeast Cox23 sequence, no significant results were obtained. However, they have been suggested to play a role in copper homeostasis in plasmodia parasites and other organisms (Tripathi *et al.,* 2009, Barros *et al.,* 2004). In the current study, we characterized *Pf*Grx1 and *Pf*SAHH and determined their potential to bind copper. Fig 1.6 shows *Pf*Ctr1 which was demonstrated to bind copper *in-vitro* and *in-vivo* (Choveaux *et al.,* 2012) and thereby proposed to have a role in the copper uptake by the parasite. Rasoloson et al., 2004, found that *Pf*CuP-ATPase binds copper and has the potential to export it from the parasite. However, no evidence has been provided

on how copper is transported from *Pf*Ctr1 to the *Pf*CuP-ATPase. In humans and yeast, the Atox1 protein which is absent in Plasmodium transfers copper from Ctr1 to the P-ATPases for export (Boyd *et al.,* 2020, Hatori *et al.,* 2016). Atox1 also transfers copper to CCS which passes the metal to the SOD1 (Chen *et al.,* 2020). The CCS and SOD1 are both absent from the parasite as can be shown in Fig 1.6, however, the parasite acquires SOD1 from the red blood cells through a process explained in section 1.20.1. Choveaux *et al.,* 2015 have shown that *Pf*Cox17 binds to copper *in-vitro* and *in-vivo*, thereby being suggested to be involved in the transfer of copper to the mitochondria as well as transfer to *Pf*Sco1 (Munsami., 2022) and *Pf*Cox11 (Salman *et al.,* 2022) for the insertion in the cytochrome *c* oxidase. *Pf*Cox19 binds copper and is suggested to play a role in *Pf*Cox11's transfer of copper to the CcO (Salman *et al.,* 2023).

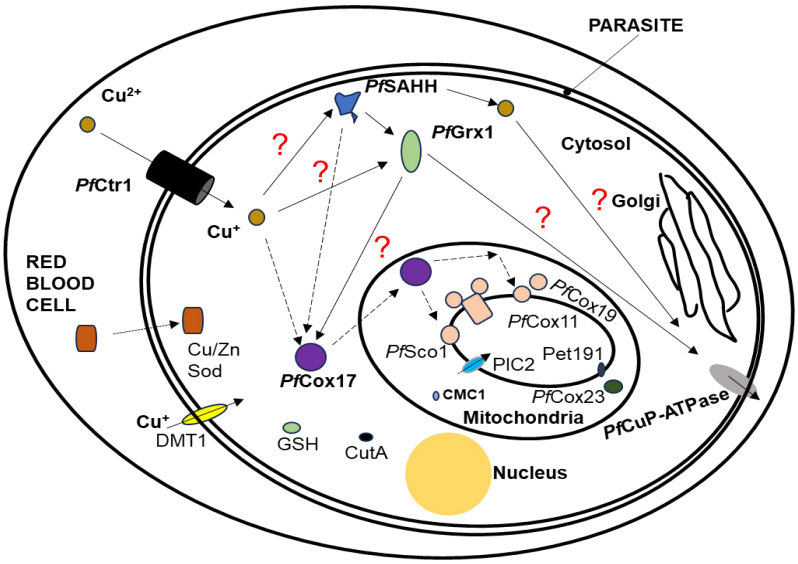

Fig 1.5 Copper proteins in *P. falciparum*. The copper binding proteins shown may be involved in the copper homeostasis in the parasite. The question marks in red indicate pathways where *Pf*Grx1 and *Pf*SAHH may potentially play a role. Source: M. Kwangu

Table 1.2 *P. falciparum* copper-dependent protein orthologs

Protein	PlasmoDB protein Identifier
Ctr1	PF3D7_1421900
Cox17	PF3D7_1025600
Cox11	PF3D7_1475300
Cox19	PF3D7_1201800
Sco1	PF3D7_0708900
Glutaredoxin1	PF3D7_0306300
S-adenosylhomocysteine hydrolase	PF3D7_0520900
CuP-ATPase	PF3D7_0904900
CMC1	PF3D7_0729600
PIC2	PF3D7_1202200
Glutathione-S-transferase	PF3D7_1419300
Pet191 (COA5 in *P. falciparum*)	PF3D7_0825600
Metallothionine (MT)	-
DMT1	PF3D7_0715800
CutA	PF3D7_1249500
Cox23	-

Source: M. Kwangu

1.20.1 Copper uptake and distribution in the *Plasmodium* parasite

Copper movement from the outside to the inside of the cell is mediated by the high-affinity copper transporter protein Ctr1 (Lutsenko *et al.,* 2010, Nayeri *et al.,* 2023). This protein is common in plants, yeast, and humans (Kim *et al.,* 2008, Kommuguri *et al.,* 2012). Similarly, in *Plasmodium falciparum*, the putative *P. falciparum* copper transport protein (*Pf*Ctr1) has been identified, and the recombinant amino terminus has been shown to bind copper *in vitro* and when expressed within *E. coli* host bacteria (Choveaux *et al.,* 2012). In humans and yeast, copper from Ctr1 is passed on to copper chaperones including copper chaperones for superoxide dismutase which traffics copper to copper/zinc superoxide dismutase (Cu/Zn SOD1) in both the cytosol and mitochondrion (Kim *et al.,* 2008, Lutsenko *et al.,* 2010). However, *P. falciparum* lacks the gene encoding cuprozinc SOD1 but synthesizes an iron/manganese Sod (Maurya *et al.,* 2022, Islam *et al.,* 2022). According to Fairfield *et al.,*1983, human SOD1 provides copper for the parasite when it ingests the host cells' cytoplasm that moves with catalase enzyme, hemoglobin, and Cu/Zn SOD1 and gets deposited in the food vacuole where Cu/Zn SOD is digested to release copper and Zinc. However, at times, it is suggested that Cu/Zn SOD1 may escape this digestive process and either remain in the vacuole or migrate to the parasite's cytoplasm (Fairfield *et al.,* 1983). Studies have shown that Cu/Zn SOD1 is an alternative source of copper for *P. falciparum* (Fairfield *et al.,* 1983, Olliaro *et al.,* 1995).

1.20.2 Copper delivery to the mitochondria

Copper delivery to the mitochondria is essential in the malaria parasite because the functionality and biogenesis of cytochrome *c* oxidase (CcO) rely on the metalation of the subunits Cu_A and Cu_B (Leary *et al.,* 2004, Llases *et al.,* 2019, Ghosh *et al.,* 2014). Cox17 in yeast has been implicated in the delivery of copper to the mitochondria owing to its cytoplasmic localization (Glerum *et al.,* 1996, Maxfield *et al.,* 2004, Horng *et al.,* 2004, Caron-Godon *et al.,* 2024). However, this thought was debated as Cox17 was found to be more effective in the delivery and metalation of copper to CcO sites through Sco1 and Cox 11 (Balandin *et al.,* 2002, Povea-Cabello *et al.,* 2024), which play a role in the insertion of copper in Cu_A and Cu_B sites of the cytochrome *c* oxidase (Cobine *et al.,* 2006). In *P. falciparum*, Cox17 was demonstrated to bind copper *in-vitro* and *in-vivo*, and it was determined to be localized in the cytoplasm and mitochondria from the ring to schizont stages (Choveaux *et al.,* 2015). Therefore, *Pf*Cox17 was thought to have a role in copper transport to the mitochondria, though there is an incomplete understanding of copper shuttling to the mitochondria in *P. falciparum* (Choveaux *et al.,* 2015). Another copper protein determined in *P. falciparum* related to copper delivery to CcO is Cox11, which was found to bind copper *in-vitro* and when expressed within *E. coli* host cells (Salman *et al.,* 2022). An alternative copper transporter that may deliver Cu to the mitochondria in yeast has been identified to be a non-proteinaceous copper ligand (CuL); however, it has not been identified in Plasmodium to this date (Cobine *et al.,* 2004, Cobine *et al.,* 2006, Vest *et al.,* 2019, Cobine *et al.,* 2021).

Another Cu transporter protein that has been identified in yeast in this regard is Pic2 (Vest *et al.,* 2013). Yeast strains lacking Pic2 were found to be deficient in CcO functionality and were observed to have decreased Cu levels compared to wild-type (WT) strains (Vest *et al.,* 2013). This suggested a critical role of Pic2 in the import of Cu into the mitochondria. In humans, SLC25A, an identical orthologue to the Pic2 protein, has been identified as the major mitochondrial transporter of both Cu and phosphate (Boulet *et al.,* 2018). In *P. falciparum*, the ability of Pic2 to bind copper has not yet been determined; however, there is a possibility that *Pf*Pic2 could have a similar role to those observed in yeast and humans.

1.20.3 Copper efflux from the parasite

Copper accumulation in a cell may lead to perturbation of metabolism and in some, impinge the development and growth (Waalkes *et al.,* 2000, Saporito-Magriñá *et al.,* 2018, Zhang *et al.,* 2024, Springer *et al.,* 2024). Therefore, copper transporter proteins that secrete Cu from cells play a role in maintaining normal copper levels (Kuo *et al.,* 2021, Tang *et al.,* 2019, Ruiz *et al.,* 2021).

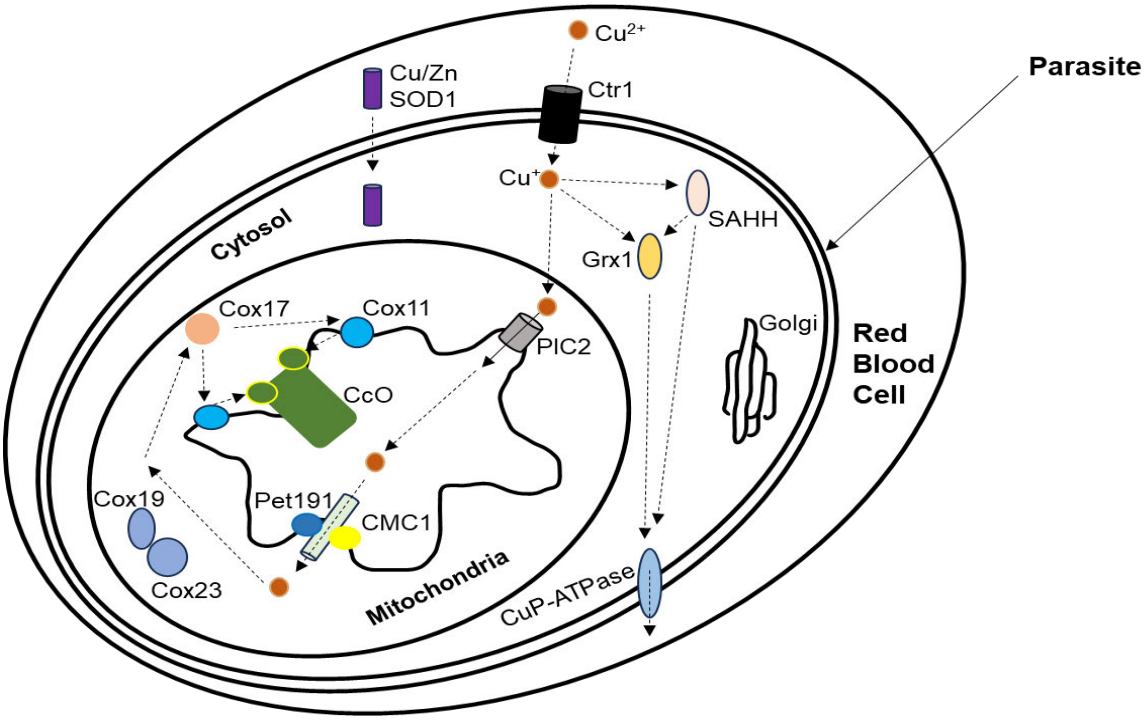

Fig 1.6 Copper metabolism in *Plasmodium falciparum*. Illustration of possible copper pathways in the *Plasmodium falciparum*. The dotted arrows show copper's suggested pathways, including the potential copper protein transporters. Source: M. Kwangu.

In yeast and human cells, copper is secreted by ATPases 7A/7B when abnormal levels are reached (Hamza *et al.,* 2003, Ding *et al.,* 2014, Gupta *et al.,* 2009). In *Plasmodium falciparum*, CuATPase protein has been suggested to have a role in the efflux of excess copper levels (Rasoloson *et al.,* 2004). *Pf*CuATPase is the largest copper transporter homolog among many other copper proteins present in *P. falciparum* and is located on the parasite's membranes as well as the surface of infected red blood cells (Rasoloson *et al.,* 2004). The *Pf*CuATPase binds copper (I) and may have a role in the export of copper to the host cell in situations when copper

surges beyond optimum concentration in the parasite. The question that begs an answer is how copper is trafficked from Ctr1 or proteins with bound copper in the cytoplasm to *Pf*CuP-ATPase because, unlike yeast and human cells, *P. falciparum* has no Atox1 to shuttle copper to the CuP-ATPase. However, *Pf*Grx1 instead is being proposed in the current study to be a potential transporter of copper between *Pf*Ctr1 and *Pf*CuP-ATPase as illustrated in Fig 1.6 due to *Pf*Grx1's similar role in copper homeostasis to that of Grx1 in humans (Maghool *et al.,* 2020). Additionally, *Pf*SAHH may also play a role in copper transport to the exporter protein as shown in Fig 1.6.

1.21 Glutaredoxins (Grxs)

Glutaredoxins are described as small ubiquitous disulfide oxidoreductases that fall in the thioredoxin superfamily (Collinson *et al.,* 2002, Stroeher *et al.,* 2012, Meyer *et al.,* 2008). A Cys-X-X-Cys/Ser active site is present in most of these proteins (Rouhier *et al.,* 2002, Ogata *et al.,* 2021). The proteins are found in almost all living organisms apart from certain bacterial and archaeal phyla (Rouhier *et al.,* 2008, Alves *et al.,* 2009). Glutaredoxins are divided into different classes based on the active site they have, i.e. CP[Y/F]C or CGFS which are dithiol and monothiol respectively (Picciocchi *et al.,* 2007). However, these have been renamed as classes I and II (Couturier *et al.,* 2009, 2013). Two additional classes (III and IV) belong to land plants and a small number of algae and animals, respectively (Meyer *et al.,* 2008, 2012). The Grx1 belongs to the class I group of glutaredoxins and has the CPYC (CXXC) motif that may be reduced by Glutathione (GSH) and has been demonstrated to bind copper (I) (Klatt *et al.,* 2000, Michelet *et al.,* 2006, Zaffagnini *et al.,* 2008, Pimentel *et al.,* 2012, Maghool *et al.,* 2020). The Glutaredoxin enzymes reduce disulfide bonds and thus participate in deglutathionylation activities of the cell (Stroeher *et al.,* 2012), nevertheless, some of the Grxs may play a role in the iron-sulfur cluster transfer proteins (Rouhier., 2010, Liedgens *et al.,* 2020, Trnka *et al.,* 2020, Chai *et al.,* 2023). Further, Grxs are known to regulate inflammation as well as play a role in the transfer of copper from Ctr1 to the P-ATPases (Liao *et al.,* 2010, Maghool *et al.,* 2020).

1.22 *Human* Glutaredoxin1 (*h*Grx1)

The *h*Grx1 is a member of the glutaredoxin class I group of enzymes and a GSH-dependent thiol-disulfide oxidoreductase (Alves *et al.,* 2009, Bouldin *et al.,* 2012, Liu *et al.,* 2015). The enzyme has a major role in the regulation and maintenance of the redox system (Cater *et al.,* 2014, Aon-Bertolino *et al.,* 2011, Begas *et al.,* 2017, Xiao *et al.,* 2019). Studies have shown that it has a C-XX-C motif between C23 and C26 which is also an active site (Berndt *et al.,* 2008). Previous studies have shown that this site has increased affinity for Cu(I) (Brose *et al.,* 2014, Xiao *et al.,* 2011, Sun *et al.,* 1998). Further studies have reported an interaction between *h*Grx1 and the Metal Binding Domains (MBDs) of ATP7A and ATP7B (Lim *et al.,* 2006). Several studies looking at the *h*Grx1 knockdown and overexpression in neurons and mouse embryonic fibroblasts have suggested a significant effect on

copper homeostasis (Cater *et al.,* 2014, Singleton *et al.,* 2010, De Benedetto *et al.,* 2014). The *h*Grx1 has been proposed to reduce oxidized Atox1 using GSH substrate (Brose *et al.,* 2014). Further, studies of the recombinant *h*Grx1 (r*h*Grx1) show its ability to bind Cu(I) through the Cys residues present in its active site (Maghool *et al.,* 2020). However, Cu(I) binding to the *h*Grx1 potentially inhibits the enzyme and makes it unavailable for various activities. In other cells like neurons, this mechanism protects the cells from the effects of copper toxicity (Cater *et al.,* 2014).

1.23 *Plasmodium falciparum* Glutaredoxin1 (*Pf*Grx1)

Plasmodium falciparum Grx1 is a small, dithiol protein, found in the cytoplasm of the parasite with a weight of approximately 12.4 kDa and has a classical motif 'CPYC' which is the active site of the protein (Rahlfs *et al.,* 2001). *P. falciparum* expresses other Grx-like proteins (GLP1, GLP2, and GLP3) which are monothiol and located in the cytosol and mitochondria respectively (Kehr *et al.,* 2010). *Pf*Grx1 is an essential protein of the parasite whose role is to decrease oxidative stress, thus increasing the survival chances of the parasite (Schirmer *et al.,*1995, Patzewitz *et al.,* 2012, Jortzik *et al.,* 2012, Djuika *et al.,* 2013). The malaria parasite is often exposed to increased amounts of reactive oxygen species (ROS) during the erythrocytic stage of development (Schwarzer *et al.,* 2003a and b, Winograd *et al.,* 2005, Tiwari *et al.,* 2021). Additionally, the heme is produced by the catabolism of the host cell hemoglobin that is ingested by the parasite leading to the production of toxic compounds that contribute to the free radical generation (Schirmer *et al.,*1995, Müller., 2015). In *Trypanosoma cruzii*, *Toxoplasma gondii*, and *Cyanobacteriium synechocystis sp*, Grx1 has been found to improve the survival chances of these organisms (Piacenza *et al.,* 2009, Rabenau *et al.,* 2001, Sánchez-Riego *et al.,* 2013).

1.24 *Pf*Grx1 and *h*Grx1

Maghool *et al.,* 2020 report the ability of *h*Grx1 to bind Cu (I) and interact with Atox1 and ATP7A/7B. Research aiming to establish the Cu (I) binding ability of *Pf*Grx1 and its interaction with *Pf*CuATPase remains to be elucidated. However, the similarities established through previous studies suggest that *Pf*Grx1 may have similar functions to *h*Grx1. More studies are required to understand the interaction of *Pf*Grx1 and other Cu transporters like *Plasmodium falciparum* Ctr1, Cox17, S-adenosylhomocysteine hydrolase (*Pf*SAHH), and *Pf*CuATPase. This will offer some insight into Cu distribution in the *Plasmodium falciparum* parasite.

1.25 Overview of S-adenosylhomocysteine hydrolase (SAHH)

SAHH is an enzyme that is conserved across most organisms and plays a role in the conversion of S-adenosyl-l-homocysteine (SAH) to L-homocysteine (HCY). The molecular weight of SAHH ranges between 45-56 kDa across the different species (Creedon *et al.,* 1994, Seo *et al.,* 1993, Tanaka *et al.,* 2004, Kusakabe *et al.,* 2015). The species have varying structures of SAHH and, thus, may have variations when it comes to functions. Various studies have reported that SAHH enzymes from *Plasmodium falciparum*, *Mycobacterium tuberculosis*

(*Mt*SAHH), rat (RnSAHH), mouse SAHH, and human (*Hs*SAHH) all form homotetramers, however, those from bacterium *Alcaligenesis faecalis* and plant *Lupinus luteus* (LISAHH) are homohexamers and homodimers respectively (Bujnicki *et al.,* 2003, Reddy *et al.,* 2008, Corrales et al., 2013, Dai *et al.,* 2022a, Kusakabe *et al.,* 2015, Singh *et al.,* 2016, Koeppl *et al.,* 2024, Brzezinski *et al.,* 2012). All the monomers have cofactor and substrate domains divided by a cleft in a deep pocket (Singh *et al.,* 2016, Tanaka *et al.,* 2004). The cofactor domain binds NAD^+ which is not covalently bound but is closely attached (Singh *et al.,* 2016). In plants, a sodium binding site close to the active site of the LISAHH has been documented (Brzezinski *et al.,* 2012). SAHH has a variety of functions, and its deficiency is associated with many conditions such as vascular disorders, myopathy, fatty liver, cancer, renal insufficiency, and diabetic nephropathy, renal insufficiency, , myopathy, cancer, and (Guo *et al.,* 2024, Fan *et al.,* 2024, Ito *et al.,* 2024, Xia *et al.,* 2024, Cueto *et al.,* 2024). SAHH has a critical role in regulating transmethylation in all eukaryotic organisms (Caracausi *et al.,* 2024).

1.26 Human S-adenosylhomocysteine hydrolase

Human SAHH forms a tetramer with similar monomers each bound with NAD^+ (Singh *et al.,* 2016, Coulter-Karis *et al.,* 1989). Amino acid residues unique to the binding of NAD^+ are asparagine, lysine, and tyrosine at positions 322, 473, and 477 respectively (Singh *et al.,* 2016). Another feature of importance that is also conserved in multiple organisms is the GYGDVGKG (GXGXXGXG) motif that has been shown to bind to NAD^+ in other organisms like *P. falciparum* SAHH (Creedon *et al.,* 1994). Mutational studies have revealed various functions of this enzyme (Yamada *et al.,* 2002). Missense mutation has been observed to lead to *h*SAHH deficiency that causes negative effects on various body systems (Dai *et al.,* 2022a and b, Bjursell *et al.,* 2011). Similarly, copper deficiency may cause a deficiency in SAHH in some organisms, i.e. in mouse hepatocytes, copper deficiency led to SAHH deficiency (Seo *et al.,* 1993, Bethin *et al.,* 1995b); however, no data suggests that copper can lead to the deficiency of SAHH in humans. Nevertheless, human SAHH has been proposed to be involved in copper metabolism as well as sulfur amino acid metabolism (Bethin *et al.,* 1995a).

1.27 Role of *Plasmodium falciparum* S-adenosyl Homocysteine Hydrolase (*Pf*SAHH) in copper metabolism

*Pf*SAHH is a highly conserved enzyme that causes a reversible hydrolysis of SAH to l-homocysteine (HCY) and adenosine (ADO) (Creedon *et al.,* 1994, Bujnicki *et al.,* 2003, Nakanishi *et al.,* 2005). The protein may play a role in copper metabolism though there are no reports regarding the ability of the *Pf*SAHH to bind copper. However, there exist structural similarities among SAHHs in various species. For this reason, *Pf*SAHH may have similar functions to those observed in other SAHHs from different organisms. Studies have indicated that *Hs*SAHH and *Rn*SAHH bind Cu, though the motif where the metal binds has not yet been studied. It can however be speculated that copper might bind to the metal-binding domain on each

monomer (Bethin *et al.,* 1995a, Bethin *et al.,* 1995b, Seo *et al.,*1993). More studies are needed to investigate the copper-binding ability of *Pf*SAHH and its interaction with other Cu chaperones which might offer alternative and novel drug targets for malaria.

1.28 Potential interaction of S-adenosylhomocysteine hydrolase, Glutathione, and Glutaredoxin 1; Implications for copper metabolism in *Plasmodium falciparum*

Human and mouse SAHH have been found to bind copper with the latter being demonstrated to be sensitive to copper deficiency, thus copper acting as a regulator of mouse SAHH derived from the hepatocytes (Bethin *et al.,* 1995a and b, Seo *et al.,* 1993). While *Pf*SAHH's role in copper metabolism remains unstudied, it possesses a co-factor binding motif (GYGDVGKG, [**GXGXXGXG]**) that is conserved in multiple organisms (Creedon *et al.,* 1993, Singh *et al.,* 2016, Tanaka *et al.,* 2004) and suggested to bind copper. Having these similarities makes us propose that *Pf*SAHH may bind copper and participate in the copper homeostasis of the parasite. Therefore, inhibition of SAHH using either compound inhibitors or copper chelators can lead to a decrease in SAHH levels. SAHH inhibitors like neplanocin A, a novel cyclopentenyl analog of adenosine, have been reported to have antimalarial activity and that PiggyBac transposon mutagenesis suggests that *Pf*SAHH is essential for parasite viability (Whaun *et al.,* 1986*,* Borchadt *et al.,* 1984, Zhang *et al.,* 2018). In humans, SAHH deficiency has many documented effects on different organs, such as muscles (Ramadza *et al.,* 2022), the heart, and blood vessels (Dai *et al.,* 2022a). In a study involving the rat SAHH deficiency, there was an increase in oxidative stress in the cerebral cortex due to the accumulation of S-adenosylmethionine (SAM) which led to decreased glutathione (GSH), increased malondialdehyde (MDA), decreased sulfhydryl content and an increase in carbonyl content (Zanatta *et al.,* 2018). One striking consequence of inhibiting SAHH is that inhibition leads to decreased glutathione where several redox enzymes like glutaredoxins and reactions depend (Djuika *et al.,* 2013, Singleton *et al.,* 2010, Urgate *et al.,* 2010). A decrease in glutathione has been suggested to inhibit copper proteins like Cu-ATPases, affecting intracellular copper concentration and decreasing glutaredoxin 1 activity (Singleton *et al.,* 2010, Liao *et al.,* 2010). Depleting GSH using L-buthionine-sulfoximine (BSO) has been shown to decrease copper entry to 50% into the HEK cells and various cell types, data which suggests glutathione's role in *h*CTr1's copper uptake (Maryon *et al.,* 2013b) and its transfer to intracellular copper chaperones. Atox1 is regulated by glutathione, and low levels of glutathione have been demonstrated to help Atox1 in its copper binding by reducing the disulfide bonds (Hatori *et al.,* 2012).

On the other hand, Glutaredoxins (GRXs) are small ubiquitous disulfide oxidoreductases known to use GSH as an electron donor (Zaffagnini *et al.,* 2008, Liao *et al.,* 2010, Saaranen *et al.,* 2009). Any perturbations regarding GSH destabilize the functionality of Glutaredoxins (Elko *et al.,* 2019). Human Glutaredoxin1 (*h*Grx1) has been found with the potential to deliver copper to ATP7B,

thus offering an alternative pathway to the maintenance of copper homeostasis (Maghool *et al.,* 2020, Singleton *et al.,* 2010). The *h*Grx1 donates copper to Atox1 and regulates its binding to protein through GSH (Brose *et al.,* 2014, Maghool *et al.,* 2020). Due to *Pf*Grx1's CXXC motif (Rahlfs *et al.,* 2001) that is present in *h*Grx1, conserved in Grx1 from many organisms, and demonstrated to bind copper, the *Pf*Grx1 is likely to have similar roles in the parasite. Evidence in humans has shown that SAHH and Grx1 may have interactions with glutathione, a situation that may be similar for *Pf*SAHH and *Pf*Grx1 more especially for the activity of *Pf*Grx1 which may be anchored on GSH (Zanatta *et al.,* 2018, Elko *et al.,* 2019). Furthermore, inhibition of *Pf*SAHH by drugs like neplanocin A may lead to the accumulation of S-adenosylmethionine (SAM) which causes a decrease in glutathione levels (Whaun *et al.,* 1986) (Fig 1.7). The low levels of glutathione may then affect the activity of copper proteins like *Pf*Ctr1, *Pf*Grx1, and *Pf*CuP-ATPases (Fig 1.7), as observed in human copper proteins.

*Pf*Grx1 might be the alternative route or link between *Pf*Ctr1 and CuATPase transporter in the copper pathway as proposed in the present study. However, *Pf*Grx1 might be inhibited due to the decrease in the levels of GSH because of the inhibition of *Pf*SAHH (Fig 1.7). These effects might affect copper transport and distribution in the parasite and therefore possibly lead to impingement on the growth and development of the parasite. It is therefore important to evaluate the copper binding abilities of *Pf*SAHH and *Pf*Grx1 and their interaction as this might offer alternative or novel drug targets for antimalarials. In addition, *Pf*Grx1 is important for the viability of the parasite (Zhang *et al.,* 2018)

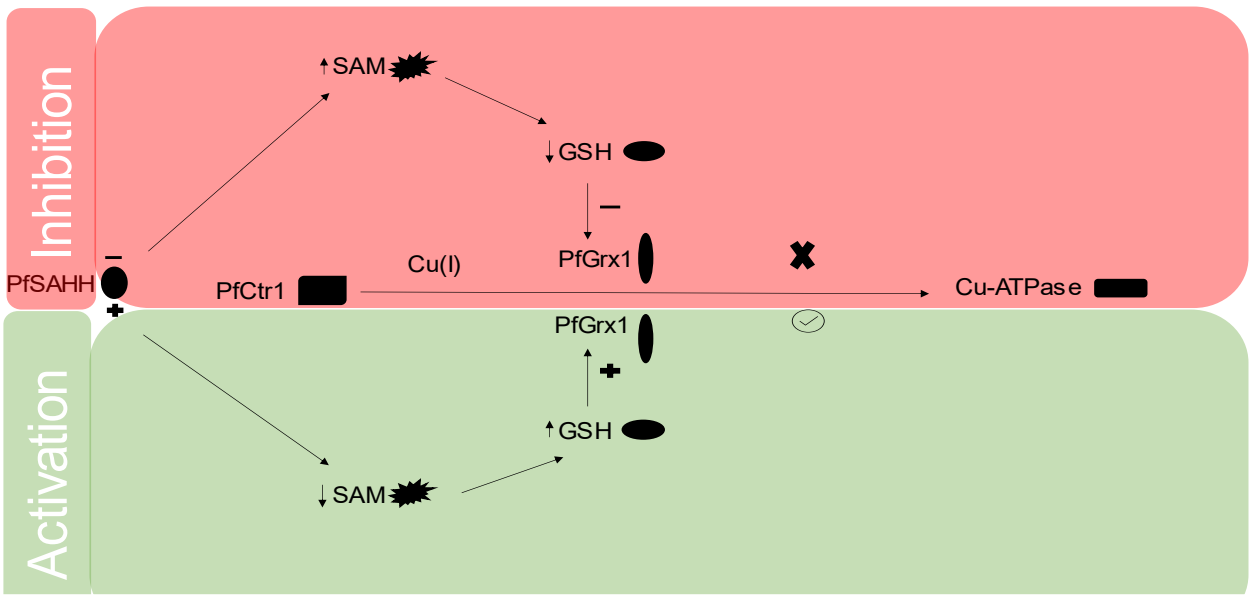

Fig. 1.7 Possible interaction of GSH, *Pf*SAHH, and *Pf*Grx1 and its implication on copper metabolism. Source: M. Kwangu

1.29 Study Outline

The *Plasmodium* parasite has in the recent past developed partial resistance to antimalarial drugs, and alarmingly, drugs (Artemisinin combination therapy) used as the first line of treatment have shown to be partially ineffective in combating malaria (Dondorp *et al.,* 2009, Noedl *et al.,* 2008, WHO., 2023). There has been renewed hope with the introduction of new pre-erythrocytic vaccines RTS, S/AS01, and R21/Matrix-M (Okombo and Fidock., 2024). Some drugs are under development as of 2022, and this list is always updated on MMV website (https://www.mmv.org/research-development/mmvs-pipeline-antimalarial-drugs). In addition, various approaches are utilized to enhance antimalarial drug discovery progress (Siqueira-Neto *et al.,* 2023). Recent reviews during the COVID pandemic revealed novel antimalarial hits that target various parasitic stages (Luo et al., 2023), It has been observed that many antimalarial candidates that end up being formulated into drugs result from phenotypic screening (Luo *et al.,* 2023). A study conducted using data from the Medicines for Malaria Venture (MMV) website, all six candidates namely, MMV533, ZY19489, INE963, GSK701/MMV367, and intravenous KAE609 significantly enhanced the treatment of malaria (Okwu *et al.,* 2025). Clinical trials were conducted to establish the effect of using combined drugs such as ganaplacide/lumefantrine-SDF, cabamiquine/pyronaridine, and both oral and intravenous cipargamin, and INE963, results are promising and resistance is likely to be evaded using such malarial regimen (Okwu *et al.,* 2025). However, the situation needs more studies to be undertaken to identify and develop new drugs to address resistance to antimalarial drugs. Genomic studies have been helpful in drug discovery though breakthroughs have eluded these efforts (Gamo *et al.,* 2010). Other methods such as the identification of malarial proteins, prediction of ligands, and simulations of various proteins present in humans and the parasite have been used to add to efforts focused on the search for alternative novel drugs to combat malaria (Joubert *et al.,* 2009). Further, different strategies must be pursued which include modifications of the available drugs to develop novel agents that focus on new targets (Rosenthal *et al.,* 2003).

Copper uptake, distribution, and efflux may provide interesting potential drug targets that deserve exploration. Focusing on the proteins involved in copper metabolism in the Plasmodia offers promising outcomes as regards alternative drugs to combat malaria. This idea is backed by studies that found that copper chelators namely neocuproine and diethyldithiocarbamate inhibit the growth of *P. falciparum* from ring to trophozoite stage (Rasoloson *et al.,* 2004, Meshnick *et al.,* 1990). Rasoloson *et al.,* 2004 report a Plasmodial copper transporter that is bound to the membrane and plays a role in the secretion of copper from the parasite. Nevertheless, it is not clearly understood how copper is trafficked from Ctr1 to the P-type ATPase copper efflux protein in times when the parasitic cell has an abnormal concentration of copper (Rasoloson *et al.,* 2004). In humans, Grx1 offers an alternative pathway for copper movement from Ctr1 to ATP7A/7B (Maghool et al., 2020). Due to structural similarities between *h*Grx1 and *Pf*Grx1, it is proposed that

*Pf*Grx1 may play a similar role in Plasmodium and provide answers to what proteins transport copper to *Pf*CuP-ATPases from *Pf*Ctr1 and intracellular pool when there is excess copper in the parasite. Another Plasmodium protein that has no information regarding the role it plays in copper metabolism but has been demonstrated to have the ability to bind copper in other species is *Plasmodium falciparum* S-adenosylhomocysteine hydrolase. The current study aimed to identify, express, and characterize copper-binding *Plasmodium falciparum* Glutaredoxin 1 and S-adenosylhomocysteine hydrolase.

1.30 Aim and Objectives

The present study aimed to gain an understanding of the plasmodia cuprome through the evaluation of the copper-binding ability of *Pf*Grx1 and *Pf*SAHH. The following objectives were formulated to address the main aim of the study.

1. To clone and recombinantly express the *Pf*Grx1 and *Pf*SAHH proteins in *Escherichia coli* (*E. coli*).
2. Evaluate the copper-binding ability of recombinant *Pf*Grx1 and *Pf*SAHH both *in-vitro* and *in-vivo* by measuring the inhibition of copper-catalyzed ascorbate oxidation assay by the two proteins, assessing the *E. coli* bacterial (with and without recombinant protein) growth in the absence and presence of toxic copper levels, and using bicinchoninic acid (BCA) copper release assay.
3. To predict protein-to-protein interaction between *Pf*Grx1 and *Pf*Ctr1, and *Pf*Grx1 and Cu-ATPase, *Pf*Grx1 and *Pf*Cox17 and *Pf*Grx1 and *Pf*SAHH using ClusPro 2.0 (https://cluspro.org)
4. Identification of copper binding sites of *Pf*Grx1, *Pf*SAHH, *Pf*Ctr1, *Pf*Sco1, *Pf*Cox11, *Pf*Cox17, and *Pf*Cox19 using the sequence alignments, BLASTp search and Metal-Ion Binding (MIB2) site prediction and modeling server (http://combio.life.nctu.edu.tw/MIB2/.

Chapter 2

Materials and Methods

2.1 Introduction

The current chapter describes general materials and methods utilized under bioinformatics, molecular biology, and biochemical techniques.

Table 2.1 Methods, materials (reagents and products), and Manufacturers.

Method	Material	Manufacturer
PCR	Oligonucleotide primers	Integrated DNA Technologies (IDT), USA
	One Taq® Polymerase	New England Biolabs (Ipswich, USA)
	10 mM dNTPs	Thermofischer Scientific (Waltham, USA)
Agarose electrophoresis	100bp DNA ladder	New England Biolabs (Ipswich, USA)
	O'GeneRuler™1kb DNA Ladder	Fermentas (Vilnius, Lithuania)
	Seakem®LE agarose	Lonza (Rockland, USA)
	Agarose, low gelling temperature	Sigma (St. Louis, USA)
	Ethidium bromide	
Cloning	Bioline Isolate II PCR and Gel kit.	Meridian Bioscience (London, England).
	pET100/D-TOPO® Expression plasmid	Invitrogen, Thermofischer Scientific (Waltham, USA)
	BamHI, and EcoRI, restriction enzymes	Thermofischer Scientific (Waltham, USA)
	GeneJet™ Plasmid Miniprep Kit, TransformAid™	Thermofischer Scientific (Waltham, USA)
	Thermo Scientific GeneJet Gel Extraction Kit	Thermofischer Scientific (Waltham, USA)
	Isopropyl β-D-1-thiogalactopyranoside (IPTG)	Thermofischer Scientific (Waltham, USA)
Bacteriological culture methods	*E. coli* JM109 and BL21(DE3) pLysS cells	Novagen (Darmstadt, Germany), Promega (Madison, USA)
	Ampicillin sodium salt	Sigma (St. Louis, USA)
	Bacteriological agar	Merck, Wadeville, Gauteng
	Tryptone	Sigma (St. Louis, USA)
	Yeast extract	Sigma (St. Louis, USA)
	Sodium Chloride	Sigma (St. Louis, USA)
	D-(+)-glucose	Merck, Wadeville, Gauteng
SDS-PAGE	Molecular weight marker	Thermofischer Scientific (Waltham, USA)
	Acrylamide	Sigma (St. Louis, USA)
	Bis-acrylamide	Sigma (St. Louis, USA)
	Sodium dodecyl sulfate (SDS)	Sigma (St. Louis, USA)
	Tetremethylethylenediamine (TEMED)	Bio-Rad Laboratories, USA
	β-mercaptoethanol	Merck, Schuchardt, Munchen
	Coomassie brilliant blue-R	Sigma (St. Louis, USA)
	Bromophenol blue	Sigma (St. Louis, USA)
	Glycerol	Merck, Wadeville, Gauteng
	Acetic acid glacial	Radchem (Pty)Ltd, SA
	Methanol	Radchem (Pty)Ltd, SA

Table 2.1 Methods, materials (reagents and products), and Manufacturers (continued).

Method	Materials	Manufacturer
SDS-PAGE	Molecular weight marker	Thermofischer Scientific (Waltham, USA)
	Acrylamide	Sigma (St. Louis, USA)
	Bis-acrylamide	Sigma (St. Louis, USA)
	Sodium dodecyl sulfate (SDS)	Sigma (St. Louis, USA)
	Tetremethylethylenediamine (TEMED)	Bio-Rad Laboratories, USA
	β-mercaptoethanol	Merck, Schuchardt, Munchen
	Tricine	Merk, Sigma-Aldrich (USA)
	Coomassie brilliant blue-R	Sigma (St. Louis, USA)
	Bromophenol blue	Sigma (St. Louis, USA)
	Glycerol	Merck, Wadeville, Gauteng
	Acetic acid glacial	Radchem (Pty)Ltd, SA
	Methanol	Minema Chemicals, South Africa.
Western Blot	Nitrocellulose 0.45 µM	Thermofischer Scientific (Waltham, USA)
	Fat-free milk powder	Spar (Pietermaritzburg, South Africa)
	Primary antibody:	Calbiochem owned by Merk KGaA, Darmstadt, Germany.
	Mouse anti-His tag	
	Secondary antibody:	Jackson ImmunoResearch Laboratories, INC Baltimore Pike, West Grove, PA 19390
	Goat-anti-mouse IgG+L peroxidase/HRP conjugate	Sigma (St. Louis, USA)
	Ponceau S	Aldrich (USA)
	Luminol ($C_8H_7N_3O_2$, 5-amino-2,3-dihydro-1,4 phthalazinedione)	Sigma (St. Louis, USA) Aldrich (USA)
	4-iodophenol	RADCHEM PTY LTD, South Africa.
	Hydrogen peroxide 30%	Minema Chemicals, South Africa.
	Methanol	
Talon Resin Affinity purification	Sodium phosphate	Merck, Germany
	Sodium Chloride	Sigma-Aldrich, USA
	Imidazole	Sigma-Aldrich, USA
	2-(N-morpholine)-ethane sulfonic acid (MES)	Sigma, St. Louis, USA
	Sodium Azide (NaN_3)	Sigma, St. Louis, USA
	Ethanol	Minema Chemicals, South Africa
	Talon Resin	Takara Bio, USA, Inc
Ascorbate oxidation assay	Ascorbic acid	Sigma (St. Louis, USA)
	Copper chloride dihydrate ($CuCl_2.2H_2O$)	Sigma (St. Louis, USA)
BCA copper-release assay	Bicinchoninic acid	Thermofischer Scientific (Waltham, USA)
	Ascorbic acid	Sigma (St. Louis, USA)
	Copper chloride dihydrate ($CuCl_2.2H_2O$)	Sigma (St. Louis, USA)
	Trichloroacetic acid	Sigma (St. Louis, USA)

Table 2.2 Composition of buffers and reagents prepared in the present study

Method	Buffer or Reagent	Composition
Agarose electrophoresis	1x Tris-acetate EDTA (TAE)	2 M Tris, 1 M glacial acetic acid, 50 mM, EDTA sodium salt, pH 8.
	Ethidium bromide	10 mg/mL ethidium bromide in 1x TAE.
	SeaKem® LE Agarose	10%w/v
	Pronasafe	1.5% (v/v).
Bacteriological culture methods	Luria-Bertani (LB)	1% (w/v) tryptone, 0.5% (w/v) yeast extract, 11 mM D-(+)-glucose, 0.5% (w/v) NaCl
	LB agar	LB with 1.5% (w/v) bacteriological agar
	Terrific broth (TB)	1.2% tryptone (w/v), 2.4% (w/v) yeast extract, 0.4% (w/v) glycerol, 17 mM KH_2PO_4, 72 mM K_2PO_4
	2xYT	1.6% (w/v) tryptone, 1% (w/v) yeast extract, 0.5% (w/v) NaCl.
	SOC media	2% (w/v) tryptone, 0.5% (w/v) yeast extract, 10 mM NaCl, 2.5 mM $MgCl_2$, 10mM $MgSO_4$, and 20 mM Glucose
	Ampicillin	100 µg/mL (*Pf*Grx1) / 75 µg/mL (*Pf*SAHH)
	IPTG	100 mM IPTG in dH2O, filter-sterilized (0.22 µM acetate filter)
Tris-Glycine SDS-PAGE	Monomer Solution	29.2% (m/v) acrylamide, 0.8% (m/v) bis-acrylamide
	Separating gel Buffer	1.5 M Tris-HCl, pH 8.8.
	Stacking gel Buffer	500 mM Tris-HCl, pH 6.8.
	SDS	10% (m/v) SDS.
	Initiator reagent	10% (m/v) ammonium persulfate.
	2x reducing treatment buffer.	125 mM Tris-HCl, 4% (m/v) SDS, 20% (v/v) glycerol, 10% (v/v) β-mercaptoethanol, pH 6.8.
	Tank buffer	250 mM Tris-HCl, 192 mM glycine, 0.1% (m/v) SDS, pH 8.3.
Tris-Tricine SDS-PAGE	Acrylamide-Bisacrylamide	49.5% (w/v) acrylamide, 3% w/v bis-acrylamide
	Gel Buffer (3x)	3 M Tris-HCL, 0.3% (m/v), pH 8.45
	Ammonium persulfate	10% (w/v) ammonium persulfate
	Anode buffer	0.1 M Tris-HCL, pH 8.9
	Cathode buffer	0.1 M Tris-HCL, 0.1 M Tricine, 0.1% (w/v) SDS, pH 8.25
	2x Reducing treatment buffer	125 mM Tris-HCl, 4% (m/v) SDS, 20% (v/v) glycerol, 10% (v/v) β-mercaptoethanol, pH 6.8.
	Stain stock solution	1% (m/v) Coomassie blue R-250
	Staining solution	0.125% (m/v) Coomassie blue R-250, 50% methanol, 10% (v/v) acetic acid.
	Destaining solution I	50% (v/v) methanol, 10% (v/v) acetic acid.
	Destaining solution II	5% (v/v) methanol, 7% (v/v) acetic acid.
Western blot	Transfer buffer.	50 mM Tris, 200 mM glycine, 20% (v/v) methanol, pH 8.3
	Tris-buffered saline (TBS)	20 mM Tris-HCl, pH 7.4, 200 mM NaCl.

	Ponceau S stain	0.2% (w/v) Ponceau S in 1% (v/v) acetic acid.
	Blocking solution	
	BSA-TBS, for antibody dilutions	5% (w/v) non-fat powdered milk in TBS. 0.5% (w/v) BSA in TBS.
	Chemiluminescent reagent	0.1 M Tris-HCl, 0.2 mg/mL luminol, 0.055 mg/mL p-iodophnol, 0.075% (v/v)
	4-Chloro-1-naphthol stock	0.03g in 10 mL Methanol, Substrate – 2 mL stock solution, 8 mL TBS, and 4 µL H_2O_2
Talon Resin Affinity purification	Phosphate/Saline solution	50 mM Sodium phosphate (NaH_2PO_4), 300 mM Sodium chloride (NaCl), pH 7.0
	Wash Buffer	50 mM Sodium phosphate, 300 Sodium chloride, 10 mM Imidazole, pH 7.0
	Elution Buffer	50 mM Sodium phosphate, 300 Sodium chloride, 500 mM Imidazole
	MES Buffer	20 mM MES, pH 5.0
	Storage Buffer	0.1% Sodium azide (NaN_3), 20 % ethanol
Bradford assay	Phosphate buffer saline (PBS)	137 mM NaCl, 2.7 mM KCl, 6.5 mM Na_2PO_4, 1.5 mM KH_2PO_4, pH 7.2
	Bovine serum albumin (BSA)	1 mg/mL BSA
E. coli copper tolerance assay	Copper (II) chloride	1 M $CuCl_2.H_2O$ in dH_2O, filter-sterilized (0.22 µM acetate filter).
Copper-catalyzed ascorbate oxidation assay (**NOTE:** Fresh ascorbic acid was prepared for each experiment)	Ascorbic acid / ascorbate solution	240 µM ascorbic acid, pH 4.5
	Copper (II) chloride	10 mM $CuCl_2.H_2O$ in dH_2O
BCA copper release assay (**NOTE:** Fresh ascorbic acid was prepared for each experiment)	Copper (II) Chloride	10 mM $CuCl_2.H_2O$ in dH_2O
	Ascorbic acid	100 mM, and 2 mM ascorbic acid solutions
	Trichloroacetic acid	30% (w/v) TCA.
	Bicinconinic acid	0.15mM Bicinchoninic acid, 0.9 M NaOH, 0.2 M HEPES

2.2 Equipment

This section provides the equipment and the source (companies). Equipment purchased from Bio-Rad (California, USA) are as follows: T100™ Thermal cycler, Basic Powerpac™, and Miniprotean®3 system with 1 mm spacer; Thermo Scientific NanoDrop™ 2000 was bought from Thermo Fisher Scientific (Massachusetts, USA); BG-subMINI horizontal electrophoresis from Baygenebiotech was obtained from China; Syngene G: Box system (UK). The centrifuge: Avanti™ X-22R was bought from Beckman colter (California, USA); Micro Tube Peristaltic pump MP-3 was purchased from EYELA Tokyo Rikakikai Co.Ltd. (Tokyo, Japan); Orbital shaking incubator from New Brunswick Scientific (New Jersey, USA); UV-1800 Shimadzu spectrophotometer from Shimadzu Corporation (Kyoto, Japan); Water bath from GFL (Burgwedel, Germany); Benchtop orbital shaker and Spectrafuge benchtop centrifuge from Labnet International Inc. (USA); Weigh balance was bought from Denver Instruments (USA); pH meter from HANNA instruments; Magnetic stirrers from Velp Scientifica (Europe).

2.3 Bioinformatics

This section describes bioinformatic methods used to characterize the two Plasmodial copper-binding proteins (Grx1 and SAHH).

2.3.1 Sequence identification and structural characterization.

An updated PlasmoDB (https://plasmodb.org/plasmo/app) was accessed on 8th September 2022 and searched for previously identified copper proteins (Choveaux *et al.,* 2012, 2015) as well as new ones. This was done by using GO terms such as CMC1, DMT1, CUTA, PIC2, and Glutaredoxin1. The present study focused on the *in-silico* analysis of *Pf*SAHH and the *Pf*Grx1 from the *Plasmodium falciparum* genome. The putative Grx1 and SAHH sequences from *P. falciparum, P. ovale, P. vivax, P. Knowlesi,* and *P. malariae* were analyzed. These amino acid sequences were aligned using ClustalW™, to identify characteristic features that may be conserved in multiple amino acid sequences from other parasites (Thompson *et al.,* 1994, 2003, Hung *et al.,* 2016). Multiple alignments of *Pf*Grx1(PF3D7_0306300) were conducted with Grx1 from other organisms (*A. thaliana* (Q8LFQ6), *S. cerevisiae* (P25373), *T. parva* (Q9BH70), *B. taurus* (P10575), *M. musculus* (Q9QUH0), and *H. sapiens* (P10575). *Pf*Grx1 was screened for acetylation (Zhao *et al.,* 2018, Yang *et al.,* 2019, Yu *et al.,* 2020) and ubiquitylation sites by using GPS-PAIL 2.0 (Deng *et al.,* 2016, Radivojac *et al.,* 2010, Cai *et al.,* 2016) (http://pail.biocuckoo.org/online.php) and UbiProber online servers (http://bioinfo.ncu.edu.cn/UbiProber.aspx). To compare the 3-dimensional structures of *Pf*Grx1 and *Hs*Grx1, both structures were obtained from Protein Data Bank (PDB) and superimposed and visualized using PyMOL (http://www.pymol.org/pymol), and the generated RMSD was used to interpret the results (Peersen *et al.,* 2019, Faure *et al.,* 2019). The copper binding motifs conserved in all sequences from the various organisms were identified using ClustalW™ and visualized through PyMOL (http://www.pymol.org/pymol). The potential presence of a transmembrane region in the *Pf*Grx1 amino acid sequence was determined by the TMHMM server (Kahsay *et al.,* 2005). It is important to predict these because membrane proteins are difficult to solubilize and purify (Kahsay *et al.,* 2005, Xu *et al.,* 2006). The characteristics of *Pf*Grx1 which include cellular and chromosome location, molecular weight, and biological and molecular functions were sourced from PlasmoDB and UniProt. Additionally, other servers like Expasy-ProtParam, and DTU-TMHMM were used to confirm the cellular location of the copper-binding proteins.

*Pf*SAHH multiple sequence alignment was performed using ClustalW™ with *A. thaliana* (Q23255), *S. cerevisiae* (P39954), *M. musculus* (P50247), and *H. sapiens* (P23526), *B. bovis* (A7AW30), *and T. annulata* (Q4UCR8). The amino acid sequences were analyzed to determine immunogenic peptides using the Predict7™ algorithm (Cármenes *et al.,* 1989) based on factors such as hydrophilicity, surface probability, flexibility, and antigenicity. The purpose of conducting this *in silico* experiment was to generate antibodies in chickens against *Pf*SAHH; however, it was not done (Hurdayal *et al.,* 2010, Chauhan *et al.,* 2005). Transmembrane regions

were screened for using the TMHMM prediction server, followed by the determination of domains, motifs, and features using the SMART program server (http://smart.embl.de/) (Letunic *et al.,* 2004, 2012). Similarities between the human and Plasmodial SAHH were established through PyMOL (http://www.pymol.org/pymol), and later sequence alignment of the SAHH amino acid sequence from *Plasmodium falciparum* and humans was performed by ClustalW™ (Yuan *et al.,* 2017, Bramucci *et al.,* 2012). Copper and NAD/H binding sites were predicted using **S**olvent accessibility-based **P**rotein-**P**rotein **I**nterface i**DE**ntification and **R**ecognition (SPPIDER) software (Porollo *et al.,* 2007). The integrity of the *Pf*SAHH structure obtained from PDB, was checked by utilizing VERIFY3D (Dym *et al.,* 2006, Eisenberg *et al.,* 1997, Adebiyi *et al.,* 2021). To establish the proteins that have been documented to interact with *Pf*grx1 and *Pf*SAHH, the STRING database was utilized (https://string-db.org/) (Mering *et al.,* 2003, Szklarczyk *et al.,* 2021)

2.4 Preparation of competent *Escherichia coli* (*E. coli*) host cells

The current study utilized a calcium chloride method in making the *E. coli* cells competent (Dagert and Ehrlich, 1979, Mandel and Higa, 1970, Sambrook *et al.,* 2006). *E. coli* JM109 and BL21 (DE3) cells were streaked on Luria Broth (LB) agar and incubated for 16 hours at 37°C. A single colony was selected from the bacterial culture and grown overnight in 5 mL LB media at 37°C with shaking at 200 revolutions per minute (RPM). The overnight culture was diluted into fresh LB media using a ratio of 1:100 and grown at 37°C with shaking until OD600 of 0.3-0.4 was achieved. The culture was transferred to pre-chilled centrifuge tubes and centrifuged at 2700 × g for 5 min at 4°C. The supernatant was then decanted, and the pellet was carefully resuspended in ice-cold autoclaved $CaCl_2$ (0.1 M) ($1/10^{th}$ of the starting culture volume). This was incubated on ice for 30 min. The cell suspension was centrifuged as before and the pellet was resuspended in ice-cold sterile $CaCl_2$, glycerol solution (0.01 M, 15% glycerol) ($1/50^{th}$ of the starting culture volume). The cells were then aliquoted in 200 µL volume using pre-chilled 1.5 mL microcentrifuge tubes and stored at -80°C until required.

2.5 Transformation of competent *E. coli* cells

Expression plasmid DNA of either *Pf*Grx1 or *Pf*SAHH was added to the aliquot of the prepared competent cells and mixed gently. The mixture was then incubated on ice for 30 min, followed by heat shock at 42°C for 60 sec (Chang *et al.,* 2017). The cells were put back on ice and incubated for 2 min. After this, Super Optimal broth with Catabolite repression (SOC) medium (800 µL) was added to the cells and incubated for 60 min with shaking at 200 RPM. The cells were later plated in duplicate on LB-agar plates containing ampicillin and incubated at 37°C overnight.

2.6 Isolation of Plasmids

DNA was isolated using the GeneJet Plasmid Miniprep Kit as per the manufacturer's instructions. The method is based on the principle of precipitating chromosomal and plasmid DNA that is found in the bacterial lysate.

2.6.1 Method

A single colony was picked from a freshly streaked plate and incubated in 5 mL of 2xYT media supplemented with 100 µg/mL (*Pf*Grx1) or 75 µg/mL (*Pf*SAHH) ampicillin at 37°C for 16 hours with shaking (200 RPM). Table 2.3 shows the strains of *E. coli* that were used in the present study. The bacterial culture (2 mL) was then centrifuged at 6800 × g for 2 min at room temperature. The supernatant was decanted to remove the remaining media. The pelleted cells were resuspended in 250 µL of resuspension buffer by vortexing until there were no more clumps. Lysis buffer (250 µL) was added, and the solution was mixed by inverting the tube 6 times till the solution turned viscous and slightly clear. Further, 350 µL neutralization solution was added to the tube and mixed immediately as before. The lysate was then centrifuged at 12000 × g for 5 min to pellet the cell debris and chromosomal DNA. The supernatant was transferred to the GeneJet spin column and centrifuged for 1 minute (Pronobis *et al.,* 2016). The flow-through was discarded and the column was placed back into the collection tube. Wash solution (500 µL) was added to the GeneJet spin column and centrifuged for 60 seconds, the flowthrough was discarded, and the step was repeated as described before. The spin column was centrifuged to remove residual ethanol from the plasmid preps. The GeneJet spin column was then transferred into a fresh 1.5 mL microcentrifuge tube, and 50 µL of elution buffer was added. This was incubated for 2 min at room temperature and centrifuged for 2 min at 12000 × g. The purified and isolated DNA was later stored at -20°C.

Table 2.3 Genotypes of *E. coli* host cells used for cloning and expression of recombinant Plasmodium falciparum copper-binding proteins.

***E. coli* Strain**	**Genotype**	**Function**
JM109	*F´ traD36 proA*B* lacI^q Δ(lacZ)M15/ Δ(lacproAB) glnV44 e14* gyrA96 recA1 relA1 ndA1 thi hsdR17(rK-mK*)*	Maintenance and propagation of recombinant plasmids for transformation into expression cells
BL21 (DE3)	*F^{-} ompT hsdS$_B$ (r_B^- m_B^-)gal dcm (DE3)*	Expression of recombinant pET100 TOPO/D containing the putative copper chaperone Grx1 and SAHH
BL21 (DE3) pLysS	*F$^-$ ompT hsdS$_B$ (r_B^- m_B^-) gal dcm (DE3) pLysS (CamR)*	Expression of recombinant pET100 TOPO/D vector containing *Pf*Grx1 and *Pf*SAHH

2.7 Restriction endonuclease digestion of plasmids

The plasmid DNA was isolated using the protocol outlined in section 2.7. The purified plasmid was digested using the following reagents: Nuclease free water (7 µL), 10 × Buffer EcoRI/BamHI (2 µL), Isolated plasmid DNA (*Pf*Grx1/*Pf*SAHH) (10 µL), EcoRI/BamHI (1 µL). The components were mixed in PCR tubes and incubated at 37°C for 1 hour. A volume of 5 µL was pipetted from the tube containing the

BamHI and later used as a sample for single digest (BamHI), the rest (15 µL) was incubated for 15 minutes at 65°C to deactivate the restriction enzyme. Then 2 µL of 500 mM Tris-HCL (pH 7.5) and 50 mM $MgCl_2$ (pH 7.5) were added plus 1 µL of EcoRI and incubated at 37°C for 2 hours. The single and double digests were confirmed using 1% (w/v) agarose gel electrophoresis (Lee *et al.,* 2012).

2.8 Agarose gel electrophoresis

A 1% agarose gel was used to monitor the restriction digests, and 0.3 g of agarose was weighed and dissolved in 30 ml of 1 × TAE buffer. The solution was then heated in a microwave until all the agarose dissolved completely and later allowed to cool. Ethidium bromide (10 mg/mL stock concentration) was added, and the gel was poured into a gel cassette and allowed to set. The samples were loaded into the wells together with the loading buffer (1:5). Electrophoresis was conducted at 70 V and the image was captured using Syngene G: Box system. The DNA bands were evaluated using a log of DNA standards [10, 000 bp, 8000, 6,000 bp, 4, 000 bp, 2, 000 bp, and 250 bp] (Thermofisher Scientific™ GeneRuler™ DNA ladders., 2018)

2.9 Expression plasmids utilized in the present study

The figures below show the expression vector that was used in the recombinant expression of the *Plasmodium falciparum* Glutaredoxin 1 (*Pf*Grx1) and *Plasmodium falciparum* S-adenosylhomocysteine hydrolase (*Pf*SAHH). Both expression plasmids were commercially synthesized by Thermofisher Scientific Company. The expression vector in Fig 2.1 A shows the total number of base pairs amounting to 6130. The insert that is located between the T7 promoter region, Xpress epitope, Enterokinase recognition site, and T7 transcription termination region has 366 bp. Furthermore, the constructs were referred to as *Pf*GLUD+thromb_cleav_pET100/D-TOPO (*Pf*Grx1).

The map in Fig 2.1 B indicates 7234 base pairs (bp) for the whole plasmid, out of which 1470 bp accounted for the insert. The name of the construct was PfADHC+thrombin_cleav_pET100D-TOPO (*Pf*SAHH). The host strain utilized for the expression was the *E. coli* BL21 (DE3) pLysS.

A. **B.**

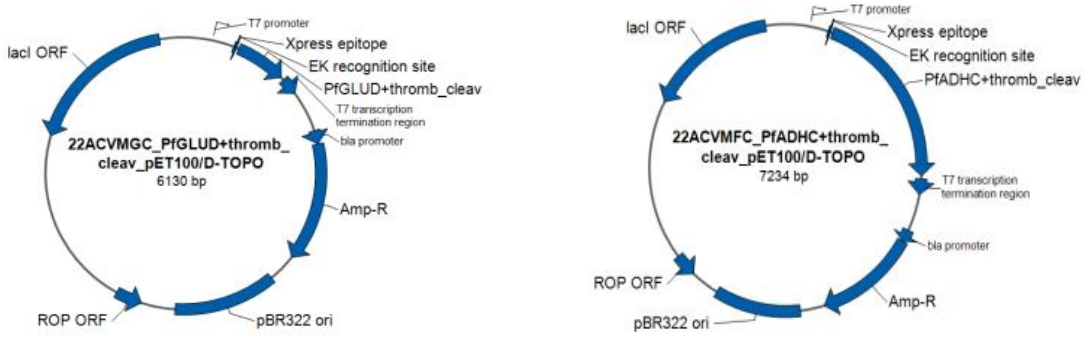

Fig 2.1 Map of the pET100/D-TOPO expression vectors. This plasmid map includes the ampicillin-resistant gene (Amp-R), thrombin cleavage site, and Enterokinase recognition sites. The inserts (*Pf*GLUD and *Pf*ADHC) were located between the EcoRI and BamHI not shown on the maps.

2.10 Polymerase chain reaction amplification of *Pf*Grx1 and *Pf*SAHH DNA

The polymerase chain reaction (PCR) was undetaken to amplify the *Pf*Grx1 and *Pf*SAHH genes. Universal primers were used to amplify both inserts. Table 2.4 shows summarized conditions used for the amplification of the genes (*Pf*Grx1 and *Pf*SAHH).

The type of the DNA polymerase that was utilized in this experiment was one Taq DNA polymerase enzyme. Additionally. parameters such as annealing temperature, and number of cycles were optimized together with other conditions summarized in Table 2.4. All the cycling conditions were determined using the NEB guidelines. Webtool oligocalc was used to establish the optimal annealing temperature. The initial denaturation temperature was set at 94°C for 3 minutes with 68°C as the extension temperature for the two amplifications that were performed in this current study (Fig 2.2). The PCR product was used to establish the presence of the inserts in the transformed *E. coli* BL 21 (DE3) cells after challenges in the expression stage for both proteins. The templates for both *Pf*SAHH and *Pf*Grx1 were isolated using the Thermo Scientific GeneJet Gel Extraction Kit as outlined in section 2.7.1. In the ideal situation, the products are mainly used as templates for secondary reactions to obtain more material. Table 2.5 shows the primers that were used in the experiment. The products were then resolved on a 1% (w/v) agarose gel and viewed under UV light.

Table 2.4 Components for the PCR amplification of *Pf*Grx1 and *Pf*SAHH DNA

Reaction Component	Concentration	Experiment (µL)	Control (µL)
5×Reaction Buffer	1×	5	5
2.5 mM dNTPs	0.2 mM	2	2
10 µM T7 promoter	0.2 µM	0.5	0.5
10 µM T7 terminator	0.2 µM	0.5	0.5
Template	256 ng	2	0
1 U/µl Taq Polymerase	0.5 U	0.5	0.5
Nuclease free water	-	14.5	16.5
Total Volume		**25**	**25**

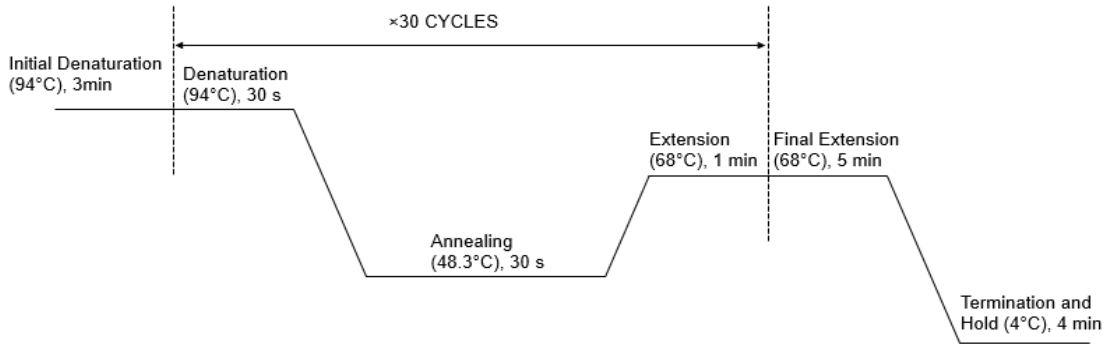

Fig 2.2 Shows PCR temperature conditions for the amplification of *Pf*Grx1 and *Pf*SAHH genes as established by NEB guidelines.

Table 2.5 Universal Primers used in the amplification of *Pf*Grx1 and *Pf*SAHH

Primer name	Sequence (5' ⟶ 3')	Melting Temperature (°C)
T7 Promoter	-TAA TAC GAC TCA CTA TAG GG-	48.3
T7 Terminator	-GCT AGT TAT TGC TCA GCG G-	53.8

2.11 Recombinant expression of *Pf*Grx1 and *Pf*SAHH

The following protocol details the procedure followed when expressing *Pf*Grx1 and *Pf*SAHH. Each plasmid was transformed in a particular *E. coli* bacterial cell line and colonies were selected for the expression of r*Pf*Grx1 and r*Pf*SAHH.

Glycerol stocks of *E. coli* BL 21 (DE3) or *E. coli* BL 21 (DE3) pLysS containing *Pf*Grx1 or *Pf*SAHH plasmids were streaked onto 2xYT agar plates containing 100 µg/mL/75 µg/mL of ampicillin and grown for 16 h at 37°C. A colony was selected and inoculated in 5 mL of bacterial medium supplemented with ampicillin at different concentrations for each plasmid (100 µg/mL (*Pf*Grx1) and 75 µg/mL (*Pf*SAHH)). It was incubated for 16 h with shaking (200 rpm) at 37°C. The overnight culture was

then diluted (1:100) in fresh media with ampicillin at the mentioned concentrations and grown at 37°C till an OD600nm of 0.5-0.6 (mid-log phase) was achieved. IPTG concentration of 0.2 mM and 1 mM was used to induce the expression of *Pf*Grx1 and *Pf*SAHH, respectively. The induced *E. coli* cultures were grown for 16 hours at 20°C. Ampicillin (100 µg/mL or 75 µg/mL) was added at the point of induction to allow *E. coli* cells to maintain the plasmid DNA. The bacteria harboring the plasmid with the resistant gene to ampicillin proliferates in the presence of antibiotics while those without the antibiotic resistance plasmid will die. This will enhance growth and efficient protein expression (Blommel *et al.,* 2007). Killing bacteria without the plasmid enhances the growth of the desired bacteria and, in turn, leads to increased protein expression (Makrides., 1996). The above conditions were selected after trying several conditions outlined in Table 2.6. After the induction period, the cells were harvested by centrifugation (4000 × g, 10 min).

Table 2.6 Variations to the culture conditions used for the recombinant expression of *Pf*Grx1 and *Pf*SAHH

Culture conditions	Medium	LB without Glucose
		LB with Glucose
		TB
		2xYT
	Temperature	20°C
		25°C
		30°C
		37°C
	OD_{600}	~0.6
		≥ 2.0

Note: The induction of *Pf*Grx1 expression was examined at all the temperatures, while *Pf*SAHH was only examined at 20ºC and 37ºC. The two recombinant proteins were induced for 16 hours.

2.12 Affinity purification of recombinant proteins

The bacteria pellets from section 2.12 were resuspended in 10% of the culture volume in wash buffer (50 mM sodium phosphate, 300 mM NaCl, 10 mM Imidazole, pH 7.0). The resuspended cells were divided into two, with one part receiving 10 mM dithiothreitol (DTT). The resuspended cells were sonicated on ice (6 cycles, 30 s/burst, and 30 s between bursts at the frequency of 25 kHz). The cell lysates were then centrifuged (14000 × g, at 4°C, 10 min). The supernatant was filtered through a 0.2 µM filter before adding to a 1 ml Talon resin. The clarified lysate in the column was incubated with resin for 1 hour (end-over-end in a cold room). The flow-through was collected and the resin was washed with three column volumes of wash buffer (50 mM sodium phosphate, 300 mM NaCl, 10 mM Imidazole, pH 7.0) until A_{280} readings were less than 0.02. *Pf*Grx1 and *Pf*SAHH were eluted with an elution buffer (50 mM sodium phosphate, 300 mM NaCl, 500 mM Imidazole, pH 7.0) in 500 µL fractions. The protein fractions were pooled and quantified using the Bradford method and stored at -20°C.

2.13 Bradford protein assay

BSA was used to construct a Bradford standard curve (Bradford., 1976; Goldring., 2015). A 1 mg/mL BSA stock was used to construct the standard curve by taking sample absorbance readings at 595 nm on a Shimadzu spectrophotometer. The quantification of the recombinant proteins was carried out by using the standard curve in Fig 2.3. Protein concentration was also determined using absorbance at 280nm.

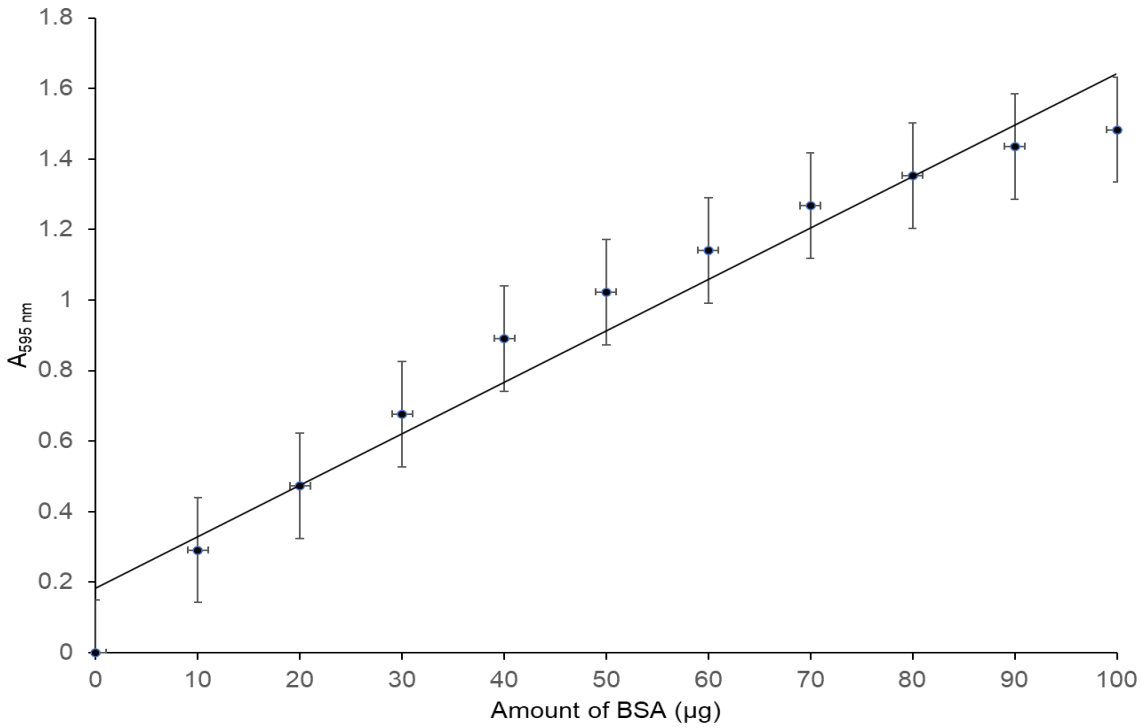

Fig 2.3 Bradford calibration curve. BSA was used in the range of 10 to 100 µg. All values are average values of triplicate readings.

2.14 Tris-Glycine Sodium dodecyl sulfate-polyacrylamide gel electrophoresis

After recombinant expression and purification of *Pf*SAHH, the samples were run on reducing SDS-PAGE according to Laemmli., 1970. A polyacrylamide gel measuring up to 1 mm thick comprising separating and stacking gels was prepared following the protocol outlined in Table 2.7. Samples were mixed in a 1:1 ratio with the reducing treatment buffer and loaded (5 µL) into the gel wells in a Bio-Rad Mini Protean II™ vertical slab electrophoresis apparatus. The running time of the electrophoresis was 1 hour using 20 mA per gel. Once the run was completed, the gel was either utilized in a western blot or stained overnight with Coomassie brilliant blue G250

Table 2.7 Recipe for SDS-PAGE gels

Reagent	Separating Gel (15%) (mL)	Stacking Gel (4%) (mL)
Monomer solution	7.5	0.94
Separating gel buffer	3.5	-
Stacking gel buffer	-	1.75
10% SDS	0.15	0.07
Distilled water	3.5	4.3
10% Ammonium persulfate	0.075	0.035
TEMED	0.0075	0.015

2.15 Tris-Tricine Sodium dodecyl sulfate-polyacrylamide gel electrophoresis

The Tris-Tricine sodium dodecyl sulfate-polyacrylamide gel electrophoresis (Schägger., 1987, 2006, Haider *et al.,* 2019) was used to analyze *Pf*Grx1. The separating and stacking gels were prepared as stated in Table 2.8. Samples that were prepared in a 1:1 ratio with reducing treatment buffer were loaded (5 µL) onto the gel wells. Electrophoresis was conducted at 30 V till the dye front crossed from the stacking to the separating gel. The voltage was then increased to 90 V and the experiment continued at this voltage till the dye front reached approximately 0.5 cm from the bottom. The gels were either stained with Brilliant Coomassie blue for visualization or used in the western blot. The stained gel was destained (Destain solution I and II) and images were obtained for analysis.

Table 2.8 Recipe for two Tricine-SDS polyacrylamide gels

Reagent	Separating (10%) (mL)	Stacking (4%) (mL)
Acrylamide-Bisacrylamide	3.0	0.5
Gel Buffer (Tris-HCL)	5.0	1.5
Glycerol	1.5g	-
Distilled water	6.0	3.95
Ammonium persulfate	0.075	0.045
TEMED	0.0075	0.0045

2.16 Western blot

The two recombinant proteins were detected by western blotting according to Towbin *et al.,* 1979, and Kurien *et al.,* 2006. After the SDS-PAGE electrophoresis, one gel was used in the western blot to transfer proteins to nitrocellulose (0.45 µM). The electro-transfer was conducted overnight in a blotting buffer at 40 mA. The success of the transfer was checked by staining the nitrocellulose with Ponceau S solution. The nitrocellulose membrane was washed using distilled water and three to four drops of NaOH. A thorough wash of the nitrocellulose with distilled water was ensured to remove any residual NaOH interfering with the blocking step. NaOH has been shown to affect milk (Law *et al.,* 2000, Sinaga *et al.,* 2017). Mouse anti-His

antibodies (primary antibody; 1:1000) and goat anti-mouse HRP conjugate (secondary antibody; 1:12000) were utilized to probe for *Pf*Grx1 and *Pf*SAHH. The proteins were detected using a chemiluminescent reagent with the recipe described in Table 2.9 (Thorpe *et al.,* 1985, Hool *et al.,* 1988, Kricka *et al.,* 1983, Yang *et al.,* 2015). The images were viewed on the Syngene G: Box system (Kulinska *et al.,* 2023). After using the first method (ECL), 4-chloro-1-napthol (Doe et al., 1988, Kobayashi *et al.,* 1989), was used to detect the protein bands of interest. The 4-chloro-1-naphthol stock was prepared by adding 0.03g in 10 mL methanol. During the staining procedure, 2 mL of the stock solution was mixed with 8 mL of TBS plus 4 µL of hydrogen peroxide. The staining takes about 10-30 minutes for the bands to show.

Table 2.9 Recipe for ECL

Reagent	Volume (µL)
Tris-HCL	10
Luminol	50
p-iodophenol (0.1 M)	25
H_2O_2	25

2.17 Copper binding studies

The recombinant proteins' ability to bind copper was determined by using the following approaches: (i) assessment of the effect of copper on the growth of *E. Coli* cells expressing the recombinant proteins (ii) inhibition of copper-catalyzed ascorbic acid oxidation assay and (ii) Bicinchoninic acid (BCA) copper release assay.

2.17.1 Effect of toxic copper on the growth of *E. coli* with or without the plasmid expressing the recombinant proteins

E. coli bacteria without or with a plasmid expressing the recombinant proteins were grown in 2xYT media at 20°C in the absence or presence of 8 mM copper. The *Pf*Grx1 and *Pf*SAHH expression were induced using 0.2 mM and 1 mM IPTG, respectively. The cultures for bacteria harboring plasmids were supplemented with ampicillin 100 µg/mL (*Pf*Grx1) and 75 µg/mL (*Pf*SAHH), respectively. Growth was monitored overnight (16 hours) by recording OD_{600} readings at the point of induction, and the end of the expression.

2.17.2 Inhibition of copper-catalyzed ascorbic acid oxidation assay

To determine whether the recombinant proteins could bind copper, r*Pf*Grx1 and r*Pf*SAHH expressed in the absence or presence of 0.5 mM copper and isolated without or with DTT (DTT protects thiols from oxidation) were subjected to the copper-catalyzed ascorbic acid oxidation assay (Jiang *et al.,* 2005). A 1 mL reaction was set up and conducted under room temperature comprising 120 µM ascorbic acid, 8 µM copper (II) chloride and 5 µM purified r*Pf*Grx1 or r*Pf*SAHH. The pH of

ascorbic acid was adjusted to 4.5 each time it was prepared, using acetic acid. All components were added to the reaction with ascorbic acid being added last to start the reaction. The absorbance at 255 nm was monitored for 300 sec at pH 4.5, in intervals of 5 seconds using a UV-1800 Shimadzu spectrophotometer. The experiment was repeated three times with the average readings being used to plot the graphs.

2.17.3 Bicinchoninic acid (BCA) copper release assay

To establish whether the two recombinant proteins bind copper (I) or copper (II), the BCA copper release assay was utilized as described by Brenner and Harris., 1995. The method involves the formation of a complex between the BCA and copper (I) (BCA-Cu (I) at alkaline pH and produces a purple color that is detected at a wavelength of 354 nm.

The r*Pf*Grx1 and r*Pf*SAHH expressed in the absence of copper and isolated without or with DTT were used in the *in-vitro* copper binding study. The purified protein samples were incubated with non-reduced or reduced copper (II) chloride by ascorbate (10 mM final concentration) equivalent to a 20-fold molar excess (1:20). Ascorbic acid creates a redox reaction in which it is oxidized, and the copper ions are reduced to Cu (I).The mixture was vortexed and incubated at room temperature for 15 min with agitation in intervals of 5 minutes. The protein sample was then passed through a 10 mL Sephadex-G10 spin column at 1000 × g for 2 mins to remove unbound copper that could interfere with the results. After removing excess copper, 750 µL of the sample was added to 250 µL trichloroacetic acid (TCA) and centrifuged at 12000 × g for 2 min after vortexing to pellet the denatured proteins. The supernatant (250 µL) was aliquoted in four microfuge tubes, after which 200 µL buffered BCA reagent was added to each of the four tubes. Since the experiment was conducted in duplicates, 50 µL of 2 mM ascorbic acid was added to two of the 4 tubes, and distilled water was added to the other two tubes. The samples were vortexed and incubated for two minutes at room temperature and absorbance readings were recorded at 354 nm. When a protein binds copper (I), the purple color change was observed without adding ascorbate, while the binding of copper (II) required the addition of ascorbic acid that reduced copper (II) to copper (I) to allow BCA to form a complex with the metal ion. The concentration of recombinant proteins was adjusted to 10 µM and applied throughout the experiments for consistency. The readings were recorded, and the student t-test was used to establish the statistical significance of the protein's ability to bind copper (I) or (II).

The *in-vivo* experiment utilized r*Pf*Grx1 and r*Pf*SAHH expressed in the presence of 0.5 mM of copper and isolated without and with DTT. The cells were harvested and washed two times with PBS equal to 50% of the culture volume. After purification, the protein was used at 10 µM in an experiment carried out as the one described *in-vitro* copper binding. Further, the *Pf*Grx1 and *Pf*SAHH that bound copper *in-vivo* previously and isolated with or without DTT were incubated with copper, and steps of the BCA copper release assay protocol were followed as outlined above in this section (2.18.3).

2.18 Protein-protein interaction and molecular docking

The interaction of *Pf*Grx1 with *Pf*SAHH and other Copper-binding proteins was determined using ClusPro version 2.0. (https://doi.org/10.1016/j.str.2020.06.006). ClusPro is a web-based server (https://cluspro.org) that is used in the direct docking of two proteins that can potentially interact at physiological conditions. The program uses Protein Data Bank (PDB) format files of proteins. ClusPro has over the years expanded and improved since its introduction, adding advanced features like the application of attraction or repulsion forces, construction of homo-multimers, and removal of unstructured protein (Kozakov *et al.,* 2017). The program can account for pairwise distance constraints, and small-angle X-ray scattering (SAXS) is considered including locating hairpin-binding sites (Kosakov *et al.,* 2017). There are mainly three main steps involved in the docking process: (i) rigid-body docking by sampling billions of conformations (Kozakov *et al.,* 2006) (ii) root-mean-square deviation (RMSD)- based clustering of 1000 lowest-energy generated structures (iii) refinement of the selected structures utilizing energy minimization. Ten models having centers with highly populated clusters of low energy docked structures are generated (Kozakov *et al.,* 2005). The runs are completed in approximately 4 hours. This method has demonstrated the first 30 largest generated clusters have near-native structures for 92% of the protein-to-protein complexes (Comeau *et al.,* 2004, Chen *et al.,* 2003, Bohnuud *et al.,* 2017). The ranking of models based on cluster size has proved to provide reliable and the best near-to-native complexes (Kosakov *et al.,* 2013). The complex was annotated in PyMOL and then analyzed in PDBsum (http://www.ebi.ac.uk/pdbsum).

Molecular docking studies were done using the MIB2 modeling server which is an updated version of MIB (Lin *et al.,* 2016, Lu *et al.,* 2022). These servers use the fragment transformation as documented by Lu *et al.,* 2006, which deals with the comparison of structures between the query protein and the MIB templates. MIB and MIB2 (http://combio.life.nctu.edu.tw/MIB2/) can dock a total number of 18 metal ions namely, Ca^{2+}, Cu^{2+}, Fe^{3+}, Mg^{2+}, Mn^{2+}, Zn^{2+}, Cd^{2+}, Fe^{2+}, Ni^{2+}, Hg^{2+}, Co^{2+}, Cu^{+}, Au^{+}, Ba^{2+}, Pb^{2+}, Pt^{2+}, Sm^{3+}, and Sr^{2+}. The source of the MIB templates is the Protein Data Bank (PDB) of structures and metal ion complexes (Lu *et al.,* 2022). The modeling makes use of protein sequences for those proteins without 3D structures by use of the PS^2 modeling method (Chen *et al.,* 2009, Lu *et al.,* 2012). There are also instances when the method uses AlphaFold structure databases (Veradi *et al.,* 2022).

Chapter 3

The Plasmodium spp. Putative Glutaredoxin 1: Bioinformatic studies, recombinant protein expression, and copper binding studies with *Plasmodium falciparum* Glutaredoxin 1 (*Pf*Grx1)

3.1 Introduction

The mapping of the *Plasmodium* genome has aided a thorough study of the parasite's proteome. This aspect has an impact on many important facets of malaria elimination, as the plasmodial mitochondrial proteome is one of the key drug targets (Antoine, 2012, Vaidya and Mather, 2009). In this important area are proteins involved in the parasite's survival, such as those in the electron transport chain. The functionality of the electron transport chain depends on the presence of copper which is supposed to be acquired and distributed by copper-dependent proteins. However, many of these proteins are yet to be characterized. Unlike *Pf*Grx1 which has not been yet characterized, *Hs*Grx1 metallochaperone has shown the potential to deliver copper to ATP7B through Atox1-independent mechanisms (Maghool *et al.,* 2020). The current section identifies the putative *Pf*Grx1 using *in-silico* analysis.

3.2 Results

3.2.1 The identification of copper-binding proteins in the *Plasmodium falciparum* database (Plasmodb)

Copper homeostasis is critical to the survival of the malaria parasite. The proteins involved in the uptake, distribution, and secretion of copper from the parasite have not been well studied. Twelve (12) copper-binding orthologs were identified by Choveaux *et al.,* 2012, and seven of these have been characterized. Table 3.1 shows the various copper-binding proteins that have been identified and characterized utilizing a BLASTp search of the PlasmoDB genome database using the *Theileria parva* polymorphic immunodominant molecule (PIM) sequence as first described by Toye *et al.,* 1996 (Toye *et al.,* 1996, Choveaux *et al.,* 2012).

Table 3.1 Copper-dependent protein orthologs identified in the *P. falciparum* proteome.

Protein[a]	Accession number	Protein characterization	PlasmoDB protein identifier	Reference
S-adenosyl-L-homocysteine hydrolase	P23526	No	PF3D7_0520900	Tanaka *et al.,* 2004
Copper transport protein (Ctr1)	L41833	Yes	PF3D7_1421900, PF3D7_1439000	Choveaux *et al.,* 2012
Ctr2	-	No	PF3D7_1421900	
Sco1	O75880	Yes	PF3D7_0708900	Choveaux et al., 2012
*Pf*CuP-ATPase		Yes	PF3D7_0904900	Rasoloson *et al.,*2004
Cox11		Yes	PF3D7_1475300	Choveaux *et al.,* 2012
Cox14		Yes	PF3D7_0825600	Watson *et al.,* 2020

Cox15	NP_510870	Yes	PF3D7_1435000	Gardner *et al.,* 2002
Cox17	Q81JE6	Yes	PF3D7_1025600	Choveaux *et al.,* 2012
Cox19	AAY35062	Yes	PF3D7_1201800	Salman *et al.,* 2023
Cytochrome-c oxidase subunit I	ACR77861	No	mal_mito_2	Gardner *et al.,* 2002
Cytochrome-c oxidase subunit II	ABU47824	No	PF3D7_1430900 PF3D7_1361700	Gardner *et al.,* 2002
Cytochrome-c oxidase subunit III	ABJ99455	No	mal_mito_1	Gardner *et al.,* 2002
Cytochrome-c oxidase subunit Vb	AAA52060	No	PF3D7_0927800	Gardner *et al.,* 2002
Cytochrome-c oxidase subunit VIb	AAP35591	No	PF3D7_0928000.1 PF3D7_0928000.2	Gardner *et al.,* 2002
Cg3	O75880	No	PF07_0034	Choveaux *et al.,* 2012
Mitochondrial phosphate carrier Protein 2 (Pic2)[b]		No	PF3D7_1202200	Bhaduri-McIntosh S and. Vaidya A.B., 1996
Glutaredoxin 1		No	PF3D7_0306300	Rahlfs *et al., 2001*
Protein CutA, putative		No	PF3D7_1249500	Gardner et al., 2002
Divalent metal transporter 1 (DMT1), putative		No	PF3D7_0715800	Loveridge *et al.,* 2024
COX assembly mitochondrial protein putative (CMC1)		Yes	PF3D7_0729600	Gardner *et al.,* 2002
Cytochrome c oxidase assembly factor 5, putative (COA5)		No	PF3D7_0825600	Hall *et al.,* 2002

a. *Pf*3D7 strain.

b. Commonly known as 'Phosphate Carrier protein' which carries copper in organisms unstudied in *Plasmodium falciparum*.

3.2.2 Identification of *Plasmodium falciparum* glutaredoxin 1 (*Pf*Grx1) in PlasmoDB

The *Pf*Grx1 amino acid sequence was identified in the Plasmodb database and was aligned with the amino acid sequence of Grx1 from six organisms (Fig 3.1, A). The sequence alignments are utilized to identify potential copper-binding motifs

and deduce common lineage. A conserved copper-binding CPYC (CXXC) motif was found in the amino acid sequences of all six organisms. Two of the amino acid sequences, *T. parva* and *A. thaliana* are longer than the rest (i.e. with an average length of 108 amino acids) of the sequences in the alignment each having 151 and 135 amino acid residues respectively. The two organisms have 45 and 25 extra amino acid residues at the N-terminal respectively, while *A. thaliana* possesses 4 extras at the C-terminal. The rest of the organisms have between 106 and 111 amino acids in their Grx1 amino acid sequences. Compared to the *S. cerevisiae* amino acid sequence, 4 amino acid sequences have one deletion, while the other 2 have 3 and 4 deletions, all located 12 to 19 amino acids from the CPYC motif and in the C-terminal region.

3.2.3 Sequence analyses of Human *Plasmodium* spp

In Fig 3.1, B, all five *Plasmodium* species that infect humans have a conserved copper binding CPYC (CXXC) motif and the serine (S) residue situated at amino acid residue 46, which is present in the *Plasmodium falciparum* sequence and absent (represented by a dash) from the remaining four species. Serine residues are often phosphorylated which could alter the activity of the protein or in the cell (Cox *et al.,* 1992). However, the serine (S) is conserved among the 19 *Plasmodium falciparum* isolates that have been sequenced up to date (Fig 3.2). The CYPC motif is positioned within a ten amino acid conserved motif. Fig 3.1, B shows an average of 46.46% amino acid identity among the aligned *Plasmodium* species.

A.

```
A.thaliana        ------MTMFRSISMVML---------LVALVTF-----ISMVSSAASSPEADFVKKTIS   40
S.cerevisiae      ---------------------------------------------MVSQETIKHVKDLIA   15
T.parva           MSSVKYLVLFTLVCVVSLFQPSQCRLDYHFFSDFLSKYSFTLPFKMAEKTPKDWVDSLVK   60
P.falciparum      ----------------------------------------MAGTSEAVKKWVNKIIE   17
B.taurus          -------------------------------------------------MAQAFVNSKIQ   11
M.musculus        -------------------------------------------------MAQEFVNCKIQ   11
H.sapiens         -------------------------------------------------MAQEFVNCKIQ   11
                                                                      *.  :

A.thaliana        SHKIVIFSKSYCPYCKKAKSVFRELDQVP----YVVELDEREDGWSIQTALGEIVGRRTV   96
S.cerevisiae      ENEIFVASKTYCPYCHAALNTLFEKLKVPRSKVLVLQLNDMKEGADIQAALYEINGQRTV   75
T.parva           KHKVVVFSKSYCPYCTRAKDALKKLN-LH--DLHVEELDSNPNMDQVQDYLNQLTGARSV  117
P.falciparum      ENIIAVFAKTECPYCIKAISILKGYN-LNSH-MHVENIEKNPDMANIQAYLKELTGKSSV   75
B.taurus          PGKVVVFIKPTCPYCRKTQELLSQLP-FKQGLLEFVDITAAGNISEIQDYLQQLTGARTV   70
M.musculus        SGKVVVFIKPTCPYCRKTQEILSQLP-FKQGLLEFVDITATNNTSAIQDYLQQLTGARTV   70
H.sapiens         PGKVVVFIKPTCPYCRRAQEILSQLP-IKQGLLEFVDITATNHTNEIQDYLQQLTGARTV   70
                     : :  *  ****  : . :    .     . ::    .   :*  * :: *  :*

A.thaliana        PQVFINGKHLGGSDDTVDAYESGELAKLLGVSGNKEAEL          135
S.cerevisiae      PNIYINGKHIGGNDDLQELRETGELEELLEPILAN----          110
T.parva           PRVFVNGRFYGDSTKTVSDVESGKFMEHYKKTDL-----          151
P.falciparum      PRIFINKDVVGGCDDLVKENDEGKLKERLQKLGLVN---          111
B.taurus          PRVFIGQECIGGCTDLVNMHERGELLTRLKQMGALQ---          106
M.musculus        PRVFIGKDCIGGCSDLISMQQTGELMTRLKQIGALQL--          107
H.sapiens         PRVFIGKDCIGGCSDLVSLQQSGELLTRLKQIGALQ---          106
                  *.::::.    *.  .  .  : *::
```

B.

```
P.vivax           MACNNEAIKKFVQKIIDENIIAVFSKTECPYCIKAISILKGYNVS-NMHVEQIEKNPNMA   59
P.falciparum      MAGTSEAVKKWVNKIIEENIIAVFAKTECPYCIKAISILKGYNLN-HMHVENIEKNPDMA   60
P.knowlesi        MACNNEGVKKFVQKIIDENVIAVFAKTECPYCIKAISILKGYNVA-NMHVEQIEKNPNMA   59
P.malariae        MGCNNEAVKKFVQKIIDDNIIAVFSKTECPYCIKAITILKGYNPN-SMHVEQIEKNPNMA   59
P.ovale           MTCNNEAIKKFVQKIIDDNVIAVFSKSECPYCIKAISILKGFNPN-NMHVEQIEKNPNMA   59
                  *  ..*.:**:*:***::*:****:*:*********:****:*    ****:*****:**

P.vivax           DIQAYLKDLTGEGERRGKAPRAPEETGPPQLNRR--------KGKNLG---           99
P.falciparum      NIQAYLKELTGKSSVPRIFINKDVVGGCDDLVKENDEGKLKERLQKLGLVN           111
P.knowlesi        DIQAYLKELTGKSSVPRIFINKEVVGGCDDLVKEKEEGKLQERLKKLGILS           110
P.malariae        DIQAYLKDLTGKSSVPRIFINKEFVGGCDDLVKENEEGKLQERLKKVGILS           110
P.ovale           DIQAYLKELTGKSSVPRIFINKEIVGGCDDLVKENEEGKLQERLKKVNVLS           110
                  :******:***:..      .     *  :* :.        : ::::.
```

Fig 3.1 Amino acid sequence alignments of *Plasmodium falciparum* glutaredoxin 1 (*Pf*Grx1) with the Grx1 orthologs present in different species. A. *Pf*Grx1 sequence was aligned with Grx1 from *A. thaliana* (Q8LFQ6), *S. cerevisiae* (P25373), *T. parva* (Q9BH70), *B. taurus* (P10575), *M. musculus* (Q9QUH0), and *H. sapiens* (P10575). **B.** Sequence alignments of Plasmodium spp that infect humans [*P. vivax* (PVP01_0833900.1), *P. falciparum* (PF3D7_0306300), *P. knowlesi* (PKNH_0836400.1), *P. malariae* (PmUG01_08049900.1), *P. ovale* (POWCR01_080040200_t1)]. The boxes in **(A)** and **(B)** indicate a conserved copper binding CPYC (CXXC) motif. The amino acid residues in yellow show acetylation sites, while that in blue indicate a serine residue. Conserved residues are indicated by *****, while **:** represents a conserved and **.** indicates a semi-conserved amino acid substitution. The alignment was performed using ClustalW (Thompson *et al.,* 2003)

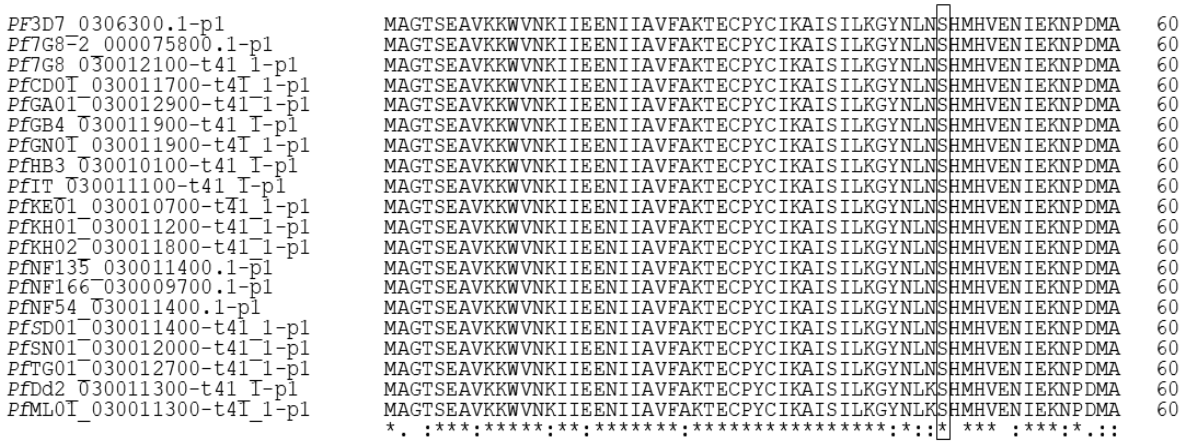

Fig 3.2 Alignments of amino acid sequence of Grx1 from 19 *Plasmodium falciparum* isolates identified in PlasmoDB. The first 60 amino acid residues of the Grx1 sequence from 19 *Plasmodium falciparum* isolates were aligned. The box indicates conserved serine (S) residue among the *Plasmodium falciparum* isolates. Conserved residues are indicated by *****, while **:** represents a conserved and **.** indicates a semi-conserved amino acid substitution. ClustalW (Thompson *et al.,* 2003) was used to perform the multiple alignment.

3.2.4 Determination of the acetylation, and ubiquitination sites among the five *Plasmodium* spp, yeast, and mammalian Grx1 sequences

Each of the *Plasmodium* Grx1 sequences in Fig 3.1, B was submitted to the GPS-PAIL online saver to predict potential acetylation sites (Deng *et al.,* 2016). Using the highest threshold, *Plasmodium falciparum* had three acetylation sites while the rest of the sequences had one each. However, no acetylation sites were predicted in mammalian, plant, or yeast sequences Fig 3.1, A. Acetylation plays a role in gene expression, for example histone acetylation relaxes the chromatin structure thereby making it easier for transcription factors and RNA polymerase to access the DNA. The lysine acyltransferase sites were specific to histone acetyltransferase p300 (EP 300) and cAMP-response element binding protein (CREBBP). KAT2B lysine acetyltransferase site was predicted in the *Plasmodium falciparum* Grx1 sequence. The EP300 acetylation sites in *Plasmodium* spp are situated at the N-terminal of the sequences, while the CREBBP acetylation sites were predicted within the C-terminal region (Fig 3.1 B). *Plasmodium falciparum* has two EP 300 sites positioned at 9 and 10 respectively, in the sequence. Using the UbiProber server, no ubiquitination site was predicted in all five *Plasmodium* species (Chen *et al.,* 2013). Ubiquitination is an important post-translational modification (PTM) that plays a role in controlling substrate degradation and mediates the quality and quantity of various proteins (Pickart *et al.,* 2001).

3.2.5 An evaluation of sequence alignments of *Plasmodium* spp that infect humans, mice, birds, and monkeys

The amino acid sequences of Grx1 belonging to *Plasmodium* spp which infects humans, mice, birds, and monkeys were identified in Plasmodb. In Fig 3.3, a conserved CPYC (CXXC) motif is shown. The serine (S) residue is present in *Plasmodium falciparum* but absent in the 11 species. Serine may play a role in the alteration of the enzyme functions especially if the protein is phosphorylated. This

deletion is positioned after 13 amino acid residues upstream of the CXXC motif. There is an average of 34.05% sequence identity among the amino acid sequences.

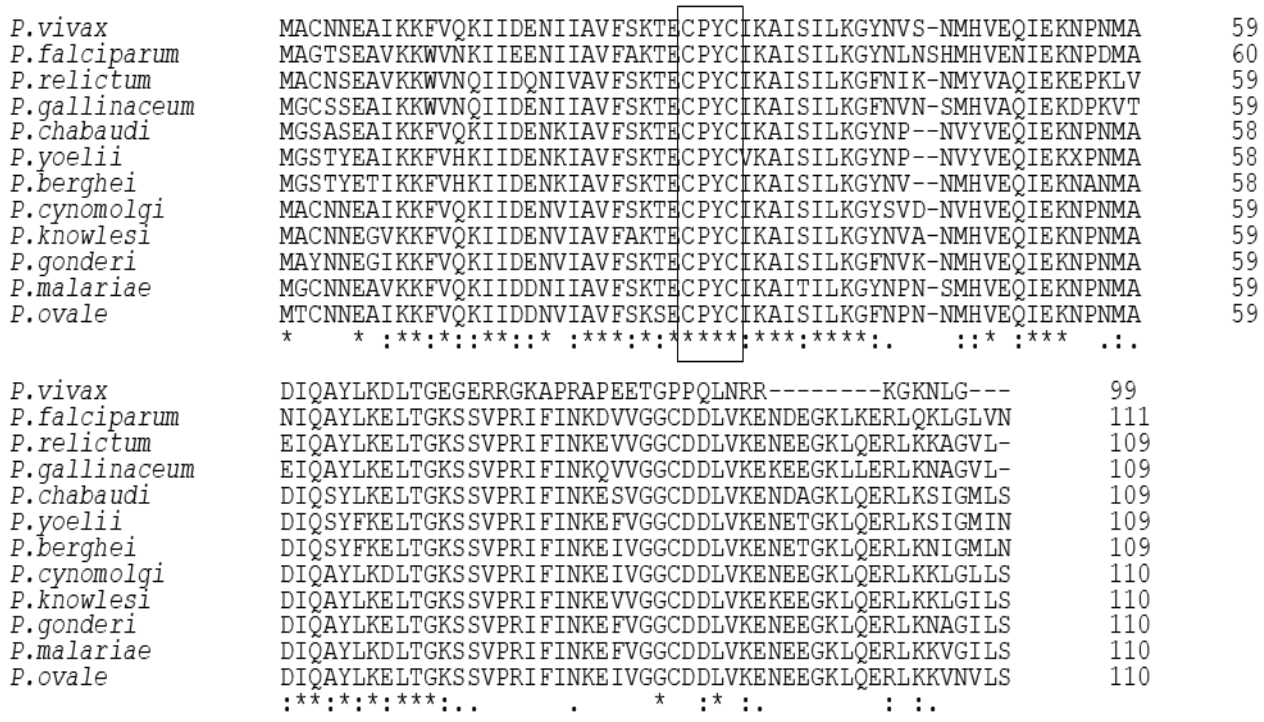

Fig 3.3 Alignments of amino acid sequence of Grx1 from 12 *Plasmodium* spp selected from PlasmoDB. The amino acid sequences of Grx1 from 12 *Plasmodium* spp that infect humans, mice, birds, and monkeys were aligned using the ClustalW (Thompson *et al.,* 2003). The box indicates a conserved copper binding CPYC (CXXC) motif. Conserved iesidues are indicated by *****, while **:** represents a conserved and **.** indicates a semi-conserved amino acid substitution.

3.2.6 Comparison between the crystal *Pf*Grx1 and NMR *Hs*Grx1 structures using a layover method in PyMOL

The *Pf*Grx1 (Fig 3.4, A) and *Hs*Grx1 (Fig 3.4, B) crystal structures were selected from the UniProt database (Manickam *et al.,* 2014, Sun *et al.,* 1998) and visualized using PyMOL (http://www.pymol.org/pymol). Fig 3.4, C indicates an overlay of *Pf*Grx and *Hs*Grx1 structures with an RMSD (0.684) less than 2Å. The generated complex showed that *Pf*Grx1 is not significantly different from *Hs*Grx1 and, thus, may potentially have similar functions. However, when sequence alignment of the two amino acid sequences (*Pf*Grx1 and *Hs*Grx1) was performed, six deletions were observed in the human sequence.

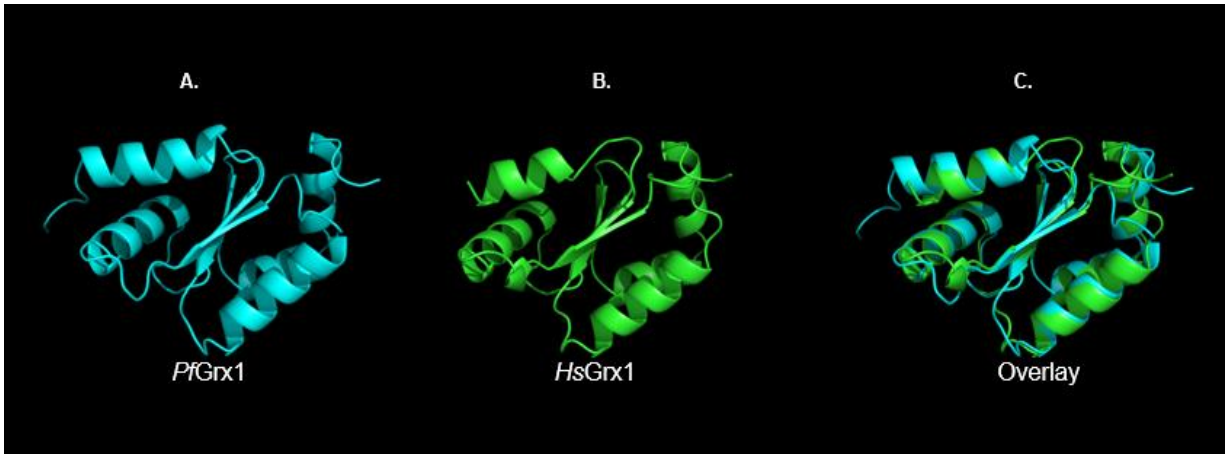

Fig 3.4 Crystal structure of *Pf*Grx1 and NMR *Hs*Grx1 structure. A. *Pf*Grx1 (4MZB) ***B.*** *Hs*Grx1 (1JHB), all obtained from the Protein Data Bank (PDB) (https://pdb101.rcsb.org/) **C.** The structures in **(A)** and **(B)** were superimposed using PyMOL software (http://www.pymol.org/pymol).

3.2.7 Position of the copper binding motif (CXXC) on the *Pf*Grx1 and *Hs*Grx1 structures

When the *Pf*Grx1 (crystal) and *Hs*Grx1 (NMR) structures were visualized using PyMOL, copper binding sites were identified and annotated. Fig 3.5 A shows the position of the CPYC (CXXC) copper-binding motif which comprises Cysteine, Proline, Tyrosine, and Cysteine that are positioned at 29, 30, 31, and 32 in the *Pf*Grx1 sequence (Rahlfs *et al.,* 2001). In Fig 3.5 B, the copper-binding motif in *hs*Grx1 spans from amino acid 23 to 26 having Cys, Pro, Tyr, and Cys. According to Maghool *et al.,* 2021, the *Hs*Grx1 CXXC motif binds copper (I) and may potentially be involved in the transportation of copper to the metal-binding domains of the ATPase.

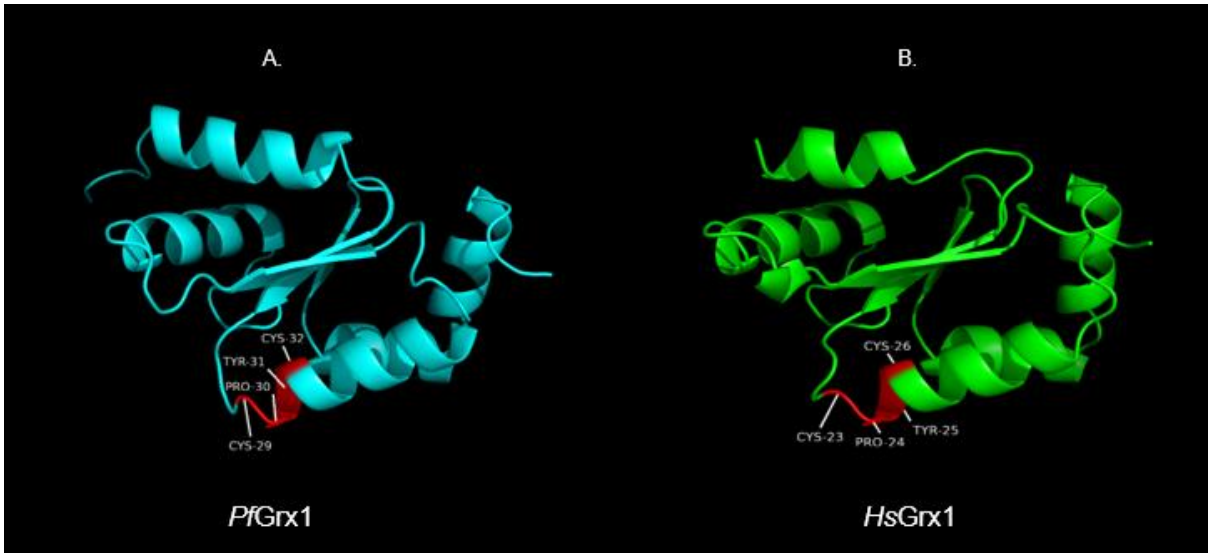

Fig 3.5. Structures of *Pf*Grx1 and *Hs*Grx1 showing copper-binding motifs. A. *Pf*Grx1 (4MZB) and **B.** *Hs*Grx1 (1JHB) show the location (red) of the conserved CPYC (CXXC). The structures (PDB) (https://pdb101.rcsb.org/) were processed and annotated using PyMOL software (http://www.pymol.org/pymol).

3.2.8 Prediction of *Pf*Grx1 transmembrane spanning regions

A prediction using DTU-TMHMM server v 2.0 was performed to determine whether the *Pf*Grx1 has any transmembrane regions. Data indicates that the protein is in the cytosol with a probability of occurrence being above 1 (Data not shown). This implies that *Pf*Grx1 has no regions situated in the membranes. Similar results are seen when PlasmoDB and UniProt are searched (https://plasmodb.org/plasmo/app, http://www.uniprot.org/).

3.2.9 Bioinformatic tools utilized in the structural identification of *Pf*Grx1

Bioinformatic tools outlined in Table 3.2 were used to evaluate the structure of *Pf*Grx1 and its characteristics. The predicted molecular weight was 12.4 kDa with an isoelectric point of 7.68. The grand average of hydropathicity has a positive value, indicating that the protein is hydrophobic. There seems to be a slight difference in the extinction coefficient between the structure that has all cysteines reduced (0.803) and that which does not have cysteines in a reduced state (0.813). The extinction coefficient of a protein enables the determination of the concentration of the pure protein. Of the amino acid residues making up this protein, 3 (2.7%) are cysteines that are positioned at numbers 29, 32, and 88. Out of these, cystines at positions 29 and 32 are involved in the CXXC motif that is important for metal binding (Stephanie *et al.,* 2021).

Table 3.2. Summary of the structural features of the putative *Pf*Grx1.

Structural features	Data	BIOINFORMATIC TOOL
Molecular weight	12.4 kDa	Expasy-ProtParam
Theoretical isoelectric point	7.68	Expasy-ProtParam
Grand average hydropathicity	50.83	Expasy-ProtParam
Number of cysteines	3	Expasy-ProtParam
Extinction coefficient when all cysteines are reduced	0.803	Expasy-ProtParam
Number of transmembrane domains	0	DTU-TMHMM
Copper-binding motifs	CXXC	Clustal Omega
Biological function	- Amino-acid transport - Ion transport - Protein transport	UniProt
Molecular function	- Antioxidant activity - Glutathione-disulphide oxidoreductase activity - Protein-disulphide reductase (glutathione) activity	UniProt, PlasmoDB
Cellular location	Cytoplasm	PlasmoDB
Chromosome location	*Plasmodium falciparum* chromosome 03	PlasmoDB

3.2.10 Cloning and expression of recombinant *Plasmodium falciparum* Glutaredoxin 1

3.3.1 The coding sequence of *Pf*Grx1

In Fig 3.6 A, the region with codons for the whole insert including those for the protein with a copper-binding motif (CXXC) is shown in yellow. The first underlined bases in red (Fig 3.6, a) show the T7 promoter region where the primers bind during the amplification process. The second underlined group of bases (Fig 3.6, b) indicates the T7 reverse region. The highlighted region has incorporated two restriction sites which are EcoRI, and BamHI respectively, all with bases shown in red on the diagram. Fig B shows the start and stop codon including the CAT repeat that codes for histidine amino acid residue.

A.

1 CAAGGAGATG GCGCCCAACA GTCCCCCGGC CACGGGGCCT GCCACCATAC CCACGCCGAA
61 ACAAGCGCTC ATGAGCCCGA AGTGGCGAGC CCGATCTTCC CCATCGGTGA TGTCGGCGAT
121 ATAGGCGCCA GCAACCGCAC CTGTGGCGCC GGTGATGCCG GCCACGATGC GTCCGGCGTA
181 GAGGATCGAG ATCTCGATCC CGCGAAATTA ATACGACTCA CTATAGGGGA ATTGTGAGCG
241 GATAACAATT CCCCTCTAGA AATAATTTTG TTTAACTTTA AGAAGGAGAT ATACATATGC
301 GGGGTTCTCA TCATCATCAT CATCATGGTA TGGCTAGCAT GACTGGTGGA CAGCAAATGG
361 GTCGGGATCT GTACGACGAT GACGATAAGG ATCATCCCTT CACCGGATCC CTGGTTCCGC
421 GTGGTAGCAT GGCAGGCACC AGCGAAGCAG TTAAAAAGTG GGTGAATAAA ATCATCGAAG
481 AAAACATTAT CGCCGTGTTT GCCAAAACCG AATGTCCGTA TTGTATTAAA GCCATCAGCA
541 TCCTGAAAGG CTATAATCTG AATAGCCATA TGCACGTGGA AAACATTGAG AAAAATCCGG
601 ATATGGCAAA CATTCAGGCC TATCTGAAAG AACTGACCGG TAAAAGCAGC GTTCCGCGTA
661 TCTTTATCAA CAAAGATGTT GTTGGTGGCT GTGATGATCT GGTGAAAGAA AATGATGAAG
721 GCAAACTGAA AGAGCGCCTG CAGAAACTGG GTTTAGTGAA TTAAGAATTC AAGGGCGAGC
781 TCAACGATCC GGCTGCTAAC AAAGCCCGAA AGGAAGCTGA GTTGGCTGCT GCCACCGCTG
841 AGCAATAACT AGCATAACCC CTTGGGGCCT CTAAACGGGT CTTGAGGAGT TTTTTGCTGA

a

b

B.

1 CAAGGAGATG GCGCCCAACA GTCCCCCGGC CACGGGGCCT GCCACCATAC CCACGCCGAA
61 ACAAGCGCTC ATGAGCCCGA AGTGGCGAGC CCGATCTTCC CCATCGGTGA TGTCGGCGAT
121 ATAGGCGCCA GCAACCGCAC CTGTGGCGCC GGTGATGCCG GCCACGATGC GTCCGGCGTA
181 GAGGATCGAG ATCTCGATCC CGCGAAATTA ATACGACTCA CTATAGGGGA ATTGTGAGCG
241 GATAACAATT CCCCTCTAGA AATAATTTTG TTTAACTTTA AGAAGGAGAT ATACATATGC
301 GGGGTTCTCA TCATCATCAT CATCATGGTA TGGCTAGCAT GACTGGTGGA CAGCAAATGG
361 GTCGGGATCT GTACGACGAT GACGATAAGG ATCATCCCTT CACCGGATCC CTGGTTCCGC
421 GTGGTAGCAT GGCAGGCACC AGCGAAGCAG TTAAAAAGTG GGTGAATAAA ATCATCGAAG
481 AAAACATTAT CGCCGTGTTT GCCAAAACCG AATGTCCGTA TTGTATTAAA GCCATCAGCA
541 TCCTGAAAGG CTATAATCTG AATAGCCATA TGCACGTGGA AAACATTGAG AAAAATCCGG
601 ATATGGCAAA CATTCAGGCC TATCTGAAAG AACTGACCGG TAAAAGCAGC GTTCCGCGTA
661 TCTTTATCAA CAAAGATGTT GTTGGTGGCT GTGATGATCT GGTGAAAGAA AATGATGAAG
721 GCAAACTGAA AGAGCGCCTG CAGAAACTGG GTTTAGTGAA TTAAGAATTC AAGGGCGAGC
781 TCAACGATCC GGCTGCTAAC AAAGCCCGAA AGGAAGCTGA GTTGGCTGCT GCCACCGCTG
841 AGCAATAACT AGCATAACCC CTTGGGGCCT CTAAACGGGT CTTGAGGAGT TTTTTGCTGA

Fig 3.6 Nucleic acid coding sequence of *Pf*Grx1. The coding sequence was obtained from the whole plasmid encoding the *Pf*Grx1 gene. The highlighted region in yellow corresponds to the gene sequence used for recombinant protein expression. **A.** The underlined bases in red indicate forward (within the T7 promoter site) and reverse primer sites, respectively. While EcoRI and BamHI are shown in red, respectively. B. The highlighted bases, ATG and TAG shows the start and stop codons, respectively. The underlined bases in blue indicate bases coding for 6×Histidine amino acid residues.

In Fig 3.6, the region with codons for the whole insert including those for the protein with a copper-binding motif (CXXC) is shown in yellow. The first underlined bases in red (Fig 3.6, a) show the T7 promoter region where the primers bind during the amplification process. The second underlined group of bases (Fig 3.6, b) indicates the T7 reverse region. The highlighted region has incorporated two restriction sites which are EcoRI, and BamHI respectively, all with bases shown in red on the diagram.

3.2.11 The amplification of *Pf*Grx1

The *Pf*Grx1 was amplified through colony PCR using Taq DNA polymerase after its *in-silico* analyses. This was performed to confirm the identity of the *Pf*Grx1 DNA in the plasmid. Fig 3.7 shows the whole plasmid in lane 2 with approximately 4000 base pairs. A PCR product with the expected ~640 bp is shown in lanes 3 and 4 when resolved on the agarose gel (Fig 3.7). There is a difference in terms of yield between lanes 3 and 4 due to the variation in the dNTPs used in the reactions. It was found that there was a greater yield of the amplicons with the use of ext. dNTPs (Fig 3.7).

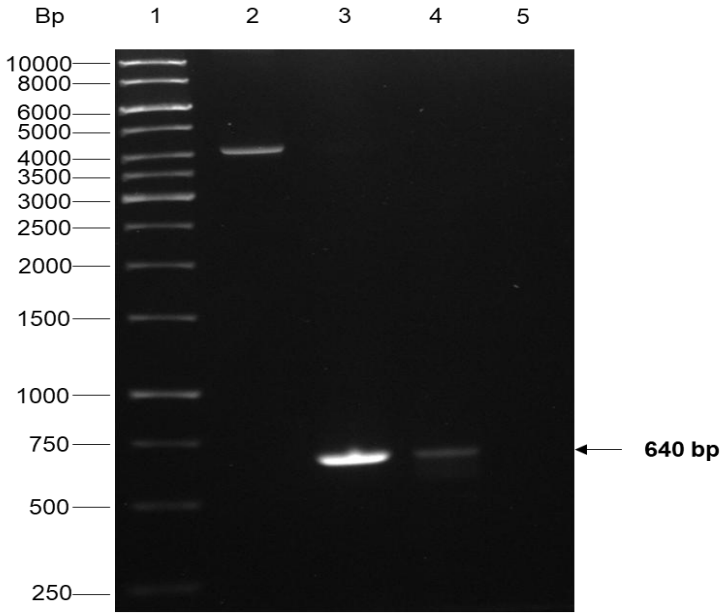

Fig 3.7 Agarose gel of the PCR product of *Pf*Grx1 gene (Commercially synthesized). The *Pf*Grx1 gene was amplified from one pET 100/D-TOPO r*Pf*Grx1 plasmid-containing bacterial colony and resolved on a 1% (w/v) agarose gel containing ethidium bromide. Lane 1, DNA ladder; Lane 2, Isolated plasmid (Grx1), Lane 3, PCR product using 2.5 mM dNTPs; Lane 4, PCR product using 10 mM dNTPs; Lane 5, template control. The arrow indicates the *Pf*Grx1 amplified product.

3.2.12 Restriction endonuclease digestion of *Pf*Grx1 pET100/TOPO expression plasmid

The restriction endonuclease digestion of pET100/TOPO expression plasmid harboring the r*Pf*Grx1 gene was performed using EcoRI and BamHI. This experiment generated the desired *Pf*Grx1 insert using BamH1 and EcoR1 restriction enzymes which confirmed the identity of the *Pf*Grx1 insert. Samples from the digestion together with the undigested *Pf*Grx1 were resolved on 1% agarose gel. (Fig 3.8) Figure 3.8, lane 2 shows three bands of the un-digested plasmid

representing nicked, linear, and supercoiled DNA. Single digests of the plasmid with EcoRI and BamHI, respectively, are seen as single bands of ~6000 bases in lanes 3 and 4. Double digestion with EcoRI and BamHI in Tris-HCl/$MgCl_2$ buffer yielded linearized *Pf*Grx1 at ~6000 bp. Another band at ~366 bp was expected in lane 5 but could not be seen. When the volume was increased to 10 µL in lane 7, four bands were visible which included a linearized DNA ~6000 bp, two feint bands, and the *Pf*GRx1 insert at ~366 bp. Lanes 6 and 8, contain samples (10 µL and 1 µL, respectively) that were digested in tango buffer. Compared to Tris-HCl/$MgCl_2$ buffer, digestion of the plasmid in tango buffer yielded star activity. Therefore, the latter was utilized for this restriction digest experiment.

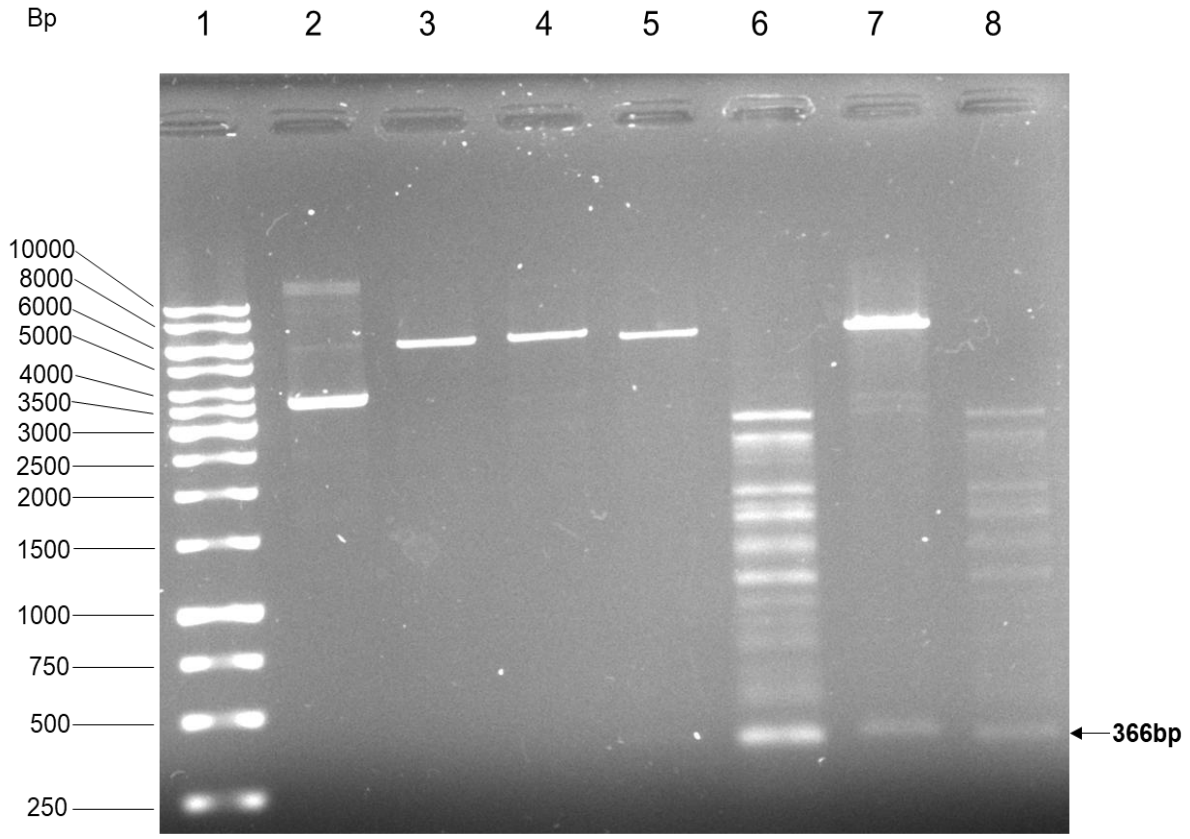

Fig 3.8 Digestion of *Pf*Grx1 pET 100/D-TOPO expression Plasmid with EcoR1 and BamH1. Samples were all resolved on 1% (w/v) agarose gel containing ethidium bromide and viewed using Ultraviolet light. Lane 1 DNA Ladder; The *Pf*Grx1 pET/D-TOPO plasmid was in Lane 2, undigested, Lane 3, digested with EcoR1; Lane 4, digested with BamH1; Lane 5, digested with EcoR1 and BamH1 in Tris-HCl/$MgCl_2$ Buffer (1 µL); Lane 6, digested with EcoR1 and BamH1 in Tango Buffer (10 µL); Lane 7, digested with EcoR1 and BamH1 in Tris-HCL/$MgCl_2$ (10 µL) Lane 8, digested with EcoR1 and BamH1 in Tango Buffer (1 µL).

3.2.13 Monitoring the growth of *E. coli* BL 21 (DE3) recombinantly expressing *Pf*Grx1

The *E. coli* BL 21 (DE3) bacteria were used for the expression of r*Pf*Grx1 in Luria broth (LB) media. The culture was grown at 37°C and induced with 1 mM IPTG for 4 hours, and bacterial growth followed at OD_{600} (Fig 3.9). All five colonies showed differences between the uninduced and induced cultures and the best were colonies 1 and 2. These were selected based on the differences in growth patterns of the host *E. coli* cells. The colony with the largest difference in growth between the uninduced

and induced cultures, was selected for subsequent experiments. Therefore, all the subsequent experiments were conducted using colony 1.

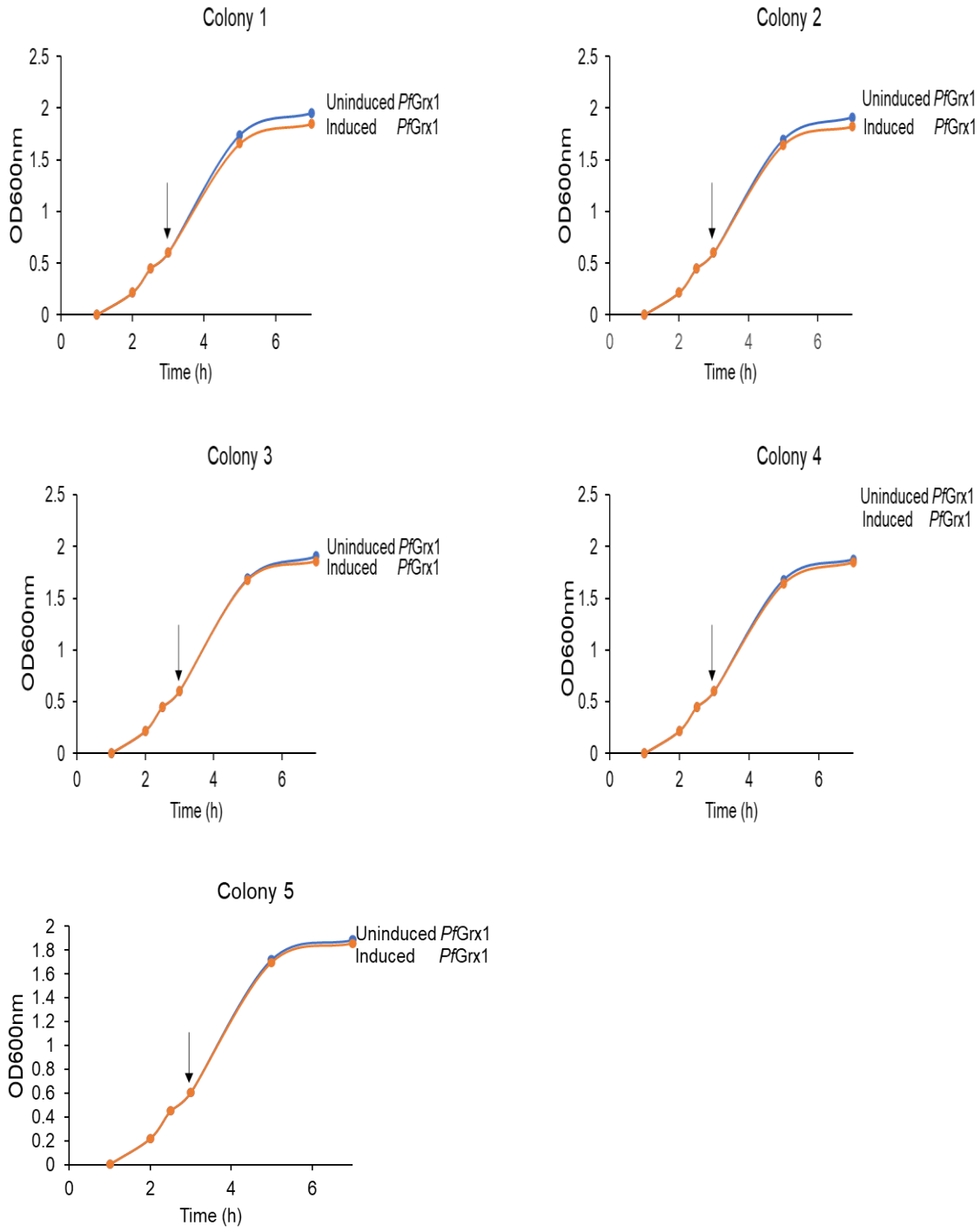

Fig 3.9 Bacterial growth curves for the expression of *Pf*Grx1 in LB media without glucose at 37°C induced with 1 mM IPTG for 4 hours. Five different *E. coli* colonies were selected and grown in the presence (induced) or absence (uninduced) of IPTG, as shown by the arrow. Growth was monitored at OD600 nm.

3.2.14 Screening for the recombinant *Pf*Grx1

The bacteria used in Figure 3.9 were lysed and electrophoresed on 15% Tris-tricine SDS-PAGE gels. In comparison with the uninduced samples in all the colonies, induced samples showed a minor protein band of approximately ~12 kDa thought to represent *Pf*Grx1 (Fig 3.10). The size of this band corresponds to the predicted size for *Pf*Grx1 of 13.4 kDa. Figure 3.10 shows that all five induced cultures have an induced protein larger than 100 kDa. However, the identity of this protein is not known. Arising from the results in Figures 3.9 and 3.10, two colonies (Colony 1 and 2) were chosen for the optimization of expression conditions for *Pf*Grx1.

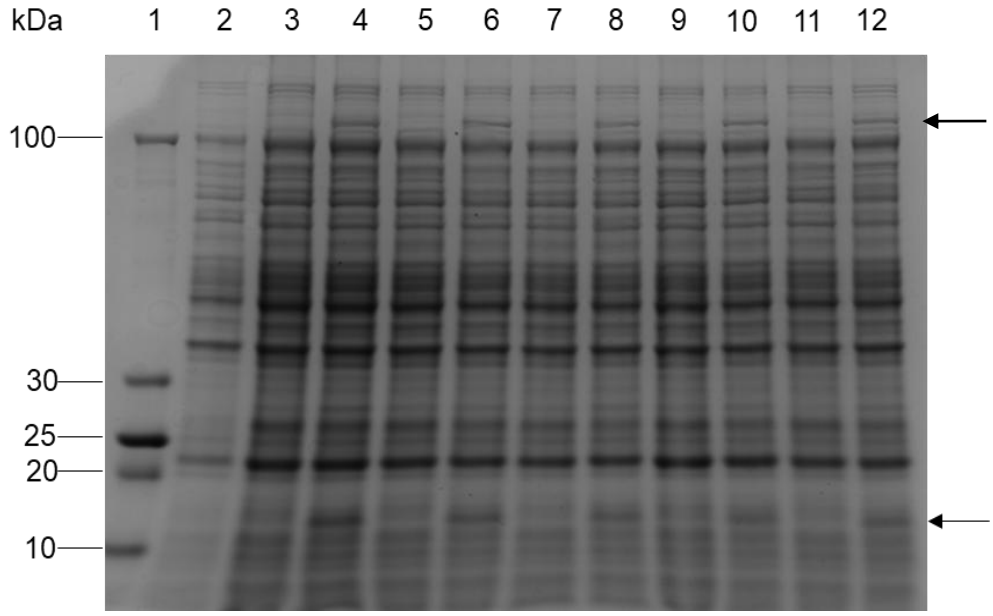

Fig 3.10 Analysis of the expression of *Pf*Grx1 in five colonies in LB media induced with 1 mM IPTG at 37ºC for 4 hours. Bacterial lysates from five cultures, each from a separate *E. coli* colony were electrophoresed on 15% reducing Tris-tricine SDS-PAGE gel stained with Coomassie brilliant blue G250. Lane 1, molecular weight marker; Lane 2, uninduced sample taken at 0.5 at OD600 nm before the addition of IPTG. Lanes 3, 5, 7, 9, and 11 uninduced, and lanes 4, 6, 8, 10, and 12 induced samples taken after the addition of IPTG. The arrow above 10 kDa on the gel shows the expressed *Pf*Grx1, while the one above 100 kDa indicates an unidentified protein.

3.2.15 Optimization of conditions utilized in the *Pf*Grx1 expression

To determine the suitable growth and expression conditions for the recombinant *Pf*Grx1, various media (Terrific broth, Luria broth, and 2xYT) were tested and 2xYT media gave the desired results (Fig 3.11). The r*Pf*Grx1 was induced with 0.2 mM IPTG for 16 hours after several induction attempts using 0.5 and 1 mM (results not shown) which did not show the band of interest with the needed intensity. The induction periods were also varied from 4 to 16 hours with the latter being optimum for the expression (Fig 3.11). The observed weight of *Pf*Grx1 was ~12 kDa which is close to the predicted size of ~13.4 kDa. The calculation of the protein size was based on plotting log molecular weight vs the distance that the protein band of interest has migrated relative to the bromophenol dye front in the SDS-PAGE gel.

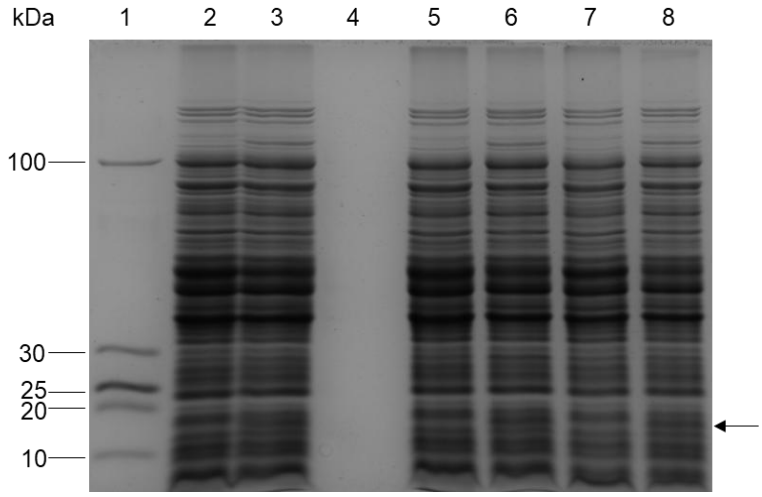

Fig 3.11 Recombinant expression of putative *Pf*Grx1 in 2XYT media at 20ºC induced with 0.2 mM IPTG for 16 hours. Bacterial lysates from one colony culture were run on 10% Tris-tricine reducing SDS-PAGE gel stained with Coomassie Blue. Lane 1, Molecular Weight Marker; Lanes 2 and 3 were loaded with 5 µL uninduced and induced samples; Lane 4, blank; while Lanes 5 and 6, and Lanes 7 and 8 with increased concentrations of 8 and 10 µL, respectively. The arrow on the indicates the size of *Pf*Grx1.

3.2.16 The effect of copper on the growth of bacterial expressing *Pf*Grx1

The host bacteria were grown in 2xYT media at 20°C for 16 hours, and 0.5 mM copper was added at the same time IPTG was added to induce expression and compared to the identical culture without copper. There was no significant difference in the intensity of the *Pf*Grx1 band between the lysate of samples grown with and without copper (Fig 3.12).

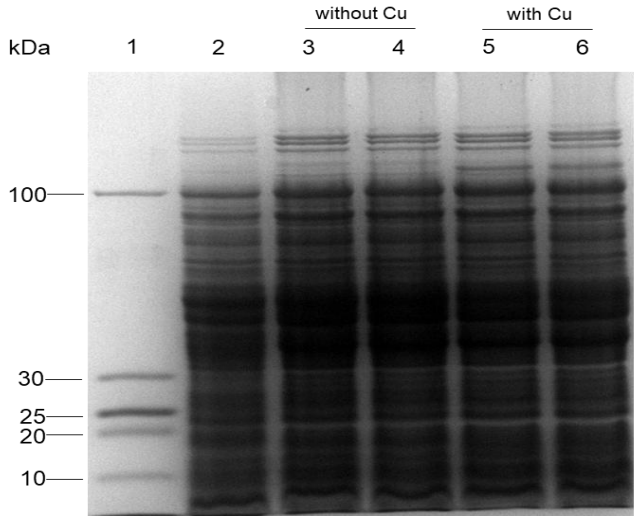

Fig 3.12 Expression of recombinant *Pf*Grx1 in 2xYT media induced with 0.2 mM IPTG at 20°C for 16 hours. *Pf*Grx1 expressed in the presence or absence of 0.5 mM copper in *E. coli* BL 21 pLysS cells were analyzed on 10% reducing Tris-tricine SDS-PAGE gel and stained with Coomassie brilliant blue G250. Lane 1, molecular weight marker; Lane 2, *E. coli* lysate without the plasmid; uninduced and induced samples grown in the absence and presence of copper were loaded in Lanes 3 and 4, and Lanes 5 and 6, respectively.

3.2.17 Expression, purification, and western blot analysis of recombinant *Pf*Grx1

Following the expression of r*Pf*Grx1, the protein was affinity purified utilizing the TALON affinity resin. The r*Pf*Grx1 was eluted using 500 mM imidazole, and a ~12 kDa protein band was identified in lanes 10 and 11 (Fig 3.13, A). Circumsporozoite (CSP) protein was included in lane 14 as a control. Fig 3.13, B, is nitrocellulose stained with Ponceau-S showing a successful western blot transfer with the protein of interest indicated by an arrow on the right side of the gel. To correctly identify the affinity purified r*Pf*Grx1, the western blot was probed with mouse anti-His and goat anti-mouse antibodies. Both r*Pf*Grx1 and CSP were detected using ECL in lanes 10 and 14, respectively (Fig 3.13, C). However, for unknown reasons, there was no signal in the lanes loaded with induced lysate, supernatant, and unbound protein where the protein of interest was expected to be. The nitrocellulose in Fig 3.13, D was viewed by incubating it with 4-chloro-1-naphthol for 30 min. The CSP band in lane 14 shows a more intense band compared to that of r*Pf*Grx1 in lane 10 (Fig 3.13, D).

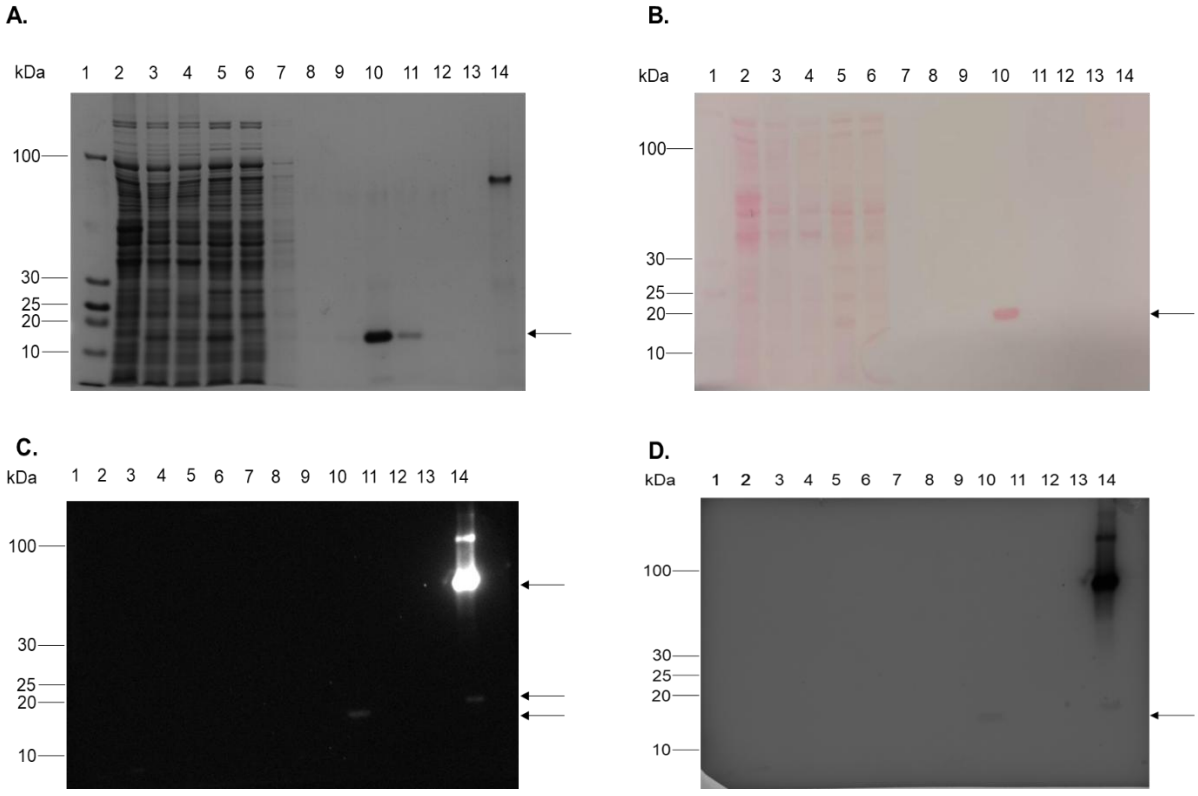

Fig 3.13 SDS-gel and Western blot analysis of recombinantly expressed and purified *Pf*Grx1 in pET100/D-TOPO expression plasmid. Samples from the expression of r*Pf*Grx1 at 20°C, induced with 0.2 mM IPTG for 16 hours were affinity purified and electrophoresed on 10% Tris-tricine SDS-PAGE and stained with Coomassie brilliant blue G250 in **(A)**, and **(B)** indicates nitrocellulose stained with Ponceau-S after the western blot transfer. **A.** Lane 1, molecular weight marker; Lane 2, uninduced bacterial lysate; Lane 3, induced bacterial lysate, Lane 4, pellet; Lane 5, unclarified supernatant; Lane 6, flow-through; Lane 7- 8, wash fractions; Lane 9-12, eluted fractions; Lane 13, Blank; Lane 14, Circumsporozoite protein (CSP) (used as a positive control because it His tagged). **C.** and **D.** show nitrocellulose with samples loaded in **(A)** and **(B)** and then viewed with ECL and 4-chloro-1-naphthol, respectively. The arrow in **A**, **B**, and **D** shows the size of the purified and transferred r*Pf*Grx1. In **C**, the arrow above 20 kDa and one between 30 and 100 kDa indicate the size of CSP.

3.2.18. Growth of *E. coli* BL21 (DE3) pLysS cells and those expressing r*Pf*Grx1 in the absence and presence of copper

According to Salman *et al.,* 2023, the growth of *E. coli* BL 21 (DE) pLysS cells is inhibited in the presence of 8 mM copper. However, bacteria harboring plasmids that express copper-binding proteins, grow in the presence of lethal concentrations of copper due to the protein's ability to bind copper. To establish whether r*Pf*Grx1 binds copper and helps the growth of the bacteria, *E. coli* BL 21 (DE3) without and with the plasmid expressing the r*Pf*Grx1 were grown in the absence or presence of copper (8 mM), and growth was monitored at OD_{600} for 16 hours. In Fig 3.14 A, the growth of *E. coli* cells was halted in the presence of copper (8 mM). *E. coli* expressing r*Pf*Grx1 showed 0.330 higher OD600nm value compared to the *E. coli* without the r*Pf*Grx1 grown in the 8 mM copper-enriched media (Fig 3.14 B) and suggests that the protein binds copper and enables bacterial growth. Uninduced and induced *E. coli* cells with r*Pf*Grx1 grown in the absence of copper indicated a marginal difference showing there was exponential growth of the bacteria (Fishov *et al.,* 1995). Induced *E. coli* expressing r*Pf*Grx1 and grown in the presence of copper (8 mM) grew marginally better than the uninduced *E. coli* carrying r*Pf*Grx1, showing that the expression of the protein helped the bacteria grow.

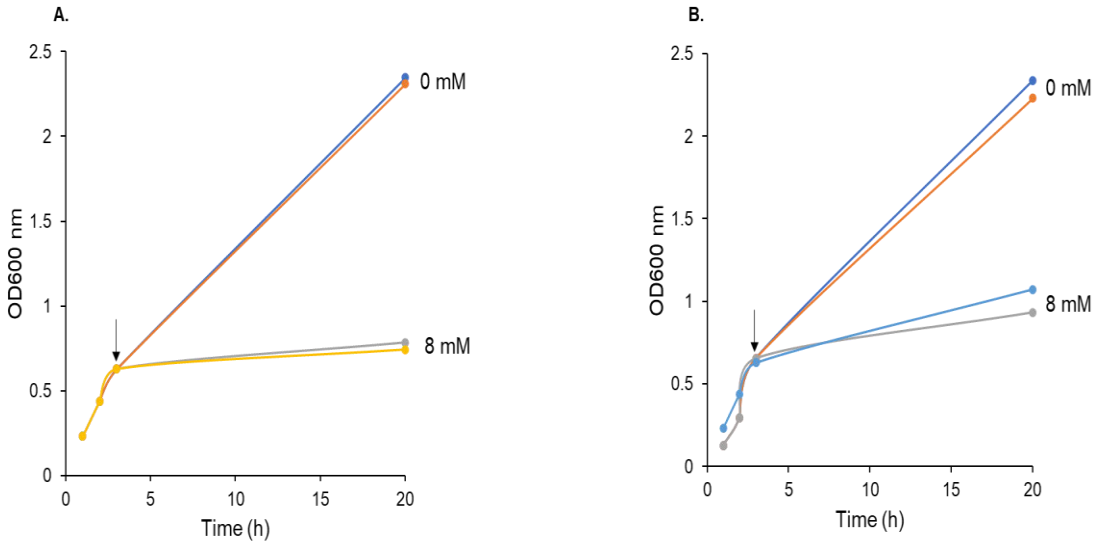

Fig 3.14 Effect of copper on the growth of *E. coli* BL 21 (DE3) pLysS cells and those expressing r*Pf*Grx1. A. The *E. coli* cells were grown in the absence (deep blue and red lines indicating uninduced and induced cultures respectively), and presence of copper (8 mM) (yellow and grey signifying uninduced and induced cultures) at 20ºC for 16 hours, after being induced with 0.2 mM IPTG. **B.** The *E. coli* cells expressing r*Pf*Grx1 were grown using the conditions in **(A)**. Uninduced and induced cultures in the absence of copper are represented in blue and orange lines respectively, while in the presence of copper, they are represented by light blue (induced) and grey (uninduced) lines. Arrows in **A** and **B** indicate the addition of copper and IPTG to the growth media. The absorbance readings in both **A** and **B** were monitored at OD600 nm.

3.2.19 Inhibition of copper-catalyzed oxidation of ascorbic acid by r*Pf*Grx1 expressed without copper and isolated without/with DTT

Jiang *et al.,* 2005 reported that oxidation of ascorbate occurs in the presence of Cu (I) and is followed by a decrease in absorbance at 255 nm over 300 s. r*Pf*Grx1 was expressed without copper and isolated without or with DTT, then followed by determining its ability to bind copper in the ascorbic acid oxidation assay over 300 s at 255 nm (Fig 3.15 A and B). DTT is widely used to prevent oxidation of thiol groups (Cleland., 1964). Ascorbic acid alone or with r*Pf*Grx1, BSA, and EDTA did not change the ascorbate oxidation over 300 s at 255 nm. Adding copper to ascorbic acid caused a 0.55 decrease in absorbance units (Fig 3.15 A). The oxidation reaction was inhibited by r*Pf*Grx1 showing that the protein bound copper (Fig 3.15 A). r*Pf*Grx1 isolated with DTT had the same effect on the assay as the protein isolated without DTT. However, r*Pf*Grx1 + DTT had a small effect on the ascorbate oxidation without copper (Fig 3.15 B). The BSA control showed (0.274 absorbance units) more inhibition of the oxidation of ascorbate than the recombinant protein either isolated without or with DTT (Fig 3.15 A and B), suggesting that BSA binds copper. BSA which has been shown to bind copper (Alhazmi *et al.,* 2023), was used as a positive control in the experiment.

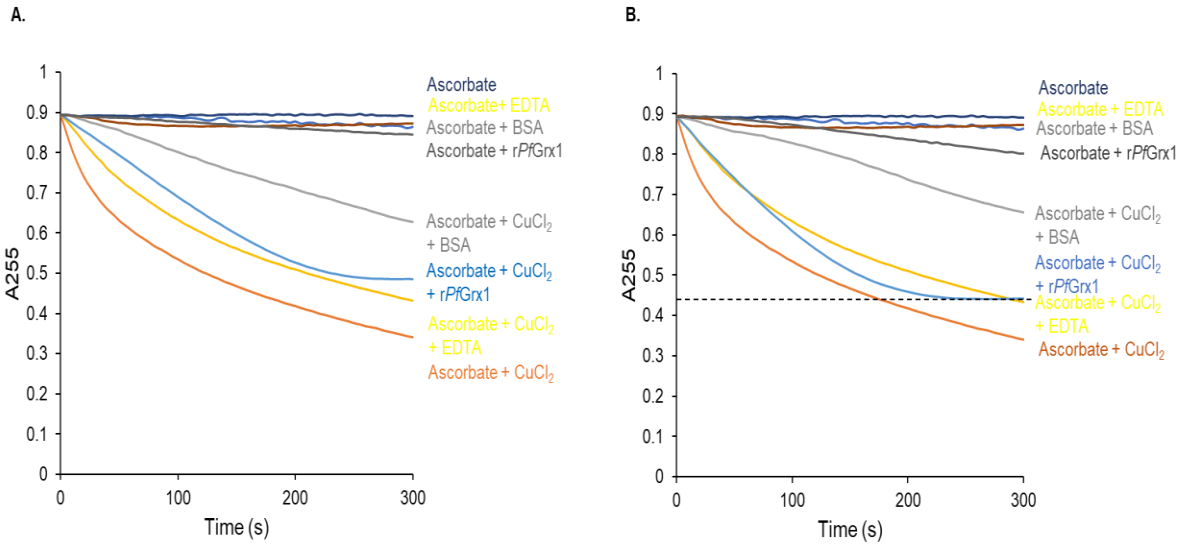

Fig 3.15 Copper-catalyzed oxidative degradation of ascorbic acid in the presence of r*Pf*Grx1 isolated from bacteria grown without Cu and isolated without/with DTT (10 mM). 120 µM Ascorbic acid (H_2Asc) was prepared and titrated to pH 4.5; 8 µM $CuCl_2$ was added to H_2Asc solution. **A.** r*Pf*Grx1 (5 µM), BSA (5 µM), or EDTA (5 µM) were added to $CuCl_2$/H_2Asc solution. **B.** r*Pf*Grx1 + DTT was treated as in A including controls (BSA and EDTA). The rate of ascorbic acid oxidation by copper in both A and B was measured for 300 s. The dotted line in **(B)** separates the reaction for *Pf*Grx1 (blue) and EDTA (yellow)

3.2.20 Inhibition of copper-catalyzed oxidation of ascorbic acid by r*Pf*Grx1 expressed in the presence of 0.5 mM of copper and isolated without/with 10 mM DTT

The binding of copper to a recombinant protein was assessed in the ascorbate assay using r*Pf*Grx1 expressed in the presence of 0.5 mM copper and

isolated without/with DTT. Ascorbate alone or with r*Pf*Grx1 + $CuCl_2$, BSA, and EDTA had little effect on the ascorbic acid oxidation at 255 nm. A decrease of 0.55 absorbance units was observed when $CuCl_2$ was added to ascorbate at 255 nm. No inhibition of the ascorbic acid oxidation was observed in the presence of r*Pf*Grx1 expressed in the presence of copper (Fig 3.16 A), suggesting that the recombinant protein had bound copper in the host bacteria and not in the assay. r*Pf*Grx1 expressed with copper and isolated with DTT showed similar results to the protein isolated without DTT (Fig 3.16 B). As earlier described in 3.4.2, BSA in Figure 3.16 A and B indicated more inhibition of the ascorbate acid than the recombinant proteins.

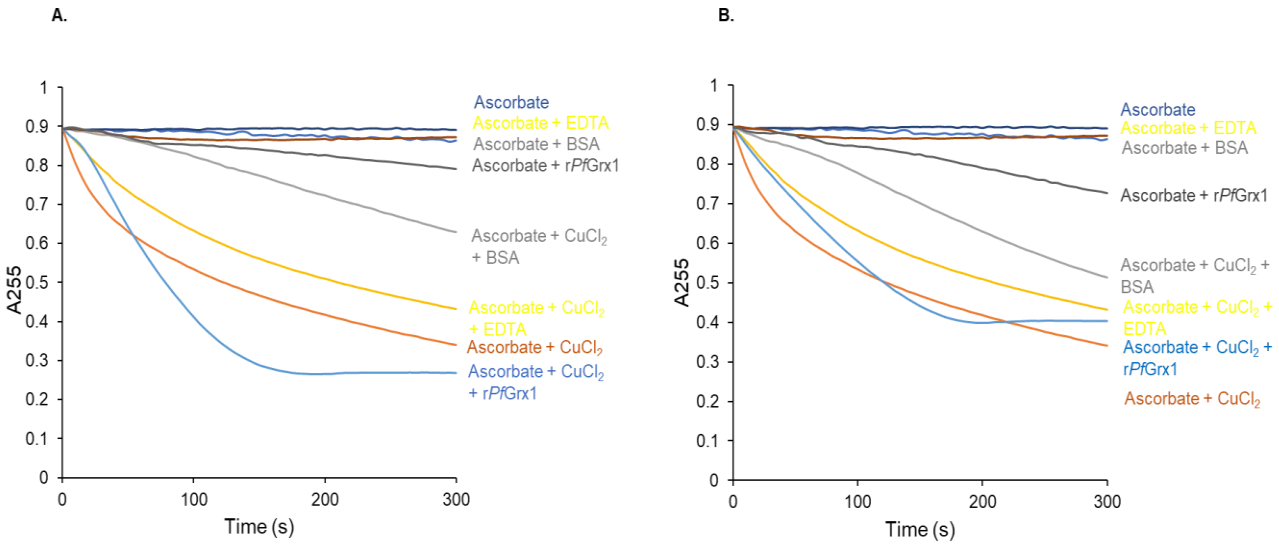

Fig 3.16 Copper-catalyzed oxidative degradation of ascorbic acid in the presence of *Pf*Grx1 expressed with Cu (0.5 mM) and isolated without/with DTT (10 mM). 120 µM Ascorbic acid (H_2Asc) was prepared and titrated to pH 4.5; 8 µM $CuCl_2$ was added to H_2Asc solution. In **A.** r*Pf*Grx1 + Cu (5 µM), BSA (5 µM), or EDTA (5 µM) were added to $CuCl_2$/H_2Asc while in **B.** r*Pf*Grx1 + Cu + DTT (5 µM), was added to the copper (II) Chloride/Ascorbate solution including the controls as mentioned in **A**. The rate of ascorbic acid oxidation by $CuCl_2$ was measured for 300 s both in **A** and **B**.

3.2.21 Measuring binding of copper to r*Pf*Grx1 using bicinchoninic acid (BCA) copper release assay

The r*Pf*Grx1 expressed without copper but isolated with/without DTT was purified and evaluated for its potential to bind copper in the BCA release assay. $CuCl_2$ alone was observed to have the highest absorbance reading in the presence of ascorbic acid (solid bars) (Fig 3.17). BSA alone did not show much increase in absorbance at 354 nm in the absence (open bars) or presence (solid bars) of ascorbic acid compared to BSA that was incubated with Cu. Identical readings at 354 nm are observed when the recombinant proteins (r*Pf*Grx1 + DTT and r*Pf*Grx1) are analyzed alone or incubated with Cu (II). Fig 3.17, shows that both r*Pf*Grx1 isolated with and without DTT, bound more copper when the proteins were incubated with reduced copper (I) compared to when the proteins were incubated with copper (II) [$P \leq 0.05$, and $P \leq 0.05$, respectively]. There was no difference between the copper bound to r*Pf*Grx1 with or without DTT ($P > 0.05$), meaning that DTT made little

difference in the ability of the r*Pf*Grx1 to bind copper (Fig 3.17). In instances where copper (II) chloride is incubated with ascorbate before being incubated with *Pf*Grx1 isolated with or without DTT, the results with and without ascorbate would be expected to be the same because copper (I) is bound to the protein. The oxidation state of the bound copper to the recombinant proteins was found to be copper (I).

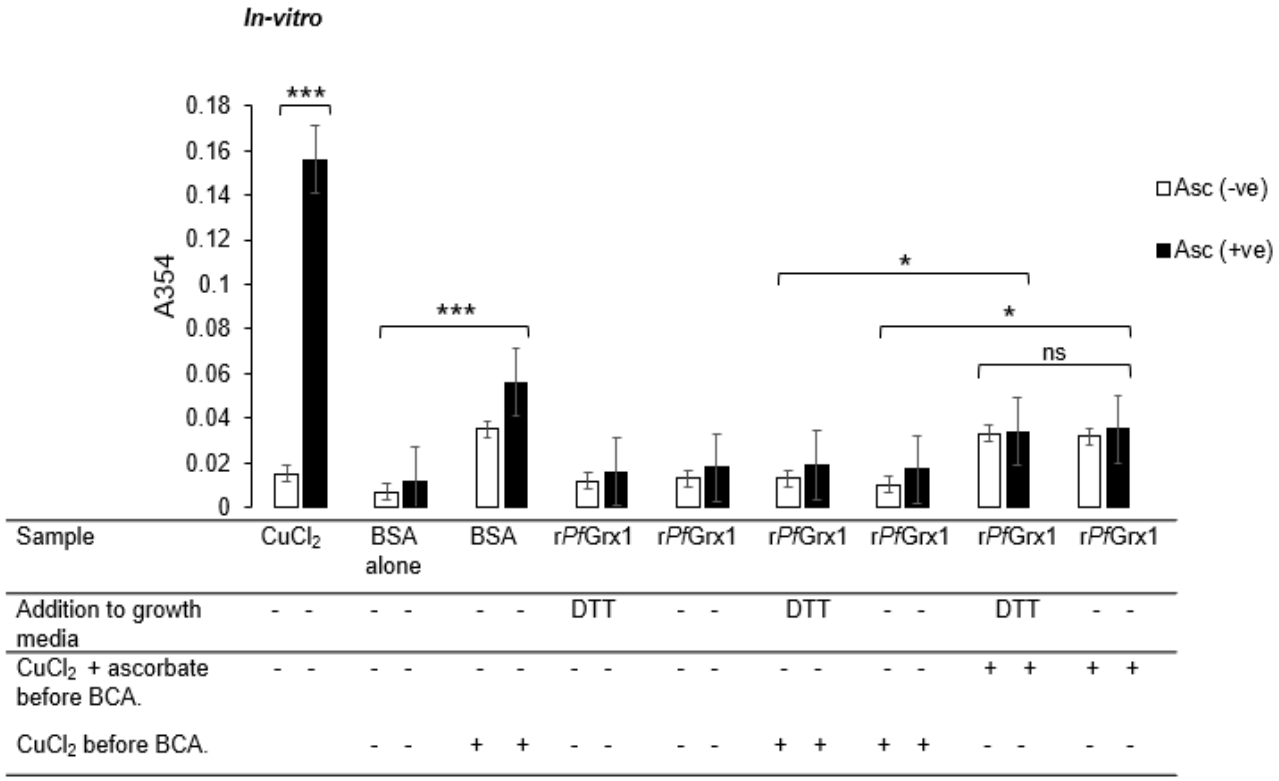

Fig 3.17 Binding of copper to *Pf*Grx1 isolated with/without DTT *in-vitro* determined by the BCA copper release assay. 10 µM affinity-purified *Pf*Grx1 + DTT or *Pf*Grx1 was incubated with copper II chloride with/without ascorbate. Excess copper from the incubation step was removed using the spun column, and the protein solution was treated with TCA. Copper was detected without (open bars) or with (solid bars) ascorbate. The experiment was performed in duplicate readings, plotting the average readings as shown in the bar graph. The experiment included BSA as a control. The data presented are mean ± SD of a duplicate. *, **, ***, and **** denote P≤ 0.05, P≤ 0.01, P≤0.001, and P≤ 0.0001, respectively, as determined by the student's t-test. The 'ns' stands for 'non-significant'.

3.2.22 An efficient method (Spin gel filtration) of removing copper from the Solution

Before the BCA release assay, the protein was incubated with copper, and any unbound copper was removed with a gel filtration spun column step. Bicinchoninic acid (BCA) release assay involves copper release from the protein with trichloroacetic acid (TCA), and Cu (I) is detected with the BCA reagent. To confirm the removal of copper, a 2 mL solution containing 5 mM of copper was passed through 1 mL, 3 mL, and 10 mL gel filtration columns. Fig 3.18, A indicates that minimal copper was eluted from three columns. Therefore, most of the copper was trapped in the columns, suggesting that the 1 mL column was sufficient to remove copper, and increasing the volume of the column did not distort the results obtained from the 1 mL gel filtration column. The gel filtration removed copper from the

solution and therefore there was no remaining copper to interfere with the BCA release experiment.

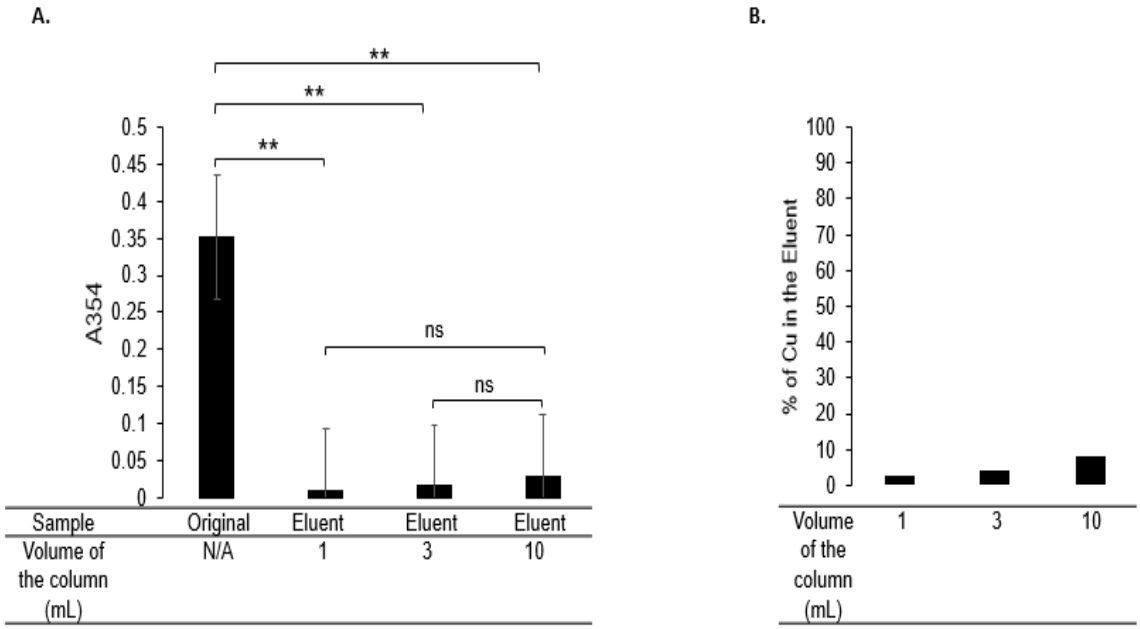

Fig 3.18 Determination of copper in eluents from spun columns of various volumes. A. $CuCl_2$ solution was eluted from spin columns of 1, 3, and 10 mL, the absorbance of the eluent from each column was measured at 354 nm, and readings presented in bar charts. **B.** The amount of $CuCl_2$ in the eluent from various columns in percent (%). *, **, ***, and **** denote P≤ 0.05, P≤ 0.01, P≤0.001, and P≤ 0.0001, respectively, as determined by the student's t-test. The 'ns' stands for 'non-significant'

3.2.23 Measuring of *in-vivo* binding of copper to r*Pf*Grx1 by bicinchoninic acid (BCA) copper release assay

The potential of r*Pf*Grx1 to bind copper intracellularly was assessed by expressing the recombinant protein in the presence of 0.5 mM copper (II) chloride, a concentration that is non-lethal to the *E. coli* bacteria carrying the plasmid expressing the protein. The protein was either isolated without or with DTT from the *E. coli* bacteria and then affinity purified. Before the isolation and purification, the host *E. coli* bacteria grown in copper-enriched media was washed to remove the extra copper. The *in-vivo* binding of copper to r*Pf*Grx1 + Cu and r*Pf*Grx1 + Cu + DTT was determined by BCA-release assay. This involved the formation of Cu(I)-BCA complex after the proteins released copper following the addition of trichloroacetic acid (TCA). The absorbance was measured at 354 nm in alkaline conditions. Copper alone had the highest absorbance readings in the presence of ascorbic acid (solid bars) (Fig 3.19). BSA alone did not indicate a significant increase in absorbance in the absence (open bars) or presence (solid bars) of ascorbic acid. However, BSA incubated with Cu (II) without a reducing agent ascorbate showed that it binds both Cu (I) and (II). Fig 3.19 showed that both r*Pf*Grx1 + Cu and r*Pf*Grx1 + Cu + DTT bound copper (I) *in-vivo* and there was no significant difference in the copper levels bound to the

protein isolated with or without DTT (P>0.05). The reason for this suggestion is that Cu exists as Cu (I) inside the cells and bound to the protein during expression.

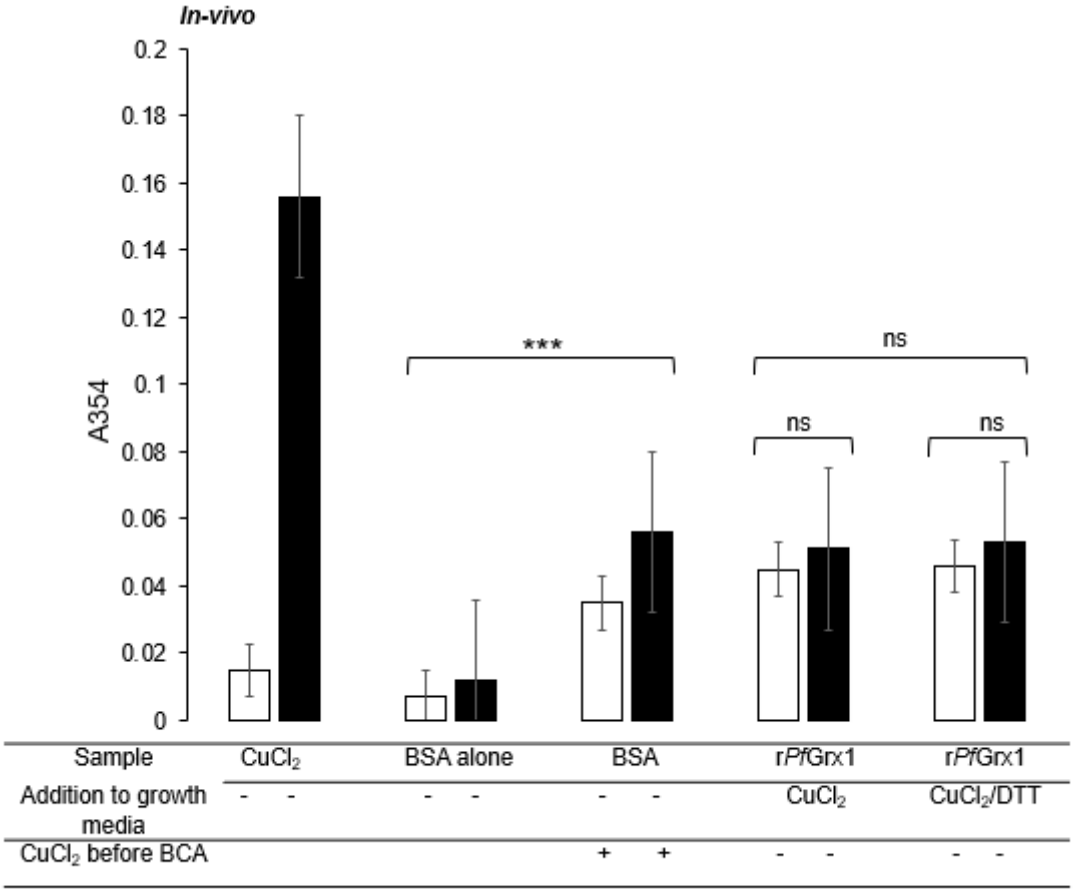

Fig 3.19 Binding of copper to *Pf*Grx1 + Cu or *Pf*Grx1 + Cu + DTT *in-vivo* determined by the BCA copper release assay. 10 µM affinity-purified *Pf*Grx1 + Cu or *Pf*Grx1 + Cu + DTT was grown with copper II chloride (0.5 mM) and treated with trichloroacetic acid (TCA). Copper was detected without (open bars) or with (solid bars) ascorbate. The experiment was performed in duplicate, and the average is presented in the figure above. The data presented are mean ± SD of a duplicate. *, **, ***, and **** denote P≤ 0.05, P≤ 0.01, P≤0.001, and P≤ 0.0001, respectively, as determined by the student's t-test. The 'ns' stands for 'non-significant'.

3.2.24 Measuring *in-vitro* copper binding to r*Pf*Grx1 with previously bound copper using bicinchoninic acid (BCA) copper release assay

The r*Pf*Grx1 that was expressed in the presence of 0.5 mM copper and isolated without/with DTT was subjected to an *in-vitro* test of its ability to bind copper using the BCA release assay (Fig 3.20). As before, copper alone which was included as a control showed higher absorbance readings when measured at 354 nm in the presence of ascorbate (solid bars). BSA alone had reduced readings when measured in the absence (open bars) or presence (solid bars) of ascorbic acid, while an increase in absorbance was observed when BSA was incubated with copper (II) in the absence of the reducing agent. The oxidation state of the bound copper was determined by the absence (open bars) and presence (solid bars) of ascorbic acid. r*Pf*Grx1 + Cu and r*Pf*Grx1 + Cu + DTT did not show a significant increase of bound copper after incubation with copper (II) without ascorbic acid, however, both

indicated an increase in the bound copper levels after incubation with reduced copper (P≤0.05 and P≤0.05 respectively) (Fig 3.20). This finding suggests that r*Pf*Grx1 prefers to bind copper(I) both *in-vivo* and *in-vitro*. There were no significant differences in the bound copper levels to the protein isolated with or without DTT (*P*>0.05).

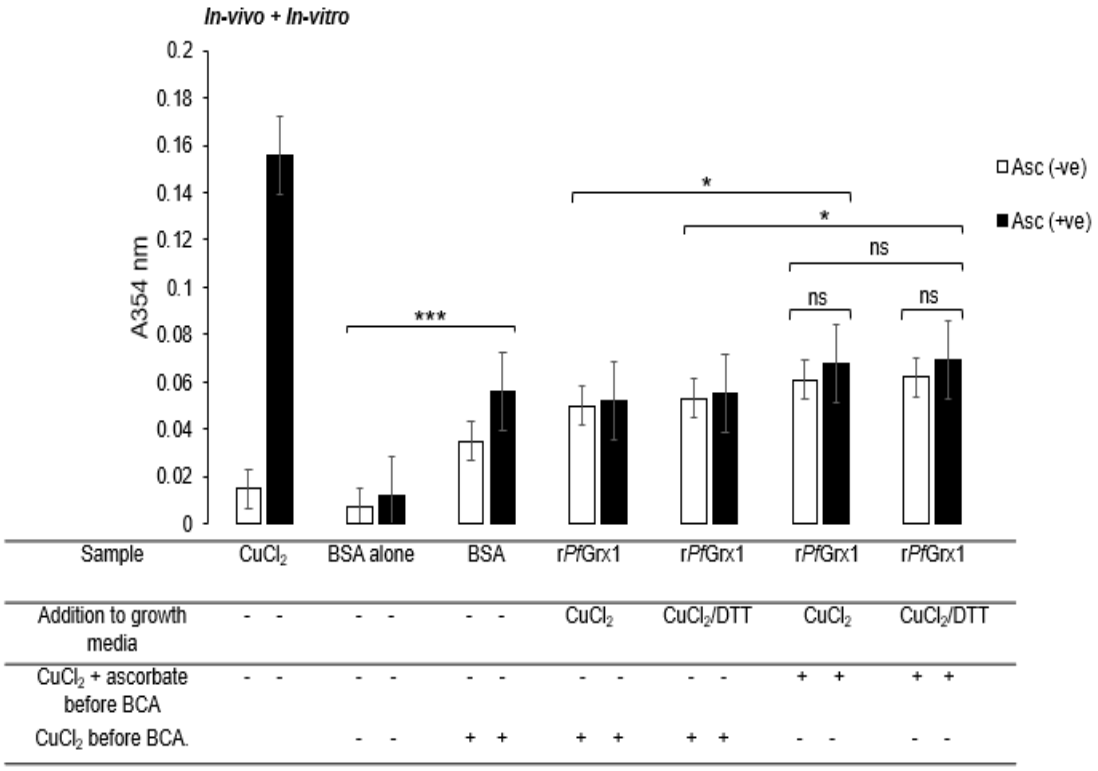

Fig 3.20 Binding of copper to *Pf*Grx1 + Cu or *Pf*Grx1 + Cu + DTT *in-vitro* determined by the BCA copper release assay. 10 µM affinity-purified *Pf*Grx1 + Cu or *Pf*Grx1 + Cu + DTT was incubated with copper II chloride with/without ascorbate. Excess copper from the incubation step was removed using a spun column, and the protein solution was treated with TCA. Copper was detected without (open bars) or with ascorbate (solid bars). The experiment was performed in duplicate, plotting the average readings as shown in the bar graph. BSA was included as a control. The data presented are mean ± SD of a duplicate *, **, ***, and **** denote P≤ 0.05, P≤ 0.01, P≤0.001, and P≤ 0.0001, respectively. This is determined by the student's t-test. The 'ns' stands for 'non-significant'.

3.2.25 Inhibition of copper-catalyzed oxidation of ascorbic acid by r*Pf*Grx1 eluent

The affinity-purified r*Pf*Grx1 + Cu and r*Pf*Grx1 + Cu + DTT were incubated with Cu (II) in the absence or presence of a reducing agent. Gel filtration to remove excess copper from the recombinant proteins was performed, followed by the determination of the effect of the eluent on the copper-catalyzed ascorbic oxidation was analyzed at 255 nm. Ascorbate alone yielded stable absorbance readings for 300s. This was followed by the addition of copper to ascorbic acid, and a large decrease in the oxidation of ascorbate was observed. In Fig 3.21, the eluent in A, B, C, and D did not inhibit the ascorbic acid oxidation. This finding suggests that the protein had already copper bound to it and thus, did not chelate copper in the

solution ($CuCl_2/H_2Asc$). The eluent was subjected to the BCA release assay which measured the amount of copper that was bound to the protein (Fig 3.21).

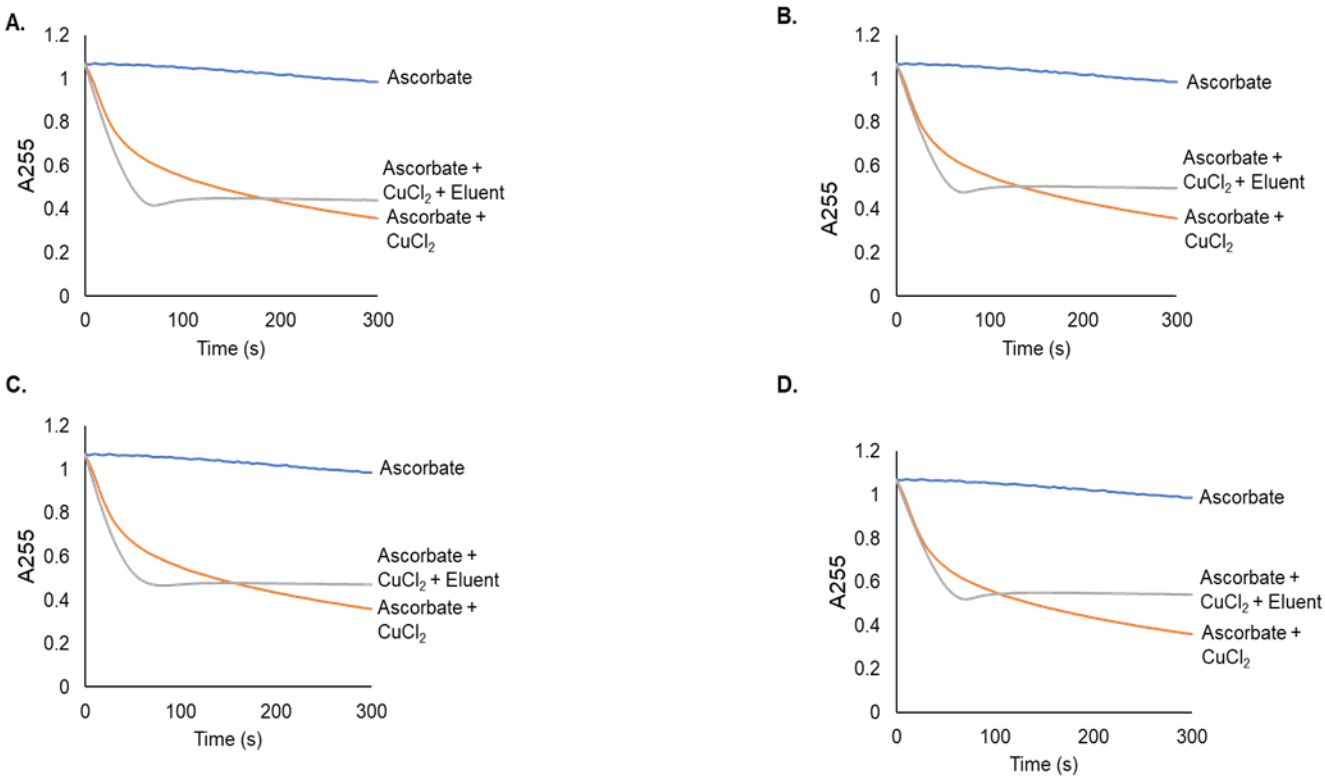

Fig 3.21 Copper-catalyzed oxidative degradation of ascorbic acid in the presence of protein solution that was eluted from the gel filtration column. 120 µM ascorbic acid (H2Asc) was prepared and titrated to pH 4.5; 8 µM $CuCl_2$ was added to H_2Asc solution; **A.** *Pf*Grx1 expressed with Cu and isolated with DTT was added to $CuCl_2$ which was reduced using 10 mM ascorbic acid and passed through gel filtration column as described earlier. **B.** The protein in **(A)** was added to $CuCl_2$ in the absence of ascorbic acid and then gel filtrated **C.** *Pf*Grx1 isolated without DTT was added to $CuCl_2$ after reduction with 10 mM ascorbic acid followed by gel filtration **D.** Protein in **(C)** was incubated with oxidized copper and gel filtrated.

3.4 Discussion

3.4.1 Introduction

The *Plasmodium falciparum* depends on copper for its development, as chelation of copper in growth media stops parasite development from the ring to the trophozoite stage (Rasoloson *et al.,* 2004). Copper-binding proteins play an important role in copper homeostasis and are possible targets for developing novel drugs to combat malaria. Choveaux *et al.,* 2012, demonstrated the potential role of *Pf*Ctr1 in the copper acquisition by the parasite, and Rasoloson *et al.,* 2004, highlighted the role of *Pf*CuATPase in copper efflux from the parasite. This section describes the identification of *Plasmodium falciparum* Glutaredoxin 1 and the copper binding characteristics of the recombinant protein using different approaches.

3.4.2 Identification of *Plasmodium falciparum* copper-binding proteins using bioinformatic tools

Our findings from the search of the PlasmoDB (https://plasmodb.org/plasmo/app, accessed on 7th June 2023) for copper-binding proteins identified some new proteins (*Pf*Grx1, CMC1, CoA5, DMT1, CutA, and *Pf*PIC) including the 12 already identified by Choveaux *et al.,* 2012 (Table 3.1). *Plasmodium falciparum* Glutaredoxin 1 (Table 3.1) belongs to a group of enzymes that reduce protein thiols and participate in the removal of free radicals. Bacterial Glutaredoxin 1 with a CXXC motif has been demonstrated to bind silver ions (Bilinovich *et al.,* 2021). Previously, glutaredoxins from bacteria and humans with CPYC motifs have been shown to bind copper and mercury (Brose *et al.,* 2014, Maghool *et al.,* 2020). Therefore, the identification and characterization of *Pf*Grx1 in the present study are important due to the role the protein might play in the cytosolic distribution of copper.

Among the 12 proteins, was *Plasmodium falciparum* S-adenosylhomocysteine hydrolase (SAHH) which has been identified to be a potential anti-malarial drug target (Singh *et al.,* 2016). SAHH from the mouse was determined to have a role in copper and sulfur amino acid metabolism (Bethin *et al.,* 1995). In the malaria parasite, *Pf*SAHH's role in copper metabolism has not been elucidated, making the current work on this protein necessary. Other copper-binding proteins (*Pf*Ctr1, *Pf*Cox17, *Pf*Sco1, *Pf*Cox11, and *Pf*Cox19), may have a potential role in the acquisition, cytosolic and mitochondrial distribution of copper (Choveaux *et al.,* 2012, Choveaux *et al.,* 2015, Salman *et al.,* 2022; 2023). Many of the proteins that have been curated with a 'Go copper-binding term in PlasmoDB have not been characterized, however, in this laboratory, five copper-binding proteins have been characterized (Choveaux *et al.,* 2012, 2015, Salman *et al.,* 2022, 2023, Munsami., 2022). The information about each protein in Table 3.1 can be accessed using protein identifiers on the PlasmoDB website (https://plasmodb.org/plasmo/app).

3.4.3 *In-silico* Identification of *Plasmodium falciparum* Glutaredoxin 1 (*Pf*Grx1)

Extensive analysis of sequences from six organisms (plant, yeast, protozoa, mouse, and human) (Fig 3.1 A) revealed some common features for *Pf*Grx1. The notable feature is the CXXC motif which has an affinity for copper (Brose *et al.,* 2014, Xiao *et al.,* 2011, Sun *et al.,* 1998). The alignment of five Grx1 amino acid sequences from human malaria species showed a conserved CXXC motif in all the sequences (Fig 3.1 B). The results may indicate that this copper-binding motif is important because it is conserved in many organisms (Bacteria, rats, and humans), and has been shown to bind copper (Cater *et al.,* 2014, Aon-Bertolino *et al*., 2011, Xiao *et al.,* 2019). Another feature worth noting is the serine residue which is observed to be present in *Plasmodium falciparum* Glutaredoxin 1 (Fig 3.1 B) and 19 other *Plasmodium falciparum* isolates (Fig 3.2). In humans, *M. musculus*, and *B. taurus*, glutamine replaces serine, while *S. cerevisiae* has arginine in that position. *T. parva* and *A. thaliana* have a deletion like the four Plasmodium species (*P. vivax*, *P. Knowlesi*, *P. malariae*, and *P. ovale*). The importance of this serine residue is not well known, however, Strader *et al.,* 1989 identified two serine residues involved in agonist activation of β-adrenergic receptors. In this regard, this residue may promote

molecular interaction with other proteins. The analysis shows that the serine residue is present in *Plasmodium falciparum* but absent in multiple species, suggesting that, the amino acid residue might not have a clear function. The Grx1 amino acid sequences from humans, mice, and monkeys all have a conserved copper-binding motif (Fig 3.3), which indicates that the motif is important in various organisms.

The *Pf*Grx1 has 3 predicted acetylation sites compared to other human infecting species that have 1 each (Fig 3.1), while the rest of the amino sequences from yeast, humans, and plants are without these sites (Fig 3.1). No ubiquitination sites were present in all the sequences analyzed, though these sites are important in aiding the protein's degradation, localization, and kinase activation (Guo and Tadi., 2020). What is not known is why these sites might be missing in these Grx1 amino acid sequences. It is documented that aberration in the ubiquitin system may breed diseases as explained by Ciechanover *et al.,* 2004). Therefore, the degradation of proteins keeps them in normal quantities, it may be suggested that there are other degradative processes that the protein from the multiple species in Fig 3.1 is subjected to.

There is no published data found during this study regarding the ability of *Pf*Grx1 to bind copper while *Hs*Grx1 has been demonstrated to bind copper through a CXXC motif and to interact with Atox1 and ATP7B Metal Binding Domains 5-6 (MBDs) (Maghool *et al.,* 2020). Models of crystal structures belonging to *Pf*Grx1 and *Hs*Grx1 were compared using superimposition in PyMoL producing an RMSD-generated value that was less than 2Å which indicated a similarity between the two models (Fig 3.4 C) (Kufareva *et al.,* 2012). The 6 extra amino acid residues that appear as a loop in the *Pf*Grx1 model are absent in the *Hs*Grx1 model. Rahlfs *et al.,* 2001 reported a 111 amino acid residues-long *Pf*Grx1 protein with a CXXC that indicates glutathione-dependent glutaredoxin activity. The *Pf*Grx1 model structure's similarity to *Hs*Grx1 could suggest similar roles of having the potential to bind copper and provide an alternative pathway for copper movement from the entry point to *Pf*CuATPases (Maghool *et al.,* 2020).

Our results identified that the copper-binding motif is located at amino acid residues 29 to 32 and 23 to 26 of the *Pf*Grx1 and *Hs*Grx1 structures, respectively (Fig 3.5 A and B). These results are supported by Yogavel *et al.,* 2014, Sun *et al.,* 1998, and Maghool *et al.,* 2020, which show the presence of a CXXC motif. The *Pf*Grx1 was predicted and shown by Kehr *et al.,* 2010, to be found in the cytosol in a study on mapping the subcellular localization of Grx1 in *Plasmodium falciparum*. The predicted molecular weight of *Pf*Grx1 using the Protparam program was 12.4 kDa, in line with reports from the current study and by Rahlf *et al.,* 2001. The presence of *Pf*Grx1 in the cytosol supports its functions regarding cell antioxidant defense and copper distribution (Rahlf *et al.,* 2001, Kehr *et al.,* 2010).

3.4.4 Expression of *Pf*Grx1 in *E. coli* BL 21 (DE3) pLysS

There are challenges in cloning a gene for heterologous recombinant expression in *E. coli*. These arise from transcription, translation, and folding in the bacterial host cells (Baneyx, 1999). Other problems may arise from the protein's coding sequence, which might possess rare codons or have more A+T bases in the

coding sequence (Birkholtz *et al.,* 2008). Analyzing the coding sequence in Fig 3.6, which was synthesized from a sequence of the genomic DNA by ThermoFisher Scientific company, indicated an inclusion of two restriction sites, EcoRI and BamHI, respectively. Further, 61.3% A+T bias was observed and slightly above the noted A+T bias in the general genome for humans (60%) but below that of the general genome belonging to the *Plasmodium falciparum* at 80.6% (Gardener *et al.,* 2002). Other studies (Mehlin *et al.,* 2006; Vedadi *et al.,* 2007) have indicated that this bias has little effect on the exogenous expression in *Plasmodium* sequences. The amplification of the coding region highlighted in Fig 3.6 produced a ~640 bp amplicon that included the T7 promoter and T7 reverse regions (Fig 3.7). Sequencing with colony PCR was not done to confirm an open reading frame (ORF) of *Pf*Grx1. However, *in-silico* analysis of the *Pf*Grx1 plasmid sequence using the MendelGene program was done to ensure that the sequence was in an open reading framework (ORF) (https://mendelgen.com).

A restriction endonuclease double digestion of the *Pf*Grx1 pET100/TOPO expression plasmid containing an insert flanked by EcoRI and BamHI restriction endonuclease sites was performed and yielded a ~366 bp *Pf*Grx1 insert (Fig 3.8). This was done to confirm the size of the fragment in the plasmid (Denomme *et al.,* 2000). Two observations were made from the restriction digestion results; (i) the insert was relatively faint, data that can be explained by a small number of base pairs of the insert that bind to the intercalating dye, thus, resulting in reduced fluorescent yield (Sambrook & Russell., 2001). The concentration of the agarose to the fragment of DNA to be resolved also plays a significant role in improving or reducing the resolution of the fragment of interest (Denomme *et al.,* 2000, Tamber and Hancock., 2001); (ii) the type of buffer in double digestion reaction of the plasmid, may have affected the results. It appeared that tango buffer may have introduced star activity and, thus, did not produce the desired results compared to Tris-HCl/$MgCl_2$ buffer. Based on this observation, it was concluded that the latter was suitable for double digestion of the expression plasmid.

3.4.5 The recombinant expression and purification of r*Pf*Grx1 from *E. coli* BL21(DE3) cells

Conducting a biochemical analysis is important for establishing the function of proteins from various organisms like the *Plasmodium* parasite (Birkholtz *et al.,* 2008). However, isolating enough protein from *Plasmodium* parasites for such functional determination is challenging, thus, *E. coli* is used to express *Pf*Grx1. The *E. coli* BL 21 (DE3) cells were transformed, and five colonies were selected for the expression of *Pf*Grx1. When the bacterial growth was analyzed, a marginal difference between the growth rates of the uninduced and induced cultures was noted (Fig 3.9). These findings do not agree with data on other malaria copper-binding proteins expressed previously (Choveaux *et al.,* 2012, 2015, Munsami., 2022, Salman *et al.,* 2022, 2023), which found a larger difference between the growth of uninduced and induced bacteria. The difference in findings could be explained by the variations in expression systems that have powerful promoters and burden the host cells metabolically (Glick, 1995, Sanden *et al.,* 2003, Haddadin and Harcum, 2005). This is due to expression difficulties that His-tag proteins come with compared to MBP tagged proteins.

Previous lab attempts to use His-tag proteins have been challenging. The addition of glucose to the LB growth media in the present study did not make a difference (Data not shown). Interestingly, even when suitable conditions are present, there are times, when the *E. coli* growth patterns may prove to be challenging leading to lack of expression. This is in spite of several studies being conducted on this bacterium (Baneyx *et al.,* 2004, Sandén *et al.,* 2003, Gill *et al.,* 2000, Sharma *et al.,* 2007).

The samples generated from the lysis of bacteria in Fig 3.9 showed two bands (see the arrows in Fig 3.10) in the induced lanes that were absent in the uninduced lanes when run on a reducing 15% Tris-tricine SDS-PAGE gel (Fig 3.10). The protein band above 100 kDa was unidentified, while the other was assumed to be *Pf*Grx1 due to its absence and presence in the uninduced and induced bacteria, respectively, and the size of the recombinant protein 13.4 kDa deduced from the band on the gel and predicted from the amino acid sequence. . This finding from the present study is like previous results with a molecular weight of 12.4 kDa belonging to *Pf*Grx1 (Rahlf *et al.,* 2001). There is a marginal difference between the predicted *Pf*Grx1's molecular weight and one observed on the SDS-PAGE gel; therefore, the protein band shows the right size of *Pf*Grx1. Two colonies with similar characteristics were selected for subsequent expressions and condition optimization.

Various factors were optimized to express *Pf*Grx1 protein effectively. Results from the use of LB and TB media did not have significant differences in protein production, therefore, enriched 2xYT media was used (de Groot *et al.,* 2006). IPTG concentration tends to affect protein expression. In our case, 0.5 mM and 1 mM of IPTG at 37°C expression temperature, and 4 hours post-induction time were used, and the expressed protein was difficult to detect. A change to a lower IPTG concentration (0.2 mM) was made as the IPTG concentration is recommended to be slightly above the critical concentration, which refers to the concentration below which the recombinant protein yield depends on IPTG (Goldberg *et al.,* 1991, Papaneophytou *et al.,* 2014). On the other hand, a concentration >5 mM of IPTG tends to overburden the host and affect the protein expression, however, between 0 and 1 mM, less effect on *E. coli* growth, and cell concentration is observed (Goldberg *et al.,* 1991, Harcum *et al.,* 1992). A lower temperature (20°C) and increased post-induction time (16 hours) were later employed, which contributed to better expression and purification of the protein (Fig 3.11). This is because a lower incubation temperature attains a reduced rate of protein synthesis, reduced aggregation, and degradation of the protein of interest (de Groot *et al.,* 2006, Khow *et al.,* 2012). All these factors affect the protein folding and solubility of the recombinant protein (Maksum *et al.,* 2023).

An attempt was made to further improve the *Pf*Grx1 expression, thus, 0.5 mM of $CuCl_2$ was added to the growth media, though no significant difference in the growth of *E. coli* cells or r*Pf*Grx1 protein was noted between cultures with and without $CuCl_2$ (Fig 3.12). However, copper addition to the *E. coli* growth media increased the yield of the recombinant *Pf*Ctr1 (Choveaux *et al.,* 2012). Interestingly, metal ions in the media contribute to the increase in the folding rate of a soluble protein being expressed, though it was not determined in the present study (Khow *et al.,* 2012). The reason for the disparities is not known. What may be true for the

*Pf*Grx1 and *Pf*Ctr1 is that both may bind copper. The expression and purification revealed a ~12 kDa *Pf*Grx1 protein band (Fig 3.13 A and B) which was consistent with the recombinant protein recognized by anti-His antibodies during the western blot (Fig 3.13 C). These findings are in line with a 12.4 kDa *Pf*Grx1 that was determined previously (Ralfs *et al.,* 2001) though it is 4 kDa less than the monothiol Glutaredoxin 1 from other parasites like the African trypanosomes (Comini *et al.,* 2008).

3.4.6 r*Pf*Grx1 enables *E. coli* host cells to tolerate toxic copper concentration levels

Copper inhibited the growth of *E. coli* without the plasmid, however, the presence of expressed r*Pf*Grx1 enabled bacterial growth in the presence of 8 mM copper and showed that the protein can bind copper in an *in-vivo* environment (Fig 3.14 A and B). This agrees with previous studies that have documented the protection that copper-binding proteins offer to *Methylosinus trichosporium*, *Bacillus subtilis*, *Lactobacillus plantarum*, and *E. coli* bacteria in the presence of toxic concentrations of copper (Vita *et al.,* 2016, Yang *et al.,* 2017, Salman *et al.,* 2023). Another notable observation in the present study is that uninduced and induced *E. coli* cells with r*Pf*Grx1 grown without copper indicated a marginal difference showing there was exponential/balanced host cell growth (Fishov *et al.,* 1995). The experiment was done three times, and results from one experiment were included. *Pf*Cox19 appeared to bind more copper than *Pf*Grx1 is higher, and therefore bacteria expressing the *Pf*Cox19 protein had higher growth rates than those observed here (Salman *et al.,* 2023).

3.4.7 Measuring inhibition of copper-catalyzed ascorbic acid oxidation by r*Pf*Grx1 expressed without copper and isolated without/with DTT

The results in Fig 3.15 A show that the copper-catalyzed oxidation was inhibited by r*Pf*Grx1 indicating that the protein bound copper. These results align well with findings that show that copper-binding proteins with methionine motifs inhibit the ascorbate assay and thus, bound copper (Jiang *et al.,* 2005). Furthermore, previous studies have determined a similar effect on copper-catalyzed ascorbic acid oxidation by other copper-binding proteins (Choveaux *et al.,* 2012, 2015, Salman *et al.,* 2022, 2023). DTT was added to protect the thiol groups from oxidation, and r*Pf*Grx1 isolated with DTT had the same levels of copper binding compared to the protein isolated without DTT (Fig 3.15 B).

3.4.8 Measuring inhibition of copper-catalyzed ascorbic acid oxidation by r*Pf*Grx1 expressed with 0.5 mM copper and isolated without/with DTT

The results from the present study show no inhibition of the ascorbic acid oxidation in the presence of r*Pf*Grx1 expressed with copper (Fig 3.16 A), suggesting that the recombinant protein had bound copper in the host bacteria and not in the assay. Although the oxidation state of copper that is bound in bacterial cells was not determined in the current study, previous studies have reported that copper is in a reduced state inside cells (Davis and O'Halloran, 2008). Another study has shown that in the Plasmodium parasite, there is a similar reducing cytoplasmic environment (Krnajski *et al.,* 2001). It was also noted that r*Pf*Grx1 expressed with copper and

isolated with DTT showed similar results to the protein isolated without DTT (Fig 3.16 B). This was because DTT just maintained the reduced state of the thiols (Cleland., 1964).

3.4.9 *In-vitro* r*Pf*Grx1 binding of copper

The third approach to determining whether r*Pf*Grx1 binds copper was the use of a BCA release assay. The protein bound copper (I) *in-vitro* and the use of DTT in the isolation step did not make a difference in the copper levels that were bound (Fig 3.17). Similar results were obtained from previous copper-binding studies involving other copper-binding proteins in bacteria and *Plasmodium falciparum (R. Sphaeroides* Cox11*, Pf*Ctr1, *Pf*Cox17, *Pf*Cox11, *Pf*Sco1, and *Pf*Cox19 (Thompson *et al.,* 2010, Choveaux *et al.,* 2012, 2015, Salman *et al.,* 2022, Munsami *et al.,* 2022). In humans, glutaredoxin 1 has been shown to bind copper (I) (Maghool *et al.,* 2020). The BCA assay was validated in this laboratory (Salman and Goldring., 2022) where it was shown to give identical results to the atomic absorption spectroscopy as described by Brener and Harris., 1995.

3.4.10 Removal of copper from solution using gel filtration

One of the factors that may affect the BCA release assay is a step that is performed to separate the protein-bound copper from unbound copper. Results measuring copper at different stages of the experiment showed that the gel filtration removed copper from the solution, thus, there was no remaining copper to interfere with the BCA release experiment (Fig 3.18 A and B). An experiment to determine the protein recovery rate in the eluents was not conducted, however, studies have shown that gel filtration can retain 85-90% of the proteins in the eluent (Nath *et al.,* 2003, Chonn *et al.,* 1991). The method allows the recovery of the protein in the eluent while excess copper is trapped in the gel filtration matrix.

3.4.11 *In-vivo* r*Pf*Grx1 binding of copper.

The r*Pf*Grx1 bound more copper (I) *in-vivo* than *in-vitro*, and there was no significant difference in the copper levels bound to the protein isolated with or without DTT (Fig 3.19). The same *in-vivo*/*in-vitro* pattern has been described for *Pf*Cox17, *Pf*Ctr1, and *Pf*Cox19 which also established copper (I) binding by these proteins within the *E. coli* bacterial cells (Choveaux *et al.,* 2012, 2015, Salman *et al.,* 2023). Copper (I) is preferred for transfer and transport in mammalian and yeast cells (Puig *et al.,* 2002, Banci *et al.,* 2004, Carr *et al.,* 2002). This supports the results in the current study that reveal the binding of copper (I) as the preferred metal ion. When copper was added to the recombinant protein that previously bound copper *in vivo,* minimal copper bound to the protein (Fig 3.20). This data suggests that r*Pf*Grx1 bound copper (I) better in *E. coli* cells as established with a study of *Pf*Sco1 (Munsami*.,* 2022). To further support the idea that r*Pf*Grx1 bound copper *in-vivo,* the affinity-purified r*Pf*Grx1 + Cu and r*Pf*Grx1 + Cu + DTT were incubated with Cu (II) in the absence or presence of a reducing agent. Gel filtration to remove excess copper from the recombinant proteins was performed, followed by the determination of the effect of the eluent on the copper-catalyzed ascorbic oxidation was analyzed at 255 nm. Results from this experiment indicated non-inhibition of the copper-catalyzed

oxidation of ascorbic acid, confirming that the protein bound copper (I) within *E. coli* cells and that binding was close to saturation.

3.4.12 Conclusion

The *in-silico* analysis of r*Pf*Grx1 using bioinformatic tools in the current study, generated results that showed that r*Pf*Grx1 has a CXXC copper-binding motif like the one present in human glutaredoxin 1, and the motif is thought to be involved in the binding of copper. Further, the *Pf*Grx1 is predicted to be in the cytosol, data that tallies well with the functions of the protein. The protein was then expressed, purified, and subjected to copper-binding studies by, analyzing the tolerance of *E. coli* cells towards high concentrations of copper, conducting experiments on the inhibition of copper-catalyzed ascorbic acid oxidation, and lastly by using a BCA release assay. All three approaches used to determine the copper binding ability of r*Pf*Grx1 indicated the protein binds copper (I) both *in-vivo* and *in-vitro*. The findings in the current study are to the best of our knowledge the first to report on the copper-binding abilities of Grx1 from the *Plasmodium* parasite.

Chapter 4

The *Plasmodium* spp. Putative S-adenosylhomocysteine hydrolase: bioinformatic studies, recombinant protein expression and copper binding studies with *Plasmodium falciparum* S-adenosylhomocysteine hydrolase

4.1 Introduction

This chapter characterizes the S-adenosylhomocysteine hydrolase using bioinformatics tools, protein expression, and copper-binding assays. Copper has various functions in the cells, e.g. the functionality of the electron transport chain depends on the presence of copper which is supposed to be acquired and distributed by copper-dependent proteins. However, many proteins are yet to be characterized. SAHH has been found to bind copper and play a role in the intracellular distribution of copper in rats (Creedon *et al.,* 1993). Therefore, *Pf*SAHH might play a similar function, hence, its characterization.

4.2 Results

4.2.1 Identification of *Plasmodium falciparum* S-adenosylhomocysteine hydrolase (*Pf*SAHH) in PlasmoDB

Following the identification of *Pf*SAHH from the Plasmodatabase, the protein sequence was aligned with the amino acid sequence of SAHH from six organisms (Fig 4.1 A). A putative copper-binding GYGDVGKG (GXGXXGXG) region was noted in the amino acid sequences of all six organisms. *B. bovis* and *T. annulata* are longer than the rest of the amino acid sequences in the alignment each having 491 and 489, respectively because of the insertion of 43 amino acid residues in their sequences (Fig 4.1 A). *M. musculus* and *H. sapiens* have the shortest sequences due to the deletions of about 73 amino acid residues. The *Pf*SAHH sequence has 479 amino acid residues with a GXGXXGXG motif like the rest of the sequences from the six organisms. The blue line indicates the NAD binding site on the *Pf*SAHH sequence. Amino acids 201, 202, 203, 235, 287, 322, 343, 391, 473, and 477 are reported to be involved in the interaction with NAD/H using hydrogen bonds, while residues 268, 288, and 320 of the *Pf*SAHH structure interact with NAD/H through hydrophobic bonds (Singh *et al.,* 2016). There is an average of 25.37% sequence identity among the amino acid sequences.

4.2.2 Analysis of amino acid sequences for Human *Plasmodium* spp

In Fig 4.1 B, four out of five *Plasmodium* species that infect humans have a conserved copper-binding GYGDVGKG (GXGXXGXG) motif while that for *Plasmodium vivax* has a GFGDVGKG motif where a phenylalanine residue replaces the tyrosine due to a single base Adenine (A) for Uracil (U) substitution in the 3´ bases. The alignment of 20 *Plasmodium falciparum* isolates SAHH amino acid sequences showed 100% identity in the GYGDVGKG motif (Fig 4.2). Fig 4.1 B shows an average of 81.06% amino acid identity among the *Plasmodium* species that infect humans.

A.

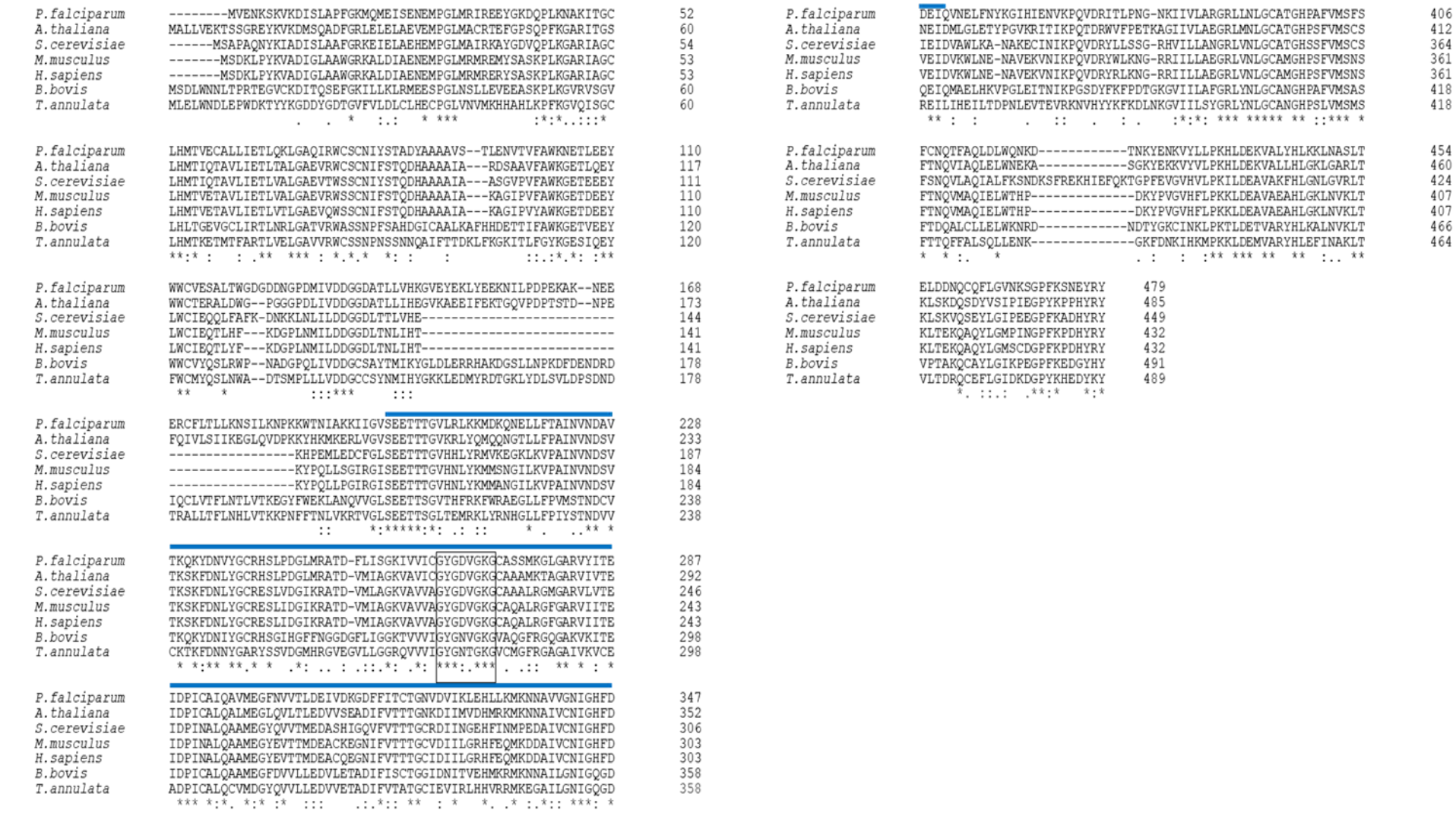
P.falciparum --------MVENKSKVKDISLAPFGKMQMEISENEMPGLMRIREEYGKDQPLKNAKITGC 52
A.thaliana MALLVEKTSSGREYKVKDMSQADFGRLELELAEVEMPGLMACRTEFGPSQPFKGARITGS 60
S.cerevisiae ------MSAPAQNYKIADISLAAFGRKEIELAEHEMPGLMAIRKAYGDVQPLKGARIAGC 54
M.musculus -------MSDKLPYKVADIGLAAWGRKALDIAENEMPGLMRMREMYSASKPLKGARIAGC 53
H.sapiens -------MSDKLPYKVADIGLAAWGRKALDIAENEMPGLMRMRERYSASKPLKGARIAGC 53
B.bovis MSDLWNNLTPRTEGVCKDITQSEFGKILLKLRMEESPGLNSLLEVEEASKPLKGVRVSGV 60
T.annulata MLELWNDLEPWDKTYYKGDDYGDTGVFVLDLCLHECPGLVNVMKHHAHLKPFKGVQISGC 60
LHMTVECALLIETLQKLGAQIRWCSCNIYSTADYAAAAVS--TLENVTVFAWKNETLEEY 110
LHMTIQTAVLIETLTALGAEVRWCSCNIFSTQDHAAAAIA---RDSAAVFAWKGETLQEY 117
LHMTIQTAVLIETLVALGAEVTWSSCNIYSTQDHAAAAIA---ASGVPVFAWKGETEEEY 111
LHMTVETAVLIETLVALGAEVRWSSCNIFSTQDHAAAAIA---KAGIPVFAWKGETDEEY 110
LHMTVETAVLIETLVTLGAEVQWSSCNIFSTQDHAAAAIA---KAGIPVYAWKGETDEEY 110
LHLTGEVGCLIRTLNRLGATVRWASSNPFSAHDGICAALKAFHHDETTIFAWKGETVEEY 120
LHMTKETMTFARTLVELGAVVRWCSSNPNSSNNQAIFTTDKLFKGKITLFGYKGESIQEY 120
WWCVESALTWGDGDDNGPDMIVDDGGDATLLVHKGVEYEKLYEEKNILPDPEKAK--NEE 168
WWCTERALDWG--PGGGPDLIVDDGGDATLLIHEGVKAEEIFEKTGQVPDPTSTD--NPE 173
LWCIEQQLFAFK-DNKKLNLILDDGGDLTTLVHE-------------------------- 144
LWCIEQTLHF---KDGPLNMILDDGGDLTNLIHT-------------------------- 141
LWCIEQTLYF---KDGPLNMILDDGGDLTNLIHT-------------------------- 141
WWCVYQSLRWP--NADGPQLIVDDGCSAYTMIKYGLDLERRHAKDGSLLNPKDFDENDRD 178
FWCMYQSLNWA--DTSMPLLLVDDGCCSYNMIHYGKKLEDMYRDTGKLYDLSVLDPSDND 178
ERCFLTLLKNSILKNPKKWTNIAKKIIGVSEETTTGVLRLKKMDKQNELLFTAINVNDAV 228
FQIVLSIIKEGLQVDPKKYHKMKERLVGVSEETTTGVKRLYQMQQNGTLLFPAINVNDSV 233
----------------KHPEMLEDCFGLSEETTTGVHHLYRMVKEGKLKVPAINVNDSV 187
----------------KYPQLLSGIRGISEETTTGVHNLYKMMSNGILKVPAINVNDSV 184
----------------KYPQLLPGIRGISEETTTGVHNLYKMMANGILKVPAINVNDSV 184
IQCLVTFLNTLVTKEGYFWEKLANQVVGLSEETTSGVTHFRKFWRAEGLLFPVMSTNDCV 238
TRALLTFLNHLVTKKPNFFTNLVKRTVGLSEETTSGLTEMRKLYRNHGLLFPIYSTNDVV 238
TKQKYDNVYGCRHSLPDGLMRATD-FLISGKIVVICGYGDVGKGCASSMKGLGARVYITE 287
TKSKFDNLYGCRHSLPDGLMRATD-VMIAGKVAVICGYGDVGKGCAAAMKTAGARVIVTE 292
TKSKFDNLYGCRESLVDGIKRATD-VMLAGKVAVVAGYGDVGKGCAAALRGMGARVLVTE 246
TKSKFDNLYGCRESLIDGIKRATD-VMIAGKVAVVAGYGDVGKGCAQALRGFGARVIITE 243
TKSKFDNLYGCRESLIDGIKRATD-VMIAGKVAVVAGYGDVGKGCAQALRGFGARVIITE 243
TKQKYDNIYGCRHSGIHGFFNGGDGFLIGGKTVVVIGYGNVGKGVAQGFRGQGAKVKITE 298
CKTKFDNNYGARYSSVDGMHRGVEGVLLGGRQVVVIGYGNTGKGVCMGFRGAGAIVKVCE 298
IDPICAIQAVMEGFNVVTLDEIVDKGDFFITCTGNVDVIKLEHLLKMKNNAVVGNIGHFD 347
IDPICALQALMEGLQVLTLEDVVSEADIFVTTTGNKDIIMVDHMRKMKNNAIVCNIGHFD 352
IDPINALQAAMEGYQVVTMEDASHIGQVFVTTTGCRDIINGEHFINMPEDAIVCNIGHFD 306
IDPINALQAAMEGYEVTTMDEACKEGNIFVTTTGCVDIILGRHFEQMKDDAIVCNIGHFD 303
IDPINALQAAMEGYEVTTMDEACQEGNIFVTTTGCIDIILGRHFEQMKDDAIVCNIGHFD 303
IDPICALQAAMEGFDVVLLEDVLETADIFISCTGGIDNITVEHMKRMKNNAILGNIGQGD 358
ADPICALQCVMDGYQVVLLEDVVETADIFVTATGCIEVIRLHHVRRMKEGAILGNIGQGD 358
DEIQVNELFNYKGIHIENVKPQVDRITLPNG-NKIIVLARGRLLNLGCATGHPAFVMSFS 406
NEIDMLGLETYPGVKRITIKPQTDRWVFPETKAGIIVLAEGRLMNLGCATGHPSFVMSCS 412
IEIDVAWLKA-NAKECINIKPQVDRYLLSSG-RHVILLANGRLVNLGCATGHSSFVMSCS 364
VEIDVKWLNE-NAVEKVNIKPQVDRYWLKNG-RRIILLAEGRLVNLGCAMGHPSFVMSNS 361
VEIDVKWLNE-NAVEKVNIKPQVDRYRLKNG-RRIILLAEGRLVNLGCAMGHPSFVMSNS 361
QEIQMAELHKVPGLEITNIKPGSDYFKFPDTGKGVIILAFGRLYNLGCANGHPAFVMSAS 418
REILIHEILTDPNLEVTEVRKNVHYYKFKDLNKGVIILSYGRLYNLGCANGHPSLVMSMS 418
FCNQTFAQLDLWQNKD------------TNKYENKVYLLPKHLDEKVALYHLKKLNASLT 454
FTNQVIAQLELWNEKA------------SGKYEKKVYVLPKHLDEKVALLHLGKLGARLT 460
FSNQVLAQIALFKSNDKSFREKHIEFQKTGPFEVGVHVLPKILDEAVAKFHLGNLGVRLT 424
FTNQVMAQIELWTHP--------------DKYPVGVHFLPKKLDEAVAEAHLGKLNVKLT 407
FTNQVMAQIELWTHP--------------DKYPVGVHFLPKKLDEAVAEAHLGKLNVKLT 407
FTDQALCLLELWKNRD------------NDTYGKCINKLPKTLDETVARYHLKALNVKLT 466
FTTQFFALSQLLENK-------------GKFDNKIHKMPKKLDEMVARYHLEFINAKLT 464
ELDDNQCQFLGVNKSGPFKSNEYRY 479
KLSKDQSDYVSIPIEGPYKPPHYRY 485
KLSKVQSEYLGIPEEGPFKADHYRY 449
KLTEKQAQYLGMPINGPFKPDHYRY 432
KLTEKQAQYLGMSCDGPFKPDHYRY 432
VPTAKQCAYLGIKPEGPFKEDGYHY 491
VLTDRQCEFLGIDKDGPYKHEDYKY 489

B.

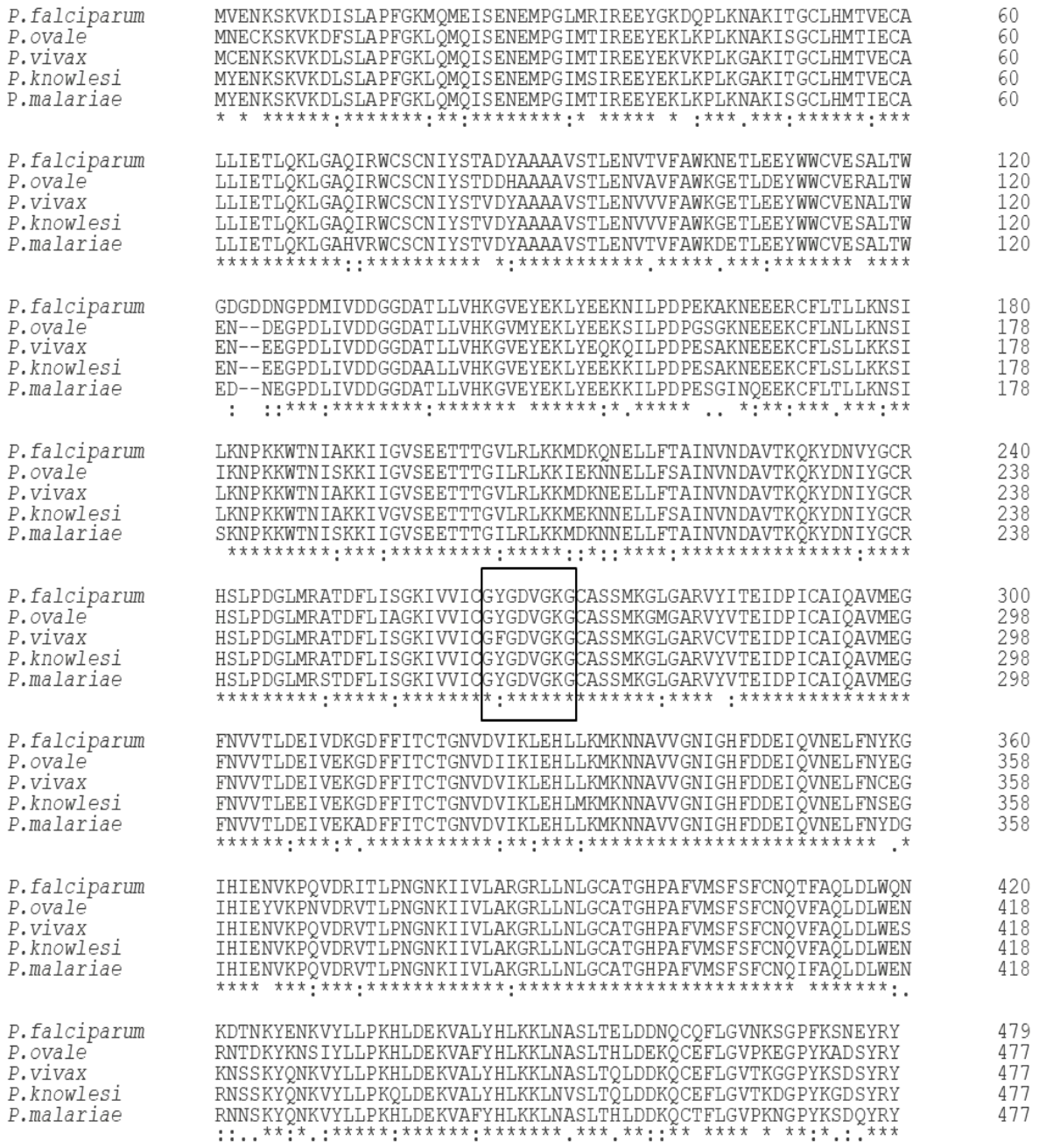

Fig 4.1 Amino acid sequence alignments of *Plasmodium falciparum* S-adenosylhomocysteine hydrolase (*Pf*SAHH, P50250) with the SAHH orthologs present in different species. A. *Plasmodium falciparum* S-adenosylhomocysteine hydrolase sequence was aligned with SAHH from *A. thaliana* (Q23255), *S. cerevisiae* (P39954), *M. musculus* (P50247), and *H. sapiens* (P23526), *B. bovis* (A7AW30), and *T. annulata* (Q4UCR8). **B.** Sequence alignments of *Plasmodium falciparum* (PF3D7_0520900.1), *P. ovale* (POWCR01_100016100), *P. vivax* (PVP01_1013000), *P. knowlesi* (PKNH_1012000), *P. malariae* (PmUG01_10023700) that infect humans. The alignments were conducted using ClustalW (Thompson *et al.,* 2003). The boxes in (A) and (B) indicate the conserved copper binding GYGDVGKG **(GXGXXGXG)** motif. The blue line in **A** shows the NAD/H binding site. Conserved residues are indicated by *****, while: represents a conserved and **.** indicates a semi-conserved amino acid substitution.

```
PF3D7_0520900.1-p1            HSLPDGLMRATDFLISGKIVVICGYGDVGKGCASSMKGLGARVYITEIDPICAIQAVMEG   300
Pf7G8-2_000140100.1-p1        HSLPDGLMRATDFLISGKIVVICGYGDVGKGCASSMKGLGARVYITEIDPICAIQAVMEG   300
Pf7G8_050026100-t41_1-p1      HSLPDGLMRATDFLISGKIVVICGYGDVGKGCASSMKGLGARVYITEIDPICAIQAVMEG   300
PfCD01_050027200-t41_1-p1     HSLPDGLMRATDFLISGKIVVICGYGDVGKGCASSMKGLGARVYITEIDPICAIQAVMEG   300
PfTG01_050026000-t41_1-p1     HSLPDGLMRATDFLISGKIVVICGYGDVGKGCASSMKGLGARVYITEIDPICAIQAVMEG   300
PfSN01_050026000-t41_1-p1     HSLPDGLMRATDFLISGKIVVICGYGDVGKGCASSMKGLGARVYITEIDPICAIQAVMEG   300
PfDd2_050025800-t41_1-p1      HSLPDGLMRATDFLISGKIVVICGYGDVGKGCASSMKGLGARVYITEIDPICAIQAVMEG   300
PfGA01_050025300-t41_1-p1     HSLPDGLMRATDFLISGKIVVICGYGDVGKGCASSMKGLGARVYITEIDPICAIQAVMEG   300
PfGB4_050026800-t41_1-p1      HSLPDGLMRATDFLISGKIVVICGYGDVGKGCASSMKGLGARVYITEIDPICAIQAVMEG   300
PfGN01_050025800-t41_1-p1     HSLPDGLMRATDFLISGKIVVICGYGDVGKGCASSMKGLGARVYITEIDPICAIQAVMEG   300
PfHB3_050025900-t41_1-p1      HSLPDGLMRATDFLISGKIVVICGYGDVGKGCASSMKGLGARVYITEIDPICAIQAVMEG   300
PfIT_050026100-t41_1-p1       HSLPDGLMRATDFLISGKIVVICGYGDVGKGCASSMKGLGARVYITEIDPICAIQAVMEG   300
PfKE01_050025300-t41_1-p1     HSLPDGLMRATDFLISGKIVVICGYGDVGKGCASSMKGLGARVYITEIDPICAIQAVMEG   300
PfKH01_050026200-t41_1-p1     HSLPDGLMRATDFLISGKIVVICGYGDVGKGCASSMKGLGARVYITEIDPICAIQAVMEG   300
PfKH02_050026400-t41_1-p1     HSLPDGLMRATDFLISGKIVVICGYGDVGKGCASSMKGLGARVYITEIDPICAIQAVMEG   300
PfML01_050025800-t41_1-p1     HSLPDGLMRATDFLISGKIVVICGYGDVGKGCASSMKGLGARVYITEIDPICAIQAVMEG   300
PfNF135_050026400.1-p1        HSLPDGLMRATDFLISGKIVVICGYGDVGKGCASSMKGLGARVYITEIDPICAIQAVMEG   300
PfNF166_050026000.1-p1        HSLPDGLMRATDFLISGKIVVICGYGDVGKGCASSMKGLGARVYITEIDPICAIQAVMEG   300
PfNF54_050025100.1-p1         HSLPDGLMRATDFLISGKIVVICGYGDVGKGCASSMKGLGARVYITEIDPICAIQAVMEG   300
PfSD01_050025800-t41_1-p1     HSLPDGLMRATDFLISGKIVVICGYGDVGKGCASSMKGLGARVYITEIDPICAIQAVMEG   300
                              ************************************************************
```

Fig 4.2 Alignments of amino acid sequence of SAHH from 20 *Plasmodium falciparum* isolates identified in PlasmoDB. A section of amino acid sequences of SAHH from 20 *Plasmodium falciparum* isolates were aligned using ClustalW (Thompson *et al.,* 2003). The box indicates the conserved GYGDVGKG motif. All the amino acid residues indicated by * are conserved among the *Plasmodium falciparum* isolates.

4.2.3 An assessment of the sequence alignment of *Plasmodium* species that infect humans, mice, birds, and monkeys

The amino acid sequences of SAHH belonging to *Plasmodium* spp which infects humans, mice, birds, and monkeys were identified in PlasmoDB. Seventeen species were aligned, and Fig 4.3 shows a conserved GYGDVGKG (GXGXXGXG) motif in 12 species while five species all of *Plasmodium vivax* origin showed a GFGDVGKG (GXGXXGXG) region indicated by a small box within a large one (Fig 4.3). The difference in the motifs is due to what is stated in 4.1.1.

```
PCHAS_1236200.1-p1            HSLPDGLMRATDFMISGKIVVICGYGDVGKGCASAMKGLGARVYVTEVDPICAIQAVMEG   299
PBANKA_1235600.1-p1           HSLPDGLMRATDFLISGKIVVICGYGDVGKGCASAMKGLGARVYVTEIDPICAIQAVMEG   299
PY02893-t26_1-p1              HSLPDGLMRATDFLISGKIVVICGYGDVGKGCASAMKGLGARVYVTEIDPICAIQAVMEG   299
PY17X_1239000.1-p1            HSLPDGLMRATDFLISGKIVVICGYGDVGKGCASAMKGLGARVYVTEIDPICAIQAVMEG   299
CDU19552.1                    HSLPDGLMRATDFLISGKIVVICGYGDVGKGCASAMKGLGARVYVTEIDPICAIQAVMEG   299
WBY59424.1                    HSLPDGLMRATDFLISGKIVVICGYGDVGKGCASAMKGLGARVYVTEIDPICAIQAVMEG   299
PF3D7_0520900.1-p1            HSLPDGLMRATDFLISGKIVVICGYGDVGKGCASSMKGLGARVYITEIDPICAIQAVMEG   300
Pf7G8_050026100-t41_1-p1      HSLPDGLMRATDFLISGKIVVICGYGDVGKGCASSMKGLGARVYITEIDPICAIQAVMEG   300
PfKH01_050026200-t41_1-p1     HSLPDGLMRATDFLISGKIVVICGYGDVGKGCASSMKGLGARVYITEIDPICAIQAVMEG   300
PCYB_102090-t26_1-p1          HSLPDGLMRATDFLISGKIVVICGYGDVGKGCASSMKGLGARVYVTEIDPICAIQAVMEG   298
PVL_100014900-t42_1-p1        HSLPDGLMRATDFLISGKIVVICGFGDVGKGCASSMKGLGARVYVTEIDPICAIQAVMEG   298
PVP01_1013000.1-p1            HSLPDGLMRATDFLISGKIVVICGFGDVGKGCASSMKGLGARVCVTEIDPICAIQAVMEG   298
CAI7720926.1                  HSLPDGLMRATDFLISGKIVVICGFGDVGKGCASSMKGLGARVCVTEIDPICAIQAVMEG   298
CAG9474863.1                  HSLPDGLMRATDFLISGKIVVICGFGDVGKGCASSMKGLGARVCVTEIDPICAIQAVMEG   298
PVX_080200.1-p1               HSLPDGLMRATDFLISGKIVVICGFGDVGKGCASSMKGLGARVCVTEIDPICAIQAVMEG   298
PGAL8A_00068200.1-p1          HSLPDGLMRSTDFLISGKIVVICGYGDVGKGCASSMKGLGARVYVTEIDPICAIQAIMEG   298
PRELSG_1010900.1-p1           HSLPDGLMRSTDFLISGKIVVICGYGDVGKGCASSMKGLGARVYVTEIDPICAIQAVMEG   298
                              *********:***:**********:********:******** :**:********:***
```

Fig 4.3 Alignments of amino acid sequence of SAHH from 17 *Plasmodium* spp selected from PlasmoDB. A section of the amino acid sequence of SAHH from 17 *Plasmodium* spp that infect humans, mice, birds, and monkeys were aligned using ClustalW (Thompson *et al*, 2003). The large and small boxes indicate conserved copper binding GYGDVGKG and GFGDVGKG (GXGXXGXG) motifs, respectively. Conserved Residues are indicated by *, while: represents a conserved and **.** indicates a semi-conserved amino acid substitution.

4.2.4 Selection of immunogenic *Pf*SAHH peptides

Martin *et al.,* 2009a report that a protein-specific antibody approach is recommended in the structural comparison between the recombinant and the native proteins (Martin *et al.,* 2009a). To achieve this, peptides from the *Pf*SAHH sequence were identified and selected using the Predict7 program (Carmenes *et al.,* 1989). The following peptides were identified after an analysis of *Pf*SAHH by Predict7; “MVENKSKVKD”, a peptide that ranges from amino acid residue 1 to 10, “QMEISENEMPGLMRIREEYGKDQPLKNAKIT” (20-50) (Fig 4.4). When the two peptide sequences were subjected to a BLASTp search against *Plasmodium*, *Homo sapiens*, *Trypanosoma*, *Mus musculus*, and *Toxoplasma* proteomes, no significant matches were observed (data not shown). This implies that antibodies generated from these peptides would be specific to the *Pf*SAHH protein and will not recognize any other protein from the four organisms. This computational analysis was done with the intention to generate peptides which could be coupled to a carrier and used for the generation of anti-peptide antibodies. Unfortunately, this experiment was not conducted.

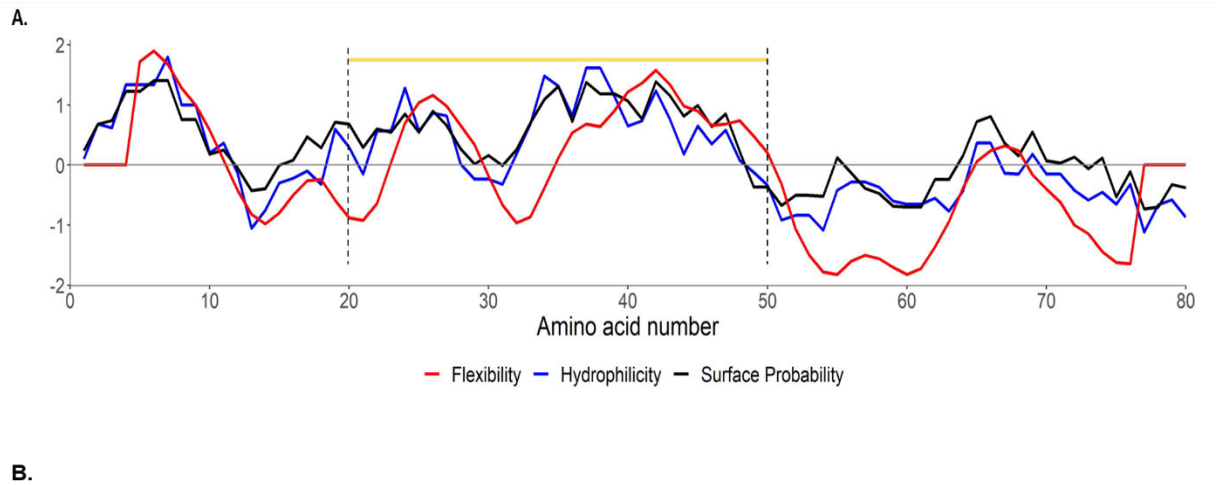

Fig 4.4 Prediction of immunogenic epitope for *Plasmodium falciparum* S-adenosylhomocysteine hydrolase. A. The flexibility, hydrophilicity, and surface probability for the *Pf*SAHH protein sequence were plotted on the horizontal axis for the *Pf*SAHH protein sequence, with the yellow line indicating the peptide with amino acid residues from 20 to 50. **B.** 20-50 peptide on the surface of *Pf*SAHH.

4.2.5 Prediction of *Pf*SAHH transmembrane spanning regions

DTU-TMHMM server v 2.0 was used to predict whether *Pf*SAHH has any transmembrane regions (Kahsay *et al.,* 2005). The findings show the protein is in the cytosol with no transmembrane-spanning regions (results not shown). There is a possibility of the protein being present in organelles, but the analysis did not predict organelle location. The prediction probability of occurrence of the transmembrane is above 1.

4.2.6 Analyses of the predicted domains, motifs, and other features of *Pf*SAHH

Using the Simple Modular Architecture Research Tool (SMART software) (Letunic *et al.,* 2004), domains belonging to *Pf*SAHH were predicted. Fig 4.5 A shows the AdoHcyase domain responsible for modulating the activity of different methyltransferases. Another domain of importance is the AdoHcyase_NAD, characterized by the glycine-rich region implicated in the NAD binding, which makes the enzyme active (Fig 4.5 B and D). The 2-Hacid_dh_c domain is a NAD-dependent 2-hydroxy-acid dehydrogenase that is specific to the D-isomer of its substrate (Fig 4.5 D). IIvN domain of *Pf*SAHH in Fig 4.5 D is related to one found in Ketoacid reductoisomerase which catalyzes the conversion of acetohydroxy acids into dihydroxy valerates in the second step of the biosynthetic pathway for the essential branched-chain amino acids such as valine, leucine, and isoleucine.

A.

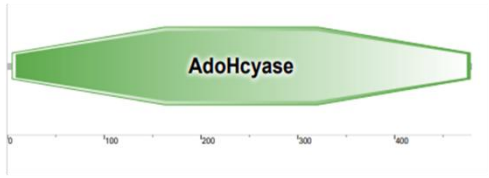

B.

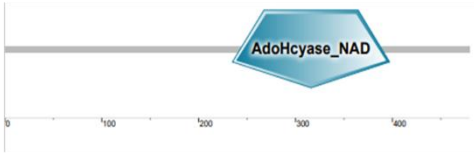

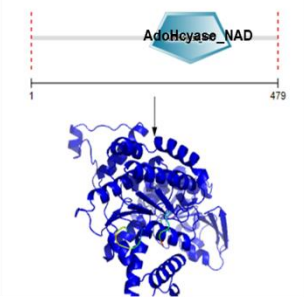

C.

Name	Start[a]	End[b]	E-value
AdoHcyase	5	478	9.7×10^{-287}
AdoHcyase_NAD	235	397	6.85×10^{-100}

a and b indicate the position of an amino acid residue

D.

Name	Start	End	E-value
Pfam: AdoHcyase	5	478	3.4×10^{-133}
Pfam:2-Hacid_dh_c	223	346	9.9×10^{-9}
Pfam: AdoHcyase_NAD	235	397	2.9×10^{-83}
Pfam: IIvN	254	341	0.0000015

Fig 4.5 Predicted domains, motifs, and features of *Pf*SAHH. SMART annotation of *Pf*SAHH protein. **A.** AdoHcyase domain **B.** AdoHcyase_NAD domain **C.** Domains of *Pf*SAHH and their positions, and confidence of prediction. **D.** other features predicted by SMART software (Letunic *et al.,* 2021).

4.2.7 Comparison between the *Pf*SAHH and *Hs*SAHH crystal structures using a layover method in PyMOL

The *Pf*SAHH (Fig 4.6 A) and *Hs*SAHH (Fig 4.6 B) crystal structures were selected from the UniProt database (Tanaka *et al*., 2004, Yang *et al.,* 2003) and visualized using PyMOL (http://www.pymol.org/mol). Fig 4.6 C shows an overlay of *Pf*SAHH and *Hs*SAHH. The *Hs*SAHH has 47 of its amino acid residues deleted compared to the *Pf*SAHH structure (Fig 4.7 and 4.8). The differences in the structure

are indicated by a box (Fig 4.7 A) and the same segment is colored red in Fig 4.7 B. This indicates a 10% difference between the *Hs*SAHH and *Pf*SAHH amino acid sequences.

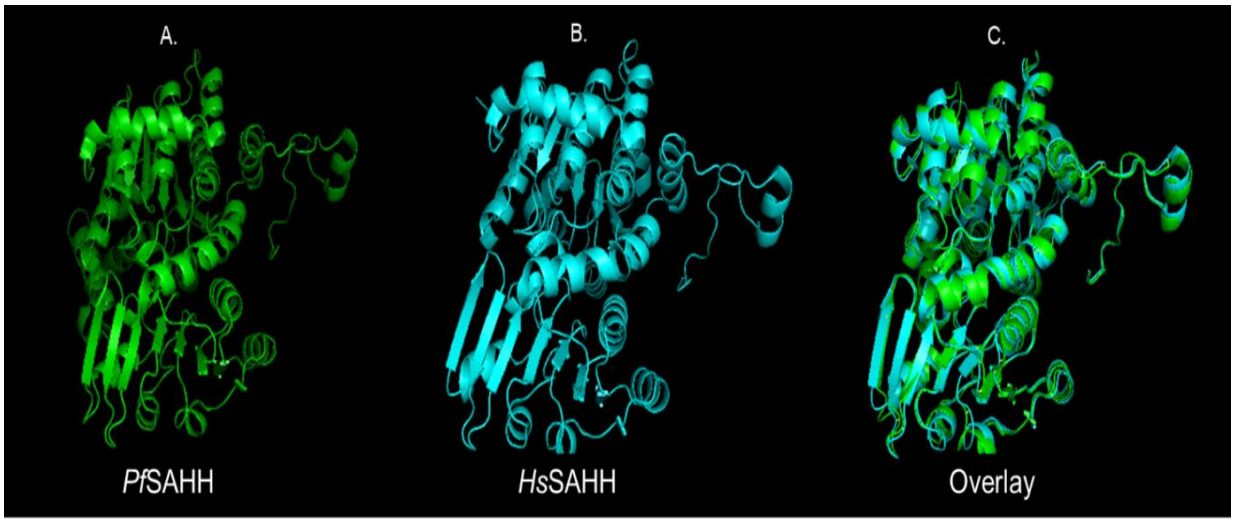

Fig 4.6 Chain A of *Pf*SAHH and *Hs*SAHH structures. A. *Pf*SAHH structure (Tanaka *et al.,* 2004) and **(B).** *Hs*SAHH structure (Yang *et al.,* 2003) obtained from protein data bank (PDB) (https://www.rcsb.org) **C.** An overlay structure of **(A)** and **(B)** superimposed using PyMOL software (http://www.pymol.org/pymol)

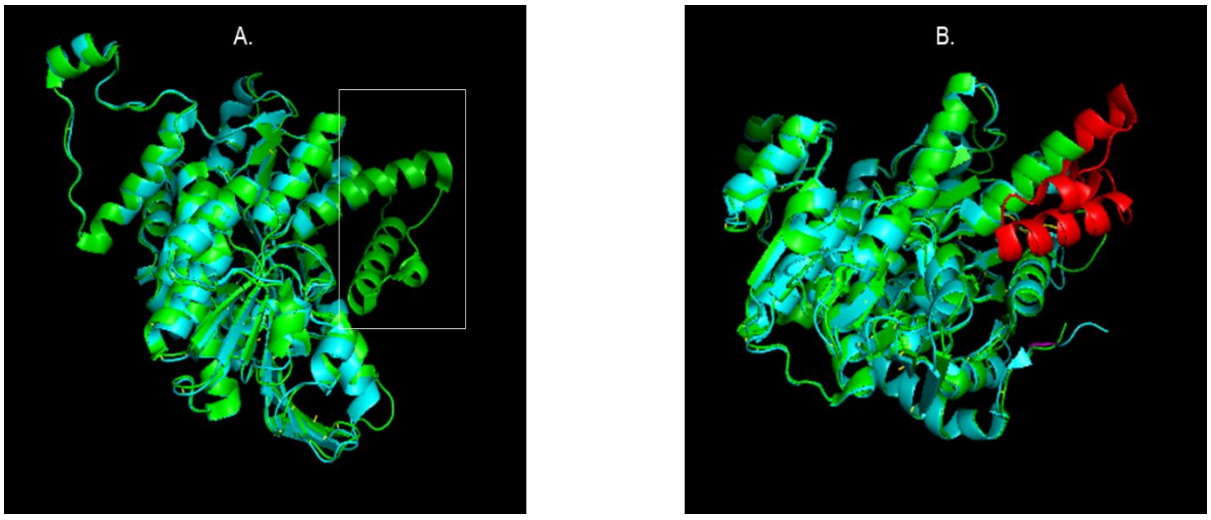

Fig 4.7 Overlay of *Pf*SAHH and *Hs*SAHH structures. *A.* An overlay structure (*Pf*SAHH (Tanaka *et al.,* 2004) and *Hs*SAHH (Yang *et al.,* 2003) obtained from PDB) with the box indicating a segment of amino acid residues that are deleted in the *Hs*SAHH sequence and in **(B),** the deleted amino acids on the *Hs*SAHH structure are shown in red and those missing in *Pf*SAHH are indicated in magenta. The structures were annotated using PyMOL software (http://www.pymol.org/pymol).

```
P.falciparum      -MVENKSKVKDISLAPFGKMQMEISENEMPGLMRIREEYGKDQPLKNAKITGCLHMTVEC    59
H.sapiens         MSDKLPYKVADIGLAAWGRKALDIAENEMPGLMRMRERYSASKPLKGARIAGCLHMTVET    60
                     :   ** **.** :*:  ::*:**********:**.*. .:***.*:*:********
P.falciparum      ALLIETLQKLGAQIRWCSCNIYSTADYAAAAVSTLENVTVFAWKNETLEEYWWCVESALT    119
H.sapiens         AVLIETLVTLGAEVQWSSCNIFSTQDHAAAAIA-KAGIPVYAWKGETDEEYLWCIEQTLY    119
                  *:***** .***:::*.****:** *:****::    .: *:***.** *** **:*.:*
P.falciparum      WGDGDDNGPDMIVDDGGDATLLVHKGVEYEKLYEEKNILPDPEKAKNEEERCFLTLLKNS    179
H.sapiens         FKDGP---LNMILDDGGDLTNLIHTK-----------------------------------    142
                  : **      :**:***** * *:*.
P.falciparum      ILKNPKKWTNIAKKIIGVSEETTTGVLRLKKMDKQNELLFTAINVNDAVTKQKYDNVYGC    239
H.sapiens         -------YPQLLPGIRGISEETTTGVHNLYKMMANGILKVPAINVNDSVTKSKFDNLYGC    195
                        : ::   * *:******** .* **  :. * . ******:***.*:**:***
P.falciparum      RHSLPDGLMRATDFLISGKIVVICGYGDVGKGCASSMKGLGARVYITEIDPICAIQAVME    299
H.sapiens         RESLIDGIKRATDVMIAGKVAVVAGYGDVGKGCAQALRGFGARVIITEIDPINALQAAME    255
                  *.** **: ****.:*:**:.*:.********** .:::*:**** ******* *:**.**
P.falciparum      GFNVVTLDEIVDKGDFFITCTGNVDVIKLEHLLKMKNNAVVGNIGHFDDEIQVNELFNYK    359
H.sapiens         GYEVTTMDEACQEGNIFVTTTGCIDIILGRHFEQMKDDAIVCNIGHFDVEIDVKWL-NEN    314
                  *::*.*:**  ::*:::*:* ** :*:*  .*: :**::*:* ****** **:*: * * :
P.falciparum      GIHIENVKPQVDRITLPNGNKIIVLARGRLLNLGCATGHPAFVMSFSFCNQTFAQLDLWQ    419
H.sapiens         AVEKVNIKPQVDRYRLKNGRRIILLAEGRLVNLGCAMGHPSFVMSNSFTNQVMAQIELWT    374
                  .:.  *:******  * **.:**:**.***:***** ***:**** ** **.:**::**
P.falciparum      NKDTNKYENKVYLLPKHLDEKVALYHLKKLNASLTELDDNQCQFLGVNKSGPFKSNEYRY    479
H.sapiens         HPD--KYPVGVHFLPKKLDEAVAEAHLGKLNVKLTKLTEKQAQYLGMSCDGPFKPDHYRY    432
                  : *  **   *::***:*** **  ** ***..**:* ::*.*:**:. .**** :.***
```

Fig 4.8 Alignment of amino acid sequence of SAHH from *P. falciparum* and *H. sapiens*. The amino acid sequence of SAHH from *P. falciparum* and *H. sapiens* were aligned using ClustalW (Thompson *et al.,* 2003). Conserved Residues are indicated by *, while: represents a conserved and **.** indicates a semi-conserved amino acid substitution.

4.2.8 Prediction of Copper binding motif GYGDVGKG (GXGXXGXG) on the *Pf*SAHH structure

According to Bethin *et al.,* 1995, the S-adenosylhomocysteine hydrolase enzyme plays a role in intracellular copper metabolism. *In-silico* determination of the copper-binding site was conducted using **S**olvent accessibility-based **P**rotein-**P**rotein **I**nterface i**DE**ntification and **R**ecognition (SPPIDER) software (Porollo *et al.,* 2007), and the sites were annotated and visualized in JMOL (Jmol development team, 2016. *Jmol*, Available at: (http://jmol.sourceforge.net/). Fig 4.9 A, B, and C show the predicted binding site (in blue color). When annotated in JMOL, a **GYGDVGKG (GXGXXGXG)** motif is situated between amino acid residues 264 and 271.

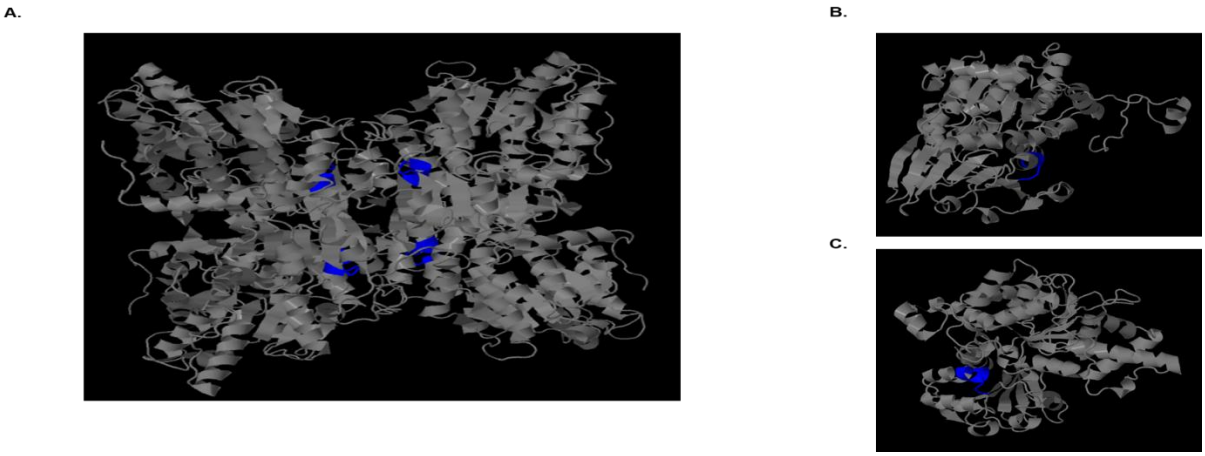

Fig 4.9 Predicted copper-binding site (GYGDVGKG) on *Pf*SAHH model. The *Pf*SAHH sequence was processed by Solvent accessibility-based Protein-Protein Interface iDEntification and Recognition (SPPIDER) software (Porollo *et al.,* 2007) and visualized in JMOL (Jmol development team, 2016. Jmol, Available at: (http://jmol.sourceforge.net/). **A.** *Pf*SAHH model homotetramer with copper binding sites indicated in blue and shown on each of the 4 chains. **B.** and **C.** different orientations of chain A of the *Pf*SAHH model illustrate the position of the copper-binding site.

4.2.9 Analyses of the NAD/H binding sites on the *Pf*SAHH structure

Exploration of the NAD/H binding sites on the *Pf*SAHH structure is important because the protein is a potential drug target against malaria. An *in-silico* experiment was performed using **S**olvent accessibility-based **P**rotein-**P**rotein **I**nterface i**DE**ntification and **R**ecognition (SPPIDER) software (Porollo *et al.,* 2007), to determine various binding sites including the binding sites for NAD/H. These were annotated and visualized in JMOL (Jmol development team, 2016. *Jmol*, Available at: (http://jmol.sourceforge.net/). Fig 4.10 shows the predicted binding sites which are shown in different colors. When viewed in Fig 4.11, amino acids 237-238, 283-292, 319-320, and 469-476, encompass the amino acid residues in the *Pf*SAHH sequence (235, 287, 288, 320, and 473) that have been reported to bind NAD/H (Singh *et al.,* 2016). Compared to the PDB structure with NAD/H (Tanaka *et al.,* 2004) the analyses from the present study revealed that only cysteine at position 263 was common with the predicted NAD/H binding sites by SPPIDER software.

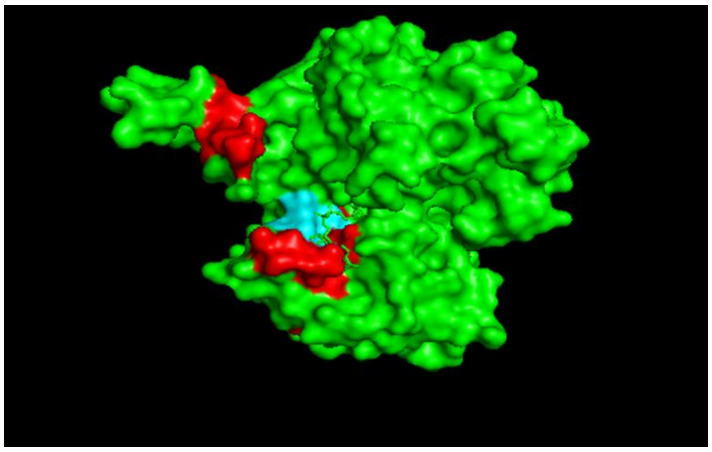

Fig 4.10 NAD/H predicted binding sites for the *Pf*SAHH model using SPPIDER software and viewed using PyMOL(http://www.pymol.org/pymol) The diagram shows the binding site of NAD/H and other ligands like copper shown in red and cyan, respectively.

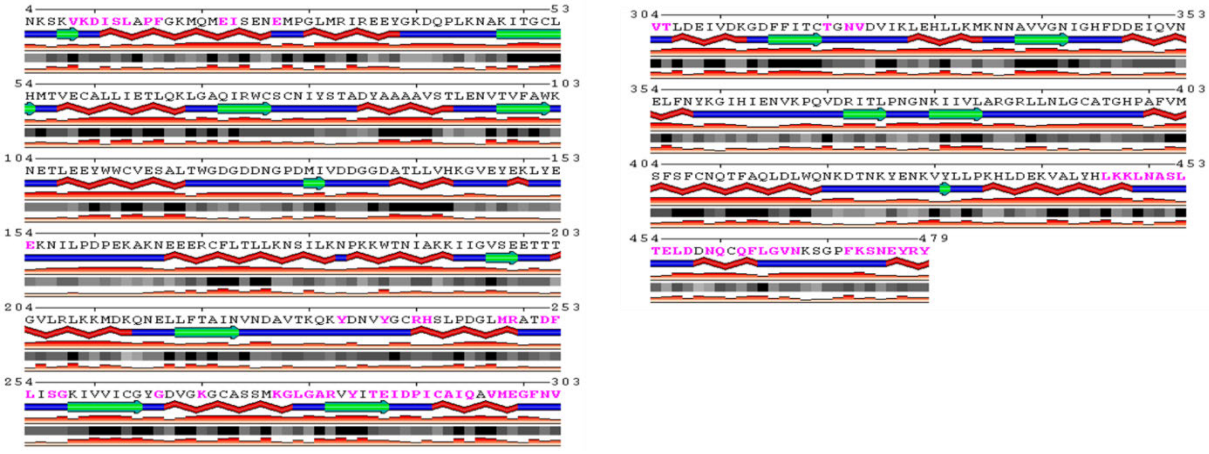

Fig 4.11 Prediction of NAD/H and other ligand binding sites of *Pf*SAHH structure using accurate sequence-based prediction of relative Solvent AccessiBiLitiEs (SABLE) secondary structure and transmembrane domains. The binding sites are represented by colored amino acids (pink). The diagram also indicates buried (blue) and accessible (red) amino acids (Adamczak *et al.,* 2004).

4.2.10 Assessment of the crystal structure of *Pf*SAHH using three-dimensional profiles

NMR and X-ray structures all have problems that are supposed to be solved by various methods that determine the quality of such structures before they can be used in docking experiments (Agnihotry *et al.,* 2022). Therefore, the VERIFY3D program was utilized to establish whether the structure was correct and not mistraced or wrongly folded. Fig 4.12 shows that 72.79% of the residues in *Pf*SAHH had an average 3D-1D score ≥ 0.1 which is near the 80% limit score. These results imply that the structure is good and can be used in molecular docking experiments.

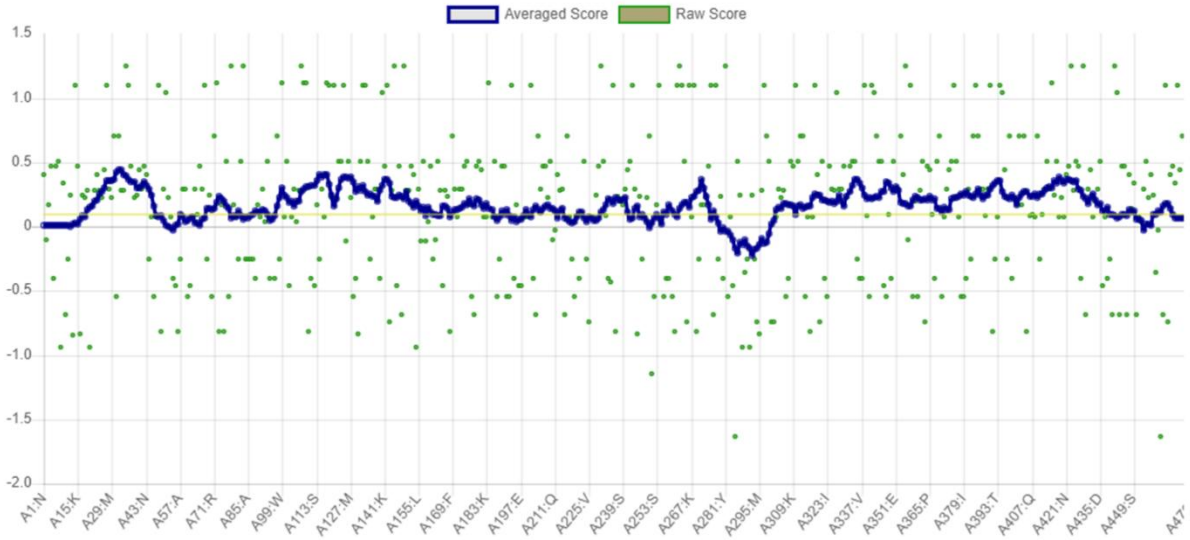

Fig 4.12 Validation of the crystal structure of *Pf*SAHH using VERIFY3D. The crystal structure of *Pf*SAHH (1v8b.pdb; Tanaka *et al.,* 2004) was obtained from a protein data bank (PDB) with 72.79% of the residues that have averaged 3D-1D score ≥ 0.1.

4.2.11 Determination of interacting partners of *Pf*SAHH using STRING Database

*Pf*SAHH interacts with various proteins to perform different functions inside the malaria parasite as shown in STRING analysis. The evidence is based on the experimental and data mining. A STRING database was evaluated to find out the interacting partners of *Pf*SAHH. Fig 4.13 shows that *Pf*SAHH interacts with many proteins that carry out notable functions that are necessary for the survival of the parasite. Table 4.1 provides partners to *Pf*SAHH determined by various methods. Those established through co-expression are S-adenosylmethionine synthase and triosephosphate isomerase which are involved in catalyzing the formation of s-adenosylmethionine and play a role in the glycolytic pathway, respectively. Adenosine deaminase which catalyzes the deamination of adenosine and *Pf*PMT which converts norepinephrine to epinephrine has been determined to be associated with *Pf*SAHH through the co-expression method (Table 4.1). The association of the rest of the partners to *Pf*SAHH in Table 4.1 was determined using text mining. These proteins are involved in various functions such as maintenance of translational

fidelity, promotion of cell growth, proliferation, and differentiation, including being involved in the purine salvage pathway.

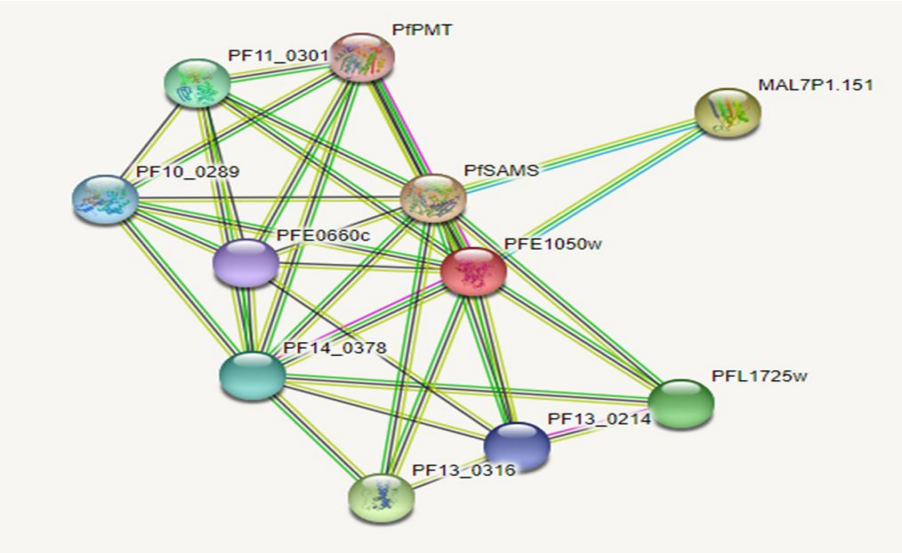

Fig 4.13 STRING database prediction of interacting partners of *Pf*SAHH (PFE1050w). The intracellular proteins that interact with *Pf*SAHH are shown in the diagram. The numbers/labels are expanded in Table 4.1 (https://string-db.org/). The lines in different colors connecting proteins signify the type of method used to determine the association of various proteins to *Pf*Grx1. Cyan – curated database; Purple – experimentally determined; Green – gene neighborhood; Red – gene fusion; Deep blue – co-occurrence; Lime green – text mining; Black – co-expression; Light blue – protein homology.

Table 4.1 Prediction of PFE1050w/PF3D7_0520900 interacting partners using the STRING database.

Predicted interacting partners of PFE1050w (*Pf*SAHH)			
STRING database name	**The current number/name of protein**	**Protein name**	**The method used in determining the interacting partners**
PfSAMS	PfSAMS	S-adenosylmethionine synthase	Neighborhood gene fusion, Coexpression, and text mining
MAL7P1.151	PF3D7_0727300	Modification methylase, putative (706aa)	Databases, and text mining
Pf13_0316	PF3D7_1358800	40s ribosomal proteins 13, putative	Textmining
PfL1725w	PF3D7_1235700	ATP synthase	Textmining
PF11_0301	PF3D7_1129000	Spermidiene synthase	Textmining
PF10_0289	PF3D7_1029600	Adenosine deaminase	Coexpression
PF13_0214	PF3D7_1338300	Uncharacterized protein, elongation factor 1-gamma, putative (411aa)	Coexpression, text mining
PFE0660c	PF3D7_0513300	Uncharacterized protein; purine nucleotide phosphorylase, (245aa)	Text mining
PfPMT	PF3D7_1343000	Uncharacteracterized protein phosphoethanolamine N-methyltransferase	Coexpression

Note: That a different pattern of interactions may be obtained if the analysis was done a year later, due to the generation of new data.

4.2.12 The amplification of *Pf*SAHH

The *Pf*SAHH was amplified through colony PCR using Taq polymerase after its *in-silico* analyses. Fig 4.14, lane 2 shows four bands of the whole plasmid representing nicked, linear, supercoiled, and circular, single-stranded plasmid DNA. A PCR product with the expected 1748 bp is shown in lanes 3 and 4. The difference in the intensity of the bands in lanes 3 and 4 is due to the variation in the dNTPs used in the reactions. Ext. dNTPs had a greater yield of amplicons (lane 3). A control without the template was run in lane 5 and shows no band (Fig 4.14).

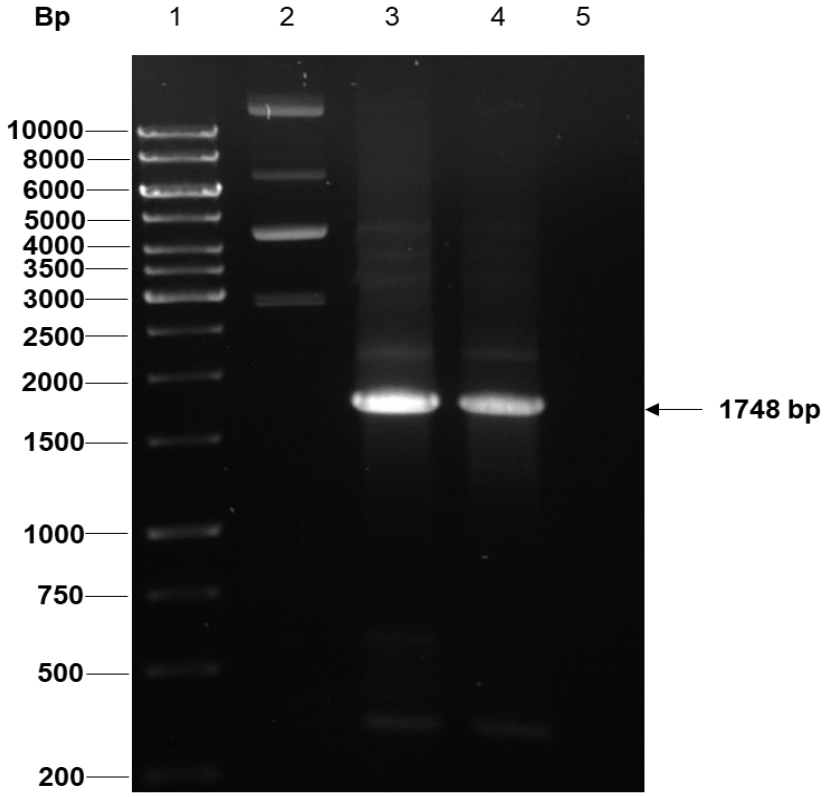

Fig 4.14 Agarose gel of the PCR product of *Pf*SAHH gene from the bacterial colony. The *Pf*SAHH gene was amplified from one pET 100/D-TOPO r*Pf*SAHH plasmid-containing bacterial colony and resolved on a 1% (w/v) agarose gel containing ethidium bromide. Lane 1, DNA ladder; Lane 2, Isolated plasmid (SAHH), Lane 3, PCR product using 2.5 mM dNTPs; Lane 4, PCR product using 10 mM dNTPs; Lane 5, Control without the template. The arrow on the shows a ~1748 bp amplicon of *Pf*SAHH.

4.2.13 Restriction endonuclease digestion of *Pf*SAHH pET100/TOPO expression plasmid

The restriction endonuclease digestion of pET/TOPO expression plasmid harboring the *Pf*SAHH gene was performed using EcoRI and BamHI. Undigested and digested *Pf*SAHH samples were resolved on 1 % agarose gel (Fig 4.15). Lane 2 of Figure 4.15 shows four bands of undigested plasmid representing nicked, linear, supercoiled, and circular, single-stranded plasmid DNA. Single digests of plasmid with EcoRI and BamHI, respectively, show prominent bands of ~7000 bases in lanes 3 and 4. There is a faint band in both lanes 3 and 4 with ~5000 and ~4500 bases, respectively. Double digestion with EcoRI and BamHI in Tris-HCI/$MgCl_2$ buffer

yielded four bands in lane 6 corresponding to linearized DNA ~6000, two faint bands, and the expected band with ~1470 bp.

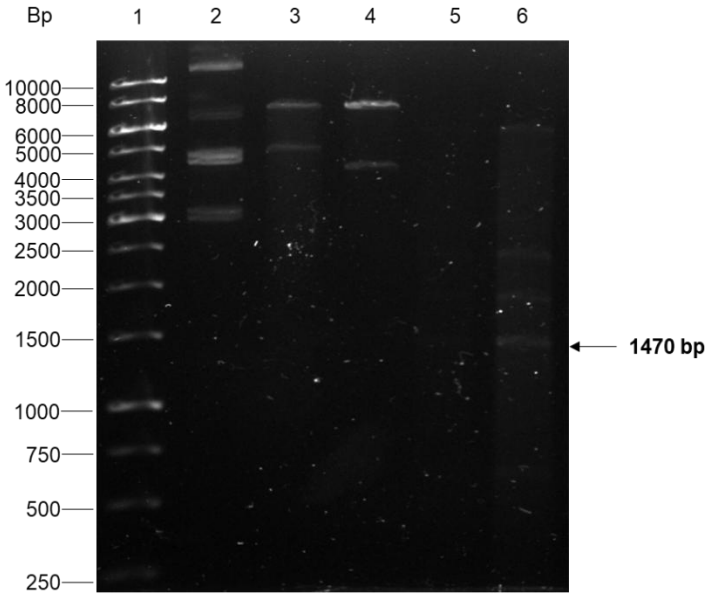

Fig 4.15 Digestion of *Pf*SAHH pET 100/D-TOPO expression plasmid (commercially synthesised)with EcoR1 and BamH1. Samples were all resolved on 1% (w/v) agarose gel containing ethidium bromide and viewed using UltraViolet light. Lane 1 DNA Ladder; The *Pf*SAHH pET 100/D-TOPO in Lane 2, was undigested, Lane 3, digested with EcoR1; Lane 4, digested with BamH1; Lane 5, digested with EcoR1 and BamH1 in Tris-HCL/$MgCl_2$ Buffer; Lane 6, digested with EcoR1 and BamH1 in Tris-HCL/$MgCl_2$. The arrow indicates a ~1470 bp insert.

4.2.14 Monitoring of the growth of *E. coli* BL 21 (DE3) expressing *Pf*SAHH

The *E. coli* BL 21 (DE3) bacteria were used for the expression of r*Pf*SAHH in Luria Broth (LB) media. The culture was grown at 37°C and induced with 1 mM IPTG for 4 hours. The bacterial growth was monitored at OD600 (Fig 4.16). The difference between the uninduced and induced cultures was marginal in the two colonies used for the experiment. This indicated that the bacteria grew exponentially (Fishov., 1995). Colony 1 was used in the subsequent experiments (Fig 4.16).

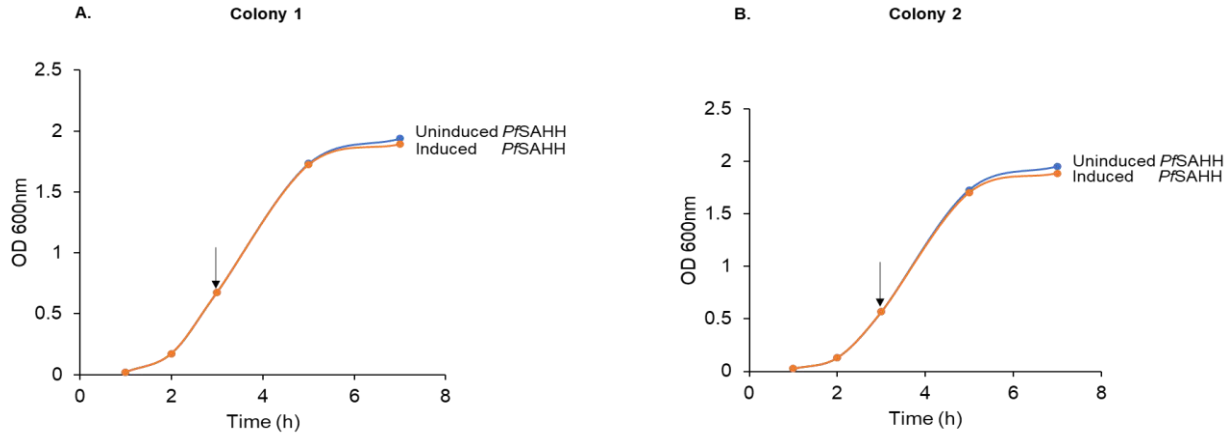

Fig 4.16 Bacterial growth curves for the expression of *Pf*SAHH in LB media without glucose at 37ºC induced with 1 mM IPTG for 4 hours. Two different *E. coli* colonies were selected and grown in the presence (induced) or absence (uninduced) of IPTG for 4 hours. Growth was monitored at OD600 nm. The arrow indicates the point at which IPTG was added.

4.2.15 Screening of the recombinant *Pf*SAHH

The bacteria utilized in Fig 4.16 were lysed and electrophoresed on a 12.5% reducing SDS-PAGE. Induced samples in lanes 4 and 6, all show a band of approximately ~116 kDa (Fig 4.17). The expected protein band of interest was supposed to be positioned between 45 and 66.2 kDa. The predicted molecular weight is 53.9 kDa. Purification of the r*Pf*SAHH grown under conditions in 4.2.4 did not show the preferred and expected band. Suggesting that the protein was not expressed and did not bind to the column during the affinity purification. In a quest to identify the protein with the right size, the expression conditions were changed, and the experiment was conducted as outlined in section 4.2.5.

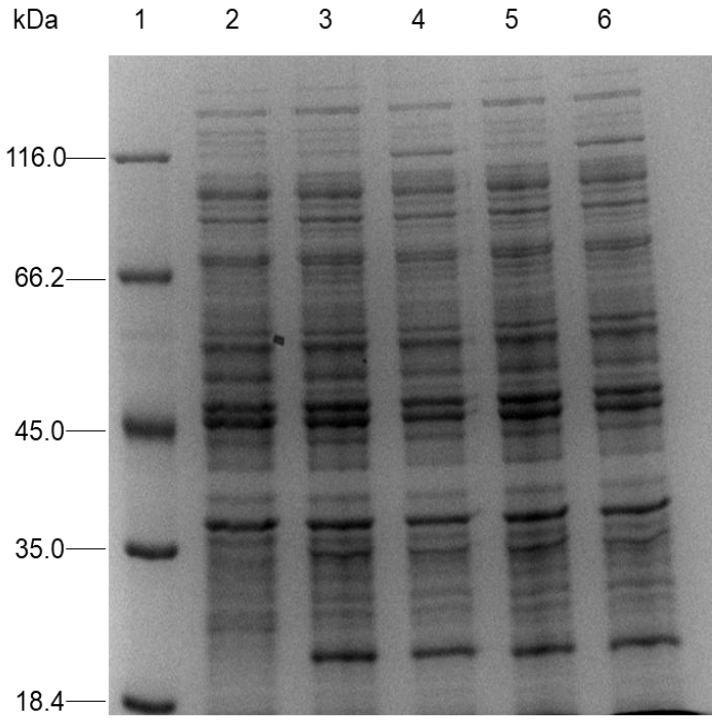

Fig 4.17 SDS-PAGE analysis of the expression of two colonies of *Pf*SAHH in LB media induced with 1 mM IPTG at 37ºC for 4 hours. Bacterial lysates from two cultures, each from a *separate E. coli* colony were electrophoresed on 12.5% reducing SDS-PAGE stained with Coomassie brilliant blue G250. Lane 1 Molecular weight marker; Lane 2 whole *E. coli* lysate (bacteria without a plasmid). Lanes 3, 5, uninduced, and lanes 4 and 6 induced samples taken after the addition of IPTG.

4.2.16 Recombinant expression of *Pf*SAHH

Following the failure to identify the band of interest in section 4.2.4, *E. coli* BL 21 (DE3) pLysS bacteria were later used for the expression of r*Pf*SAHH. The culture was grown at 20°C and induced with 1 mM IPTG for 16 hours. The bacteria were lysed and run on 15% reducing SDS-PAGE. A notable band (~116 kDa) was identified as earlier observed in 4.2.4. When r*Pf*SAHH was affinity purified, a band of approximately ~53 kDa was confirmed through western blot Fig 4.19 C. It was then concluded that the band of interest in Fig 4.18 was situated between ~45 and ~66.2 kDa.

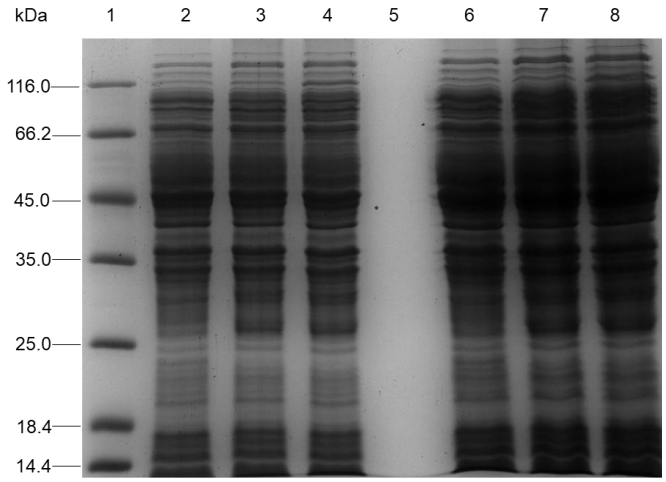

Fig 4.18 Recombinant expression of *Pf*SAHH in 2xYT media induced with 1 mM IPTG for 16 hours at 20°C. Bacterial lysates from one colony culture were electrophoresed on 15% reducing SDS-PAGE gel stained with Coomassie brilliant blue G250. Lane 1, molecular weight marker; Lanes 2, whole *E. coli* lysate; uninduced and induced samples of 5 µL were loaded in lanes 3 and 4, respectively; Lane 5, blank; Lanes 6, 7, and 8 were loaded with double the volume of the samples in lanes 2, 3, and 4.

4.2.6 Expression, purification, and characterization of recombinant *Pf*SAHH

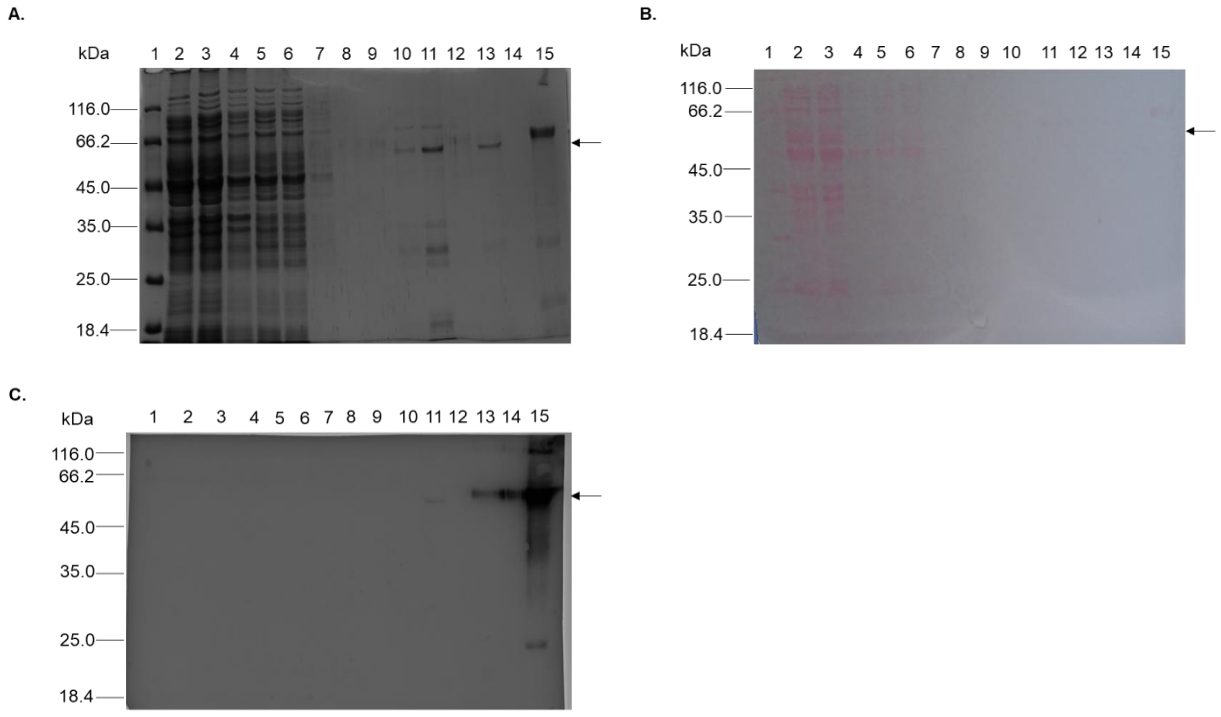

Fig 4.19 SDS-gel and western blot analysis of recombinantly expressed and purified *Pf*SAHH in pET100/D-TOPO. Samples from the expression of r*Pf*SAHH at 20°C, induced with 1 mM IPTG for 16 hours and affinity purified were electrophoresed on 15% reducing SDS-PAGE and stained with Coomassie brilliant blue G250 in **(A)**. **B**. and C indicate nitrocellulose stained with Ponceau S after western blot transfer and detection of r*Pf*SAHH using 4-Chloro-1-napthol, respectively. In **A**, **B**, and **C**, lanes were loaded with the following samples: Lane 1, molecular weight marker; Lane 2, uninduced whole lysate; Lane 3, induced whole lysate, Lane 4, pellet; Lane 5, unclarified supernatant; Lane 6, flow-through; Lane 7- 9, wash fractions; Lane 10-13, eluted fractions; Lane 14, blank; Lane 15, Circumsporozoite protein (CSP). The arrow shows the predicted size of r*Pf*SAHH (~53 kDa).

The recombinant *Pf*SAHH protein was expressed and purified by Ni-NTA column chromatography. The protein elution was done using 500 mM imidazole with an estimated molecular weight of ~53 kDa protein band being identified in lanes 10, 11, and 13 (Fig 4.19 A) corresponding to the predicted molecular weight of 53.9 kDa. Fig 4.19, B, is nitrocellulose stained with Ponceau-S showing a successful western blot transfer with r*Pf*SAHH indicated by an arrow on the right side of the gel. The purity of the r*Pf*SAHH was ascertained by probing the western blot with mouse anti-His antibody and detected with 4-chloro-1-naphthol (Fig 4.19 C). For unknown reasons, the protein of interest could not be detected in the induced culture and supernatant as expected. If the gel in (A) is analyzed carefully, you will notice that lanes 10, 11, and 13 show the band of the protein of interest (*Pf*SAHH). In (B), the protein bands were washed away with distilled water. However, protein transfer was successful. In (C) lanes 11 and 13 have a faint protein band for *Pf*SAHH. Lane 14 is supposed to be blank but poor loading of the sample in the adjacent lane has led to the spill over of the sample.

4.2.17 Monitoring of *E. coli* BL 21 (DE3) pLysS bacteria growth with and without rPfSAHH in the absence and presence of copper

An experiment was carried out to determine the effect of r*Pf*SAHH on the growth of *E. coli* host cells in the presence of toxic copper (8 mM) concentrations. *E. coli* BL 21 (DE3) pLysS cells with and without r*Pf*SAHH were grown for 16 hours and monitored at OD_{600}. Fig 4.20 A shows that there was minimal *E. coli* cell growth in copper (8 mM) enriched media. Contrary to this, *E. coli* with expressed r*Pf*SAHH protein, indicated increased growth by 0.248 absorbance units (Fig 4.20 B). This data suggests that r*Pf*SAHH binds copper inside cells and aids bacterial cell growth. Uninduced and induced *E. coli* cells with r*Pf*SAHH showed marginal differences in the absence of copper, showing balanced growth (Fig 4.20 B). The data indicates that the uninduced bacteria expressed some *Pf*SAHH protein which enabled them to grow in the presence of 8mM copper, and this may be due to the leaky expression of the *Pf*SAHH protein.

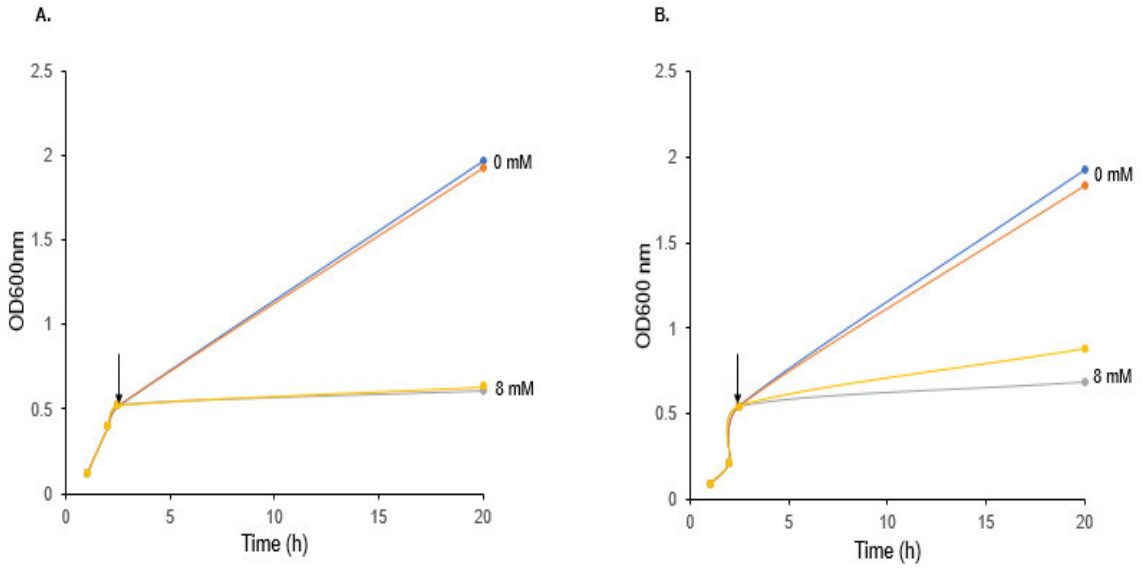

Fig 4.20 Growth of *E. coli* BL 21 (DE3) pLysS cells and expressing r*Pf*SAHH in the absence or presence of copper. A. The *E. coli* cells were grown in the absence (red and blue lines) and presence of copper (8 mM) (yellow and grey) at 20ºC for 16 hours, after being induced with 0.2 mM IPTG. **B.** The *E. coli* cells expressing r*Pf*SAHH were grown using the conditions in **(A).** Uninduced and induced cultures in the absence of copper are represented in blue and orange respectively, while in the presence of copper (yellow (induced) and grey (uninduced)**.** Arrows in **A** and **B** indicate the addition of copper and IPTG to the media. The absorbance readings in **A** and **B** were monitored at OD600 nm.

4.2.18 Inhibition of copper-catalyzed oxidation of ascorbic acid by r*Pf*SAHH expressed without copper and isolated without/with DTT

r*Pf*SAHH was expressed without copper, isolated without or with DTT, and added to the ascorbate oxidation assay (Fig 4.21 A and B). Ascorbic acid alone or with r*Pf*SAHH, EDTA (control), and BSA had little effect on the ascorbic acid oxidation at 255 nm for 300 s. Adding $CuCl_2$ to the ascorbate oxidation led to a 0.57 decrease in absorbance units (Fig 4.21 A). The ascorbic acid oxidation was inhibited by r*Pf*SAHH, causing a 0.46 less change in absorbance units. This finding indicates that the protein bound copper (Fig 4.21 A). Isolating r*Pf*SAHH with DTT and adding it to the assay, did not produce results different from those obtained from using r*Pf*SAHH isolated without DTT (Fig 4.21 B). As shown in 3.4.2, there was more inhibition of the ascorbate oxidation by BSA than r*Pf*SAHH isolated with and without DTT (Fig 4.21 A and B), thus BSA binds copper.

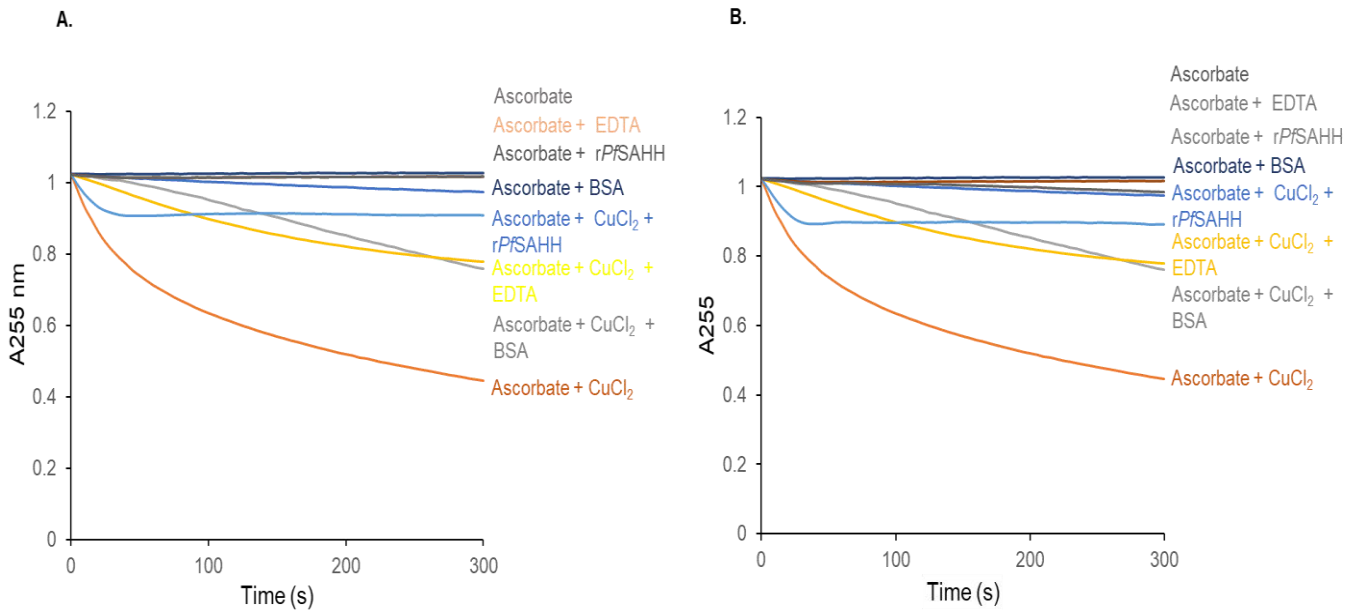

Fig 4.21 Copper-catalyzed oxidative degradation of ascorbic acid in the presence of r*Pf*SAHH grown without Cu and isolated without/with DTT (10 mM). 120 µM ascorbic acid (H_2Asc) was prepared and titrated to pH 4.5; 8 µM $CuCl_2$ was added to H_2Asc solution. A. r*Pf*SAHH (5 µM), BSA (5 µM), or EDTA (5 µM) were added to $CuCl_2$/H_2Asc solution. B. r*Pf*SAHH + DTT was treated as in A including controls (BSA and EDTA). The rate of ascorbic acid oxidation by copper in A and B was measured for 300 s.

4.2.19 Inhibition of copper-catalyzed oxidation of ascorbic acid by r*Pf*SAHH expressed with 0.5 mM of copper and isolated without/with 10 mM DTT

r*Pf*SAHH was expressed in the presence of 0.5 mM copper and isolated without/with DTT, then followed by addition to the ascorbate oxidation assay (Fig 4.22 A and B). Ascorbic acid alone or with r*Pf*SAHH + $CuCl_2$, BSA, and EDTA had little effect on the ascorbate oxidation assay. When $CuCl_2$ was added to the ascorbate, a 0.57 decrease in absorbance readings was seen. r*Pf*SAHH expressed with copper had no inhibitory effects on the ascorbate oxidation assay (Fig 4.22 A), suggesting that the protein bound copper inside of the host bacterial cells. The data obtained from the assay by using r*Pf*SAHH isolated with or without DTT did not significantly differ (Fig 4.22 B).

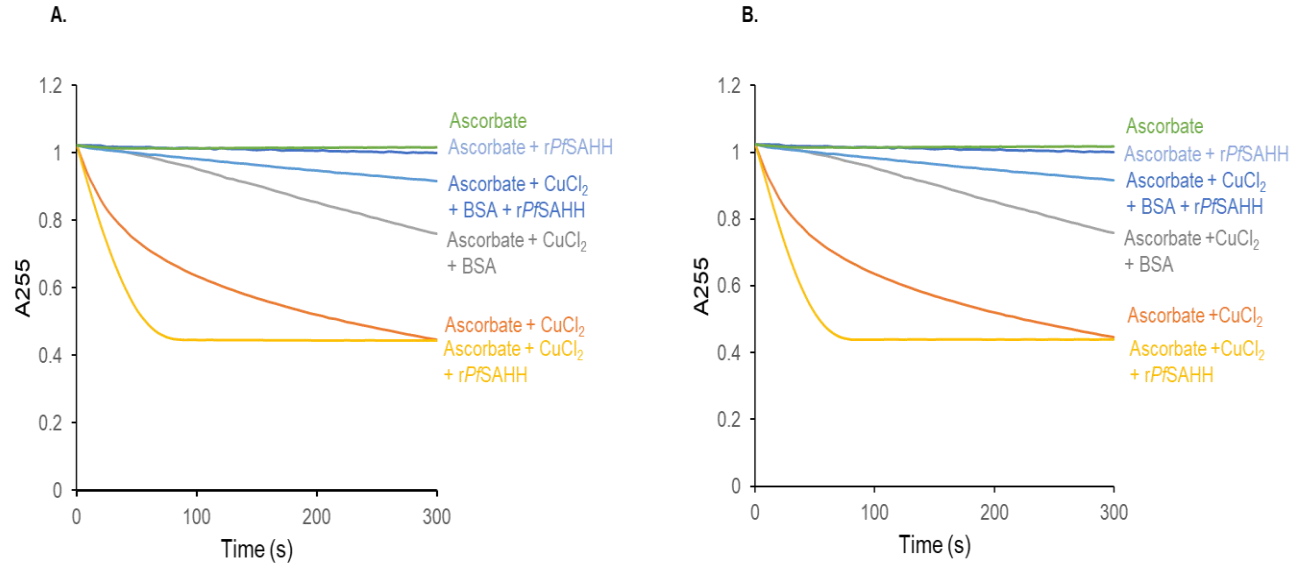

Fig 4.22 Copper-catalyzed oxidative degradation of ascorbic acid in the presence of r*Pf*SAHH grown with Cu (0.5mM) and isolated without/with DTT (10 mM). 120 µM Ascorbic acid (H_2Asc) was prepared and titrated to pH 4.5; 8 µM $CuCl_2$ was added to H_2Asc solution. In A, r*Pf*SAHH + Cu (5 µM), and BSA (5 µM) were added to $CuCl_2$/H_2Asc while in **B.** r*Pf*SAHH + Cu + DTT (5 µM), was added to the copper (II) Chloride/Ascorbate solution including the control as mentioned in **A**. The rate of ascorbic acid oxidation by $CuCl_2$ was measured for 300 s both in **A** and **B**.

4.2.20 Binding of copper to r*Pf*SAHH measured with the bicinchoninic acid (BCA) copper release assay

r*Pf*SAHH was expressed without copper and isolated with/without DTT followed by purification and analysis of its ability to bind copper in the BCA release assay. Dithiothreitol (DTT) was included during the isolation of the recombinant protein because it is a strong reducing agent at low (1-10 mM) concentrations, and maintains reduced states of thiol groups (Cleland, 1964). Fig 4.23 shows $CuCl_2$ absorbance readings in the presence of ascorbic acid (solid bars) which are higher than the rest of the samples (P≤0.001). Little copper was detected when r*Pf*SAHH isolated with/without DTT and BSA were assessed alone or incubated with Cu (II) (Fig 4.23). r*Pf*SAHH isolated with or without DTT and BSA control bound copper after incubation with Cu (I) (P≤ 0.05). The binding ability of copper to r*Pf*SAHH with or without DTT was not significantly different (P>0.05) (Fig 4.23).

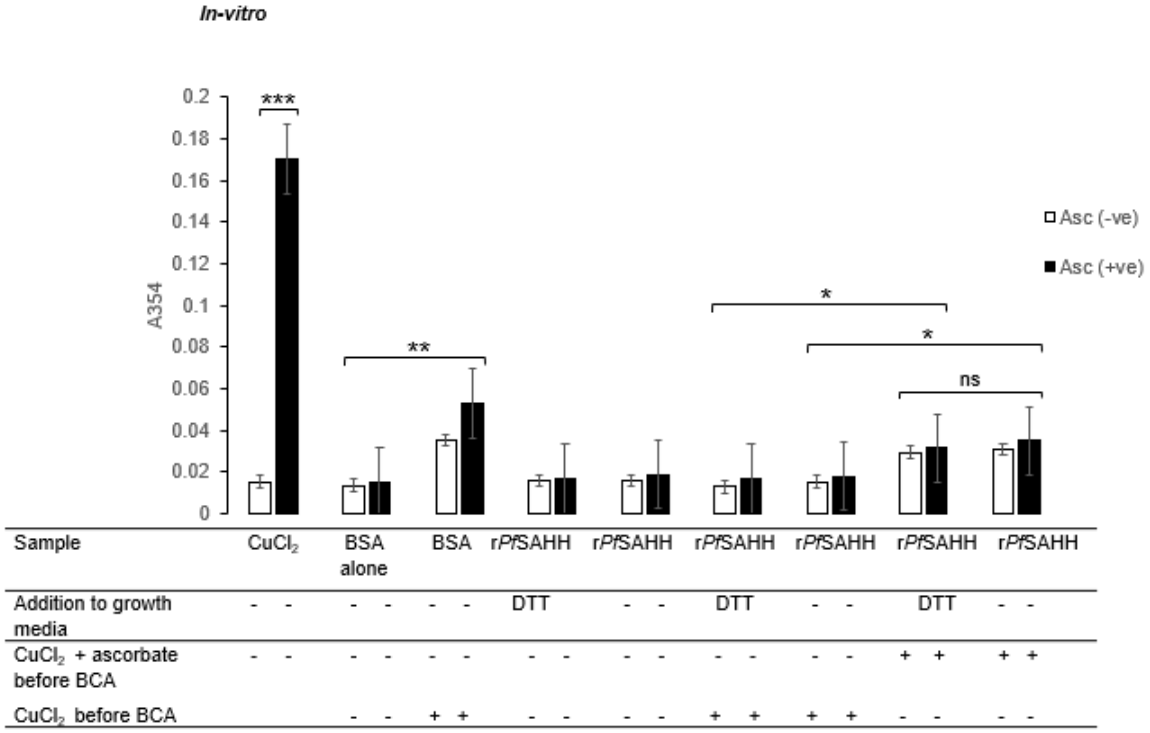

Fig 4.23 Binding of copper to *Pf*SAHH isolated with/without DTT *in-vitro* determined by the BCA copper release assay. 10 µM affinity-purified *Pf*SAHH + DTT or *Pf*SAHH was incubated with copper II chloride with/without ascorbate. Excess copper from the incubation step was removed using a spun column, and the protein solution was treated with TCA. Copper was detected without (open bars) or with ascorbate (solid bars). The experiment was performed in duplicate, and the average readings were plotted as shown in the bar graph. The experiment included BSA as a control. The data presented are mean ± SD of a duplicate. *, **, ***, and **** denote P≤ 0.05, P≤ 0.01, P≤0.001, and P≤ 0.0001, respectively, as determined by the student's t-test. The 'ns' stands for 'non-significant'

4.2.21 Measuring the copper bound *in-vivo* to r*Pf*SAHH using the bicinchoninic acid (BCA) copper release assay

Low concentrations (0.5 mM) of copper do not influence the growth of *E. coli* cells (Lutsenko *et al.,* 1997). For this reason, r*Pf*SAHH was expressed in the presence of 0.5 mM copper (II) chloride to establish whether r*Pf*SAHH binds copper in the host cell. The protein was isolated without or with DTT before being affinity purified and analyzed in the BCA release assay. *E. coli* host cells were washed to remove excess copper. Copper alone had the highest absorbance readings in the presence of ascorbic acid (Solid bars) (Fig 4.24). BSA alone and r*Pf*SAHH had minimal copper bound compared to when the proteins were incubated with Cu (II) in the absence of ascorbate. BSA bound both Cu (I) and Cu (II) in tandem with reports by Suzuki *et al.,* 1989 and Alhazmi *et al.,*2023. r*Pf*SAHH bound Cu (I) and there was no significant difference in copper levels between the recombinant proteins isolated with DTT or not (P>0.05) (Fig 4.24).

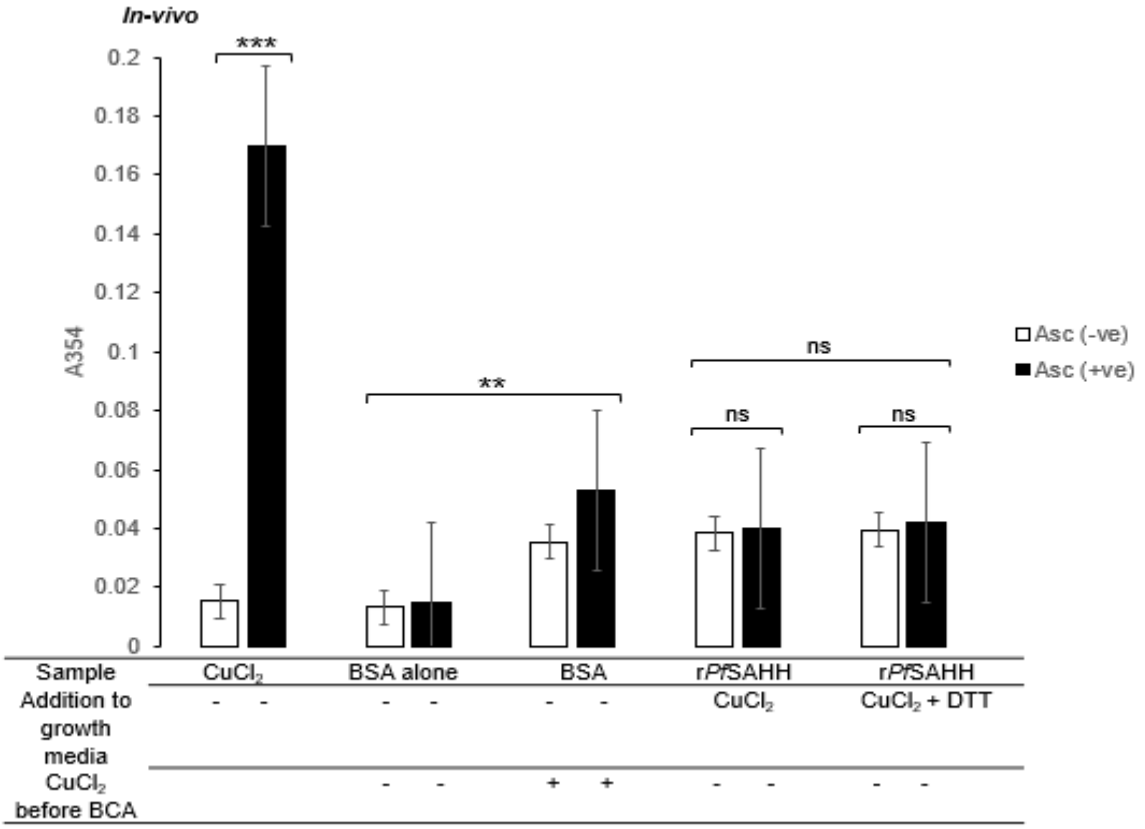

Fig 4.24 Binding of copper to *Pf*SAHH + Cu or *Pf*SAHH + Cu + DTT *in-vivo* determined by the BCA copper release Assay. 10 µM affinity-purified *Pf*SAHH + Cu or *Pf*SAHH + Cu + DTT was expressed with copper II chloride (0.5 mM) and treated with TCA. Copper was detected without (open bars) or with ascorbate (solid bars). The experiment was performed in duplicate, and the average readings are presented in the figure above. The data presented are mean ± SD of a duplicate. *, **, ***, and **** denote P≤ 0.05, P≤ 0.01, P≤0.001, and P≤ 0.0001, respectively, as determined by the student's t-test. The 'ns' stands for 'non-significant'

4.2.22 Measuring *in-vitro* copper binding to r*Pf*SAHH with previously bound copper using bicinchoninic acid (BCA) release assay

To determine the ability of r*Pf*SAHH to bind more copper, the protein was expressed in copper-rich (0.5 mM) media and isolated without/with DTT. r*Pf*SAHH was incubated with copper in the absence and presence of ascorbate before evaluating it in the BCA release assay (Fig 4.25). As before, copper measured in the presence of ascorbate (solid bars) had the highest absorbance readings at 354 nm. BSA alone had little copper, and bound copper when copper was added to the protein without ascorbic acid. There was more copper bound to r*Pf*SAHH expressed with copper and isolated without or with DTT when the recombinant proteins were incubated with copper (I), and the proteins did not bind copper when copper (II) was added (Fig 4.25). This finding suggests that r*Pf*SAHH expressed in the presence of copper bound more copper, thus the protein was not saturated. r*Pf*SAHH isolated with DTT bound a similar amount of copper to the protein isolated without DTT(P>0.05).

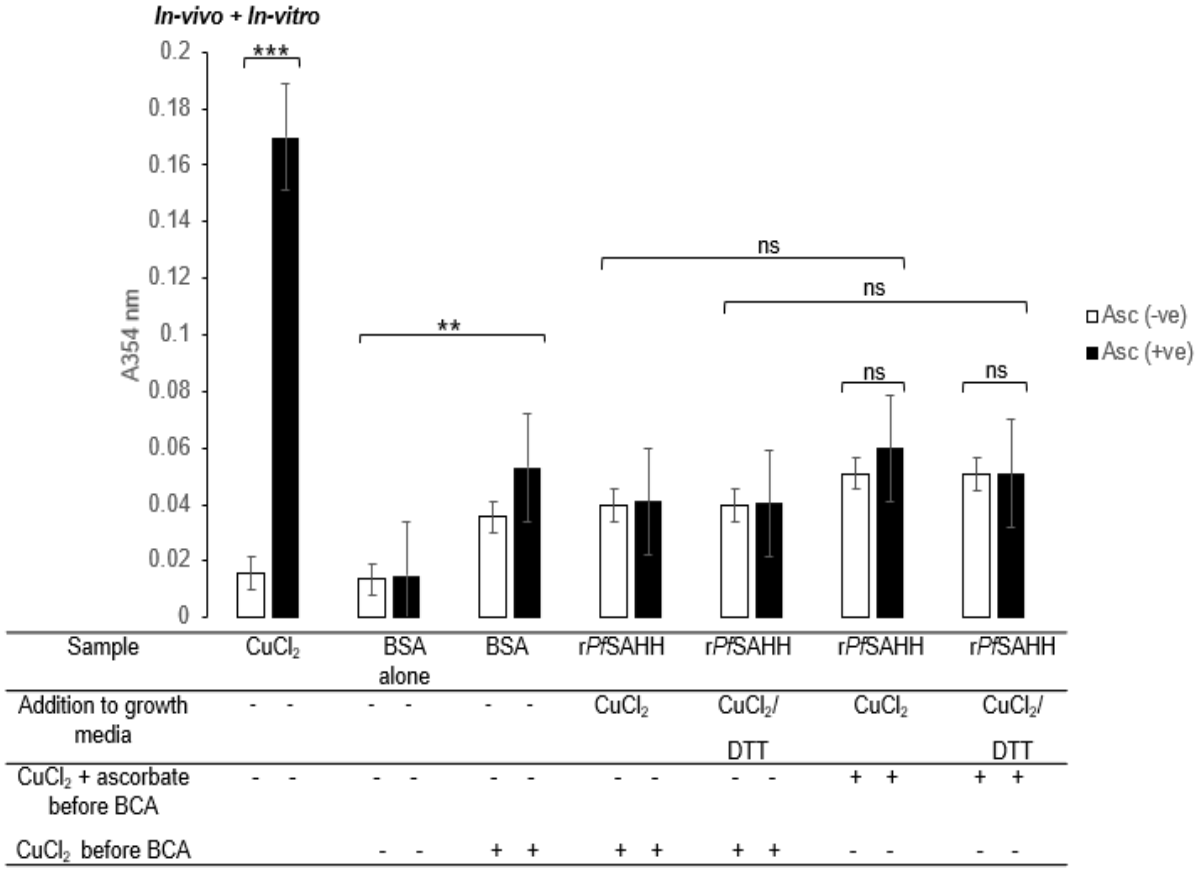

Fig 4.25 Binding of copper to *Pf*SAHH + Cu or *Pf*SAHH + Cu + DTT *in-vitro* determined by the BCA copper release assay. 10 µM affinity-purified *Pf*SAHH + Cu or *Pf*SAHH + Cu + DTT was incubated with copper II chloride with/without ascorbate. Excess copper from the incubation step was removed using a spun column, and the protein solution was treated with TCA. Copper was detected without (open bars) or with ascorbate (solid bars). The experiment was performed in duplicate, and the average readings were plotted in the bar graph. BSA was included as a control. The data presented are mean ± SD of a duplicate *, **, ***, and **** denote P≤ 0.05, P≤ 0.01, P≤0.001, and P≤ 0.0001, respectively, as determined by the student's t-test. The 'ns' stands for 'non-significant'.

4.2.23 The effect of r*Pf*SAHH eluent on the copper-catalyzed oxidation of ascorbic

r*Pf*SAHH expressed in the presence of 0.5 mM copper and isolated without/with DTT, then followed by purification and incubation with more copper in the presence or absence of ascorbate. Before the sample could be added to the ascorbic acid oxidation assay, it was passed through a spin column to remove excess copper. Ascorbic acid alone had a minimal effect on ascorbate oxidation at 255 nm. A decrease of 0.64 absorbance units was observed when $CuCl_2$ was added to ascorbic acid (Fig 4.26 A, B, C, and D). The recombinant proteins that were incubated with copper and then passed through the gel filtration column did not inhibit copper-catalyzed ascorbic acid oxidation, suggesting that the recombinant proteins had bound copper in the host bacteria cells.

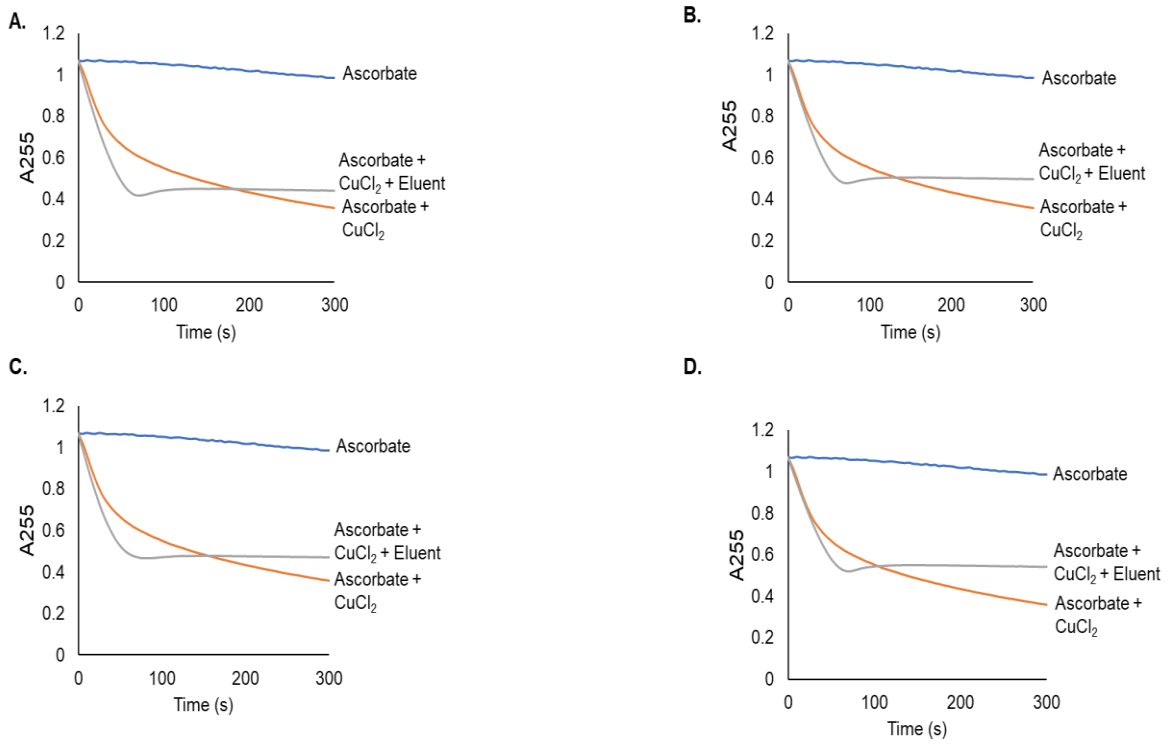

Fig 4.26 Copper-catalyzed oxidative degradation of ascorbic acid in the presence of eluent. 120 µM ascorbic acid (H_2Asc) was prepared and titrated to pH 4.5; 8 µM $CuCl_2$ was added to H_2Asc solution; **A.** *Pf*SAHH expressed with Cu and isolated with DTT was added to $CuCl_2$ which was reduced using 10 mM ascorbic acid and passed through gel filtration column as described earlier. **B.** The protein in **(A)** was added to $CuCl_2$ in the absence of ascorbic acid and then gel filtrated **C.** *Pf*SAHH isolated without DTT was added to $CuCl_2$ after reduction with 10 mM ascorbic acid followed by gel filtration **D.** Protein in **(C)** was incubated with oxidized copper and was passed through a gel filtration column.

4.3. Discussion

4.3.1 Introduction

Copper has been documented to be important to all organisms because it is a cofactor of many different enzymes. However, it may be harmful due to its capacity to undergo redox reactions that increase free radicals causing peroxidation of cell membranes (O'Halloran *et al.,* 2000). For this reason, cells have mechanisms that reduce the effects of elevated levels of copper. The role of copper-binding proteins in ensuring optimum levels of copper are present in cells cannot be over-emphasized. In *Plasmodium falciparum*, the addition of 5 µM of copper sulfate stops 50% growth of the parasite (Marva *et al.,* 1989). Copper must be regulated through a balance between the influx, and efflux. To achieve this, the parasite has copper transporters and metallochaperones that aid copper acquisition, distribution, and efflux. Cytosolic copper distribution is poorly documented in *Plasmodium falciparum*, therefore, the study to examine S-adenosylhomocysteine hydrolase documented to have a role in intracellular copper metabolism in mouse hepatic cells (Seo *et al.,* 1993) was undertaken. This section will describe the identification of *P. falciparum* S-adenosylhomocysteine hydrolase and its copper-binding characteristics.

4.3.2 Analysis and identification of *Pf*SAHH using computational methods.

Analysis of the amino acid sequence alignment of SAHH from protozoa, yeast, mice, and humans revealed a conserved copper binding motif GYGDVGKG-GXGXXGXG (Fig 4.1 A), which is situated in the cofactor domain (Tanaka *et al.,* 2004). The results are supported by previous studies in protozoa, rats, mice, and humans (Bujnicki *et al.,* 2003, Gomi *et al.,* 1989, Seo *et al.,* 1993, Tanaka *et al.,* 2004). Further, the results highlighted the NAD^+/H binding region (Fig 4.1 A). This is in line with findings in mice that have the NAD site ranging from amino acid residue 197 to 351 (Kusakabe *et al.,* 2015), and in humans, this is located between amino acid residue 226 to 339 (Tanaka *et al.,* 2004). Singh *et al.,* 2016 reported a 13 amino acid residue involvement in NAD binding on *Pf*SAHH structure compared to the three documented by Creedon *et al.,* 1994. The latter was the first to express and purify the SAHH from the *Plasmodium falciparum* and established that NAD bound to glycine residues located on positions 264, 266, and 269, amino acids that are part of the GXGXXGXG copper-binding motif (Creedon *et al.,* 1994). These results demonstrate that the GXGXXGXG motif is common in most organisms, thus making it an important part of the functionality of the enzyme.

When amino acid sequences of SAHH for the five *Plasmodium* species that infect humans were aligned, a GYGDVGKG motif was common to the other four amino acid sequences apart from *Plasmodium vivax* that had a GFGDVGKG motif (Fig 4.1 B). The GYGDVGKG motif has also been found to be conserved in the SAHH sequences from bacteria, plants, nematodes, soil-dwelling amoeba, and leishmania species (Creedon *et al.,* 1994). An alignment of 20 amino acid sequences from *Plasmodium falciparum* isolates, showed a conserved GYGDVGKG in all isolates and a 100% conservation of all the amino acid residues (Fig 4.2). Alignment of SAHH sequences from Plasmodium species infecting humans, mice, birds, and monkeys, still indicated the GYGDVGKG motif to be common apart from the *Plasmodium vivax* isolates that had GFGDVGKG motif (Fig 4.3). The reason for the substitution of tyrosine for phenylalanine is not known.

The study identified and selected two immunogenic peptides from the *Pf*SAHH sequence which are “MVENKSKVKD”, a peptide that ranges from amino acid residue 1 to 10, and “QMEISENEMPGLMRIREEYGKDQPLKNAKIT”, ranging from 20 to 50) (Fig 4.4). These peptides were to be injected into chickens to generate antibodies, an activity that was not undertaken. Due to these peptides being on the surface, they might provide several epitopes that are accessible to antibodies like those reported on Cox17 by Beers *et al.,* 1997. Generation of chicken antibodies of *Pf*SAHH could be useful because they would help in identifying the protein and would confirm that the recombinant protein shared structural motifs with the native *Pf*SAHH protein structure. When the r*Pf*SAHH is injected into the chickens, antibodies will be purified and used in western blot to detect both the native and recombinant *Pf*SAHH.

The enzyme S-adenosylhomocysteine hydrolase (SAHH) catalyzes S-adenosyl-L-homocysteine hydrolysis to adenosine and homocysteine. It is also reported that it plays a role in regulating physiological methylation. Additionally, S-adenosyl-L-homocysteine may act as an inhibitor of methionine (SAM)-dependent

methylation. In other instances, SAM may have a part in the methylation of biomolecules and other small molecules (Yuan *et al.,* 1999). For the above functions to be performed, the protein has domains that participate in such reactions. The AdoHyase_NAD domain was predicted (Fig 4.5), and this result is in tandem with what is documented by Creedon *et al.,* 1994, Seo *et al.,* 1993, and Singh *et al.,* 2016.

No studies have determined the ability of *Pf*SAHH to bind copper. However, SAHH from mouse hepatic cells has been found to have a role in intracellular copper metabolism (Bethin *et al.,* 1995 a and b). The *Pf*SAHH model crystal structure was compared to that of *Hs*SAHH using superimposition in PyMOL (Fig 4.6 A, B, and C), with an overlay structure generating an RSMD value of less than 2Å. This is supported by Singh *et al.,* 2016, who established similarity with an RSMD of 0.749 Å. However, mouse SAHH is 97% identical to the *Hs*SAHH (Coulter-Karis *et al.,* 1989), suggesting that it would be very similar to *Pf*SAHH structure Multiple sequence alignments have revealed identical motifs and NAD binding sites among SAHH amino acid residue sequences from mice, *P. falciparum,* and humans; thus, SAHH protein is similar among these organisms. Therefore, if mouse SAHH binds copper and plays a role in intracellular copper metabolism, *Pf*SAHH has the potential to bind and distribute copper in the malaria parasite.

Various studies have determined that mouse SAHH binds copper (Seo et al., 1993, Bethin *et al.,* 1995); however, the site has not been established. Using SPPIDER, the copper-binding motif (GXGXXGXG) motif was predicted (Fig 4.9) and we think that this is the likely copper binding site due to the GXXG copper-binding motif present in another copper binding protein (Ctr1) (Puig *et al.,* 2002, Choveaux *et al.,* 2012) that was implicated in copper binding. Additionally, this site is shown to bind copper in section 6.1.4. using the MIB2 modeling server. Other sites predicted are NAD/H sites in Fig 10 and 11. These align well with previous studies (Singh *et al.,* 2016, Tanaka *et al.,* 2004, Yang *et al.,* 2002, Kusakabe *et al.,* 2015). VERIFY3D program was utilized to establish whether the *Pf*SAHH structure was correct and not mistraced or wrongly folded. The results indicated that 72.79% of the residues in *Pf*SAHH had an average 3D-1D score ≥ 0.1 which is near the 80% limit score (Fig 4.12). Data that shows that the structure was good (Agnihotry *et al.,* 2022).

*Pf*SAHH has various roles in the malaria parasite, some of which depend on its interaction with other proteins. Using the STRING database, the interacting partners of this protein were predicted (Fig 4.13). Notably, *Pf*SAHH was observed to be associated with triosephosphate isomerase, adenosine deaminase, and *Pf*PMT, proteins that have a role in glycolysis, and deamination. *Pf*SAHH has been reported to be involved in nitrogen, sulfur, and carbon metabolisms (Balmer *et al.,* 2003, Lemaire *et al.,* 2004, Lindahl *et al.,* 2003). The pull-down assay experiment by Sturm *et al.,* 2009 reports that *Pf*SAHH also interacts with *Pf*Grx1 through the formation of a disulfide bond at an amino acid residue 88 of *Pf*Grx1. The interaction with these proteins provides insight into the potential for *Pf*SAHH to interact with other copper proteins and thus, may play a role in the cytosolic copper distribution and contribute to the parasite's survival.

4.3.3 PCR amplification of *Pf*SAHH in *E. coli* BL 21 (DE3) pLysS

The *Plasmodium falciparum* gene is located on chromosome 5 which codes for 479 amino acid residues (Bujnicki *et al.,* 2003). The gene coding for the *Pf*SAHH is transcribed as a 2.8 kilobase mRNA in the parasite at the erythrocytic blood stage (Creedon *et al.,* 1994). The coding sequence was amplified, revealing a 1748 bp amplicon (Fig 4.14) that included T7 promoter and T7 reverse regions (coding sequence not shown). The amplicon was however not sequenced to confirm the Open Reading Frame (ORF). However, an analysis using the MendelGen program was conducted to verify that the coding sequence was in an Open Reading Frame. Further, a restriction digest of the *Pf*SAHH plasmid was performed with restriction enzymes (EcoRI and BamHI) used individually and in combination to establish that the right size of the SAHH fragment was inserted. The results of the double digestion showed a 1470 bp (Fig 4.15) similar to sizes obtained in previous studies (Creedon *et al.,* 1994, Bujnicki *et al.,* 2003).

4.3.4 Recombinant expression and purification of *Pf*SAHH in *E. coli* BL 21 (DE3) pLysS

Research studies in biological sciences require recombinant proteins, which are used to establish enzyme activity, protein interactions, and binding capacities of different ligands like metal ions. Many other functions can be sought to be established in both *in-vivo* and *in-vitro* experiments (Bondos *et al.,* 2003, Casteleigjn *et al.,* 2013). Therefore, *E. coli* BL 21 (DE3) cells were transformed, and two colonies were selected for the expression of *Pf*SAHH. Monitoring the *E. coli* growth revealed no significant difference between the uninduced and induced cultures (Fig 4.16) like a study by Ramirez *et al.,* 1994 that reported that IPTG between 0- and 1-mM concentration does not affect bacterial growth and cell concentration. In contrast to these findings is a report by Harcum *et al.,* 1992 that states that IPTG slows the growth of *E. coli*. Additionally, previous studies on copper-binding proteins indicated a large difference between the uninduced and induced cultures (Choveaux *et al.,* 2015, Salman *et al.,* 2022). One colony with the best growth rate was selected for subsequent expression optimization.

The bacteria grown in Fig 4.16 were lysed and run on a 12.5% reducing SDS-PAGE gel (Fig 4.17). It was difficult to identify the size of *Pf*SAHH protein in the induced cultures which was supposed to be between 45 to 66.2 kDa like reports in previous studies (Seo *et al.,* 1993, Creedon *et al.,* 1994). There was an unidentified protein in the induced lanes with a molecular weight of 116 kDa (Fig 4.17). Efforts to purify the *Pf*SAHH protein proved fruitless, and the results were not very significant. There were various reasons why the results could have been the way they were; (i) there could have been low or no protein expression because of expression conditions that may have affected the protein integrity (Malhotra., 2009). (ii) The other reason would be due to the efficiency of the purification that could have been affected by protein tags that function in both the affinity and solubility roles (e.g. MBP and GST tags have been used to improve affinity and solubility) (Malhotra., 2009). Previous studies indicated challenges in expressing His-tagged proteins (Carr *et al.,* 2002, Banci *et al.,* 2004, Salman *et al.,* 2022). The molecular weight markers were used to calculate the approximate size of the expressed protein by plotting the log

mw vs the distance travelled by each protein relative to the Bromophenol blue and comparing the distance moved by protein band of interest on the graph. To improve the expression of *Pf*SAHH, the expression conditions were altered, and the following were the conditions used for the expression of *Pf*SAHH; 2xYT growth media, 20°C expression temperature, 16 hours induction time, and 1 mM IPTG inducer concentration. Fig 4.18 shows the results obtained from the change in expression conditions though only the 116 kDa band differentiated the induced from the uninduced lanes. The size of *Pf*SAHH could still not be identified using the 15% reducing SDS PAGE gel (Fig 4.18). Unfortunately, *E. coli* proteins of a similar size to the expected protein, masked the expression of the recombinant protein. Purification and later western blot results identified a ~53 kDa *Pf*SAHH that was like the predicted molecular weight of 53.9 kDa (Fig 4.19 A, B, and C). This is slightly different from the report by Creedon *et al.,* 1994 which found a molecular weight of 56 kDa, during the same study, SAHH from a rat with a 44 kDa was identified. Nakanishi *et al.,* 2001 reported a 55 kDa, and Bujnicki *et al.,* 2003, found a molecular weight of 50 kDa all from *Plasmodium falciparum*. The size of the protein in all these reports is deduced from electrophoresis gels which give an approximate measure of molecular weight. SAHH in mouse has a reported molecular weight of 50 kDa (Seo *et al.,* 1993), and in humans, it has a molecular weight of 54 kDa (Creedon *et al.,* 1993, Tanaka *et al.,* 2004) These molecular weights fall within the same range as that of SAHH from a rat liver (45 kDa) (Gomi *et al.,* 1989).

4.3.5 r*Pf*SAHH enables *E. coli* host cells to tolerate toxic copper concentrations

The results in Fig 4.20 A and B show minimal *E. coli* cell growth in copper (8 mM) enriched media while in *E. coli* which had expressed r*Pf*SAHH protein, there was increased growth, indicating that the protein bound copper. This is like other studies that established the survival of bacteria and human cells in the presence of toxic copper levels (Rensing *et al.,* 2013, Öztürk *et al.,* 2020, Burkitt., 2001, Gaetke *et al.,* 2014). In previous studies, *E. coli* expression of recombinant copper-binding proteins has been demonstrated to enable the growth of *E. coli* cells in the presence of toxic levels of copper (Salman *et al.,* 2022, 2023). Another observation made from the results is that there was a marginal difference between the uninduced and induced *E. coli* cells with r*Pf*SAHH grown in the absence of copper. This data may be explained by the exponential/balanced growth of the bacterial host cells (Fishov *et al,* 1995).

4.3.6 Inhibition of copper-catalyzed ascorbic acid oxidation by r*Pf*SAHH expressed without copper and isolated without/with DTT

The findings in Fig 4.21 A show that ascorbic acid oxidation was inhibited by r*Pf*SAHH, indicating that the protein bound copper in the assay (Fig A and B). Previous studies have established similar results for r*Pf*Ctr1 and r*Pf*Cox17's effect on the ascorbic acid assay (Choveaux *et al.,* 2012, 2015). BSA, which has been shown to bind copper, was used in the assay as a positive control for the assay (Fig 4.21 A and B) (Musuoka *et al.,* 1994., Alhazmi *et al.,* 2023). However, the experiment does not determine which form [copper (I) or (II)] of copper that BSA bound. BSA has been shown to bind both copper (I) and (II) and prefers copper (II) (Peters and

Blumenstock., 1967, Alhazmi *et al.,* 2023). Isolating r*Pf*SAHH with or without DTT did not generate any variation in the results (Fig 4.21 A and B).

4.3.7 Inhibition of copper-catalyzed ascorbic acid oxidation by r*Pf*SAHH expressed with 0.5 mM copper and isolated without/with DTT

r*Pf*SAHH expressed with copper had no inhibitory effects on the ascorbate oxidation assay (Fig 4.22 A), suggesting that the protein bound copper inside the host bacterial cells and therefore no longer could bind copper in the assay. The data obtained from the assay using r*Pf*SAHH isolated with or without DTT were not significantly different (Fig 4.22 B). This is in line with studies that have documented that copper (I) compared to copper (II) is in abundance in bacterial cells during reducing conditions found in the cytoplasm, like the reduced plasmodial cytoplasmic environment (Krnajski *et al.,* 2001, Davis and O'Halloran, 2008, Foster *et al.,* 2014). DTT plays a role in protecting thiol groups from oxidation. Sensor proteins in bacteria have also shown a high binding affinity towards copper (I) that is in abundance and, thus, stimulating an upregulation of cytosolic mechanisms that prevent stress on the cells (Tottey *et al.,* 2005, Ma *et al.,* 2009). This evidence shows the form [copper (I)] of copper that is predominant in the cells, and most likely, this is the form that r*Pf*SAHH bound when expressed in a bacterial environment.

4.3.8 *In-vitro* r*Pf*SAHH binding of copper

The BCA release assay results showed that r*Pf*SAHH isolated with or without DTT and BSA control bound copper after incubation with Cu (I). This aligns with results on mouse SAHH, which established the role of this protein in copper and sulfur metabolism (Creedon *et al.,* 1993). Immunoblot results, from another study by the same author, stated the direct effect of copper deficiency on the levels and functionality of the SAHH in the mouse liver (Bethin *et al.,* 1995 a and b). Seo *et al.,* 1993 reported a copper-binding SAHH purified from the brindled mouse hepatic cytosols with a role in intracellular copper metabolism. Other studies equally show that *Plasmodium falciparum* proteins and Trypanosoma proteins bind copper (I) in the BCA release assay (Rasoloson *et al.,* 2004, Salman *et al.,* 2022, Isah *et al.,* 2020). The binding ability of copper to r*Pf*SAHH with or without DTT was not significantly different (Fig 4.23).

4.3.9 *In-vivo* r*Pf*SAHH binding of copper

The r*Pf*SAHH bound more copper *in-vivo* than *in-vitro*, and no significant difference was seen between the copper bound to the protein isolated with or without DTT (4.24). The results from *in-vivo* analysis are like those from the expression of copper-binding proteins and their binding of copper in the *E. coli* cells (Lutsenko *et al.,* 1997). A comparison between *in-vivo* and *in-vitro* results in the present study gives similar results to those obtained from the expression of *Pf*Cox17 (Choveaux *et al.,* 2015). Using the protein that previously bound copper in *E. coli*, an *in-vitro* examination of the copper binding abilities of the protein revealed that the protein bound copper though at minimal levels (Fig 4.25). This is supported well by results from Munsami's study on *Pf*Sco1 (Munsami., 2022). Another experiment was done to confirm that r*Pf*SAHH bound copper *in-vivo*, and results in Fig 4.26 show that the recombinant protein bound copper in the bacteria as there was no inhibition of the

copper-catalyzed ascorbate oxidation assay. All these results suggest that no copper (II) was bound by r*Pf*SAHH, instead, the protein bound copper (I), data that is supported by published studies (Choveaux *et al.,* 2012, 2015).

4.3.10 Conclusion

The results from the current study indicated that *Pf*SAHH has a GXGXXGXG copper-binding motif and is common in all the organisms analyzed. The protein is in the cytosol, thus, there is a likelihood of it taking part in intracellular copper metabolism including other cellular activities. The three methods used to establish whether *Pf*SAHH binds copper revealed that it binds copper *in-vivo* and *in-vitro*. This is the first time *Pf*SAHH is being assessed for its ability to bind copper.

Chapter 5

The protein-protein interaction studies of *Pf*Grx1, *Pf*Ctr1, and *Pf*CuATPAse using ClusPro 2.0, and molecular docking of copper with plasmodial copper-binding proteins.

5.1 Introduction

This chapter describes the protein-protein interaction of copper-binding proteins using bioinformatic tools. A brief overview of the predicted interaction using the STRING database of *Pf*Grx1 with other proteins is given Additionally, ClusPro online saver was used to establish the interaction of *Pf*Grx1, *Pf*Ctr1 and *Pf*CuATPase. The PDBSum programme was utilized to determine the amino acid residues, type and number of bonds involved in the complex generated from the ClusPro programme. Molecular Dynamics Simulation (MDS) performed on CABS-flex 2.0 server established protein changes after formation of the protein complex, in this regard, *Pf*Ctr1-*Pf*Grx1 complex was analysed.

5.2 Results and Discussion

5.2.1 STRING prediction of proteins interacting with *Pf*Grx1(PF3D7_0306300) inside the parasite.

The proteins that interact with *Pf*Grx1 in the parasite were determined using the STRING database (https://string-db.org). In Fig 5.1, the analysis showed that PF3D7_0306300 (*Pf*Grx1) interacts with many different intracellular *Plasmodium* proteins with various cellular functions. Among the partners established through coexpression are ribonucleotide reductase and glutathione peroxidase, which are involved in the provision of precursors for DNA synthesis and maintenance of the antioxidant status of organisms, respectively. Other partners like glutathione and thioredoxin reductases are involved in maintaining reduced glutathione and catalysis of the reduction of thioredoxin, respectively. Thioredoxin 2 keeps low levels of free radicals (Stanely *et al.,* 2011), and dihydrolipoyl dehydrogenase plays a role in the Krebs cycle, photorespiration, and degradation of branched-chain alpha-ketoacids. *Pf*Grx1 is associated with Tip1, a truncated isoform *Pf*Ctr1, which represents the Nt domain and lacks transmembrane domains. This interaction is proposed to be vital to the survival of the parasite. Table 5.1 shows the accession numbers and identity of the proteins in Fig 5.1.

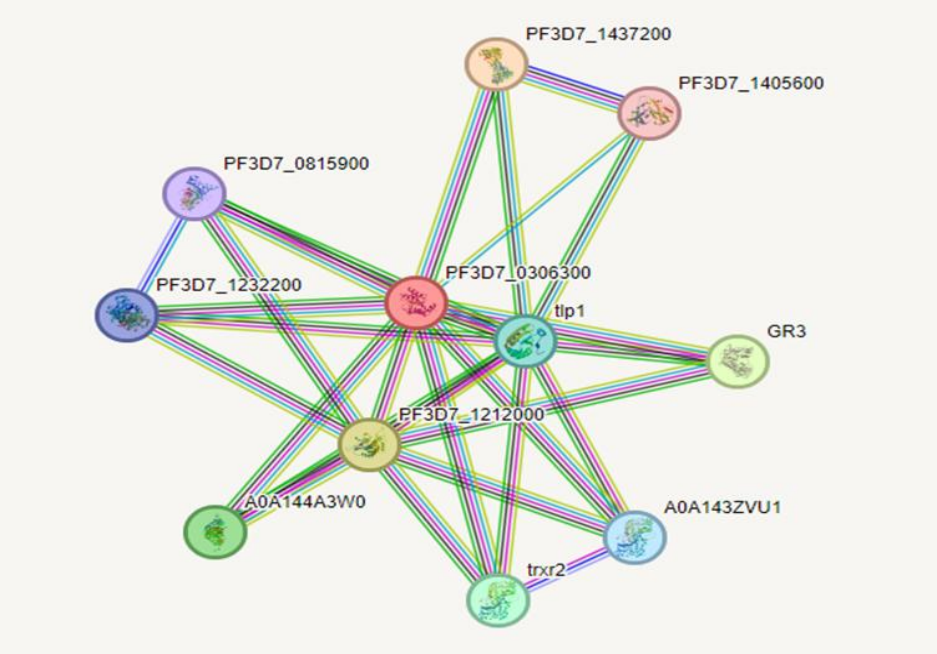

Fig 5.1 STRING database prediction of interacting partners of PF3D7_0306300. The intracellular proteins that interact with glutaredoxin 1 are shown in the diagram (https://string-db.org). The lines in different colors connecting proteins signify the method used to determine the association of various proteins to *Pf*Grx1. Cyan – curated database; Purple – experimentally determined; Green – gene neighborhood; Red – gene fusion; Deep blue – co-occurrence; Lime green – text mining; Black – co-expression; Light blue – protein homology.

Table 5.1 Prediction of *Pf*Grx1 interacting partners using the STRING database.

Predicted interacting partners of PF3D7_0306300 Glutaredoxin 1			
Nomenclature assigned on Fig 5.1	**Current accession number**	**Protein Name**	**The method used in determining the interacting partners**
PF3D7_1437200	PF3D7_1437200	Ribonucleoside-diphosphate reductase	Coexpression, experiments, and text mining
PF3D7_1212000	PF3D7_1212000	Glutathione peroxidase	Neighborhood gene fusion, Coexpression, text mining
GR3	PF3D7_1419800	Glutathione reductase	Databases, text mining
AOA144A3WO	PF3D7_1419800	Glutathione reductase	Databases, text mining
trxr2	AF508128	Thioredoxin reductase 2	Databases, text mining
AOA143ZVU1	PF3D7_0923800	Thioredoxin reductase	Databases, text mining
PF3D7_1232200	PF3D7_1232200	Dihydrolipoyl dehydrogenase	Databases, text mining
PF3D7_0815900	PF3D7_0815900	Dihydrolipoyl dehydrogenase, apicoplast	Databases, text mining
PF3D7_1405600	PF3D7_1405600	Ribonuclease-diphosphate reductase-small chain, putative	Databases
Tip1	-	Truncated isoform *Pf*Ctr1	Databases, text mining, coexpression, gene fusion

5.2.2 An analysis of the AlphaFold structure of *Pf*Ctr1 and crystal structure of *Pf*Grx1 using a Ramachandran plot

A Ramachandran plot is a graphical representation of dihedral angles belonging to amino acids in proteins. It is used to authenticate protein structures. In the present study, a Ramachandran plot was generated through PROCHECK to establish the accuracy of the AlphaFold *Pf*Ctr1 (Q8IL79) and *Pf*Grx1 crystal structure (Q9NLB2) obtained from UniProt (https://www.uniprot.org) and Protein Data Base (https://www.rcsb.org), respectively, and used in ClusPro 2.0 protein- protein interaction studies. The PROCHECK software evaluates the residue's geometry and gives a stereochemical quality of the structure in use (Agnihotry *et al.,* 2022). Fig 5.2 A shows that *Pf*Ctr1 has 83.3% (184), 14% (31), 1.4% (3), and 1.4% (3) residues that belong to the favored regions, additionally allowed regions, generously allowed regions, and disallowed regions, respectively. *Pf*Grx1 in Fig 5.2 B has no residues in the disallowed regions, while 94% (94), 4% (4), and 1% (1) of the residues belong to favored, additionally allowed, and generously allowed regions, respectively. This shows that both structures are of good quality because *Pf*Ctr1 has few residues in the disallowed region, while *Pf*Grx1 has none.

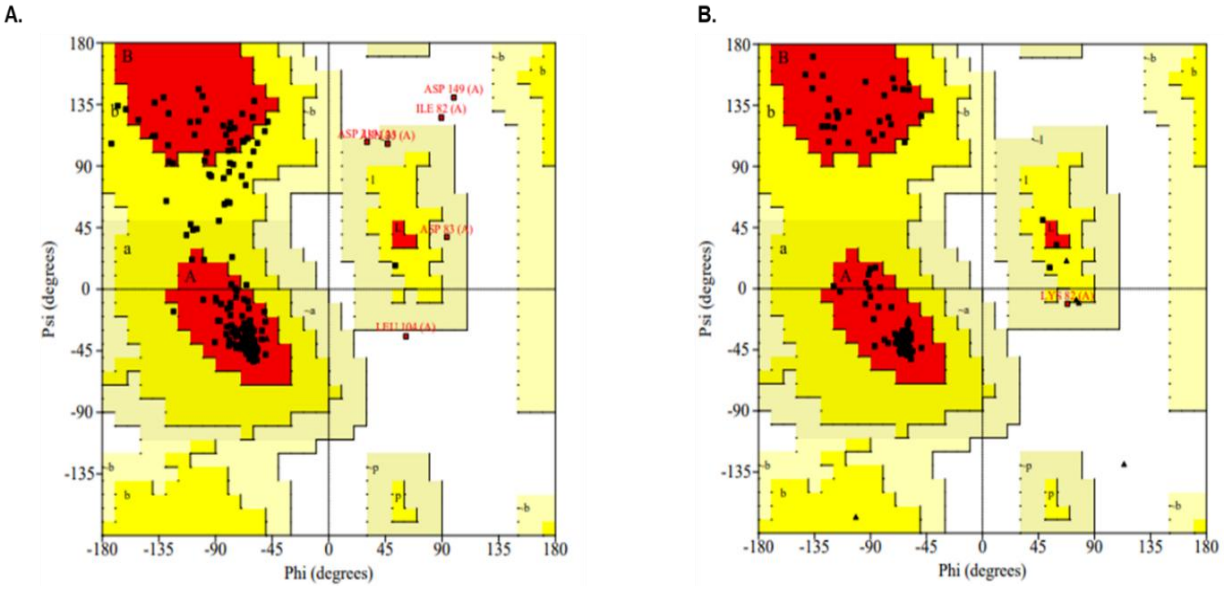

Fig 5.2 Ramachandran plot of AlphaFold *Pf*Ctr1 and *Pf*Grx1 crystal structures using PROCHECK software. A and **B** illustrate the distribution of the protein's (*Pf*Ctr1 and *Pf*Grx1, respectively) main φ-ψ torsion angles (black squares) relative to the "core" (red) and "allowed" (yellow) regions, with residues falling in "generously allowed" (dark yellow), and "disallowed" (light green/ and white) regions plotted as red squares and labeled.

5.2.3 Validation of AlphaFold structure of *Pf*Ctr1 and crystal structure of *Pf*Grx1 using the ERRAT program

The ERRAT program verifies protein structures and uses scores to rate overall protein quality. The ERRAT program validated the AlphaFold *Pf*Ctr1 and *Pf*Grx1 crystal structures used in the interaction studies. The database belonging to ERRAT has highly refined structures. The plot usually involves the value graph of a nine-amino acid residue sliding window versus the error function (Colovos and Yeates, 1993). The basis of the plot is centered on the non-bonded interaction statistics between various types of atoms which are calculated by their structure in the database. In Fig 5.3 A and B, the overall quality of the input structures (*Pf*Ctr1 and *Pf*Grx1) was 91.4% and 100%, respectively. This implies that the resolution of the two structures is between 2-3 Å because the overall score is more than 90%. Fig 5.3 A has a few red and yellow bars that stand for parts of the structure that are problematic in the *in-silico* analysis regarding the interaction of the two proteins. On the other hand, Fig 5.3 B, has no problematic regions, and therefore, reasonably accurate results from modeling studies are more likely.

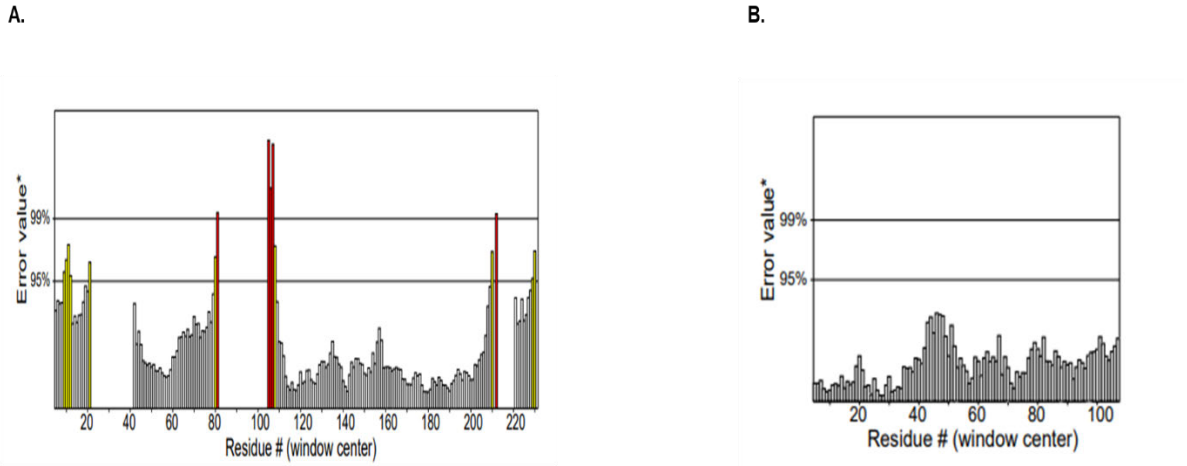

Fig 5.3 Validation of the AlphaFold *Pf*Ctr1 and *Pf*Grx1 crystal structures. Result ERRAT server shows graphs between residues and error values. The overall quality score of the input structure in **(A)** *Pf*Ctr1 is 91.379%, while that in **(B)** *Pf*Grx1 is 100%.

5.2.4 Determination of protein interaction between *Pf*Ctr1 and *Pf*Grx1 using ClusPro 2.0 and visualized using PyMOL software.

Copper transport in *Plasmodium falciparum* requires protein interaction between the protein with bound copper and one without. A protein is required for copper to gain entry into and a second protein for copper to be distributed in the parasite. Such interaction should occur between the copper transporters involved in the copper entry and passing on the copper to another protein for its distribution in the parasite. *In-silico* analysis of the interaction between *Pf*Ctr1 and *Pf*Grx1 was conducted through ClusPro 2.0 (Desta *et al.,* 2020, Vajda *et al.,* 2017, Kozakov *et al.,*2017, Kozakov *et al.,* 2013) and visualized using PyMOL (http://www.pymol.org/pymol). Fig 5.4, A and B show the *Pf*Ctr1 and *Pf*Grx1 structures, respectively, *Pf*Ctr1 obtained from UniProt (Yogavel *et al.,* 2014, Varadi

et al., 2024), and *Pf*Grx1 from a protein data bank (PDB). Fig 5.4 C illustrates the highest-ranked docked complex out of the ten models generated. For each cluster, the table indicated the docked structures, the structure with the highest number of neighbor structures, and the energy of the lowest energy structure in the cluster (Table shown in additional information A1). The complex shown is the most populated cluster with 124 members and has a center structure with -927.1 kcal/mol of energy, and the energy of the lowest energy structure amounting to -1030.5 kcal/mol. Lower binding energy implies stronger attractive forces between the receptor and ligand, which in turn stabilizes the complex (Qureshi *et al.,* 2022).

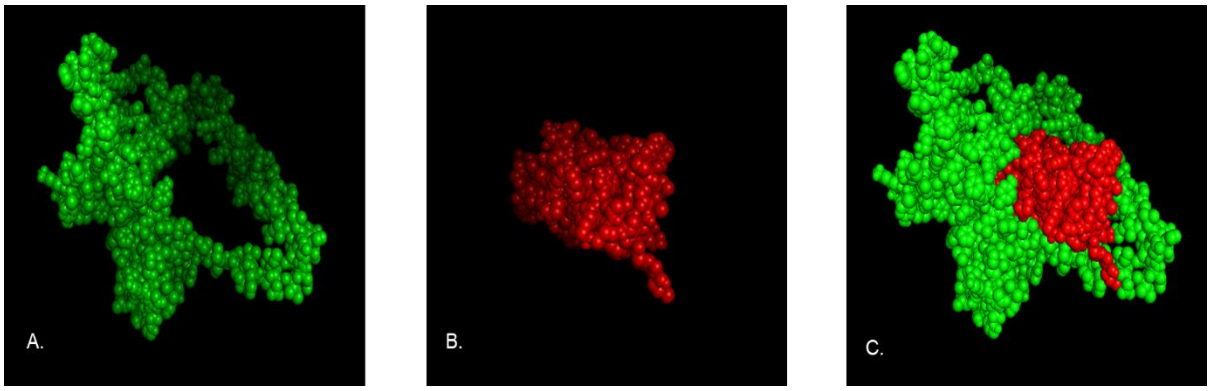

Fig 5.4 Interaction between *Pf*Ctr1 and *Pf*Grx1 using ClusPro. A. AlphaFold *Pf*Ctr1 (Q81L79) structure B. *Pf*Grx1 (Q9NLB2) crystal structure **C.** Complex formed between *Pf*Ctr1 and *Pf*Grx1 in ClusPro and visualized in PyMOL.

5.2.5 Potential Interactions between AlphaFold *Pf*Ctr1 and *Pf*Grx1 using PDBSum program

To analyze the type of bonds involved in the potential interaction between *Pf*Ctr1 and *Pf*Grx1, the selected complex generated from ClusPro 2.0 was submitted to the PDBSum server to identify the number of amino acids and type of bonds involved in the interaction (Fig 5.5 A, and B). Fig 5.5, A, shows the interaction between two proteins through an interface of 35 amino acid residues from *Pf*Ctr1 and 36 amino acid residues from *Pf*Grx1. The complex (*Pf*Ctr1-*Pf*Grx1) is held by four salt bridges, and thirteen hydrogen bonds. There are 226 non-bonded contacts between the two proteins. In Fig 5.5, B a summary of the statistics of the interface residues, number of disulfide and hydrogen bonds, and non-bonded contacts are shown, data that indicates a potential interaction between *Pf*Ctr1 and *Pf*Grx1.

A.

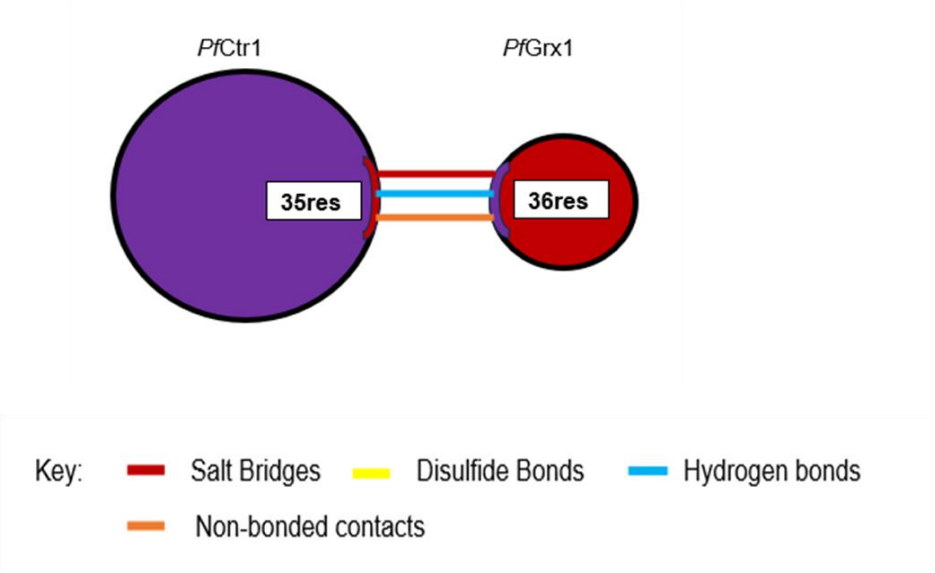

B.

Interface statistics						
Protein name	No. of interface residues	Interface area (Å^2)	No. of salt bridges	No. of disulfide bonds	No. of hydrogen bonds	No. of non-bonded contacts
*Pf*Ctr1	35	1953	4	-	13	226
*Pf*Grx1	36	1867				

Fig 5.5 Schematic diagram of the interactions between *Pf*Ctr1 and *Pf*Grx1 of the PDBSum generated complex. A. Interacting chains are joined by colored lines, each representing a different type of interaction, as per the key above. The area of each circle is proportional to the surface area of the corresponding protein. The extent of the interface region on each chain is represented by the wedge (red and purple) whose size signifies the interface surface area. **B.** Indicates the interface statistics. Data was generated from PDBsum (Laskowski., 2001).

5.2.6 Interaction plot for the complex formed between *Pf*Ctr1 and *Pf*Grx1 as generated by PDBsum software

PDBSum software was used to establish the amino acid residues and type of bonds used to interact with the proteins in the complex generated from ClusPro 2.0. In Fig 5.6, many amino acids are shown to be involved in the interaction between the proteins. *Pf*Ctr1 has three transmembrane regions that span from amino acid residues 116-133, 166-183, and 188-205 (Choveaux *et al.,* 2012). Therefore, any possible interaction with this protein in biological processes in the cytoplasm is only

likely to occur with amino acid residues in positions 134-165 and 206-235 (Fig 5.7). When the diagram is analyzed, the *Pf*Grx1 interacts with *Pf*Ctr1 using aspartate and phenylalanine at positions 229 and 226, respectively, through two hydrogen bonds, one salt bridge, and hydrophobic interaction (Fig 5.6, 5.7). This result suggests that there is a possibility that *Pf*Grx1 can interact with and receive copper from *Pf*Ctr1. The ClusPro program results also show that *Pf*Grx1 can potentially interact with amino residues located between the 2nd and 3rd transmembrane regions from the N-terminus of *Pf*Ctr1 and with amino acid residues at 180, 183, and 199, which are part of the MXXXM and GXXXG copper-binding motifs (Fig 5.7). However, this is unlikely under physiological conditions as the *Pf*Grx1 is on the cytosolic side of the membrane (Fig 5.7). Interestingly, human red blood cell Grx1 (*Hs*RBC Grx1) which shares valine, leucine, isoleucine, phenylalanine, asparagine, lysine, tyrosine, proline, glycine, glutamine, threonine and arginine with *Pf*Grx1 protein (Fig 5.8), may interact with residues on the N-terminal and some residues that are part of the MXXXM and GXXXG copper-binding motifs (Fig 5.9). These findings suggest that there is a possibility that *Hs*RBC Grx1, which is located extracellularly, may interact with *Pf*Ctr1 due to the shared residues with *Pf*Grx1 that participate in the interaction (additional information A2).

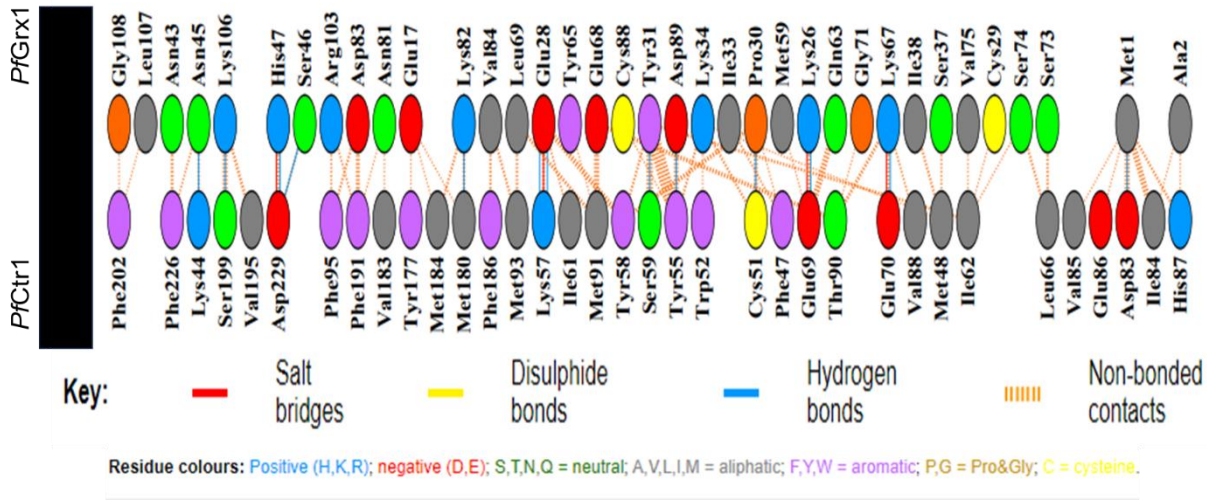

Fig 5.6 PDBsum interaction plot for AlphaFold *Pf*Ctr1 and *Pf*Grx1 crystal structures. The plot indicates hydrogen bonds (blue lines), nonbonded contacts (orange tick marks (banding pattern), and salt bridges (red lines) between residues on either side of the protein-protein interface.

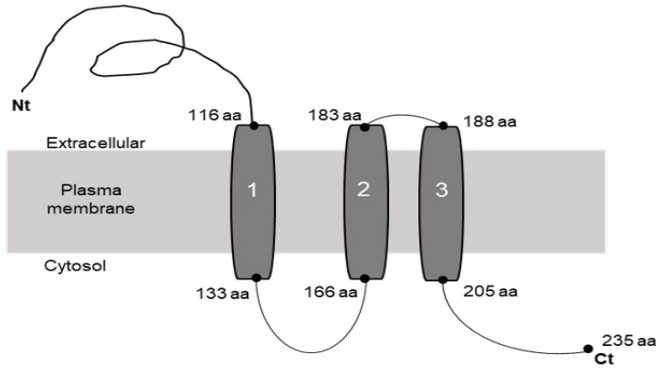

Fig 5.7 Schematic picture of the membrane topology and key features of *Pf*Ctr1. Three transmembrane (TM) (1-3), extracellular amino-terminal (Nt), and intracellular carboxy-terminal (Ct) domains. The start and end of each TM is shown on the diagram (116-133, 166-183, and 188-205).

```
P.falciparum      MAGTSEAVKKWVNKIIEENIIAVFAKTECPYCIKAISILKGYNLNSH-MHVENIEKNPDM     59
H.sapiens         ------MAQEFVNCKIQPGKVVVFIKPTCPYCRRAQEILSQLPIKQGLLEFVDITATNHT     54
                        .:::**  *: . :.** *  **** :* .**.   ::.  :.. :*  . .

P.falciparum      ANIQAYLKELTGKSSVPRIFINKDVVGGCDDLVKENDEGKLKERLQKLGLVN      111
H.sapiens         NEIQDYLQQLTGARTVPRVFIGKDCIGGCSDLVSLQQSGELLTRLKQIGALQ      106
                   :** **::***  :***:**.** :***.***. ::.*:*  **:::* ::
```

Fig 5.8 Alignments of amino acid sequence of Grx1 from *Plasmodium falciparum* and *Homo sapiens*. The amino acid sequence of Grx1 from *P. falciparum* and *H. sapiens* were aligned using ClustalW (Thompson et al., 2003). Conserved Residues are indicated by *, while : represents a conserved and . indicates a semi-conserved amino acid substitution. The amino acids in yellow are common in both amino acid sequences *Pf*Grx1 and *Hs*Grx1 (https://www.ebi.ac.uk › thornton-srv › databases › pdbsum)

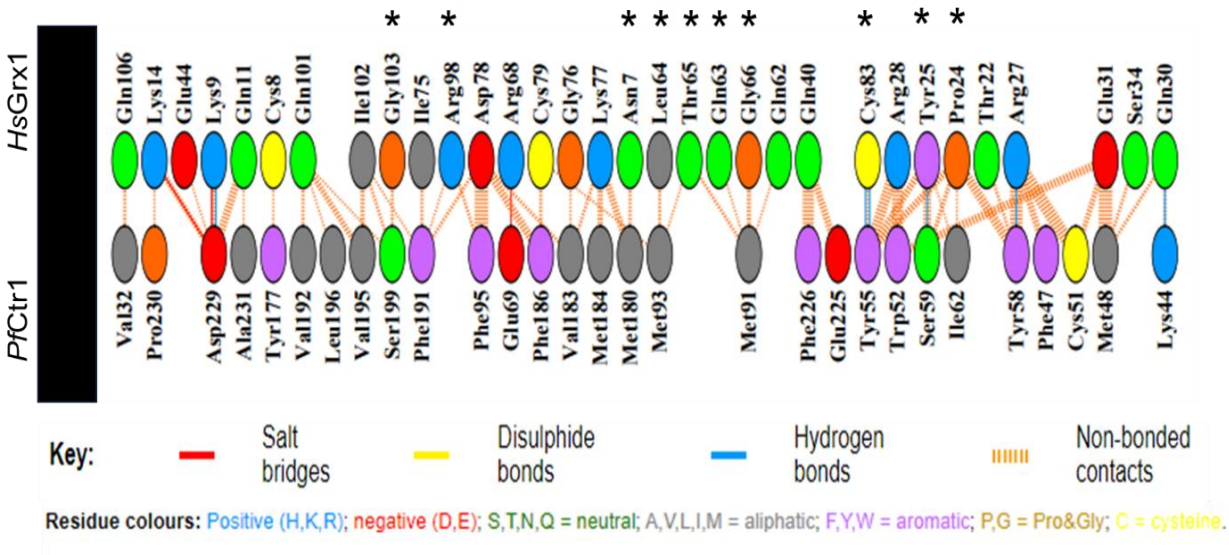

Fig 5.9 PDBsum interaction plots for the interface between the *Pf*Ctr1 and *Hs*Grx1. A plot of hydrogen bonds (blue lines), non-bonded contacts (orange tick marks (banding pattern), and salt bridges (red lines) between residues on either side of the protein-protein interface are shown on the diagram. The * indicates the amino acid residues common in both *Pf*Grx1 and *Hs*Grx1 that interact with *Pf*Ctr1(https://www.ebi.ac.uk › thornton-srv › databases › pdbsum)

5.2.7 Prediction of possible clefts on AlphaFold *Pf*Ctr1 structure using the SURFNET program

The size of the cleft in the protein's surface is of primary importance in determining how proteins interact with one another (Laskowski *et al.,* 1996). The PDBSum predicted clefts on the *Pf*Ctr1 where *Pf*Grx1 could bind. In Fig 5.10, A, B, and C, three different orientations of *Pf*Ctr1 with clefts indicated in different colors according to their size and volume are shown. Other characteristics are outlined in table (D) on the right of Fig 5.10. The calculation of the cleft regions in PDBsum is done via the SURFNET program (https://www.ebi.ac.uk). The analysis shows that the red cleft is the largest and deepest cleft. According to Laskowski *et al.,* 2017, the largest cleft is the most probable binding site of a ligand (Laskowski *et al.,* 2017). Interestingly, this cleft contains aspartate that appears to bind with two hydrogen bonds and a salt bridge to histidine and serine of *Pf*Grx1 (Fig 5.7, 5.8 D). Phenylalanine is also part of the cleft and interacts through hydrophobic bonds with glycine and leucine amino acids (Fig 5.7, 5.10 D). This data implies that *Pf*Grx1 may bind in the largest cleft colored red (Fig 5.10 D).

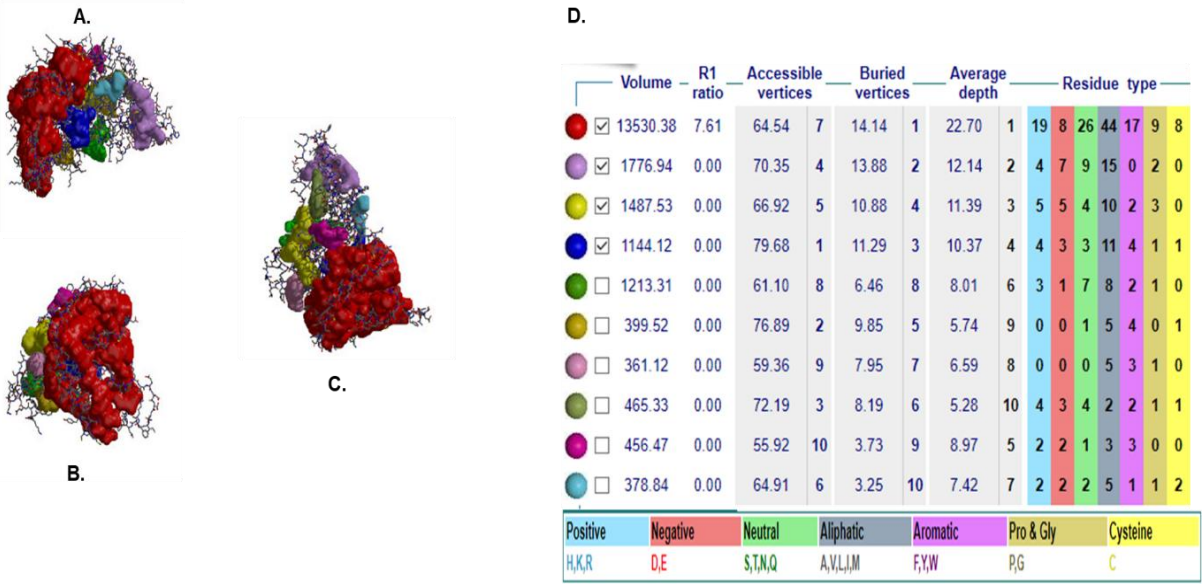

Fig 5.10 Clefts on the protein AlphaFold surface structure of *Pf*Ctr1. Three orientations (**A**, **B**, and **C**) of protein structure with highlighted clefts (marked in various colors that correspond to those in Table **D**) are illustrated for the protein. A table is included with details on the pocket's volume, R1 ratio, depth, and residue type are visible on the right; the coloring of the residues involved is below the table. Data is generated from PDBsum (Laskowski., 2001).

5.2.8 Molecular Dynamics Simulation (MDS)

The CABS-flex 2.0 server was utilized to perform a molecular dynamics simulation (MDS) at default settings to determine the changes the protein structures will have after the two proteins have interacted. This algorithm used by the server emulates the alterations in biological structures (Badar *et al.,* 2022). The fluctuations in the amino acids during a 10 ns molecular dynamics simulation of unbound *Pf*Grx1 and the structure of *Pf*Grx1 bound to *Pf*Ctr1 are shown in Fig 5.11 A. The use of 10 ns molecular dynamics simulation is supported by Bourne *et al.,* 1995).

Additionally, Fig 5.11, B shows the unbound *Pf*Ctr1 and bound structure of *Pf*Ctr1 to *Pf*Grx1. There was a significant statistical difference between the unbound (*Pf*Grx1 and *Pf*Ctr1) and bound *Pf*Ctr1 (P≤ 0.0001), and *Pf*Grx1 (P≤ 0.05) structures, respectively. This suggests a potential interaction between the two proteins. Further analysis of the *Pf*Grx1 simulation showed that between amino acid residues 40 to 60, and 60 to 80 in Fig 5.11 A is where possible interaction would occur. These two regions encompass amino acid residues at 46, 47, and 67 (Fig 5.7, 5.11 A). *Pf*Ctr1 equally has two regions starting from amino acids 0 to 50, and 150 to 200 which corresponds to a likely interaction at positions 32 – 48 and 183 – 191 as shown in Fig 5.7, and 5.11 B. This suggests a potential interaction between *Pf*Ctr1 and *Pf*Grx1 as predicted by the ClusPro 2.0 program. However, the interaction regions of *Pf*Ctr1 are either on the extracellular N-terminus or the loop with the MXXM copper-binding motif which makes the potential interaction with *Pf*Grx1 less likely unless *h*RBC Grx1 is involved as earlier explained in 5.2.6.

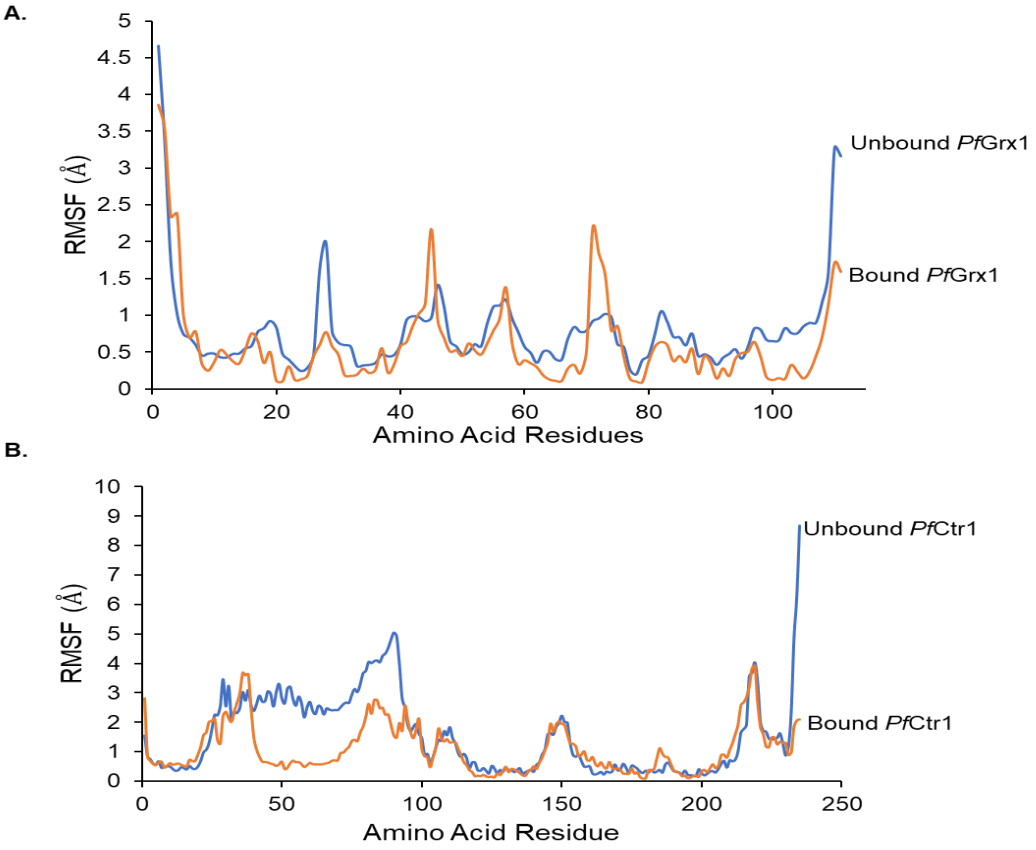

Fig 5.11 Molecular dynamics simulation of the unbound and bound crystal structure of *Pf*Grx1 and AlphaFold *Pf*Ctr1 structure, respectively. A. Fluctuation plot of the number of amino acid residues of unbound (blue) and bound (orange) *Pf*Grx1. **B.** Fluctuation plot of the number of the amino acid residues of unbound (blue) and bound (orange) *Pf*Ctr1. The results indicate a significant difference between the unbound and bound structures of *Pf*Grx1(P≤ 0.05) and *Pf*Ctr1 (P≤ 0.0001), respectively (Karplus and Petsko., 1990).

5.2.9 An assessment of AlphaFold *Pf*CuATPase and *Pf*Grx1 crystal structures using Ramachandran plot

PROCHECK software was used to assess the quality of AlphaFold *Pf*CuATPase (Q813A0) and *Pf*Grx1 (Q9NLB2) crystal structures by utilizing the Ramachandran plot. Fig 5.12, A shows that 55.2% of the residues belong to the most favored regions, while additional allowed, generously allowed, and disallowed regions accounted for 18.8%, 10.3%, and 15.7%, respectively. However, a good-quality structure should have >90% of its amino acid residues in the most favored regions (Rai *et al.,* 2012). Protein-to-protein analysis using a structure such as this one still produces good results because more than half of the residues are found in the most favored regions. Refinement of *Pf*CuATPase could have helped with the upward adjustment of the structure quality, nevertheless, *Pf*CuATPase has more than 1000 amino acid residues which was the limit in the GalaxyWEB refinement server (Ko *et al.,* 2012) (http://www.galux.co.kr/). Fig 5.12 B shows the results highlighted in section 5.2.2.

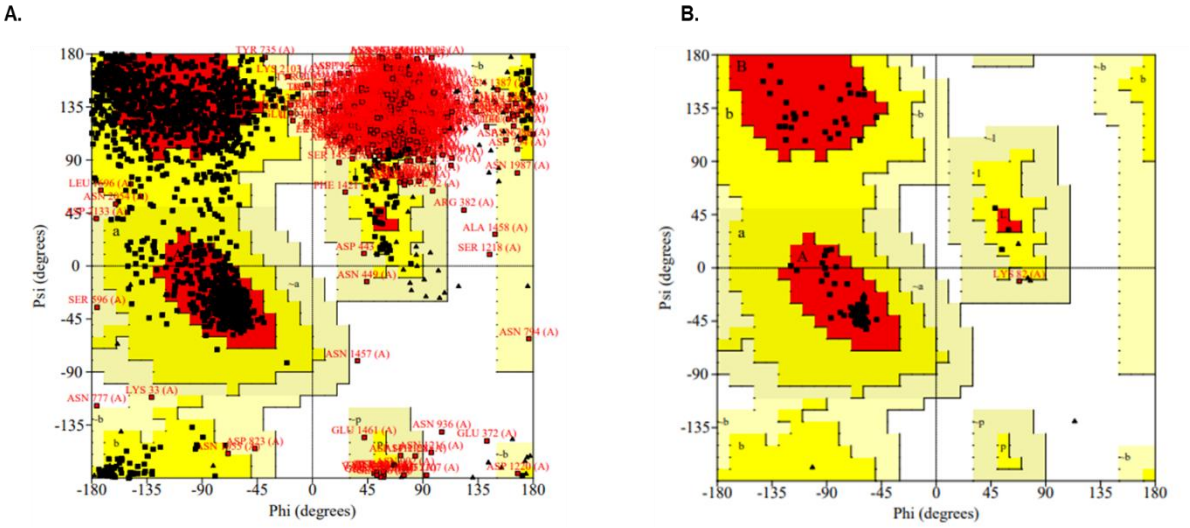

Fig 5.12 Ramachandran plot of the AlphaFold *Pf*CuATPase and *Pf*Grx1 crystal structures using PROCHECK. A *Pf*CuATPase and **B** *Pf*Grx1 illustrate the distribution of the protein's (*Pf*CuATPase and *Pf*Grx1, respectively main φ-ψ torsion angles (black squares) relative to the "core" (red) and "allowed" (yellow) regions, with residues falling in "generously allowed" (dark yellow), and "disallowed" (light green/ and white) regions plotted as red squares and labeled.

5.2.10 Evaluation of the AlphaFold *Pf*CuATPase and *Pf*Grx1 crystal structures using ERRAT program

In Fig 5.13 A (i-ix), the ERRAT score for *Pf*CuATPase was 58.229%, which is below the recommended threshold percentage. When the graph was analyzed, there were many red bars between 80-380 amino acid residues, and above 600 to 1480 amino acid residues. The red and yellow bars are not predominant above 1480 amino acid residues (Fig 5.13 A (v-ix). This shows that the software could not detect the problematic regions of the protein with accuracy, a fact that affects the quality of the structure. Those regions of the structure that are yellow can be rejected at a 95% confidence level; 5% of a good protein structure may have an error value above this level. Those regions in red are rejected above 99% level of confidence. However, the

structure was used in the interaction studies because the quality of the structure was above 50% (Messaoudi *et al.,* 2013). Fig 5.13 B shows a 100% score for *Pf*Grx1 as earlier determined in section 5.2.2. The reason for the low percentage of ERRAT score of AlphaFold *Pf*CuATPase structure may emanate from a lack of cofactors, metal ions, or bound ligands, factors that affect the quality of AlphaFold structures. The AlphaFold *Pf*CuATPase structure has no ADP or ATP bound (Hekkelman *et al.,* 2023).

A.

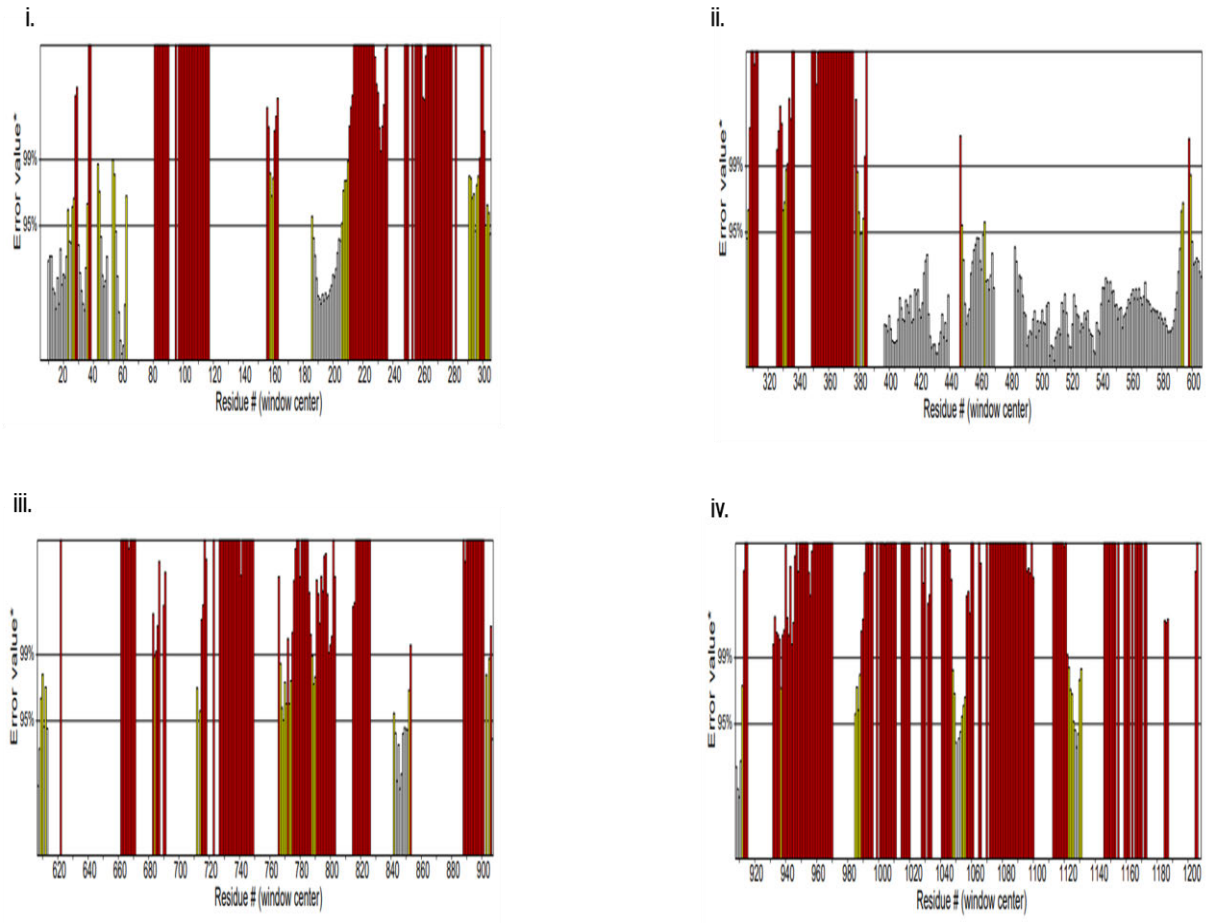

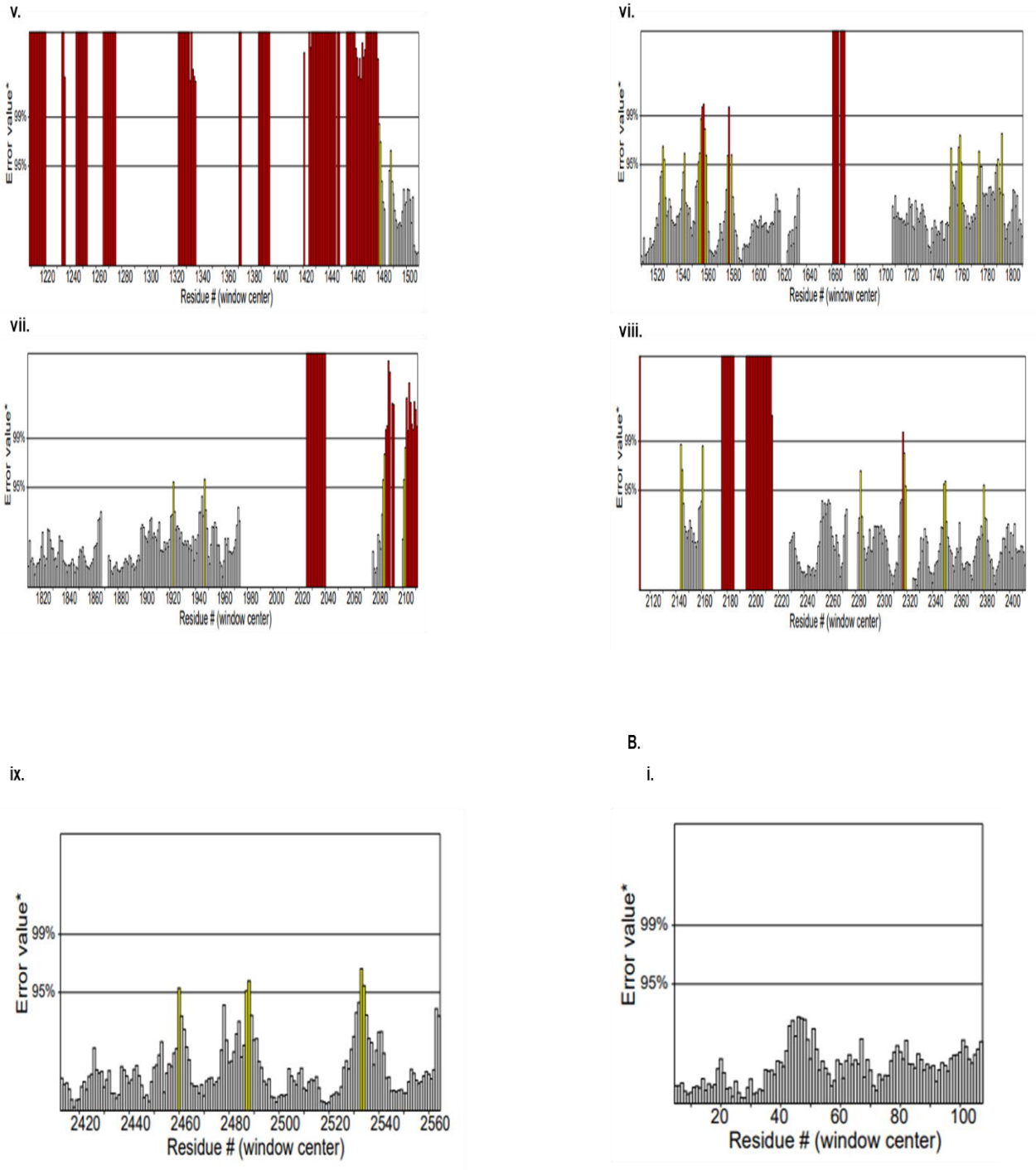

Fig 5.13 Validation of the AlphaFold *Pf*CuATPase, and *Pf*Grx1 crystal structures. ERRAT server illustrates the graphs between residues and error values. The overall quality score of the input structure of **A.** *Pf*CuATPase in (**Q813A0**) [(i-ix)]) is 58.229%, while that for **B.** *Pf*Grx1 in (**Q9NLB2**) [(i)]) is 100%.

5.2.11 Interaction analysis between AlphaFold *Pf*CuATPase and *Pf*Grx1 crystal structures using ClusPro 2.0

Fig 5.14 A and B show the AlphaFold *Pf*CuATPase and *Pf*Grx1 crystal structures obtained from UniProt (https://www.uniprot.org) and the protein data bank, respectively. Fig 5.14 C shows a complex structure of *Pf*CuATPase and *Pf*Grx1, which was selected based on the high number of members (107) in the set of structures. The center structure has an energy of -846.3 kcal/mol, while the energy of the lowest energy structure in the cluster is -1029.2 kcal/mol (Table is shown in additional information B1). This suggests that the complex generated by the ClusPro program is stable (Qureshi *et al.,* 2022).

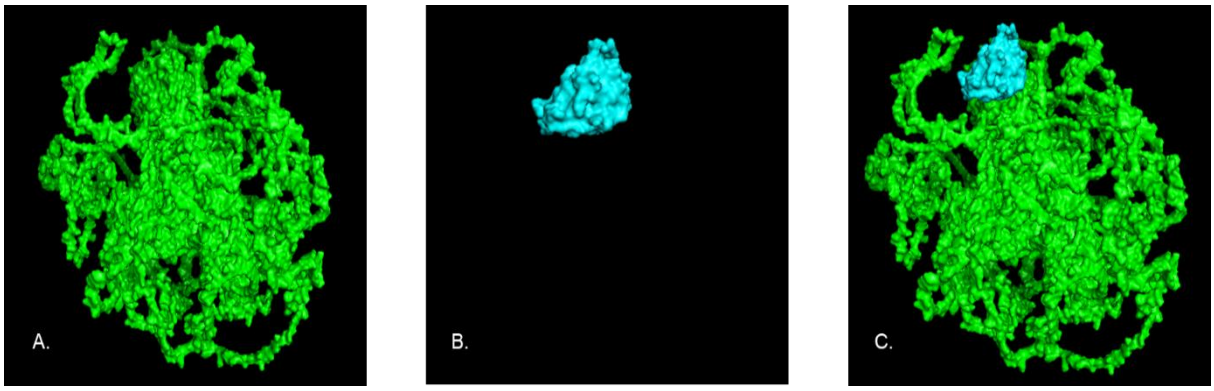

Fig 5.14 Interaction between *Pf*CuATPase and *Pf*Grx1 using ClusPro 2.0. A. *Pf*CuATPase AlphaFold structure (Q813A0) B. *Pf*Grx1 crystal structure (Q9NLB2) **C.** Complex formed between *Pf*CuATPase and *Pf*grx1 in ClusPro and visualized in PyMOL. NOTE: The protein structures are sized and position so exposed the point of attachment when a complex is formed.

5.2.12 Statistical descriptives for the interaction between *Pf*CuATPase and *Pf*Grx1 complex as established by the PDBsum program

Using a complex of *Pf*CuATPase and *Pf*Grx1, analyses from the PDBSum program produced statistical data that showed the potential interaction between the two proteins. It was observed that the proteins in the complex interacted through an interface of 20 amino acid residues from *Pf*CuATPase and 18 from *Pf*Grx1 (Fig 5.15 A). The complex is held by two hydrogen bonds and 155 non-bonded contacts, as indicated in the statistical summary table in Fig 5.15 B. When Fig 5.16 is analyzed, the interaction occurs through two hydrogen bonds at amino acid residues 1560 located in the transmembrane two region and 1876 on the extracellular loop connecting the transmembrane regions three and four. This data suggests that *Pf*CuATPase may potentially interact with *Pf*Grx1 on the outside of the cell though not at physiological conditions because *Pf*Grx1 is located intracellularly, thus, the likely interaction with *Pf*CuATPase is on the N-terminus, intracellular loops, transmembrane regions and the C-terminus all of which are intracellular (Fig 5.16).

A.

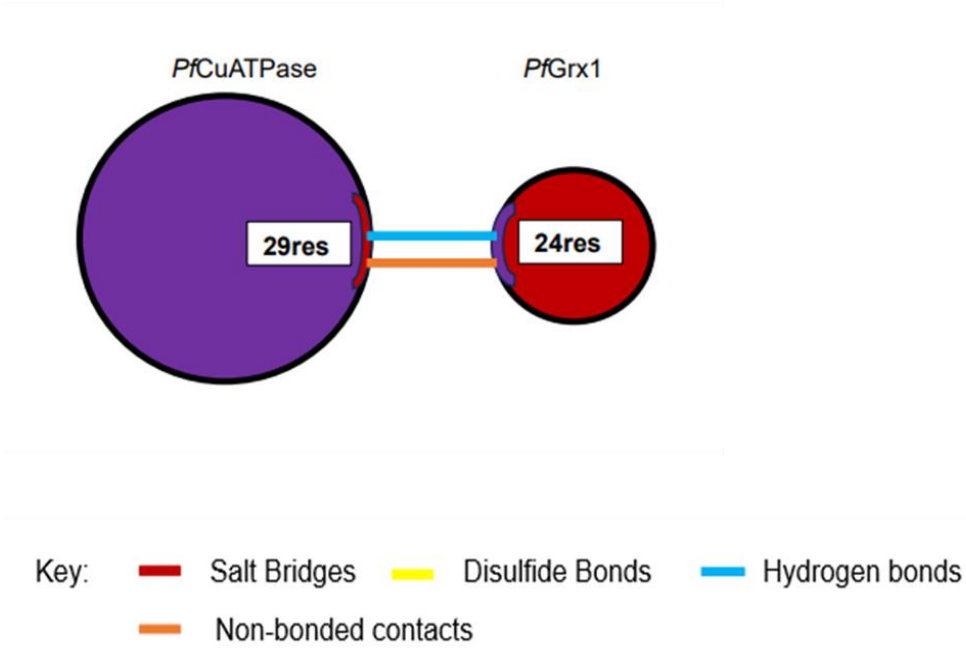

B.

Interface statistics						
Protein name	No. of interface residues	Interface area (Å^2)	No. of salt bridges	No. of disulfide bonds	No. of hydrogen bonds	No. of non-bonded contacts
*Pf*CuATPase	20	1144	-	-	2	155
*Pf*Grx1	18	1183				

Fig 5.15 Schematic diagram of the interaction between *Pf*CuATPase and *Pf*Grx1 of the PDBsum generated complex. A. Colored lines join interacting proteins, each representing a different type of interaction, as shown in the key above. The area of each circle is proportional to the surface area of the corresponding protein chain. The extent of the interface region on each chain is represented by the wedge (red and purple) whose size signifies the interface surface area. **B.** Indicates the interface statistics concerning the number of residues involved in the interface of each chain, interface area, number of salt bridges, number of disulfide bonds, and number of non-bonded contacts (Laskowski, 2001)

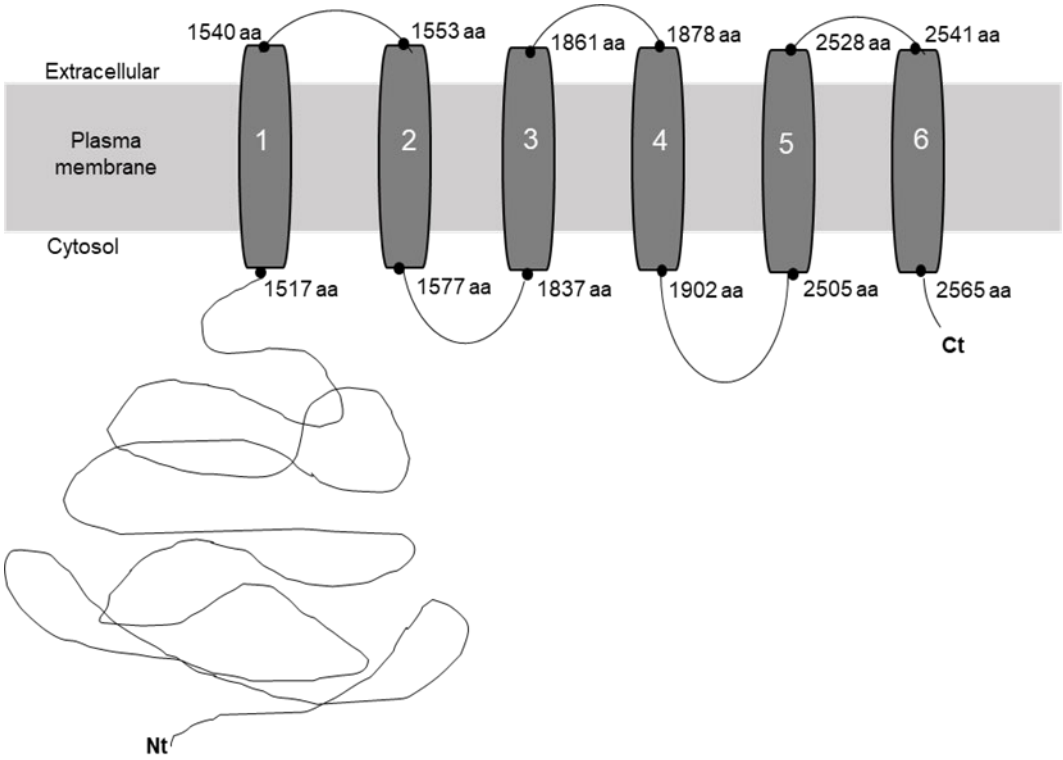

Fig 5.16 Schematic picture of the membrane topology and key features of *Pf*CuATPase. Six transmembrane (TM) (1-6), intracellular amino-terminal (Nt), and carboxy-terminal (Ct) domains. The amino acid residue involved in the start and end of each TM is shown on the diagram (1517-1540, 1553-1553, 1837-1861, 1878-1902, 2505-2528, 2441-2565). Source: M. Kwangu.

5.2.13 Interaction plot for the complex formed between AlphaFold *Pf*CuATPase and *Pf*Grx1 crystal structures.

When the *Pf*CuATPase-*Pf*Grx1 complex was submitted to the PDBsum server for analysis, the interaction in Fig 5.17 between the two proteins was generated. Fig 5.17 shows the type of bonds involved and the amino acid residues forming these bonds. *Pf*CuATPase is a P1B-1 type of ATPase that possesses transmembrane helices with Metal Binding Domains (MBD) in the cytosolic N-terminal region and serves to export copper from inside cells (Palmgren, 2023; Lutsenko *et al.,* 2007; Arguello *et al.,* 2007). Prediction of transmembrane regions using the HMMTOP server (http://www.enzim.hu>hmmtop) yielded six transmembrane helices (Fig 5.16). The most important feature of these Cu-ATPases from bacteria, and humans, is the presence of transmembrane metal-binding sites (Arguello *et al.,* 2003; Gonzalez-Guerrero *et al.,* 2008a; Mandal *et al.,* 2004). The transmembrane helices of *Pf*CuATPases span from amino acid residue 1517 – 1540, 1553 – 1577, 1837 – 1861, 1878 – 1902, 2505 – 2528, and 2541 – 2565 (Fig 5.16). Therefore, *Pf*Grx1 will potentially interact with the cytosolic N- and C- terminus, and cytosolic loops of *Pf*CuATPase under physiological conditions. However, findings from the modeling show that the potential interaction occurs with amino residues in transmembrane helices number 2, 3, and 4 of *Pf*CuATPase (Fig 5.16, 5.17). According to Solioz and Vulpe., 1996, *Pf*CuATPase has a metal-binding motif that stretches from amino acid residue 403 to 408 at the N-terminal region before the first

predicted transmembrane helix, and Rasoloson *et al.,* 2004 showed that this region in malaria protein binds copper (I). Nevertheless, copper (I) in some instances is delivered directly to the transmembrane metal binding sites (without involving N-terminal metal binding domains) through a copper chaperone, which is required to be near the transmembrane-metal binding sites for the transfer of copper to take place (Gonzalez-Guerrero *et al.,* 2008b; 2009). Using this scenario, it is proposed that there is a likelihood that *Pf*Grx1 may pass copper (I) to the *Pf*CuATPase for secretion, provided the *Pf*Grx1 is near the amino acid residues that are part of the transmembrane metal binding sites. Other interactions between *Pf*CuATPase and *Pf*Grx1 that are unlikely to occur under physiological conditions include interactions with amino acids at positions 1861, 1862, and 1876 located on the extracellular side of the membrane (Fig 5.16, 5.17), This is because *Pf*Grx1 is located in the cytoplasm of the parasite hence it is unlikely to interact with amino acids on the extracellular loop.

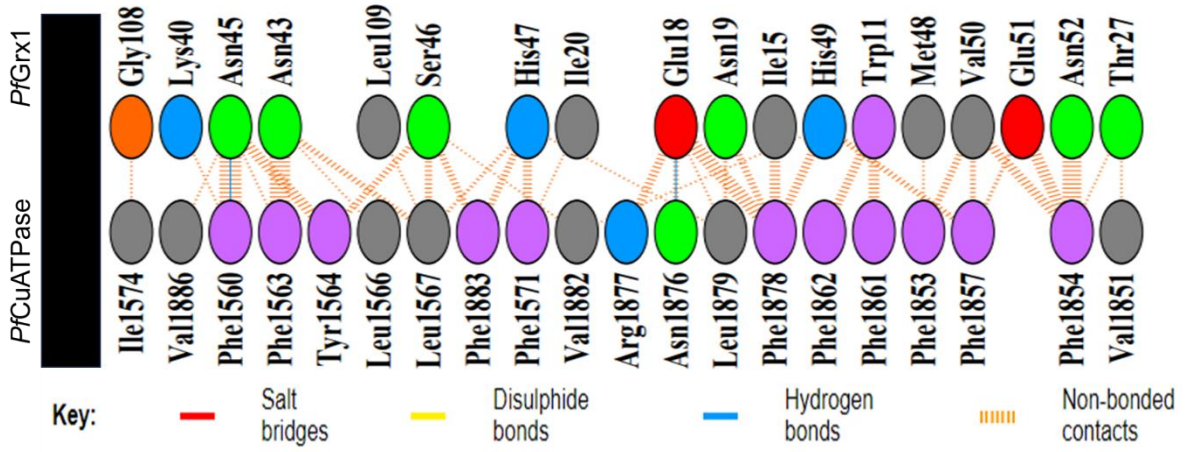

Fig 5.17 PDBsum interaction between the *Pf*CuATPase and *Pf*Grx1. Hydrogen bonds (blue lines), non-bonded contacts (orange tick marks/banding pattern), and salt bridges (red lines) between residues on either side of the protein-protein interface are shown on the diagram.

5.2.14 Prediction of possible *Pf*CuATPase's clefts used for the possible interaction with *Pf*Grx1

PDBSum servers generated possible interaction sites of *Pf*CuATPase with *Pf*Grx1. Fig 5.18 A, B, and C show three different orientations of the *Pf*CuATPase structure with clefts indicated in various colors. These are in different sizes and depths as shown in Fig 5.18, D. The cleft in red is the largest and deepest, thus the most likely interaction site with *Pf*Grx1 protein (Leskowski *et al.,* 2017). The amino acids belonging to *Pf*CuATPase shown to interact with *Pf*Grx1 (Fig 5.15) seem to be concentrated in the red cleft, making it a likely site for the protein-to-protein interaction (Fig 5.18 D). This association may aid the movement of copper from *Pf*Grx1 to the *Pf*CuATPase and finally out of the parasitic cell in scenarios explained in 5.3.3.

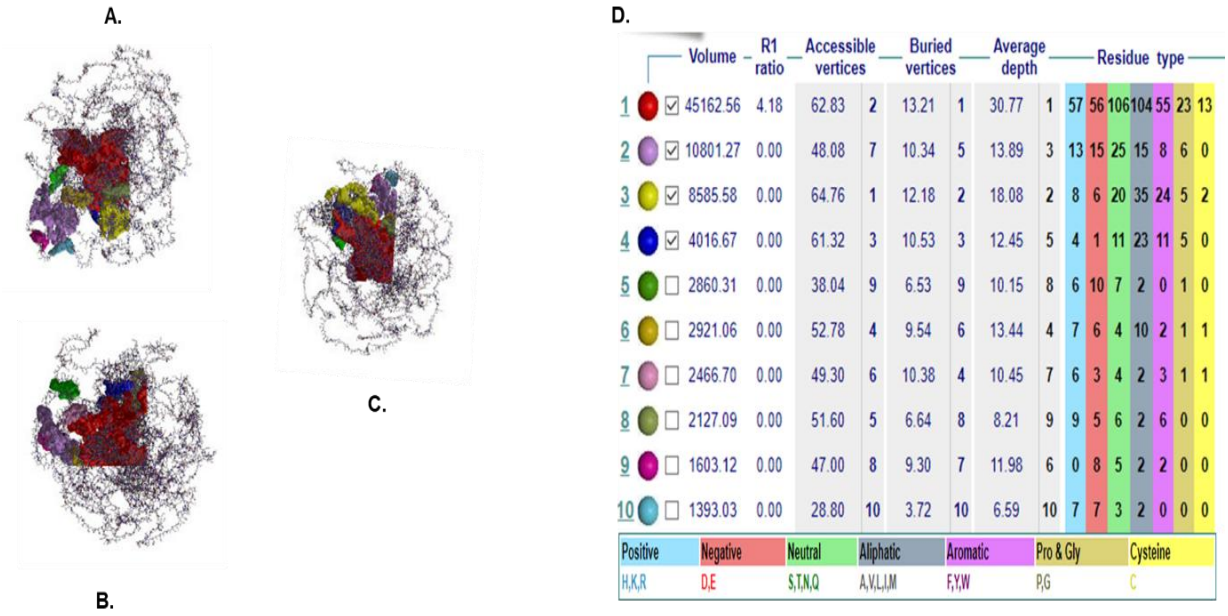

	Volume	R1 ratio	Accessible vertices		Buried vertices		Average depth		Residue type						
1	45162.56	4.18	62.83	2	13.21	1	30.77	1	57	56	106	104	55	23	13
2	10801.27	0.00	48.08	7	10.34	5	13.89	3	13	15	25	15	8	6	0
3	8585.58	0.00	64.76	1	12.18	2	18.08	2	8	6	20	35	24	5	2
4	4016.67	0.00	61.32	3	10.53	3	12.45	5	4	1	11	23	11	5	0
5	2860.31	0.00	38.04	9	6.53	9	10.15	8	6	10	7	2	0	1	0
6	2921.06	0.00	52.78	4	9.54	6	13.44	4	7	6	4	10	2	1	1
7	2466.70	0.00	49.30	6	10.38	4	10.45	7	6	3	4	2	3	1	1
8	2127.09	0.00	51.60	5	6.64	8	8.21	9	9	5	6	2	6	0	0
9	1603.12	0.00	47.00	8	9.30	7	11.98	6	0	8	5	2	2	0	0
10	1393.03	0.00	28.80	10	3.72	10	6.59	10	7	7	3	2	0	0	0

Positive	Negative	Neutral	Aliphatic	Aromatic	Pro & Gly	Cysteine
H,K,R	D,E	S,T,N,Q	A,V,L,I,M	F,Y,W	P,G	C

Fig 5.18 Surface clefts of the AlphaFold *Pf*CuATPase structure. Three orientations of the protein structure with different sizes and depths of the clefts (**A**, **B**, and **C**) (marked in various colors that correspond to those in Table **D**) are shown in the diagram. **D.** Table with details on the pocket's volume, R1 ratio, depth, and residue type. Additionally, the colors representing residues involved are indicated below the table. Data is generated from PDBsum (Laskowski., 2001).

5.2.15 Validation of AlphaFold *Pf*Cox17 and *Pf*Grx1 crystal structures

The PROCHECK ERRAT and Ramachandran plot online programs validated the AlphaFold *Pf*Cox17 (Q8IJE6, from UniProt) and *Pf*Grx1 crystal structures. The results for *Pf*Cox17 showed 1.7% of amino acid residues in the disallowed region and 85% of the amino acid residues in the most favored region (Fig 5.19). The result from the ERRAT quality check was 94.872% (Fig 5.20 A). This implied that the *Pf*Cox17 structure was of good quality and good for the modeling studies. The results for the *Pf*Grx1 crystal structure are as outlined in section 5.2.2.

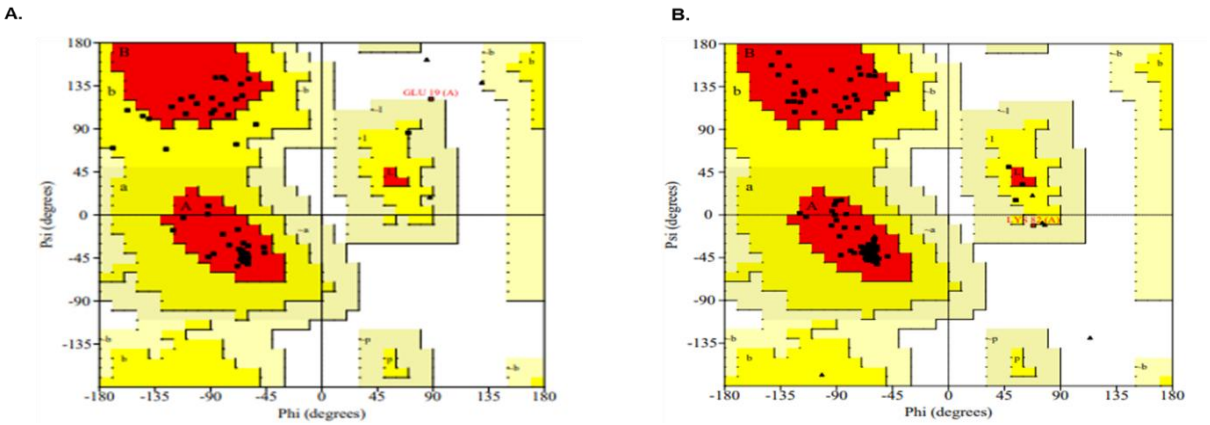

Fig 5.19 Ramachandran plot of AlphaFold *Pf*Cox17 and *Pf*Grx1 crystal structures using PROCHECK software. A *Pf*Cox17 and **B.** *Pf*Grx1 illustrate the distribution of the protein's (*Pf*Cox17 and *Pf*Grx1, respectively) main φ-ψ torsion angles (black squares) relative to the "core" (red) and "allowed" (yellow) regions, with residues falling in "generously allowed" (dark yellow), and "disallowed" (light green/ and white) regions plotted as red squares and labeled.

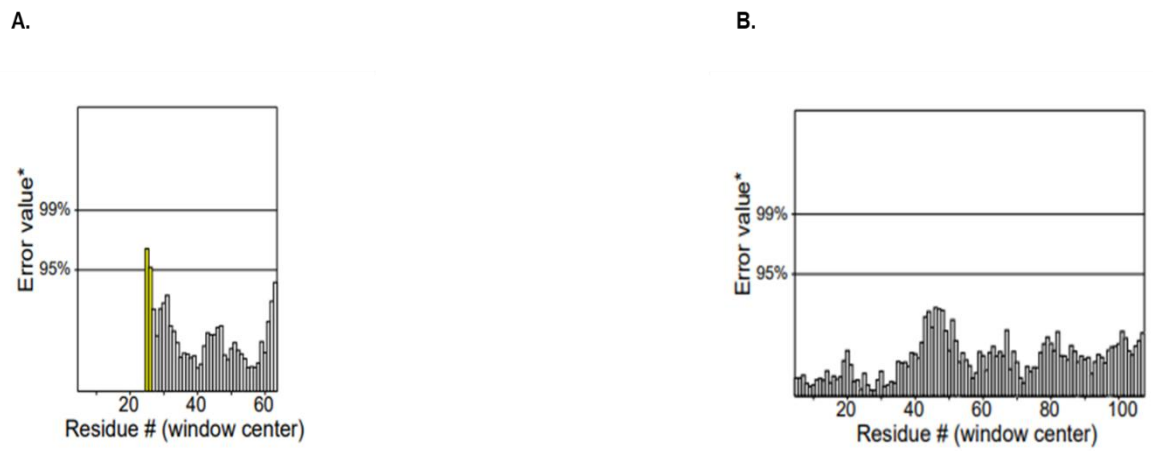

Fig 5.20 Validation of the AlphaFold *Pf*Cox17, and *Pf*Grx1 crystal structures. Result ERRAT server shows graphs between residues and error values. The overall quality score of the input structure in **(A)** *Pf*Cox17 is 94.872%, while that in **(B)** *Pf*Grx1 is 100%.

5.2.16 Potential interaction between AlphaFold *Pf*Cox17 and *Pf*Grx1 crystal structures

Understanding the entry and distribution of copper in the malaria parasite is important to unlocking some potential drug targets. The interaction between *Pf*Cox17 and *Pf*Grx1 may provide answers to questions surrounding copper movement from the parasite plasma membrane, through the cytosol and to the mitochondria. Subcellular fractionation experiments in yeast reveal that Cox17 is localized in both the cytosol and intermembrane space (Beers *et al.,* 1997). Choveaux *et al.,* 2015 demonstrated that *Pf*Cox17 is present in the cytosol in all three erythrocytic parasitic asexual developmental stages. Having established a possible interaction between *Pf*Grx1 and *Pf*Ctr1 in section 5.2.5, *Pf*Grx1 may interact with *Pf*Cox17 and provide a model for copper movement from *Pf*Ctr1 to the mitochondria. To achieve the latter, modeling to determine the potential interaction between *Pf*Cox17 and *Pf*Grx1 was conducted using ClusPro 2.0. Fig 5.21 A and B indicate *Pf*Cox17 and *Pf*Grx1 structures, respectively. In Fig 5.21 C a complex of *Pf*Cox17_*Pf*Grx1 is shown as generated from the ClusPro program (Table with cluster scores indicated in additional information C1). *Pf*Cox17 and *Pf*Grx1 interact through interfaces formed by 13 residues from *Pf*Cox17 and 18 residues from *Pf*Grx1, including six salt bridges, nine hydrogen bonds, and 199 non-bonded contacts (Fig 5.22, A and B). Fig 5.23 shows the interaction diagram between *Pf*Cox17 and *Pf*Grx1, notably, cysteine residues (C26 and C27) are thought to bind copper (I) (Choveaux *et al.,* 2015) and interact with *Pf*Grx1 on amino acid residues 7 and 11 (5.23). This may suggest that *Pf*Cox17 may receive copper (I) from *Pf*Grx1 and potentially shuttle it to the mitochondria. The table in Fig 5.24 D, shows the various sizes and depths of the clefts indicated by different colors. The interaction of *Pf*Grx1 could have potentially been in the cleft with red color as shown in Fig 5.24 A, B, and C.

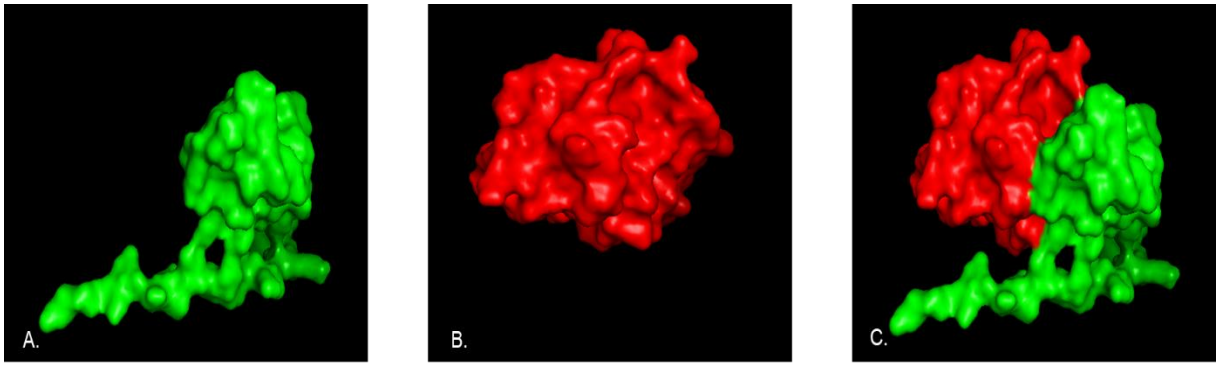

Fig 5.21 Interaction between *Pf*Cox17 and *Pf*Grx1 using ClusPro. A. AlphaFold *Pf*Cox17 structure (UniProt, Q8IJE6) B. *Pf*Grx1 crystal structure (PDB, Yogavel *et al.,* 2014) **C.** Complex formed between *Pf*Cox17 and *Pf*Grx1 in ClusPro and visualized in PyMOL.

A.

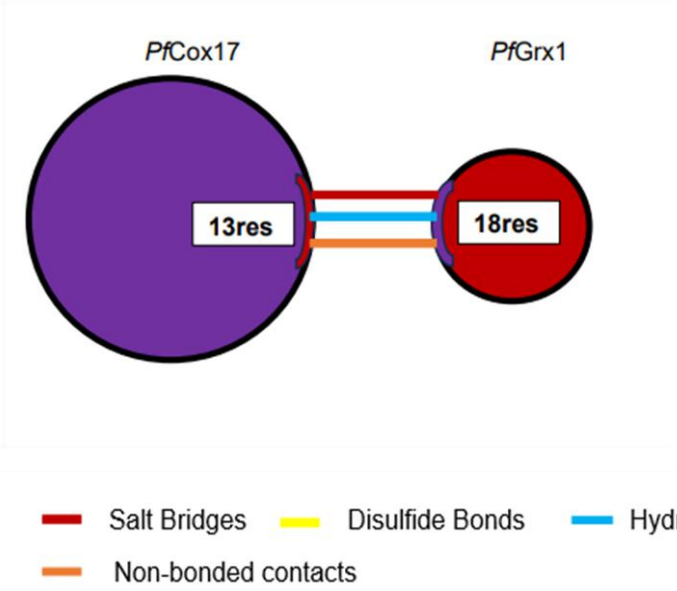

B.

Interface statistics						
Protein name	No. of interface residues	Interface area (Å^2)	No. of salt bridges	No. of disulfide bonds	No. of hydrogen bonds	No. of non-bonded contacts
*Pf*Cox17	13	892	6	-	9	109
*Pf*Grx1	18	763				

Fig 5.22 Schematic diagram of the interaction between *Pf*Cox17 and *Pf*Grx1 of the PDBSum generated complex. A. Interacting chains are joined by colored lines, each representing a different type of interaction, as shown in the key above. The area of each circle is proportional to the surface area of the corresponding protein chain. The extent of the interface region on each chain is represented by the wedge (red and purple) showing the interface surface area. **B.** Indicates the interface statistics concerning the number of residues involved in the interface of each chain, interface area, number of salt bridges, number of disulfide bonds, and number of non-bonded contacts.

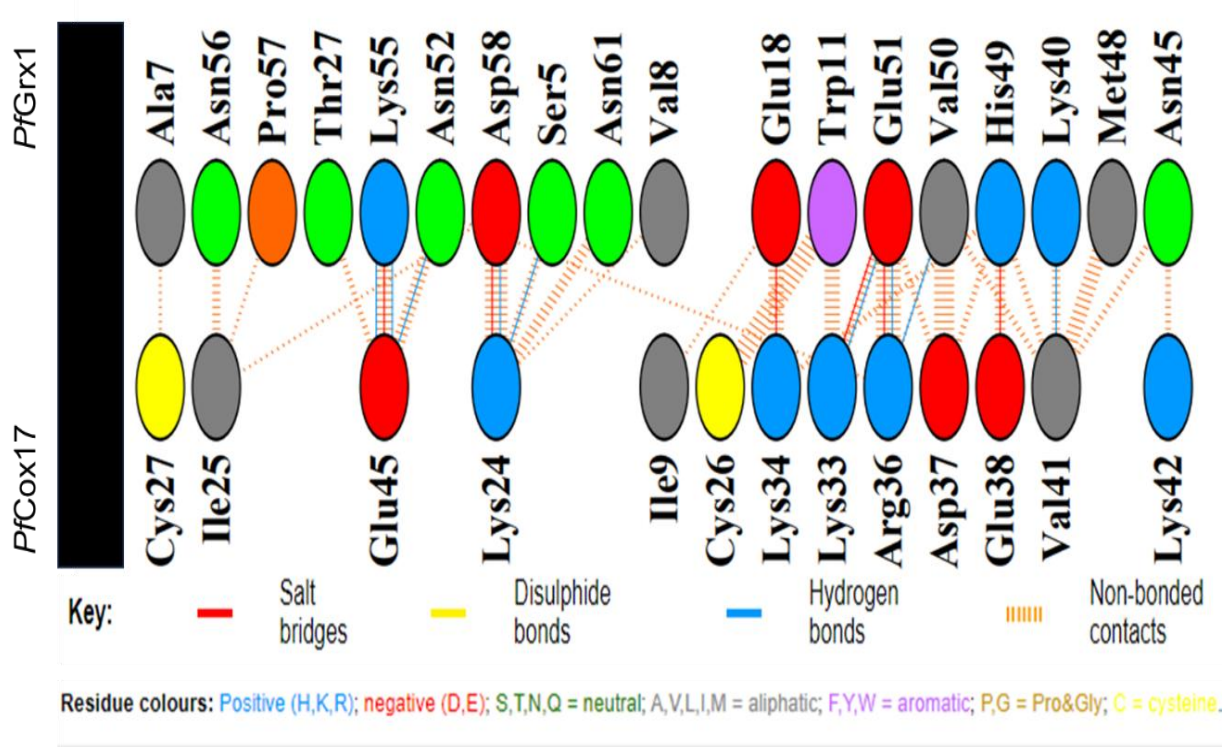

Fig 5.23 PDBsum interaction plots for the interface between the *Pf*Cox17 and *Pf*Grx1. Hydrogen bonds (blue lines), non-bonded contacts (orange tick-marks/banding pattern), and salt bridges (red lines) between residues on either side of the protein-protein interface are shown on the diagram.

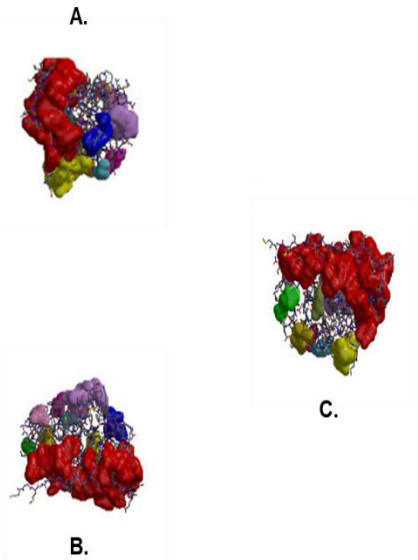

D.

	Volume	R1 ratio	Accessible vertices		Buried vertices		Average depth		Residue type					
1	6722.58	6.35	61.24	3	12.91	1	16.53	1	15	10	15	19	2	7	4
2	1058.06	0.00	64.52	2	9.66	2	9.57	3	5	3	3	9	0	1	1
3	801.14	0.00	53.09	9	6.80	5	9.79	2	1	1	4	5	0	1	0
4	504.56	0.00	59.00	6	8.30	3	8.36	4	3	2	2	3	0	1	0
5	300.80	0.00	60.98	4	7.32	4	5.74	8	3	2	1	2	0	0	0
6	283.92	0.00	59.72	5	3.50	10	5.08	9	4	4	1	2	0	1	0
7	226.55	0.00	48.20	10	5.72	6	6.20	6	1	0	2	3	1	1	0
8	182.67	0.00	78.07	1	3.69	8	0.00	10	1	2	1	3	2	0	0
9	191.95	0.00	56.88	7	4.45	7	6.24	5	2	1	0	1	1	1	1
10	178.88	0.00	56.81	8	3.62	9	5.90	7	0	1	1	1	1	0	2

Fig 5.24 Clefts on the protein AlphaFold surface structure of *Pf*Cox17. Three orientations (**A**, **B**, and **C**) of protein structure with highlighted clefts (marked in various colors that correspond to those in Table D) are illustrated for the protein. A table is included with details on the pocket's volume, R1 ratio, depth, and residue type are visible on the right; the coloring of the residues involved is below the table. Data is generated from PDBsum (Laskowski, 2001).

Chapter 6

Molecular docking of copper onto seven plasmodial copper-binding proteins

6.1 Introduction

Various proteins bind metals, and those that bind metal ions such as iron are important in cellular biological processes (Crichton *et al.,* 2002). Copper is vital for the survival of the malaria parasite (Asahi *et al.,* 2014). The parasite appears to obtain copper through the Ctr1 protein and secrete copper via CuATPases (Öhrvik *et al.,* 2017). Human Grx1 has been shown to play a role in the cytosolic movement of copper from Ctr1 to the copper-secreting ATPase protein (Maghool *et al.,* 2020), thus, the *Pf*Grx1 may play a similar function. *Pf*SAHH may be involved in cytosolic copper metabolism (Bethin *et al.,* 1995). Inside the parasite mitochondrion, Cox17 passes copper to Cox11 and Sco1 which metalates CuA sites of cytochrome c oxidase (Robison and Winge., 2010). Information on human Cox19 shows that it interacts with Cox11 (Nývltová *et al.,* 2022). All these proteins have been reported to bind copper. However, experimental determination of metal-binding sites on proteins is a difficult and involved process. Different specialized techniques like absorption spectroscopy, and resonance spectroscopy are required. Computational methods have been employed to analyze the metal-binding sites of proteins to provide an accessible evaluation (Lu *et al.,* 2022).

6.2 Results and Discussion

6.2.1 Molecular docking of copper with *Pf*Ctr1 involved in the potential uptake of copper

Molecular docking was conducted to establish the copper binding and binding sites for *Pf*Ctr1 using a Metal Ion-Binding (MIB2) site prediction and modeling server (http://combio.life.nctu.edu.tw/MIB2/). According to Puig *et al.,* 2002, copper may bind to the MXXXM (180-185) copper-binding motif of the *Pf*Ctr1 protein. The GXXXG motif is conserved in Ctr1s from most species (Choveaux *et al.,* 2012) and may play a role in the ability of Ctr1 to bind copper. Fig 6.1 A, I, and II show the complex of *Pf*Ctr1 and copper (I) with the highest score of 4.929 and binding residues histidine (H) and aspartate (D) at positions 79 and 80, respectively. Human Ctr1 has two Histidine-rich regions thought to have a role in copper binding (Puig *et al.,* 2002). Therefore, there is a possibility that H79 in *Pf*Ctr1 could be involved in copper binding (Fig 6.1 A I). Fig 6.1, III shows the top four complexes with the highest binding scores and the most likely copper binding sites which are 79H and 80D, 36C, 38H, and 41C, 38H and 40C, and 119S and 123C. The additional information section shows the table showing the remaining complexes with lower scores generated during the docking experiment.

A.

i. *Pf*Ctr1_Cu (H79, D80)

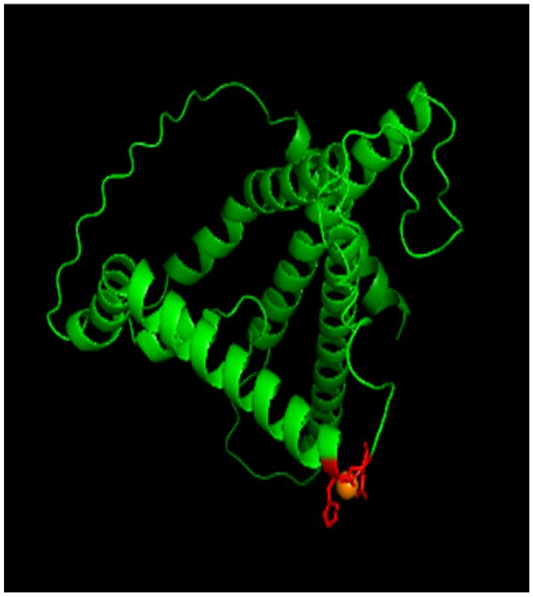

ii.

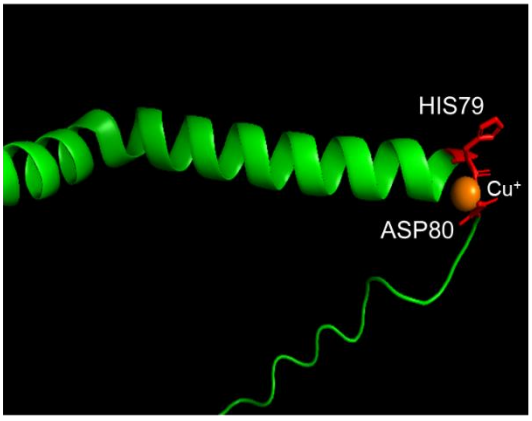

iii.

No.	Binding Residues	Template	Score
1	79H , 80D	5arnA1	4.929
2	36C , 38H , 41C	5fjeA1	4.229
3	38H , 40C	1zpuA3	3.804
4	119S , 123C	5fjeA5	3.448

Fig 6.1 Docking of copper (I) onto *Pf*Ctr1 which is involved in copper entry into the *Plasmodium falciparum* parasite. A, I. The *Pf*Ctr1 crystal structure with copper (I) bound. **II.** *Pf*Ctr1_Cu complex (binding score of 4.929) with histidine (79) and aspartate (D) as copper-binding amino acid residues. **III.** The table contains four *Pf*Ctr1_Cu complexes with the highest binding scores.

6.2.2 Determination of copper-binding to *Plasmodium falciparum* proteins involved in cytosolic copper distribution in the parasite

Like the human Grx1, *Pf*Grx1 may have a role in the cytosolic distribution of copper. Cytosolic *Pf*SAHH is involved in copper metabolism though the exact role is not yet established. Computational analyses in Figs 6.2 A, I, and II show that copper (I) binds to cysteine 29, 32 (CXXC), and serine residue at position 74 of *Pf*Grx1. Kusakabe *et al.,* 2015, showed that copper may bind to the cofactor binding glycine-rich (264-271) region (GXGXXGXG) of the SAHH protein. In Fig 6.2 B I and II, *Pf*SAHH docking results indicated that copper (I) may bind to glutamate (E) and cysteine (C) positioned at amino acid residues 167 and 171, respectively. Further analysis indicated that another *Pf*SAHH_Cu complex may bind copper (I) at amino acid residues 239 (cysteine), 271 (glycine), 272 (cysteine), and 319 (cysteine) with a low binding score (2.953) (Fig 6.2 B IV and V). This finding aligns with what Kusakabe *et al.,* 2015 reported in mouse SAHH where cofactors like metal ions like copper bind in the glycine-rich region. Mouse SAHH is 97% identical to *hs*SAHH which is similar to *Pf*SAHH (Coulter-Karis *et al.,* 1989). Amino acid residue at 271 which has been shown to bind copper in the model is part of the glycine-rich region (Singh *et al.,* 2016).

A.

i. *Pf*Grx1_Cu (C29, C32, S74)

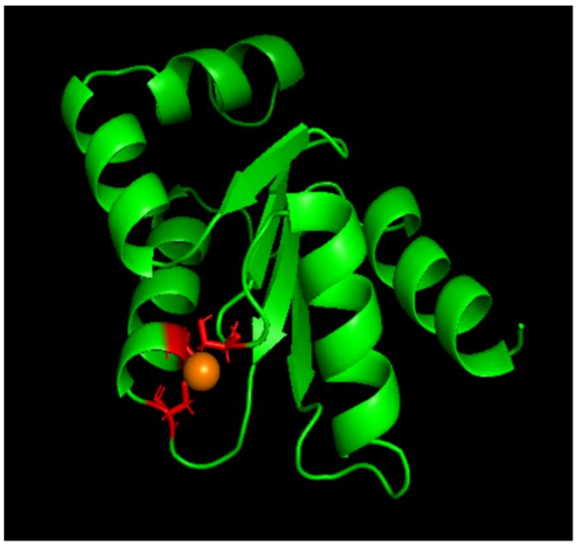

ii.

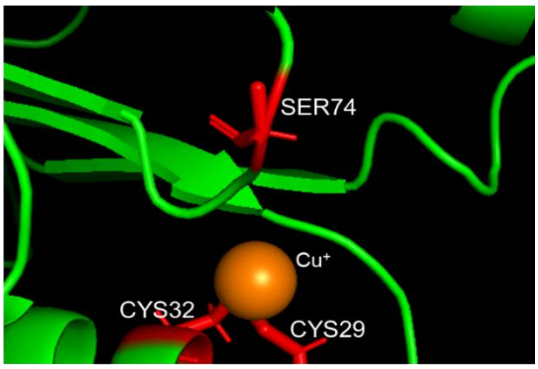

iii.

No.	Binding Residues	Template	Score
1	29C , 32C , 74S	6n5uA0	4.141
2	29C , 32C , 75V , 88C	5arnA6	4.047
3	29C , 32C , 75V , 88C	5arnA4	3.751
4	29C , 32C , 75V	5arnA1	3.650

B.

i. *Pf*SAHH_Cu (C239, G271, C272, C319)

ii.

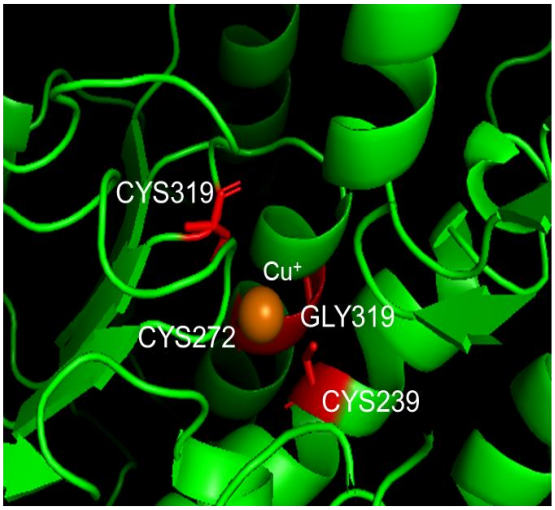

iii.

13	239C , 271G , 272C , 319C	5arnA4	2.953
14	28M , 30G , 445H	5fejA0	2.882

Fig 6.2 Analyses of copper (I) docking onto *Pf*Grx1 (Q9NLB2) and *Pf*SAHH (P50250) involved in cytosolic copper distribution in the parasite. A, I. The *Pf*Grx1 crystal structure is complexed with copper (I). II. *Pf*Grx1_Cu complex (binding score of 4.141) with cysteines 29, and 32, and serine at position 74 as copper-binding amino acid residues. **III.** The table contains four *Pf*Grx1_Cu complexes with the highest binding scores. **B. I** and **II,** Crystal structure of *Pf*SAHH with copper bound to cysteines 239, 272, and 319, and glycine at 271, **III** Table showing the position of the complexes generated from MIB2 server (Lu *et al.,* 2022).

6.2.3 Computational analyses of copper binding to plasmodial proteins involved in the mitochondrial distribution of copper

Molecular docking of copper onto different copper-binding proteins (*Pf*Cox17, *Pf*Cox11, and *Pf*Sco1) was performed and analyzed. Fig 6.3 A I and II indicate that copper (I) binds to histidine 55 and cysteine 58 (binding score 2.760), though laboratory evidence in yeast shows that any cysteine outside the CCXC motif is non-essential for copper (I) binding (Heaton *et al.,* 2000). When the rest of the *Pf*Cox17_Cu complexes were further examined, one complex with a lower binding score (1.279) compared to the one presented in Fig 6.3 A I and II was found to bind copper (I) at cysteine 26 and 27, residues that form **CCXC** motif in *P. falciparum* Cox17. In yeast, the substitution of C23, C24, or C26, (C23C24XC26, **CCXC**) of Cox17 led to the decreased binding capacity of the protein while a double mutant of C23, and C24 completely made the protein fail to bind copper (I) (Heaton *et al.,* 2000). However, another report in yeast by Abajian *et al.,* 2004, demonstrated that copper (I) binds to amino acid residues C23 and C26 which are still part of the CCXC motif. Copper (I) in human Cox17 is held by C22 and C23 which are part of the C22C23XC24 (**CCXC**) motif (Banci *et al.,* 2008). Further, Choveaux *et al.,* 2015, suggested that copper (I) binds to the C26C27XC29 **(CCXC)** motif of *Pf*Cox17 at amino acid residues 26 and 27 respectively. In the present docking study, copper (I) is shown to bind to C26 and C27 which are part of the CCXC motif of the *P. falciparum* Cox17. This finding supports the previous laboratory findings in yeast and mammalian cells that determined that copper (I) binds to the CCXC motif. Fig 6.3 B I and II are *Pf*Cox11 with copper (I) bound to cysteine residues at positions 155 and 157 that form the CXC motif. Salman *et al.,* 2022, demonstrated that C157 is essential for copper (I) binding compared to C60 when site-directed mutagenesis was performed; however, C155 was not mutated. In yeast, mutation of the two cysteines that form the C208XC210 (CXC) motif led to a significant loss of copper from the protein (Carr *et al.,* 2002). When copper (I) was docked with *Pf*Sco1, C159, C163 (CXXXC), and H264 was found to coordinate the binding of copper (I) (Fig 6.3 C, I and II). Mutating the two cysteines in the CXXXC motif has been shown to affect the copper binding function of Sco1 in yeast cells (Rentzsch *et al.,* 1999). In human Sco1, C169, and C173 that form the CXXXC motif has been shown to bind copper (I) together with amino acid residue histidine at position 260 (Banci *et al.,* 2006). *Bacillus subtilis* Sco1 has been shown to bind copper (I) through C45, and C49 which are part of the CXXXC motif and histidine at position 135 (Balatri *et al.,* 2003). The docking results, therefore, support the laboratory findings of Sco1 from other organisms. Interacting with *Pf*Cox11, one of the copper-binding proteins known to distribute copper in the mitochondria, is *Pf*Cox19 (Bode *et al.,* 2015). After molecular docking with copper (I), C34 and C45 ($CX_{10}C$) were identified as copper-binding residues (Fig 6.3 D, I and II). Another complex of *Pf*Cox19_Cu generated from the MIB2 server showed a CX_9CC motif with copper binding residues located at C34, C44, and C45), with a binding score (3.239) lower than the highest-ranked complex which had a binding score of 5.362 (Fig 6.3, D III and VI). In yeast, proximal cysteine amino acid residues (C30 and C62) in the CX_9C motif are essential in copper (I) binding (Rigby *et al.,* 2007). Salman *et al.,*2023, suggested in their report that the CX_9C copper-binding motif might be involved in copper (I) binding that was observed in various copper binding assays conducted, though site-directed mutagenesis

experiments were not carried out to establish which cysteines are involved. The bioinformatics analyses indicate also that proximal cysteines are involved in copper binding like what is observed in yeast cells (Rigby *et al.,* 2007)

A.

i. *Pf*Cox17_Cu (H55, C58)

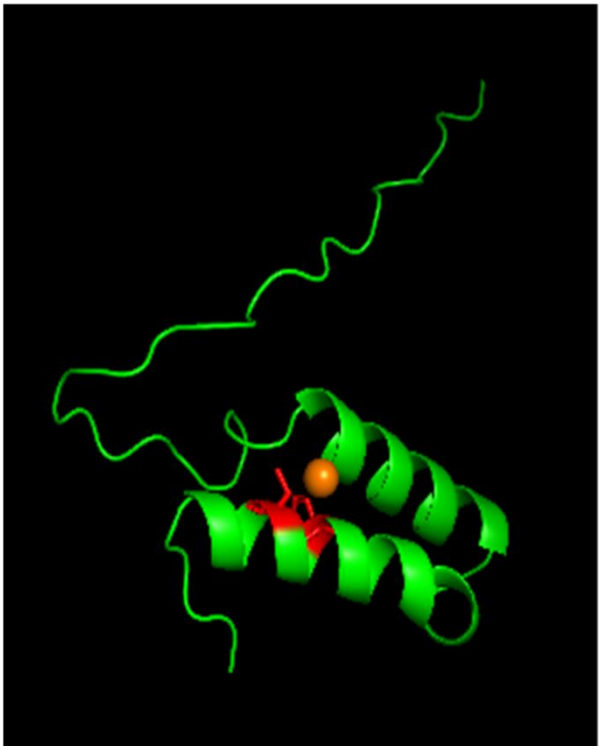

ii.

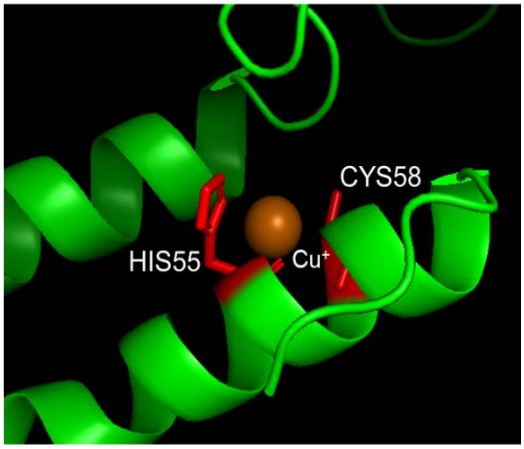

iii.

No.	Binding Residues	Template	Score
1	55H , 58C	4m1pA0	2.760
2	29C , 32T , 58C , 61S	5fjeA2	2.663
3	29C , 55H	4f2fA0	2.207
4	39C , 43L , 48C	5arnA1	1.449

iv. *Pf*Cox17_Cu (C26, C27)

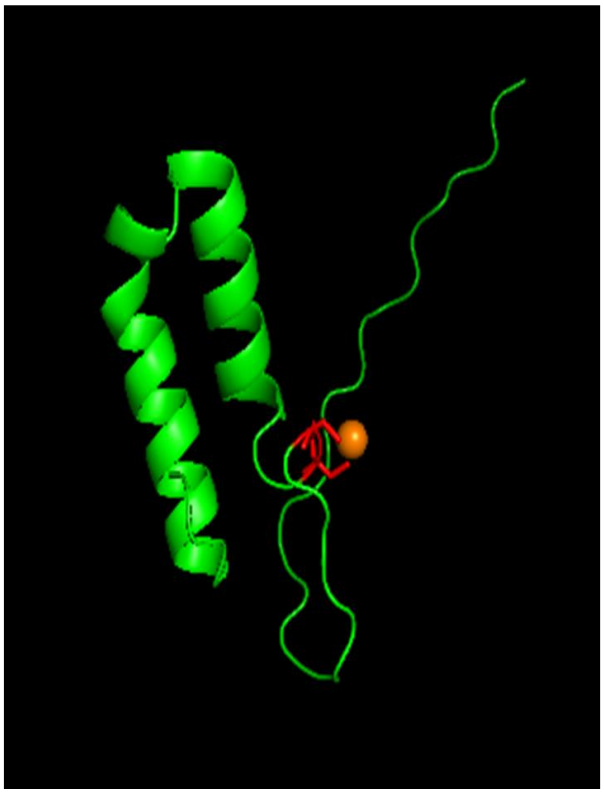

v.

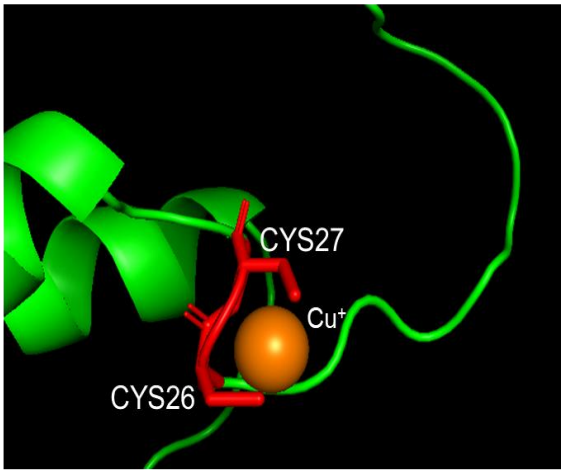

vi.

7	26C , 27C	1rjuV1	1.279
8	54D , 58C	5arnA7	1.246
9	29C , 58C	5fjeA8	1.198
10	26C , 29C , 36R , 55H	3hb3B1	1.162

B.

i. *Pf*Cox11_Cu (C155, C157)

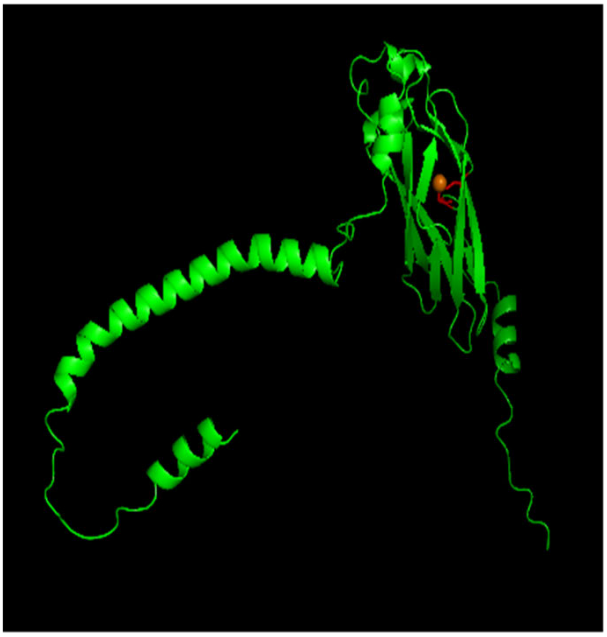

ii.

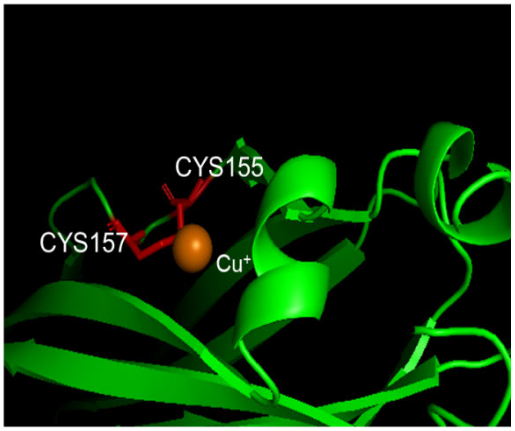

iii.

No.	Binding Residues	Template	Score
1	155C , 157C	1rjuV4	8.256
2	155C , 157C	1rjuV5	4.255
3	140H , 144E	4tm7A0	3.438
4	139Y , 155C , 157C	2ppeA0	2.887

C.

i. *Pf*Sco1_Cu (C159, C163, H264)

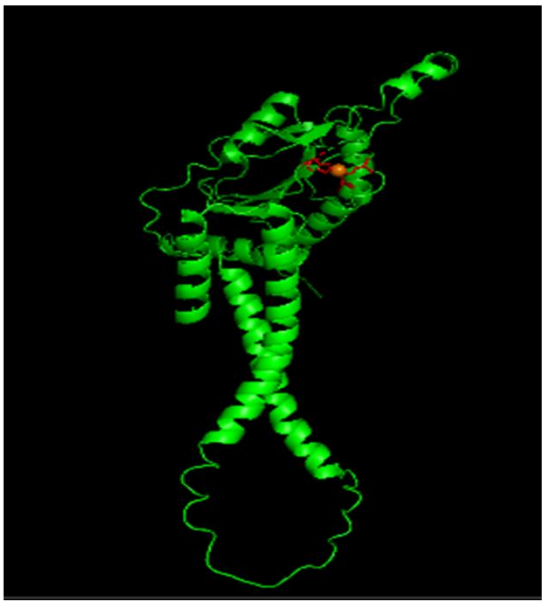

ii.

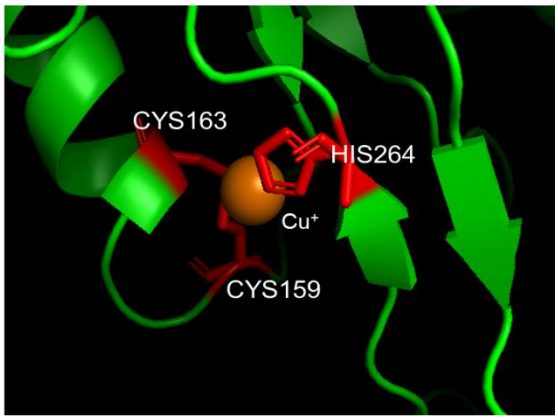

iii.

No.	Binding Residues	Template	Score
1	159C , 163C , 264H	6n5uA0	8.385
2	159C , 163C , 264H	5arnA1	4.313
3	135H , 136H	3eh3A0	4.052
4	159C , 163C , 264H	5fjeA3	3.543

D.

i. *Pf*Cox19_Cu (C34, C45)

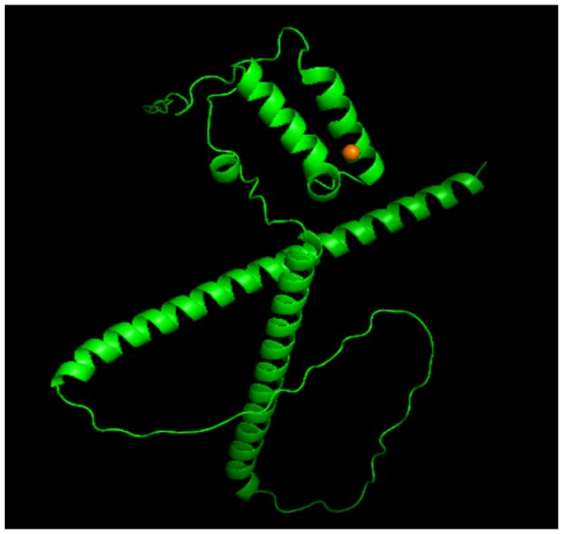

ii.

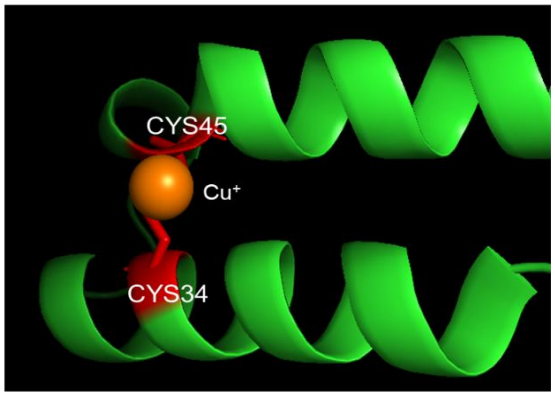

iii.

No.	Binding Residues	Template	Score
1	34C , 45C	5arnA1	5.362
2	34C , 45C	2z8yM0	4.442
3	34C , 38N , 43I , 45C	5fjeA1	3.764
4	107H , 108D	5arnA1	3.703

iv. *Pf*Cox19_Cu (C34, C44, C45)

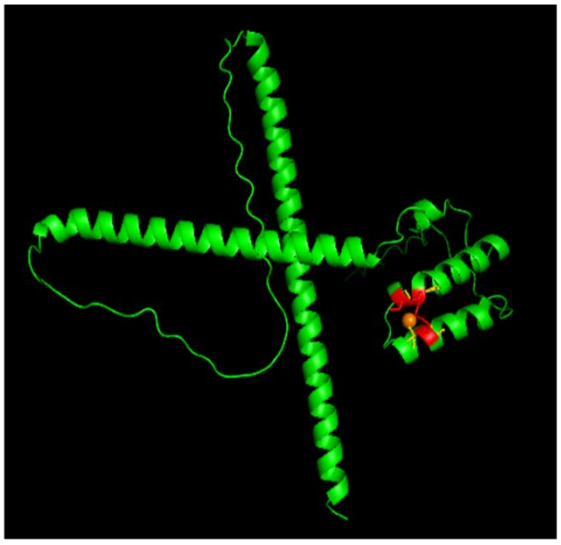

v.

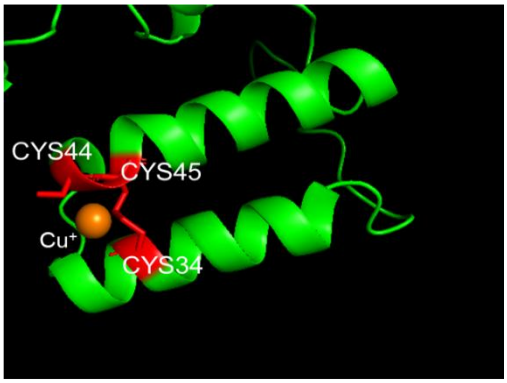

vi.

5	34C , 44C , 45C	1rjuV1	3.239
6	40N , 42H	2fk2A0	2.887
7	24C , 55C	5fjeA4	2.273
8	46R , 75H	1zpuA3	2.191
9	24C , 55C , 59N	5arnA1	2.043
10	34C , 38N , 45C	5arnA1	1.928

Fig 6.3 Docking of copper (I) with *Pf*Cox17(Q8IJE6), *Pf*Cox11(Q8IK85), *Pf*Sco1(Q8IC00), and *Pf*Cox19(Q8I627). A, I. The *Pf*Cox17 crystal structure, with copper (I) bound. **II.** *Pf*Cox17_Cu complex (binding score of 2.760) with histidine and cysteine at 55 and 58 respectively, as copper-binding sites. **IV.** and **V** *Pf*Cox17_Cu complex (with a binding score of 1.279) with C26, and C27, as binding amino acid residues for copper (I). **III** and **VI.** Tables that contain *Pf*Cox17_Cu complexes with binding scores. **B. I** and **II** *Pf*Cox11 crystal structure complexed with copper (I) (with a binding score of 8.256) at cysteines 155 and 157. **C. I** and **II** Crystal structure of *Pf*Sco1 (binding score of 8.385) with copper bound to C159, C163, and H264. **D.** *Pf*Cox19 crystal structure (**I, II, IV,** and **V**) with bound copper and binding sites at C34 and C45 in the complex ranked number 1, and C34, C44, and C45 in structure ranked 5 with a binding score of 3.239 respectively. The docking was performed using an MIB2 server (Lu *et al.,* 2022).

Chapter 7

General Discussion

7.1 Overview of Malaria

Malaria causes severe loss of human life in Africa particularly in sub-Saharan Africa where the disease is endemic. The groups at higher risk are children under the age of five and expecting mothers. This has prompted many interventions toward the elimination of malaria (Shretta *et al.,* 2018). However, the parasite has a complicated life cycle that makes prevention and treatment options difficult (Greenwood., 2017, Marsh *et al.,* 2024). Despite a breakthrough with the malaria vaccine that was announced in 2021 by the WHO, malaria elimination has remained challenging (WHO., 2021, Hassan *et al.,* 2022, Duffy., 2022). Additionally, there is a reported emergence of drug-resistant parasites in Uganda against the artemisinin-based combination therapies (ACT) which is the first-line treatment for *Plasmodium falciparum* (Ikeda *et al.,* 2018, Conrad *et al.,* 2023, Rosenthal *et al.,* 2024a, Rosenthal *et al.,* 2024b). Arising from this, a search for new antimalarial drug targets is important. To effectively eliminate the parasite, various drug developments have targeted the transcription and protein synthesis, transport, and membrane structure of the malaria parasite (Flannery *et al.,* 2013, Cowman *et al.,* 2016, Blasco *et al.,* 2017). Similarly, copper transport in the parasite can be investigated to determine whether it is a potential novel drug target. Such undertakings may contribute to the fight against malaria because the survival of the malaria parasites depends on the use of membrane transport proteins in the uptake of nutrients, waste product discharge from the cell, and safeguarding ion homeostasis (Weiner *et al.,* 2016). The membrane transport proteins perform these functions in conjunction with intracellular transport proteins that also play a role in the distribution of various nutrients including metal ions (Martin., 2020)

7.2 The current knowledge on the copper homeostasis in *Plasmodium falciparum*

The previous and present studies have identified 19 genes that code for copper-binding proteins from the Plasmodial genome. However, only 7 have been characterized (Rasoloson *et al.,* 2004, Choveaux *et al.,* 2012, 2015, Munsami., 2022, Salman *et al.,* 2022, 2023). Copper sources for the parasite may be from the host cells through different channels. The parasites ingest the host's cytoplasm at the blood stage with Cu/Zn superoxide dismutase enzyme, catalase, and hemoglobin. These are taken up through the cytostome and deposited in the food vacuole where copper is released from the digestion of Cu/Zn SOD (Rasoloson *et al.,* 2004, Olliaro *et al.,* 1995). However, some Cu/Zn SOD may escape digestion and remain in the vacuole or move to the cytosol of the parasite (Olliaro *et al.,* 1995). Previous studies have established that the malaria parasites are deficient in Cu/Zn and catalase enzymes, thus making the host cellular proteins one of the possible sources (Fairfield *et al.,* 1983. 1986). However, the copper present in the parasite is more than that in Cu/Zn SOD (Fairfield *et al.,* 1983); therefore, there must be another source of copper for the parasite. Another way that copper gets into the parasite has been proposed to be through transport across the parasitic membrane by *Pf*Ctr1, while *Pf*CuP-ATPase has been proposed to export copper from the parasite to the

host red blood cell (Choveaux *et al.,* 2012, Rasoloson *et al.,* 2004). CuATPase attached to intracellular organelles like endoplasmic reticulum in *P. berghei* is proposed to have a role in copper homeostasis and is more likely to be implicated in copper export to the host cells when the CuATPase translocates to the parasite membrane (Kenthirapalan *et al.,* 2014, Docampo., 2024). This evidence suggests that ATPases in most organisms maintain the level of copper below the toxic concentrations inside cells. This is done by exporting the excess copper to the extracellular compartment. The function of the ATPases in *Plasmodium* is comparable to the role of ATP7A/7B in humans (Hasan and Lutsenko., 2012, La Fontaine and Mercer., 2007). The movement of copper in the *Plasmodium falciparum* from Ctr1 to the *Pf*CuP-ATPase has not been elucidated. In humans, plants, and yeast, Atox1 transports copper from Ctr1 to ATP7B (Lin *et al.,* 1995, Öhrvik *et al.,* 2014, Maghool *et al.,* 2020, Lutsenko., 2021), nevertheless, in humans, Grx1 has been proposed to offer an alternative pathway for the transport of copper to ATP7B (Maghool *et al.,* 2020). ATP7A/B are located in the trans-Golgi network (TGN) and move to the parasitic membrane to give off excess copper to the host cells (Yamaguchi *et al.,* 1996, Hung *et al.,* 1997, Petris *et al.,* 1996). Another suggestion is that there may be another, as yet unidentified proteins that move copper to ATPases. In *Plasmodium falciparum*, copper distribution in the cytosol and mitochondria is not well documented though some studies have suggested *Pf*Cox17 to be involved in copper transport into the mitochondria (Choveaux *et al.,* 2015). In mammalian and yeast cells, Cox17's role in copper movement to the mitochondria has been proposed (Beers *et al.,* 1997, Banci *et al.,* 2008). However, it has been demonstrated that copper import into the mitochondria does not depend on the presence or activity of Cox17 in yeast cells even though Cox17 is localized both in the cytosol and the IMS of the mitochondria (Boulet *et al.,* 2018). Other proteins implicated in human cells regarding copper import into the mitochondria and its distribution therein are SLC25A3 and a copper ligand (CuL) (Boulet *et al.,* 2018, Cobine *et al.,* 2006). Identical to the SLC25A3 protein, a gene coding for mitochondrial phosphate carrier or PIC2 protein from *P. falciparum* has been identified and cloned (Bhaduri-McIntosh and Vaidya., 1996) though, its potential to bind copper has not been established. However, it can be suggested that it is likely to play a similar role in *P. falciparum*. Additionally, a copper ligand (CuL) which is present in mammalian cells has not been found in malaria parasites (Cobine *et al.,* 2006). What copper proteins then, does *P. falciparum* use in its cytosolic distribution, mitochondrial supply, and transfer of copper to the *Pf*CuP-ATPase? Investigating and understanding how copper is transported in Plasmodia may contribute to efforts towards the discovery of novel drug targets and drugs to combat malaria.

7.3 Copper homeostasis as a possible novel drug target in the malaria parasite

Copper is important to the malaria parasite's growth and development. Its chelation stops the development from ring to trophozoite stages of the *Plasmodium falciparum* (Rasoloson *et al.,* 2004). Due to this reason, novel drugs with the potential to disrupt copper transport in the malaria parasite can be identified including sites where they are likely to act. The removal of copper from the parasite has severe effects that range from inhibition of development to lowered fertility levels during the liver blood, and sexual stages of the parasite (Rasoloson *et al.,* 2004,

Kenthirapalan *et al.,* 2014, 2016, Voorberg-van der Wel *et al.,* 2017). When copper (I) chelators such as neocuproine and diethyldithiocarbamate (DDC) were used, the malaria parasites' development from ring to trophozoite was inhibited (Meshnick *et al.,* 1990, Rasoloson *et al.,* 2004, Asahi *et al.,* 2014). All liver-stage *Plasmodium vivax* parasites were inhibited when exposed to neocuproine, suggesting that copper (I) is important for the parasites' growth at the schizonts stage (Voorberg-van der Wel *et al.,* 2017). Therefore, the development of inhibitors of copper-binding proteins is likely to affect the parasites on two fronts; (i) there would be no copper available for the parasite assuming that the entry channel (*Pf*Ctr1) is blocked and this will inhibit growth i.e. Thiosemicarbazone NSC73306 has been shown to lower the human Ctr1 levels, an action likely to lead to cellular copper deficiency (Fung *et al.,* 2014), while three selected semi-substituted steroids [3β-hydroxy-16-aminomethylen-androst-5-en-17- one **(4)**, 3β-hydroxy-16 (N-benzyl) aminomethylenandrost-5-en-17-one (**5)**, and 16(N--hydroxyethyl)aminomethylene-3-methoxy-estra-1,3,5(10)-trien-17- one **(25)**] have been demonstrated to bind to Ctr1 more strongly than the known inhibitor cimetidine thereby preventing copper transfer into the cells (Kadioglu *et al.,* 2015, Serly *et al.,* 2011). Liang *et al.,* 2014, report that cisplatin is a competitor with copper for *h*Ctr1, leading to decreased intracellular copper levels when cisplatin binds to *h*Ctr1. The binding of cisplatin to *h*Ctr1 has been shown by mutagenesis studies that revealed 2 methionine-rich clusters that are present in the extracellular N-terminal region of the protein and form cross-links between the *h*Ctr1 polypeptide chains (Guo *et al.,* 2004). (ii) lack of distribution and efflux of copper from the parasite, which might lead to copper accumulation leading to a free radical generation that harms the parasitic cell i.e. in a mouse model with breast cancer, TM is reported to have improved the efficacy of cisplatin resulting in decreased ATP7A levels, on the other hand, D-penicillamine strengthened the effect of oxaliplatin in human cervical cancer leading to a downregulation of ATP7A (Chisholm *et al.,* 2016, Chen *et al.,* 2015). ATP7A/B belong to a subfamily of P1B heavy metal-transporting ATPases common in prokaryotes and eukaryotes (Argüello *et al.,* 2007). Additionally, findings from the gene knock-out of Ctr1 and Cu-ATPase in *P. berghei* led to decreased fertility and transmission to the vector, strengthening the suggestion that copper-binding proteins may contribute to the propagation and continuity of the parasite. Additionally, they can potentially be drug targets for new drugs against malaria (Kenthirapalan *et al.,* 2014, 2016). Thus, when such proteins are inhibited, or genes coding for the copper proteins are silenced or knocked out, the result is an aberration of cellular functions that negatively affects the organism to the extent of cellular death in case of a disturbance of an essential protein (Narayanan *et al.,* 2013).

7.4 Transcription levels of *P. falciparum* Glutaredoxin 1 (*Pf*Grx1) and S-adenosylhomocysteine hydrolase (*Pf*SAHH)

The life cycle of *P. falciparum* was analyzed for the expression of *Pf*Grx1 during the blood stage and asexual stages and then compared to the expression of *Pf*SAHH in similar stages (Wichers *et al.,* 2019, López-Barragán *et al.,* 2011). Further analysis of previously studied copper proteins was made (Le Roch *et al.,* 2003). The examination of *Pf*Grx1 indicated the highest expression occurred in the mid-trophozoite developmental stage of the blood stage while the expression of *Pf*SAHH was more compared to that of *Pf*Grx1 and showed a climax during the late

trophozoite developmental stage. Nevertheless, both proteins expressed in mid and late trophozoite stages with *Pf*SAHH showing more expression in both stages (Fig A10). Interestingly, the trend of expression is the opposite during the asexual stage. *Pf*Grx1 protein is observed to express more than *Pf*SAHH during the two gametocyte stages (Gametocyte II and V) (Fig A11). Previously, Lactate Dehydrogenase (LDH) showed expression during all blood stages with decreased expression in the gametocyte stage, a trend similar to *Pf*SAHH. The data on *Pf*Grx1 and *Pf*SAHH including other copper proteins previously analyzed indicates that the expression of copper proteins differs during the *P. falciparum* life cycle. This creates an opportunity for attempts to develop drugs targeting these proteins that are essential in copper homeostasis. Additionally, copper (I) is shown to be important in the parasites' development from the ring-trophozoite-schizont stages of the *P. falciparum* life cycle (Asahi *et al.,* 2013). The role of copper (I) in the arrest of the parasite development has been studied using copper (I) chelators and observed that copper (I) has a vital role in the early development stages of *Plasmodium falciparum* (Asahi *et al.,* 2014). When parasites were cultured in a chemically defined medium containing hexadecenoic acid alone, growth was arrested, a result suggested to be associated with the downregulation of genes coding for copper-binding proteins (Asahi *et al.,* 2014). Similarly, *trans*-9-octadecenoic has been noted to have similar effects on the development and growth of the parasite (Asahi *et al.,* 2016). The major stages that the parasite develops within the red blood cells (RBCs) take approximately 48 hours and these are the ring, trophozoite, and schizont stages (Bannister *et al.,* 2000). An understanding of the parasite biology and the functional molecules such as copper proteins that may play a role in the developmental succession or arrest of the parasites' growth may contribute to efforts of identification of drug targets and formulation of drugs aimed at malaria eradication (Ridley., 2002, Asahi *et al.,* 2014).

7.5 Methods utilized in the present study to identify and characterize the two recombinant proteins (*Pf*Grx1 and *Pf*SAHH) and proposed techniques for future studies

Several methods were used to identify and characterize the two recombinant proteins. Bioinformatics tools were utilized to identify the two proteins from PlasmoDB (www.plasmodb.org) where copper-binding motifs common to other copper-binding proteins were noted. Multiple sequence alignments were performed using ClustalW for the structure and function of the two recombinant proteins (Thompson *et al.,* 2003, Pais *et al.,* 2014, Edgar *et al.,* 2006). Further analysis of the structure of *Pf*Grx1 and *Pf*SAHH was done by comparing them to Grx1 and SAHH from humans using PyMOL (Bramucci *et al.,* 2012, El Khoury *et al.,* 2023, Sehnal *et al.,* 2009). The two recombinant proteins were expressed and purified before being subjected to copper binding studies (Spriestersbach *et al.,* 2015, Scheich *et al.,* 2003, Kimple *et al.,* 2013). These copper-binding studies included an assessment of *E. coli* growth without/with protein expression induction in the presence and absence of harmful levels of copper, copper-catalyzed inhibition of the ascorbate oxidation assay, and bicinchoninic acid release assay (Jiang *et a.,* 2005, Lutsenko *et al.,* 1997, Davis and O'Halloran, 2008). Protein-to-protein interactions were performed using the ClusPro program, to establish the interaction possibility of *Pf*Grx1 and *Pf*SAHH with other copper-binding proteins involved in copper entry into

the parasitic cytoplasm and its distribution path to the mitochondria and the host cell when the levels of copper exceed the normal (Kozakov *et al.,* 2013, Kangueane *et al.,* 2018). To support laboratory confirmation of the copper binding abilities of *Pf*Grx1 and *Pf*SAHH and other proteins studied previously, molecular docking studies were conducted to predict copper binding sites (Lu *et al.,* 2022, Lin *et al.,* 2016). The two expressed and purified recombinant proteins were shown to bind copper; however, more characterization could be undertaken using various methods, which were not done due to resource limitations.

The localization of the two native proteins can be achieved by performing immunolocalization studies i.e. polyclonal antibodies against an amino-terminal third of Menkes protein (ATP7A; MNK) were generated by immunizing rabbits. The results show that MNK protein was localized in the Golgi complex (Dierick *et al.,* 1997). *Pf*Ctr1 has been shown to translocate from the erythrocytic plasma membrane during the ring stage to the membrane of the parasite during the early schizonts (Choveaux *et al.,* 2012). Both immunolocalization and electron microscopy indicate that *Pf*CuP-ATPase is localized on the surface of the infected erythrocytes and parasite membranes during the schizont stage (Rasoloson *et al.,* 2004). In plants, similar work using polyclonal antibodies against peroxisomal Cu/Zn SOD1 from watermelon cotyledons indicated an intracellular localization of the enzyme (Sandalio *et al.,* 1997), with western blot and electron microscopy. Electron microscopy can also detect the *Pf*Grx1 and *Pf*SAHH proteins in the current study by utilizing metallothionein (MT) tags i.e. MT tags have been demonstrated to be employed in detecting intracellular proteins of interest in bacteria and eukaryotic cells using transmission microscopy. In this method, the MT tag is fused with either *Pf*Grx1 or *Pf*SAHH, and then *in vitro,* treatment of the complex (protein-tag) is undertaken with gold salts (de Castro *et al.,* 2014). When viewed under the transmission electron microscope, the MT tag produces an electron-dense cluster that allows the protein of interest to be located (de Castro *et al.,* 2014). Further, the specificity of this MT-gold method can be confirmed by immunogold labeling, which involves the use of a primary antibody that recognizes the protein and the secondary antibody with a colloidal gold attached to it. The last part is the viewing of the complex [MT-Protein-primary antibody-secondary antibody (with colloidal gold)] using electron-dense markers such as undecagold clusters (Wall *et al.,* 1982, Hermann *et al.,* 1996, de Castro *et al.,* 2014, Martin *et al.,* 2009, Agarwal *et al.,* 2011). The elastic scattering contrast in annular dark-field images scanning transmission electron microscopy (STEM) can be used to generate 3D reconstructions from cryo-STEM images which can detect trace metals bound to proteins of interest like the detection of Zn and Fe bound to ferritin that was done at very low stoichiometry (Elad *et al.,* 2017). This demonstration showed trends of interactions that could occur in a physiological environment and further illustrates a possibility for protein labeling with heavy metals (Elad *et al.,* 2017). Protein-to-protein interactions and copper coordination can be studied using surface plasmon resonance (SPR) i.e. in *Enterococcus hirae* the interaction between CopZ and CopA ATPase was established using SPR (Multhaup *et al* 2001), similarly, the interaction modeling study results obtained from the present study can support results that can be generated from studying the interactions of *Pf*Grx1 and *Pf*SAHH with other copper-binding proteins using SPR. In addition to the

protein-to-protein interaction determination, copper proteins, and copper can also be investigated using SPR, i.e. a flow-injection surface plasmon resonance spectrometry demonstrated the interactions between Alzheimer's $A\beta_{1-16}$ and copper (Yao *et al.,* 2012), a study that can be supported well by the docking studies that have been done in the present study. Thermal melt analysis and differential scanning fluorimetry have been used to determine the copper binding capacity of copper proteins (Saman et al., 2022, 2023). Another method that can be used to determine which amino acids are involved in copper binding is site-directed mutagenesis, like one conducted to determine which cysteine in the CFCF motif is essential for copper binding (Salman *et al.,* 2022). This method brings about changes in the functionality of either the protein or the motif (Punter *et al.,* 2003). Gene knock-out experiments have been used to establish the importance of the copper proteins in question (Günther *et al.,* 2009, Douradinha *et al.,* 2011), i.e. complementary site-directed mutagenesis was utilized to determine which residues are involved in copper (I) delivery by Menkes ATPase (Jones *et al.,* 2003).

7.6 Identification of *Plasmodium falciparum* Grx1 and SAHH

The *Plasmodium falciparum* clone 3D7 is a 23-megabase nuclear genome that contains 14 chromosomes that encode 5, 300 genes (Gardner *et al.,* 2002). In comparison with free-living eukaryotic parasites, *Plasmodium falciparum* encodes few transporters, enzymes, and copper-binding proteins (Kita *et al.,* 1998). However, more genes encoded enhance the virulence of the parasite as well as function in host-parasite interactions (Gardner *et al.,* 2002, Singh *et al.,* 2010). In eukaryotes and prokaryotes, the copper proteome accounts for less than 1% of the proteome in an organism (Andreini *et al.,* 2008, Banci *et al.,* 2010).

To address the identification of *Pf*Grx1 and *Pf*SAHH, bioinformatic tools were utilized. *In-silico* analysis of the Grx1 amino acid sequence from plants, yeast, mouse, and Plasmodium species that infect humans (Fig 3.1) all revealed a CXXC motif common to some known copper-binding proteins. Interestingly, the Grx1 from humans has an identical motif which has a high affinity for copper (I) (Brose *et al.,* 2014) and has been proposed to provide an alternative pathway for copper to ATP7B in human cells (Maghool *et al.,* 2020). This supports a suggestion that *Pf*Grx1 may be involved in the copper transport from *Pf*Ctr1 to *Pf*CuP-ATPase, just like *Hs*Grx1 which transfers copper to Atox1 and ATP7B (Maghool, *et al.,* 2020, Brose *et al.,* 2014). However, Plasmodia lacks Atox1, a protein known to transfer copper to ATP7A/B from Ctr1 (Grechnikova *et al.,* 2023). Therefore, it is suggested that *Pf*Grx1 may interact with *Pf*Ctr1 directly in its quest to transport copper to the copper exporter when the copper levels are above normal within the parasite. Grx1 has various functions in different cells or organisms, such as the maintenance of antioxidant status through the interaction with glutathione (Saaranen *et al.,* 2009), improving the prognosis of diabetes mellitus and other metabolic diseases, slowing aging (Urgate *et al.,* 2010), and working to reduce inflammatory processes through the regulation of NF-kB inactivation (Liao *et al.,* 2010). In neuroblastoma cells, overexpression of Grx1 leads to a decrease in copper accumulation in the mitochondria and arguably modulates the expression of Ctr1 (De Benedetto *et al.,* 2014). In the *Plasmodium* parasite, Grx1 lowers free radicals and prevents cell

membrane peroxidation thereby increasing the chances of the parasite's survival in the host cells (Tiwari *et al.,* 2021). These functions suggest that *Pf*Grx1 is an essential protein and has a potential role in copper transport in the malaria parasite (Gonzales *et al.,* 2008a and b). If the described functions are disrupted, the parasite is likely to become dysfunctional, therefore, this data may show that the protein is a likely drug target for antimalarials. Similarly in humans, disruption of copper homeostasis in neurons has been reported to give rise to neuronal diseases (Kardos *et al.,* 2018)

S-adenosylhomocysteine hydrolase is a copper-dependent enzyme identified from Plasmodb (Choveaux *et al.,* 2012). Analysis of SAHH amino acid sequences from different organisms (plant, yeast, mouse, protozoa, and human), the multiple sequence alignments showed a copper-binding motif and NAD/H binding site (Fig 4.1). In *Plasmodium falciparum*, the GXGXXGXG motif is suggested to be involved in copper binding and has a part in intracellular copper metabolism. The ability of the GXGXXGXG to be involved in copper binding is supported by experiments done in brindled mice (Seo *et al.,* 1993). Usually in these animals, the uptake and efflux of copper-binding proteins in hepatocytes, fibroblasts, and Menkes lymphoblasts are normal (Mann *et al.,* 1979). In the same paper, the copper binding protein is referred to as copper binding protein (CuBP) and later confirmed to be mouse S-adenosylhomocysteine hydrolase (SAHH) with a role in intracellular copper and sulfur amino acid metabolism (Bethin *et al.,* 1995a). With *Pf*SAHH protein having similar features to SAHH from mice as well as other organisms (humans and plants), and the conserved copper binding motif, it is suggested that *Pf*SAHH is essential to the malaria parasite and may be involved in copper delivery to other cupro enzymes in the parasite's cytosol (Gonzales *et al.,* 2008a and b).

7.7 Recombinant expression and purification of *Plasmodium falciparum* Grx1 and SAHH

Further characterization of the two recombinant proteins was achieved through the expression and purification methods of both proteins. The *Pf*Grx1 and *Pf*SAHH which are 111 and 479 amino acid residues long respectively, were expressed as complete amino acid sequences as they do not have transmembrane regions. Difficulties in the expression of His tagged recombinant proteins have been reported in previous studies (Choveaux., 2011, Salman., 2019). The challenges can be due to A+T bias in the DNA coding sequence for the proteins which affects mRNA level because of effects on transcription activity and mRNA stability (Hia and Takeuchi *et al.,* 2021, Birkholtz *et al.,* 2008). Another reason would be the presence of rare codons which affect the protein expression arising from variations in the utilization of codons between the *E. coli* host cells and the heterologous target gene (Gustafsson *et al.,* 2004). The disturbance in translation occurs because of the need for one or more tRNAs by *E. coli* host cells which may be missing or is rare (Makrides., 1996). Additionally, the most problematic codons i.e. AGA and AGG which encode arginine (Kurland and Gallant., 1996) play a role in the non-expression of proteins. The gene sequences were checked using MendelGene for the possibility of rare codon occurrence. Conditions such as type of media, expression temperature, IPTG concentration, and induction time were evaluated and optimized

to enable the expression of the two proteins. All the other expression conditions were the same apart from the concentration of IPTG (0.2 mM and 1 mM for *Pf*Grx1 and *Pf*SAHH, respectively). Both recombinant proteins were identified through a western blot using mouse anti-His antibodies which confirmed the identity of individual protein bands at the appropriate positions (protein sizes) in an SDS-PAGE gel (Debeljak *et al.,* 2006).

7.8 Copper binds to *Plasmodium falciparum* Grx1 and SAHH

Copper binding by the two recombinant proteins (*Pf*Grx1 and *Pf*SAHH) was demonstrated by evaluating the copper tolerance of *E. coli* cells with or without the expressed recombinant proteins, inhibition of copper-catalyzed ascorbate oxidation, and utilizing the bicinchoninic acid (BCA) copper release assay. All these approaches showed that the two proteins bound copper. Further, the BCA release assay findings show the two recombinant proteins bound reduced copper (copper I) (Asahi *et al.,* 2014). Neocuproine, a compound that selectively chelates copper (I) was found to result in the inhibition of parasitic development in the erythrocytes. On the other hand, cuprizone that chelates copper (II) did not affect the growth and development of the parasite (Ding *et al.,* 2011, Asahi *et al.,* 2014). The assays showing copper binding by the two recombinant proteins are supported by molecular docking results that show where copper potentially binds in the two 3D amino acid structures. In the *Pf*Grx1 structure, copper (I) was shown to bind to cysteine residues at positions 29 and 32 (Fig 6.2), which are part of the CXXC motif that was identified and conserved in amino acid sequence alignments of Grx1 from yeast, plants, protozoa, mice, and humans (Fig 3.1 A and B). In human Grx1, copper (I) is bound to cysteines at 23, and 26 (Fig A5) which form the copper binding motif documented by Maghool *et al.,* 2020. Both *Pf*Grx1 and *Hs*Grx1 are found in the cytosol, however only the latter has been determined to bind copper at the CXXC motif common in both proteins (Cater *et al.,* 2014, Rahlfs *et al.,* 2001, Maghool *et al.,* 2020). In humans, Grx1 transfers copper to Atox1 and ATPases. In addition, Grx1 is implicated in redox regulation of ATPase through cysteine motif modulation and the ability to bind copper (Singleton *et al.,* 2010, Maghool *et al.,* 2020). The intramolecular disulfide bond inside Atox1 is reduced in the presence of Grx1 and glutathione (Hatori *et al.,* 2012). However, the parasite lacks Atox1, but *Pf*CuP-ATPase has been implicated in the export of copper (Rasoloson *et al.,* 2004). No information exists on copper movement from *Pf*Ctr1 to *Pf*CuP-ATPase though with the similarities between the Plasmodial and human Grx1, one could suggest that *Pf*Grx1 whose copper binding ability has been described in the present study has a role in the copper movement from *Pf*Ctr1 to *Pf*CuP-ATPase.

The binding of copper to *Pf*SAHH is suggested by modeling studies to be coordinated by amino acid residues at 239, 271, 272, and 319 (Fig 6.2). From these sites, only one amino acid residue at position 271 is part of the GXGXXGXG copper-binding motif. Mouse SAHH from hepatocytes was found to bind copper at a single site and had a role in intracellular copper metabolism (Bethin *et al.,* 1995b). In brindled mice, the binding of copper by CuBP (Seo *et al.,* 1993) which was later identified as mouse hepatic SAHH was determined (Bethin *et al.,* 1995a). The CuBP was linked to functions regarding copper delivery to other copper enzymes like

Atox1, Sod1, and metallothioneins all located in the cytosol of hepatic cells. Atox1 and Sod1 are not present in *Pf*SAHH, however, other proteins like *Pf*Grx1 may interact with and receive copper from *Pf*SAHH. NAD has been noted to be essential for enzyme functionality. Creedon *et al.,* 1994 reported that 3 glycine amino acid residues at 264, 266, and 269, are involved in the binding of NAD. Contrary to what Creedon *et al.,* 1994 established on the NAD binding site, Singh *et al.,* 2016 found 11 amino acids that are involved in the binding of the cofactor NAD with only one amino acid residue (valine at 268) from the GXGXXGXG motif being involved. The cofactor binds one amino acid residue away from where copper is predicted to bind using the MIB2 modeling server. There is no reported interference from NAD with copper binding to the motif. Bethin *et al.,* 1995a determined that mouse SAHH binds copper, and the protein regulates hepatic copper metabolism, another study established that intracellular copper deficiency leads to a decrease in mouse hepatic SAHH (Bethin et al., 1995b). The mouse SAHH has been documented to deliver copper to other metallocheperones that transfer copper to proteins either responsible for storage or export (Seo *et al.,* 1993). The involvement of *Pf*SAHH in the intracellular copper movement has not well been elucidated. Thus, the described *Pf*SAHH's ability to bind copper *in vivo* and *in vitro* in the present study together with the evidence from previous studies on SAHH's role in the cytosolic distribution of copper in mice, strengthens the suggestion that Plasmodial SAHH could transfer copper to *Pf*Grx1 that can potentially deliver copper to *Pf*CuP-ATPase. The proposed interaction between *Pf*Grx1 and *Pf*SAHH has been supported by evidence from a pull-down assay that showed an association between the two malaria proteins (Sturm *et al.,* 2009), thereby suggesting a possible copper transfer from *Pf*SAHH to *Pf*Grx1 at physiological conditions. There is also a possibility that *Pf*SAHH may transfer copper directly to other copper proteins as illustrated in Fig 7.1. Additionally, both *Pf*SAHH and *Pf*Grx1 are expressed during the mid and late trophozoite stages of the life cycle for *P. falciparum* (Wichers *et al.,* 2019, López-Barragán *et al.,* 2011). However, the interaction may be less during the asexual stages due to the *Pf*SAHH's decreased expression during this stage.

7.9 Copper-binding proteins characterized in previous studies

Seven copper-binding proteins in *Plasmodium falciparum* have been evaluated and observed to bind copper (I) and potentially have a role in copper uptake (*Pf*Ctr1), mitochondrial import and distribution to other copper proteins (*Pf*Cox17) (Choveaux *et al.,* 2012, 2015, Azucenas *et al.,* 2020**,** Wee *et al.,* 2013), including efflux from the parasite (*Pf*CuATPase) (Rasoloson *et al.,* 2004). *Pf*Cox17 has been linked to the supply of copper to Cox11 and Sco1 which metalates cytochrome *c* oxidase (Banci *et al.,* 2011, Banci *et al.,* 2008, Palumaa *et al.,* 2004, Oswald *et al.,* 2009). The *Pf*Cox11 and *Pf*Sco1 have been suggested to play a role in the provision of copper for the metalation of the cytochrome *c* oxidase (Salman *et al.,* 2022, Munsami., 2022). In bacteria and yeast, Cox11 is essential for the biogenesis of the cytochrome *c* oxidase (Banci *et al.,* 2004, Carr *et al.,* 2002, Thompson *et al.,* 2010). On the other hand, mutations in Sco1 destabilize the protein, thus making it lose the ability to bind copper leading to copper deficiency and inefficient biogenesis of the cytochrome c oxidase (Leary *et al.,* 2004, Stiburek *et al.,* 2009, Horng *et al.,* 2005, Banci *et al.,* 2007). The *Pf*Cox19 was suggested to interact with *Pf*Cox11 and

possibly distribute copper in the mitochondria (Salman *et al.,* 2023). An interplay between Cox19 and Cox11 in the intermembrane space of the mitochondria helps in the CcO assembly (Bode *et al.,* 2015, Nobrega *et al.,* 2002). Further, Cox 19 in humans may regulate the ATPase ability to export copper through a signal by Sco1 (Leary *et al.,* 2013). The binding of copper by the six copper proteins excluding *Pf*CuATPase is supported and strengthened by molecular docking studies that indicate where copper binds (Fig 6.3). Copper could not be docked onto the *Pf*CuATPase protein using the MIB2 modeling server due to the size of the protein (Lu *et al.,* 2022). The bioinformatics results from the present study agree with those determined in the laboratory. This is the first time Plasmodial copper proteins are subjected to *in-silico* analysis to determine where copper binds. Interestingly, results from the modeling show that copper binds to the earlier predicted copper-binding motifs belonging to the various proteins mentioned in this section. Only Ctr1 protein has shown lower scores than the rest of the previous characterized copper-binding proteins for the predicter copper binding motif, however, the protein has been shown experimentally to bind copper.

7.10 *Pf*Grx1 Interaction with other copper-binding proteins involved in copper pathways in the malaria parasite

Copper transfer from one site to the other within and outside of cells requires the interaction of copper proteins. Various cellular processes are facilitated by interactions of proteins (Banci *et al.,* 2009, De Rienzo *et al.,* 2000, Österberg., 1974). In addition, the transfer of copper from metallocheperones to the target protein is promoted by complex formation (Kay *et al.,* 2017). Proteins interact in the complex through hydrogen, ionic, and hydrophobic bonds (Arnesano *et al.,* 2004). There is no evidence in *P. falciparum* of how copper is transferred from *Pf*Ctr1 to *Pf*CuP-ATPase, or copper binding proteins found in the mitochondria. In humans, Atox1 shuttles copper from Ctr1 to ATP7B and *Hs*Grx1 offers an independent copper pathway to the efflux protein by interacting with copper proteins at the entry, with Atox1 and ATPase (Maghool *et al.,* 2020), while Pic2 has been implicated in the mitochondria copper import (Cobine *et al.,* 2021). The protein-to-protein interaction study in Chapter 5 indicated the possibility of *Pf*Grx1 interacting with *Pf*Ctr1, *Pf*CuP-ATPase, *Pf*Cox17, and *Pf*SAHH (Figs 5.6, 5.16, and 5.22). The interactions produce complexes held by different bonds, and these bonds require energy to be broken. Therefore, the more energy required for bond disruption, the more stable a complex is (Honig *et al.,* 1989, Carruth *et al.,* 2002, Petrucci *et al.,* 2007). Using average bond energies for each bond from literature (Carruth *et al.,* 2002, Xu *et al.,* 1997, Albeck *et al.,* 2000), the calculation of the total energies involved indicated the strongest interaction was between *Pf*Grx1 and *Pf*SAHH (five salt bridges, 13 hydrogen bonds) as well as the *Pf*Ctr1 and *Pf*Grx1 (four salt bridges, 13 hydrogen bonds) (Table A8). In a pull-down assay, Sturm *et al.,* 2009 reported an interaction between *Pf*Grx1 and *Pf*SAHH, the computer modeling therefore supports the experimental result (Fig A7). The strength of interaction between *Pf*Grx1 and *Pf*Cox17 was second with six salt bridges and nine hydrogen bonds. *Pf*Grx1's association with *Pf*CuP-ATPase was through two hydrogen bonds showing a relatively weak interaction as indicated by the energy involved (Table A8). Maghool *et al.,* 2020 further suggest that affinities of protein-protein interactions together with the copper (I) binding of each protein establish

copper movement inside the cell. Metal binding and transfer occur through protein-to-protein interactions, in yeast, Atx1 interacts with Ctr1, Ccc, and ATPase, which enables copper transfer from Ctr1 to the exporter protein (Lin *et al.,* 1997, O'Halloran *et al.,* 2000, Harrison *et al.,* 2000). In humans, Atox1 interacts with Ctr1 and ATP7B (Puig *et al.,* 2002). Atox1 or Atx1 are not present in *Plasmodium falciparum*, however, *Pf*Grx1 a cytosolic protein has shown possible interaction with the C-terminal of *Pf*Ctr1. In humans, Ctr1's C-terminal region functions as a channel gate and a shuttle helping in the delivery of copper from outside to intracellular copper proteins possibly *Hs*Grx1 (Walke *et al.,* 2022). With the similarities that exist between *Pf*Grx1 and *Hs*Grx1, we suggest that *Pf*Grx1 may transfer copper from *Pf*Ctr1 to *Pf*CuP-ATPase. *Pf*SAHH may as well possibly pass on copper to *Pf*Grx1 due to the interaction shown in the pull-down assay and supported by the modeling protein-to-protein interaction studies. The findings from the experiments and supported by the modeling studies may point to the roles of *Pf*Grx1 and *Pf*SAHH in the Plasmodial copper pathway.

7.11 Proposed Roles of *Plasmodium falciparum* Grx1 and SAHH in Copper transport pathways

Copper is important to many organisms including *Plasmodium falciparum* (Krupanidhi *et al.,* 2008, Senior *et al.,* 2020, Pavelková *et al.,* 2018). In yeast and humans, copper movement from Ctr1 to the cytoplasm and eventually to the mitochondria and ATPase exporter protein is well coordinated (Nevitt *et al.,* 2018, Harris *et al.,* 2000, Tapiero *et al.,* 2003). In these organisms, Atox1 transfers copper (I) to ATP7B for export. The Atox1 may also transfer metal ions to CCC2 and Sod1 for storage (Hatori *et al.,* 2013, Zhalsanova *et al.,* 2023, Simon *et al.,* 2008). The picture of copper movement in humans is like in yeast (Cankorur-Cetinkaya *et al.,* 2016, Flores *et al.,* 2013). However, in *Plasmodium falciparum*, Atox1 or Atx1 are absent. Copper has been documented to be exported through *Pf*CuP-ATPase and has been reported by various authors to be transferred to the cytochrome *c* oxidase (Rasolosone *et al.,* 2004, Horn *et al.,* 2008, Hamza *et al.,* 2002, Punter *et al.,* 2003, Morgada *et al.,* 2015). In the *Plasmodium* parasite, how copper moves from PfCtr1 to *Pf*CuP-ATPase and the mitochondria is not known. What is interesting is copper has been documented to be delivered in those two sites (Rasoloson *et al.,* 2004). For this reason, *Pf*Grx1 and *Pf*SAHH have been proposed to play a role in copper movement as illustrated by red arrows in Fig 7.1. Apart from transporting copper from that *Pf*Ctr1, we suggest that the two proteins may transport excess copper that comes from the digestion of Cu/Zn SOD1 (Fairfield *et al.,* 1983, Rasoloson *et al.,* 2004)

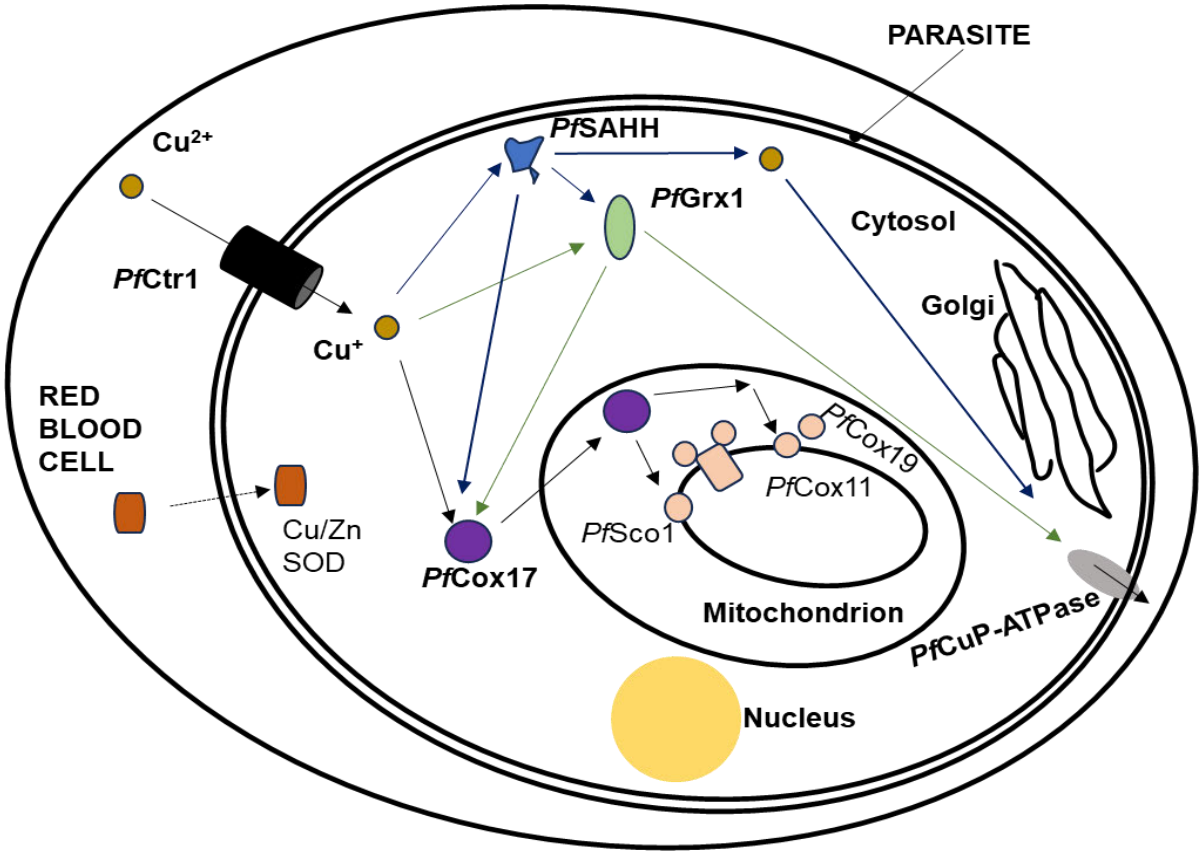

Fig 7.1 Possible roles of *Pf*Grx1 and *Pf*SAHH in Plasmodia copper pathways. The schematic diagram shows the possible roles of *Pf*Grx1 and *Pf*SAHH indicated in red arrows.

The *Pf*Grx1 has a copper-binding motif (CXXC) and is predicted to be in the cytosol (Fig 3.1 A and B), data, that suggests that the protein may participate in intracellular copper distribution (Rahlfs *et al.,* 2001). This distribution can involve transferring copper to other cytosolic copper proteins for its transport. This is supported by protein-to-protein modeling results from the current study that established strong interactions between *Pf*Grx1 and other copper proteins (*Pf*Cox17 and *Pf*SAHH). We suggest that there is a possibility of *Pf*Grx1 transferring copper to *Pf*Cox17, as Cox17 from humans and yeast has been proposed to have a role in mitochondrial copper import (Maxfield *et al.,* 2004, Banci *et al.,* 2008, Kim *et al.,* 2008, Lutsenko, 2010). This will provide a pathway for copper from the entry into the mitochondria (Fig 7.1). The *Pf*Grx1 may also play a role in copper trafficking from *Pf*Ctr1 to *Pf*Cu-ATPase, and previous studies in humans have shown the regulation of Ctr1 by Grx1 as well as its interaction with the N-terminal domain of ATP7B (Lim *et al.,* 2006, Singleton *et al.,* 2010, De Benedetto *et al.,* 2014). Modeling in the current study showed interactions with the *Pf*Ctr1 and *Pf*Cu-ATPase copper proteins, thereby supporting the previous results and indicating a possible role in the copper trafficking pathway shown in Fig 7.1. In humans, Grx1 offers an alternative copper pathway to apo Atox1 and ATP7B (Mercer *et al.,* 2016, Maghool *et al.,* 2020), this may mean that Grx1 gets copper from human Ctr1. Due to the features shared with *Pf*Grx1, it is proposed that the latter can potentially perform a similar role in the parasite. *Pf*SAHH can also be linked to intracellular copper metabolism, this is because mouse SAHH was suggested to have a part in the delivery of copper to

other copper enzymes in the hepatic cells (Seo *et al.,* 1993). Additionally, copper deficiency causes a reduction in the activity of the protein in hepatocytes (Bethin *et al.,* 1995b). It is proposed that *Pf*SAHH's interaction with *Pf*Grx1 (Sturm *et al.,* 2009), might lead to copper transfer from *Pf*SAHH to *Pf*Grx1 as illustrated in Fig 7.1. This diagram shows possible distribution pathways of copper from *Pf*Ctr1 to *Pf*Cu-ATPase and the mitochondria (Fig 7.1). Disruption of the activity of the copper proteins may lead to the impairment of the parasite's survival, as observed from the chelation of copper (I) from the parasite causes impingement on the erythrocytic development from ring to trophozoite stage (Rasoloson *et al.,* 2004).

7.12 Plasmodial Grx1 and SAHH as potential novel drug targets

Copper is important in the development and growth of the *Plasmodium falciparum* (Asahi *et al.,* 2016, Maya-Maldonado *et al.,* 2021). Prevention of acquisition, distribution, and efflux adversely affects the malarial parasite (Asahi *et al.,* 2014, Rasoloson *et al.,* 2004). Different copper proteins are specialized in the acquisition (*Pf*Ctr1), distribution in the cytosol (*Pf*Cox17), and the mitochondria (*Pf*Cox17, *Pf*Cox11, *Pf*Cox19, and *Pf*Sco1) and removal of copper from the parasite (*Pf*CuP-ATPase) (Choveaux *et al.,* 2012, 2015, Salman *et al.,* 2022, 2023, Rasoloson *et al.,* 2004, Kenthirapalan *et al.,* 2014). These proteins may be important drug targets in antimalarial drug development, i.e. Tetrathiomolybdate (TM) inhibits copper trafficking proteins by forming metal clusters (Alvarez *et al.,* 2010). In bacteria, yeast, and humans, Tetrathiomolybdate inhibits various copper proteins namely, CopB ATPases, cytochrome oxidase, superoxide dismutase (SOD1), and ceruloplasmin (cp) (Bissing *et al.,* 2001, Chidambaram *et al.,* 1984). Human copper transporter 1 in colorectal cancer has shown sensitivity to oxaliplatin though the drug does not inhibit its expression completely. Instead, Ctr1 aids the transport of oxaliplatin across the membranes, into the cytoplasm, thus, killing the cancer cells (Cui *et al.,* 2017). *Pf*Grx1 has been detected at the trophozoite stage of the parasites there is no difference in terms of activity in parasites sensitive and those resistant to antimalarials (Rahlfs *et al.,* 2001). Nevertheless, methylene blue inhibited 90% of the enzyme's activity (Rahlfs *et al.,* 2001), suggesting an effect on the functions of the *Pf*Grx1. What is not known is whether the inhibition of *Pf*Grx1's activity leads to a decreased ability to bind copper. However, six copper-containing amine oxidases lost function from inhibition by tranylcypromine (TCP) (Shepard *et al.,* 2003). Additionally, drugs containing metal ions such as platinum and gold including soft acids like mercury, chromium, and arsenic have an inhibitory effect on the thioredoxin and glutaredoxin systems (Ouyang *et al.,* 2018). Inhibitors such as 2-Fluoroaristeromycin bind with *Pf*SAHH and produce an antimalarial effect (Singh *et al.,* 2016, Nakanishi *et al.,* 2005, 2007). However, no data shows *Pf*SAHH's ability to bind copper and its role in Plasmodia copper homeostasis. Although more work needs to be done to develop inhibitors that can stop the two copper proteins from providing copper to the parasite, results from the present study provide a foundation for further investigation. Inhibiting these two proteins may affect the cytosolic copper distribution and arguably the import into the mitochondrial, an action that affects the electron transport chain of the parasite (Painter *et al.,* 2007, Asahi *et al.,* 2013, 2014). Effective inhibitors and novel drug targets will have been potentially elucidated when this is achieved.

7.13 Conclusion

The current study describes the binding of copper by *Pf*Grx1 and *Pf*SAHH and their possible interaction with other copper proteins involved in the trafficking of copper in the malaria parasite. This suggests a role of the two copper proteins in malaria copper homeostasis. These results and those proposed from previous studies that have demonstrated the importance of copper in the parasite could provide alternative novel drug targets that may further be exploited in the development of antimalarial drugs. Inhibiting these copper proteins could provide an effective way of stopping the development and growth of the parasite as observed in the exposure of *P. falciparum* culture to neocuproine an intracellular copper chelator (Rasoloson *et al.,* 2004), thereby contributing to the elimination of malaria. Wang *et al.,* 2015 showed that depleting copper availability inside cells by inhibiting or knocking human Atox1 and CCS, led to decreased growth of cancer cells, showing that the two copper proteins could be novel targets for anticancer drugs. Additionally, cisplatin and oxaliplatin have been shown to have effects on Ctr1 thereby affecting copper homeostasis, an action leading to arrests in the growth of cancerous cells (Howell *et al.,* 2010, Larson *et al.,* 2009, Holzer *et al.,* 2006, Larson *et al.,* 2010). The cancerous cells are stopped from proliferation due to the inhibition of the copper proteins. This shows the importance of copper to the growth of cancer cells. Similarly, copper is needed to grow and develop malaria parasites (Asahi *et al.,* 2014, Rasoloson *et al.,* 2004). *In vitro,* experiments have demonstrated that cisplatin can completely inhibit the growth of *P. falciparum* at a dose of 30 ng/mL within 48 hours and the same drug cures mice infected with *P. berghei* (Nair *et al.,* 1994), cisplatin has been observed to cause death of the *P. falciparum* parasites Murray *et al.,* 2011). With *Pf*Grx1 being like *Hs*Grx1 which has been documented to bind copper and suggested to transport copper from Ctr1 to ATP7A/B, the former would play a similar role, inhibiting *Pf*Grx1 may lead to the disruption of copper transfer for export, an action that may increase copper accumulation in the parasite and later cause cell death due to free radical generation from high levels of copper (Valko *et al.,* 2016, Bremner., 1998). Therefore, *Pf*Grx1 may be a potential novel drug target. Analogs of 3-deaza-adenosine (DZA) have been shown to bind to *Pf*SAHH and inhibit the growth of *Plasmodium falciparum in vitro* (Bujnicki *et al.,* 2003), suggesting that *Pf*SAHH may be a novel drug target for future developments of new antimalarials. In yeast, disruption of SAHH may cause signs of copper abnormalities (Zhou., 1998), therefore, inhibiting *Pf*SAHH may have similar effects on the copper homeostasis of the parasite. In the present study, both *Pf*Grx1 and *Pf*SAHH have been suggested to play a role in the copper secretory pathway. However, more studies are needed to elucidate how copper is transported in *Plasmodium falciparum* from *Pf*Ctr1 to *Pf*CuP-ATPase and the mitochondria. This would only be possible if each copper protein's directional transport and location could be investigated using methods outlined in section 7.5. Conducting these experiments on the two copper proteins (*Pf*Grx1 and *Pf*SAHH) may offer further knowledge of their role in the copper pathways and establish how close they are to the copper proteins found in yeast and humans. The binding of copper by Plasmodial Grx1 and SAHH, and their interactions with each other and other copper proteins provide a basis for molecular docking studies that may evaluate potential novel drug targets and antimalarials through

identifying inhibitors. The current study has determined the ability of the two recombinant proteins to bind copper and suggested their potential role in copper homeostasis, especially the secretory pathway; however, more studies are required to establish their likelihood of being novel drug targets.

Bibliography

Abajian, C., Yatsunyk, L.A., Ramirez, B.E. and Rosenzweig, A.C. (2004). Yeast Cox17 solution structure and copper (I) binding. *Journal of Biological Chemistry*, 279 (51), pp.53584-53592.

Abdalla, Z.A., Rahma, N.A., Hassan, E.E., Abdallah, T.M., Hamad, H.E., Omer, S.A. and Adam, I. (2019). The diagnostic performance of rapid diagnostic tests and microscopy for malaria diagnosis in eastern Sudan using a nested polymerase chain reaction assay as a reference standard. *Transactions of The Royal Society of Tropical Medicine and Hygiene*, 113 (11), pp.701-705.

Abiodun, G.J., Adebiyi, B.O., Abiodun, R.O., Oladimeji, O., Oladimeji, K.E., Adeola, A.M., Makinde, O.S., Okosun, K.O., Djidjou-Demasse, R., Semegni, Y.J. and Njabo, K.Y. (2020). Investigating the resurgence of malaria prevalence in South Africa between 2015 and 2018: a scoping review. *The Open Public Health Journal*, 13 (1), pp.119-125.

Adamczak, R., Porollo, A. and Meller, J. (2004). Accurate prediction of solvent accessibility using neural networks–based regression. *Proteins: Structure, Function, and Bioinformatics*, 56 (4), pp.753-767.

Adebiyi, M. and Olugbara, O. (2021). Binding site identification of COVID-19 main protease 3D structure by homology modeling. *Indonesian Journal of Electrical Engineering and Computer Science*, 21 (3), p.1713.

Adjekukor, C. (2018). Past and current findings in antimalarial drug resistance molecular markers in endemic areas of Africa. *International Journal of Tropical Disease & Health*, 30 (3), pp.1-11.

Agarwal, S., Kern, S., Halbert, J., Przyborski, J.M., Baumeister, S., Dandekar, T., Doerig, C. and Pradel, G. (2011). Two nucleus-localized CDK-like kinases with crucial roles for malaria parasite erythrocytic replication are involved in the phosphorylation of the splicing factor. *Journal of Cellular Biochemistry*, 112 (5), pp.1295-1310.

Agnihotry, S., Pathak, R.K., Singh, D.B., Tiwari, A. and Hussain, I. (2022). Protein structure prediction. In *Bioinformatics*. Academic Press. pp. 177-188

Alam, M.S., Mohon, A.N., Mustafa, S., Khan, W.A., Islam, N., Karim, M.J., Khanum, H., Sullivan, D.J. and Haque, R. (2011). Real-time PCR assay and rapid diagnostic tests for the diagnosis of clinically suspected malaria patients in Bangladesh. *Malaria Journal*, 10, pp.1-9.

Albeck, S., Unger, R. and Schreiber, G. (2000). Evaluation of direct and cooperative contributions towards the strength of buried hydrogen bonds and salt bridges. *Journal of Molecular Biology*, 298 (3), pp.503-520.

Alhazmi, H.A., Alam, M.S., Albratty, M. Najmi, A., Abdulhaq, A.A., Hassani, R., Ahsan, W. and Qramish, A.N. (2023). Binding investigation of some important metal ions copper (I), nickel (II), and aluminum (III) with bovine serum albumin using valid spectroscopic techniques. *Journal of Chemistry*, pp.1-10.

Alhazmi, H.A., Alam, M.S., Albratty, M., Najmi, A., Abdulhaq, A.A., Hassani, R., Ahsan, W. and Qramish, A.N. (2023) Binding investigation of some important metal ions copper (I), nickel (II), and aluminium (III) with Bovine Serum Albumin using Valid Spectroscopic Techniques. *Journal of Chemistry*, 2023 (1), p.2581653.

Al-Sa'doni, H.H., Megson, I.L., Bisland, S., Butler, A.R. and Flitney, F.W. (1997). Neocuproine, a selective Cu (I) chelator, and the relaxation of rat vascular smooth muscle by S-nitrosothiols. *British Journal of Pharmacology*, 121 (6), pp.1047-1050.

Alvarez, H.M., Xue, Y., Robinson, C.D., Canalizo-Hernández, M.A., Marvin, R.G., Kelly, R.A., Mondragón, A., Penner-Hahn, J.E. and O'Halloran, T.V. (2010). Tetrathiomolybdate inhibits copper trafficking proteins through metal cluster formation. *Science*, 327 (5963), pp.331-334.

Alves, R., Vilaprinyo, E. and Sorribas, A., i Herrero, E. (2009). Evolution based on domain combinations: the case of glutaredoxins. *BMC Evolutionary Biology*, 9, p.66.

Amato, R., Lim, P., Miotto, O., Amaratunga, C., Dek, D., Pearson, R.D., Almagro-Garcia, J., Neal, A.T., Sreng, S., Suon, S. and Drury, E. (2017). Genetic markers associated with dihydroartemisinin–piperaquine failure in *Plasmodium falciparum* malaria in Cambodia: a genotype-phenotype association study. *The Lancet Infectious Diseases*, 17 (2), pp.164-173.

Amelo, W. and Makonnen, E. (2021). Efforts Made to Eliminate Drug-Resistant Malaria and Its Challenges. *BioMed Research International*, (1), p.5539544.

Ameri, E., Cheraghi, E. and Moheb, A. (2001). Rapid immunochromatography test "ict malaria Pf" in diagnosis of *Plasmodium falciparum* and its application in the in vivo drug susceptibility test. *Archives of Iranian Medicine,* 4 (1), pp 14-17

Amino, R., Thiberge, S., Martin, B., Celli, S., Shorte, S., Frischknecht, F. and Ménard, R. (2006). Quantitative imaging of Plasmodium transmission from mosquito to mammal. *Nature Medicine*, 12 (2), pp.220-224.

Andrei, A., Öztürk, Y., Khalfaoui-Hassani, B., Rauch, J., Marckmann, D., Trasnea, P.I., Daldal, F. and Koch, H.G. (2020). Cu homeostasis in bacteria: the ins and outs. *Membranes*, 10 (9), p.242.

Andrei, A., Öztürk, Y., Khalfaoui-Hassani, B., Rauch, J., Marckmann, D., Trasnea, P.I., Daldal, F. and Koch, H.G. (2020). Cu homeostasis in bacteria: the ins and outs. *Membranes*, 10 (9), p.242.

Andreini, C., Banci, L., Bertini, I. and Rosato, A. (2008). Occurrence of copper proteins through the three domains of life: a Bioinformatic approach. *The Journal of Proteome Research*, 7 (01), pp.209-216.

Antoine, T. (2012). *Molecular and biochemical characterization of the electron transport chain of Plasmodium falciparum* (Doctoral dissertation, University of Liverpool).

Antony, H.A., Pathak, V., Parija, S.C., Ghosh, K. and Bhattacherjee, A. (2016). Transcriptomic analysis of chloroquine-sensitive and chloroquine-resistant strains of Plasmodium falciparum: toward malaria diagnostics and therapeutics for global health. *OMICS: A Journal of Integrative Biology*, 20 (7), pp.424-432.

Aon-Bertolino, M.L., Romero, J.I., Galeano, P., Holubiec, M., Badorrey, M.S., Saraceno, G.E., Hanschmann, E.M., Lillig, C.H. and Capani, F. (2011). Thioredoxin and glutaredoxin system proteins—immunolocalization in the rat central nervous system. *Biochimica et Biophysica Acta (BBA)-General Subjects*, 1810 (1), pp.93-110.

Appetecchia, F., Fabbrizi, E., Fiorentino, F., Consalvi, S., Biava, M., Poce, G. and Rotili, D. (2024). Transmission-Blocking Strategies for Malaria Eradication: Recent Advances in Small-Molecule Drug Development. *Pharmaceuticals*, 17 (7), p.962.

Araki, T., Kawai, S., Kakuta, S., Kobayashi, H., Umeki, Y., Saito-Nakano, Y., Sasaki, T., Nagamune, K., Yasutomi, Y., Nozaki, T. and Franke-Fayard, B. (2020). Three-dimensional electron microscopy analysis reveals endopolygeny-like nuclear architecture segregation in Plasmodium oocyst development. *Parasitology International*, 76, p.102034.

Argüello, J.M. (2003). Identification of ion-selectivity determinants in heavy-metal transport P 1B-type ATPases. *The Journal of Membrane Biology*, 195, pp.93-108.

Argüello, J.M., Eren, E. and González-Guerrero, M. (2007). The structure and function of heavy metal transport P 1B-ATPases. *Biometals*, 20, pp.233-248.

Argüello, J.M., Raimunda, D. and Padilla-Benavides, T. (2013). Mechanisms of copper homeostasis in bacteria. *Frontiers in Cellular and Infection Microbiology*, 3, p.73.

Ariey, F., Witkowski, B., Amaratunga, C., Beghain, J., Langlois, A.C., Khim, N., Kim, S., Duru, V., Bouchier, C., Ma, L. and Lim, P. (2014). A molecular marker of artemisinin-resistant *Plasmodium falciparum* malaria. *Nature*, 505 (7481), pp.50-55.

Arnesano, F., Banci, L., Bertini, I. and Bonvin, A.M. (2004). A docking approach to the study of copper trafficking proteins: Interaction between metallochaperones and soluble domains of copper ATPases. *Structure*, 12 (4), pp.669-676.

Arya, A., Foko, L.P.K., Chaudhry, S., Sharma, A. and Singh, V. (2021). Artemisinin-based combination therapy (ACT) and drug resistance molecular markers: A systematic review of clinical studies from two malaria endemic regions–India and sub-Saharan Africa. *International Journal for Parasitology: Drugs and Drug Resistance*, 15, pp.43-56.

Asahi, H., Kobayashi, F., Inoue, S.I., Niikura, M., Yagita, K. and Essa Marghany Tolba, M. (2016). Copper homeostasis for the developmental progression of intraerythrocytic malarial parasite. *Current Topics in Medicinal Chemistry*, 16 (27), pp.3048-3057.

Asahi, H., Tolba, M.E.M., Tanabe, M. and Ohmae, H. (2013). Molecular factors that are associated with early developmental arrest of intraerythrocytic *Plasmodium falciparum*. *Canadian Journal of Microbiology*, 59 (7), pp.485-493.

Asahi, H., Tolba, M.E.M., Tanabe, M., Sugano, S., Abe, K. and Kawamoto, F. (2014) Perturbation of copper homeostasis is instrumental in early developmental arrest of intraerythrocytic *Plasmodium falciparum*. *BMC microbiology*, 14, pp.1-11.

Ashley EA, Pyae Phyo A, Woodrow CJ. (2018) Malaria. *Lancet*; pp.1608-1621.

Ashley, E.A., Dhorda, M., Fairhurst, R.M., Amaratunga, C., Lim, P., Suon, S., Sreng, S., Anderson, J.M., Mao, S., Sam, B. and Sopha, C. (2014). Spread of artemisinin resistance in *Plasmodium falciparum* malaria. *New England Journal of Medicine*, 371 (5), pp.411-423.

Aweeka, F.T. and German, P.I. (2008). Clinical pharmacology of artemisinin-based combination therapies. *Clinical pharmacokinetics*, 47, pp.91-102.

Azucenas, C.R., Shawki, A., Logeman, B.L., Niespodzany, E.J., Dunham, J.L., Ruwe, T.A., Thiele, D.J. and Mackenzie, B. (2020). Iron and copper transport activities of the mammalian metal-ion transporters DMT1 and Ctr1. *The FASEB Journal*, 34 (S1), pp.1-1.

Babiker, H.A., Gadalla, A.A. and Ranford-Cartwright, L.C. (2013). The role of asymptomatic *P. falciparum* parasitemia in the evolution of antimalarial drug resistance in areas of seasonal transmission. *Drug Resistance Updates*, 16 (1-2), pp.1-9.

Badar, M.S., Shamsi, S., Ahmed, J. and Alam, M.A. (2022). Molecular dynamics simulations: concept, methods, and applications. In *Transdisciplinarity* (pp. 131-151). Cham: Springer International Publishing.

Balandin, T. and Castresana, C. (2002). *At*Cox17, an *Arabidopsis* homolog of the yeast copper chaperone Cox17. *Plant Physiology*, 129 (4), pp.1852-1857.

Balatri, E., Banci, L., Bertini, I., Cantini, F. and Ciofi-Baffoni, S. (2003). Solution structure of Sco1: a thioredoxin-like protein involved in cytochrome c oxidase assembly. *Structure*, 11 (11), pp.1431-1443.

Baliraine, F.N. and Rosenthal, P.J. (2011). Prolonged selection of pfmdr1 polymorphisms after treatment of *falciparum* malaria with artemether-lumefantrine in Uganda. *Journal of Infectious Diseases*, 204 (7), pp.1120-1124.

Balmer, Y., Koller, A., del Val, G., Manieri, W., Schürmann, P. and Buchanan, B.B. (2003). Proteomics gives insight into the regulatory function of chloroplast thioredoxins. *Proceedings of the National Academy of Sciences*, 100 (1), pp.370-375.

Balmith, M., Basson, C., and Brand, S.J. (2024). The Malaria Burden: A South African Perspective. *Journal of Tropical Medicine*, 2024 (1), p.6619010.

Bancells, C., Llorà-Batlle, O., Poran, A., Nötzel, C., Rovira-Graells, N., Elemento, O., Kafsack, B.F. and Cortés, A. (2019). Revisiting the initial steps of sexual development in the malaria parasite *Plasmodium falciparum*. *Nature Microbiology*, 4 (1), pp.144-154.

Banci, L., Bertini, I., Calderone, V., Ciofi-Baffoni, S., Mangani, S., Martinelli, M., Palumaa, P. and Wang, S. (2006). A hint for the function of human Sco1 from different structures. *Proceedings of the National Academy of Sciences*, 103 (23), pp.8595-8600.

Banci, L., Bertini, I., Calderone, V., Della-Malva, N., Felli, I.C., Neri, S., Pavelkova, A., and Rosato, A. (2009). Copper (I)-mediated protein-protein interactions result from suboptimal interaction surfaces. *Biochemical Journal*, 422 (1), pp.37-42.

Banci, L., Bertini, I., Cantini, F. and Ciofi-Baffoni, S. (2010). Cellular copper distribution: a mechanistic systems biology approach. *Cellular and Molecular Life Sciences*, 67, pp.2563-2589.

Banci, L., Bertini, I., Cantini, F., Ciofi-Baffoni, S., Gonnelli, L. and Mangani, S. (2004). Solution structure of Cox11, a novel type of β-immunoglobulin-like fold involved in CuB site formation of cytochrome c oxidase. *Journal of Biological Chemistry*, 279 (33), pp.34833-34839.

Banci, L., Bertini, I., Cefaro, C., Ciofi-Baffoni, S. and Gallo, A. (2011). Functional role of two interhelical disulfide bonds in human Cox17 protein from a structural perspective. *Journal of Biological Chemistry*, *286* (39), pp.34382-34390. Cox17. *Journal of Biological Chemistry*, 283 (12), pp.7912-7920.

Banci, L., Bertini, I., Ciofi-Baffoni, S., Del Conte, R. and Gonnelli, L. (2003). Understanding copper trafficking in bacteria: interaction between the copper transport protein CopZ and the N-terminal domain of the copper ATPase CopA from Bacillus subtilis. *Biochemistry*, 42 (7), pp.1939-1949.

Banci, L., Bertini, I., Ciofi-Baffoni, S., Janicka, A., Martinelli, M., Kozlowski, H. and Palumaa, P. (2008). A structural-dynamical characterization of human Cox17. *Journal of Biological Chemistry*, 283 (12), pp.7912-7920.

Banci, L., Bertini, I., Ciofi-Baffoni, S., Kozyreva, T., Zovo, K. and Palumaa, P. (2010). Affinity gradients drive copper to cellular destinations. *Nature*, 465 (7298), pp.645-648.

Baneyx, F. (1999). Recombinant protein expression in *Escherichia coli*. *Current Opinion in Biotechnology*, 10 (5), pp.411-421.

Baneyx, F. and Mujacic, M. (2004). Recombinant protein folding and misfolding in *Escherichia coli*. *Nature Biotechnology*, 22 (11), pp.1399-1408.

Bank, P.D. (1971). Protein data bank. *Nature New Biology*, 233 (223), pp.10-1038. Available at: (https://pdb101.rcsb.org/)

Bannister, L.H., Hopkins, J.M., Fowler, R.E., Krishna, S., and Mitchell, G.H. (2000). A brief illustrated guide to the ultrastructure of *Plasmodium falciparum* asexual blood stages. *Parasitology Today*, 16 (10), pp.427-433.

Baraka, V., Mavoko, H.M., Nabasumba, C., Francis, F., Lutumba, P., Alifrangis, M. and Van Geertruyden, J.P. (2018). Impact of treatment and re-treatment with artemether-lumefantrine and artesunate-amodiaquine on selection of *Plasmodium falciparum* multidrug resistance gene-1 polymorphisms in the Democratic Republic of Congo and Uganda. *PLoS One*, 13 (2), p.e0191922.

Barney, R., Velasco, M., Cooper, C.A., Rashid, A., Kyle, D.E., Moon, R.W., Domingo, G.J. and Jang, I.K. (2022). Diagnostic characteristics of lactate dehydrogenase on a multiplex assay for malaria detection including the zoonotic parasite Plasmodium knowlesi. *The American Journal of Tropical Medicine and Hygiene*, 106 (1), p.275.

Barros, M.H., Johnson, A. and Tzagoloff, A. (2004). COX23, a homologue of COX17, is required for cytochrome oxidase assembly. *Journal of Biological Chemistry*, 279 (30), pp.31943-31947.

Beers, J., Glerum, D.M. and Tzagoloff, A. (1997). Purification, characterization, and localization of yeast Cox17p, a mitochondrial copper shuttle. *Journal of Biological Chemistry*, 272 (52), pp.33191-33196.

Begas, P., Liedgens, L., Moseler, A., Meyer, A.J. and Deponte, M. (2017). Glutaredoxin catalysis requires two distinct glutathione interaction sites. *Nature communications*, 8 (1), p.14835.

Belachew, M., Wolde, M., Nega, D., Gidey, B., Negash, L., Assefa, A., Tasew, G., Woyessa, A. and Abera, A. (2022). Evaluating performance of multiplex real-time PCR for the diagnosis of malaria at elimination targeted low transmission settings of Ethiopia. *Malaria Journal*, 21, pp.1-9.

Bennett, A., Bisanzio, D., Yukich, J.O., Mappin, B., Fergus, C.A., Lynch, M., Cibulskis, R.E., Bhatt, S., Weiss, D.J., Cameron, E. and Gething, P.W. (2017). Population coverage of artemisinin-based combination treatment in children younger than 5 years with fever and *Plasmodium falciparum* infection in Africa, 2003–2015: a modeling study using data from national surveys. *The Lancet Global Health*, 5 (4), pp.e418-e427.

Bennink, S., Kiesow, M.J. and Pradel, G. (2016). The development of malaria parasites in the mosquito midgut. *Cellular Microbiology*, 18 (7), pp.905-918.

Berndt, C., Lillig, C.H. and Holmgren, A., (2008). Thioredoxins and glutaredoxins as facilitators of protein folding. *Biochimica Et Biophysica Acta (BBA)-Molecular Cell Research*, 1783 (4), pp.641-650.

Bethin, K.E., Cimato, T.R. and Ettinger, M.J. (1995a). Copper Binding to Mouse Liver S-Adenosylhomocysteine Hydrolase and the Effects of Copper on Its Levels. *Journal of Biological Chemistry*, 270 (35), pp.20703-20711.

Bethin, K.E., Petrovic, N. and Ettinger, M.J. (1995b). Identification of a Major Hepatic Copper Binding Protein as S-Adenosylhomocysteine Hydrolase. *Journal of Biological Chemistry*, 270 (35), pp.20698-20702.

Beutler, E. (1995) in Williams Hematology (Beutler, E., Lichtman, M., Coller, B. and Kipps, T., eds.), McGraw-Hill, New York, pp. 364–369.

Bhaduri-McIntosh, S., and Vaidya, A.B. (1996). Molecular characterization of a *Plasmodium falciparum* gene encoding the mitochondrial phosphate carrier. *Molecular and Biochemical Parasitology*, 78 (1-2), pp 297-301

Bhatt, S., Weiss, D.J., Cameron, E., Bisanzio, D., Mappin, B., Dalrymple, U., Battle, K.E., Moyes, C.L., Henry, A., Eckhoff, P.A. and Wenger, E.A. (2015). The effect of malaria control on *Plasmodium falciparum* in Africa between 2000 and 2015. *Nature*, 526 (7572), pp.207-211.

Bilinovich, S.M., Morris, D.L., Prokop, J.W., Caporoso, J.A., Taraboletti, A., Duangjumpa, N., Panzner, M.J., Shriver, L.P. and Leeper, T.C. (2021). Silver binding to bacterial glutaredoxins observed by NMR. *Biophysica*, 1 (4), pp.359-376.

Binder, B.M. (2020). Ethylene signaling in plants. *Journal of Biological Chemistry*, 295 (22), pp.7710-7725.

Birkholtz, L., Van Brummelen, A.C., Clark, K., Niemand, J., Maréchal, E., Llinas, M., and Louw, A.I. (2008). Exploring functional genomics for drug target and therapeutics discovery in Plasmodia. *Acta Tropica*, 105 (2), pp.113-123.

Birkholtz, L.M., Bornman, R., Focke, W., Mutero, C. and De Jager, C. (2012). Sustainable malaria control: transdisciplinary approaches for translational applications. *Malaria Journal*, 11, pp.1-11.

Bishop, Ö.T., Musyoka, T.M. and Barozi, V. (2022). Allostery and missense mutations as intermittently linked promising aspects of modern computational drug discovery. *Journal of Molecular Biology*, 434 (17), p.167610.

Bissig, K.D., Voegelin, T.C. and Solioz, M. (2001). Tetrathiomolybdate inhibition of the *Enterococcus hirae* CopB copper ATPase. *FEBS letters*, 507 (3), pp.367-370.

Bjursell, M.K., Blom, H.J., Cayuela, J.A., Engvall, M.L., Lesko, N., Balasubramaniam, S., Brandberg, G., Halldin, M., Falkenberg, M., Jakobs, C. and Smith, D. (2011). Adenosine kinase deficiency disrupts the methionine cycle and causes hypermethioninemia, encephalopathy, and abnormal liver function. *The American Journal of Human Genetics*, 89 (4), pp.507-515.

Blasco, B., Leroy, D. and Fidock, D.A. (2017). Antimalarial drug resistance: linking *Plasmodium falciparum* parasite biology to the clinic. *Nature Medicine*, 23 (8), pp.917-928.

Blommel, P.G., Becker, K.J., Duvnjak, P. and Fox, B.G. (2007). Enhanced bacterial protein expression during auto-induction obtained by alteration of lac repressor dosage and medium composition. *Biotechnology Progress*, 23 (3), pp.585-598.

Bode, M., Woellhaf, M.W., Bohnert, M., Laan, M.V.D., Sommer, F., Jung, M., Zimmermann, R., Schroda, M. and Herrmann, J.M. (2015). Redox-regulated dynamic interplay between Cox19 and the copper-binding protein Cox11 in the intermembrane space of mitochondria facilitates the biogenesis of cytochrome *c* oxidase. *Molecular Biology of the cell*, 26 (13), pp.2385-2401.

Bohnuud, T., Luo, L., Wodak, S.J., Bonvin, A.M., Weng, Z., Vajda, S., Schueler-Furman, O. and Kozakov, D. (2017). A benchmark testing ground for integrating homology modeling and protein docking. *Proteins: Structure, Function, and Bioinformatics*, 85 (1), pp.10-16.

Bondos, S.E. and Bicknell, A. (2003). Detection and prevention of protein aggregation before, during, and after purification. *Analytical Biochemistry*, *316* (2), pp.223-231.

Bopp, S.E., Manary, M.J., Bright, A.T., Johnston, G.L., Dharia, N.V., Luna, F.L., McCormack, S., Plouffe, D., McNamara, C.W., Walker, J.R. and Fidock, D.A. (2013). The mitotic evolution of *Plasmodium falciparum* shows a stable core genome but recombination in antigen families. *PLoS Genetics*, 9 (2), p.e1003293.

Borchardt, R.T., Keller, B.T., and Patel-Thombre, U. (1984). Neplanocin A. A potent inhibitor of S-adenosylhomocysteine hydrolase and of *vaccinia virus* multiplication in mouse L929 cells. *Journal of Biological Chemistry*, 259 (7), pp.4353-4358.

Bouldin, S.D., Darch, M.A., Hart, P.J. and Outten, C.E. (2012). Redox properties of the disulfide bond of human Cu, Zn superoxide dismutase, and the effects of human glutaredoxin 1. *Biochemical Journal*, 446 (1), pp.59-67.

Boulet, A., Vest, K.E., Maynard, M.K., Gammon, M.G., Russell, A.C., Mathews, A.T., Cole, S.E., Zhu, X., Phillips, C.B., Kwong, J.Q. and Dodani, S.C. (2018). The mammalian phosphate carrier SLC25A3 is a mitochondrial copper transporter required for cytochrome *c* oxidase biogenesis. *Journal of Biological Chemistry*, 293 (6), pp.1887-1896.

Bourne, Y., Taylor, P. and Marchot, P. (1995). Acetylcholinesterase inhibition by fasciculin: crystal structure of the complex. *Cell*, 83 (3), pp.503-512.

Boyce, R.M., Muiru, A., Reyes, R., Ntaro, M., Mulogo, E., Matte, M. and Siedner, M.J. (2015). Impact of rapid diagnostic tests for the diagnosis and treatment of malaria at a peripheral health facility in Western Uganda: an interrupted time series analysis. *Malaria Journal*, 14, pp.1-7.

Boyd, S.D., Ullrich, M.S., Skopp, A. and Winkler, D.D. (2020). Copper sources for Sod1 activation. *Antioxidants*, 9 (6), p.500.

Bradford, M.M. (1976). A rapid and sensitive method for the quantitation of microgram quantities of protein utilizing the principle of protein-dye binding. *Analytical biochemistry*, 72 (1-2), pp.248-254.

Bramucci, E., Paiardini, A., Bossa, F. and Pascarella, S. (2012). PyMod: sequence similarity searches, multiple sequence-structure alignments, and homology modeling within PyMOL. *BMC bioinformatics*, 13, pp.1-6.

Bremner, I. (1998). Manifestations of copper excess. *The American Journal of Clinical Nutrition*, 67 (5), pp.1069S-1073S.

Brenner, A.J. and Harris, E.D. (1995). A quantitative test for copper using bicinchoninic acid. *Analytical Biochemistry*, 226 (1), pp.80-84.

Brose, J., La Fontaine, S., Wedd, A.G. and Xiao, Z. (2014). Redox sulfur chemistry of the copper chaperone Atox1 is regulated by the enzyme glutaredoxin 1, the reduction potential of the glutathione couple GSSG/2GSH, and the availability of Cu (I). *Metallomics*, 6 (4), pp.793-808.

Bruce, M.C., Macheso, A., Galinski, M.R. and Barnwell, J.W. (2006). Characterization and application of multiple genetic markers for *Plasmodium malariae*. *Parasitology*, 134 (5), pp.637-650.

Brzezinski, K., Dauter, Z. and Jaskolski, M. (2012). High-resolution structures of complexes of plant S-adenosyl-L-homocysteine hydrolase (Lupinus luteus). *Acta Crystallographica Section D: Biological Crystallography*, 68 (3), pp.218-231.

Bujnicki, J.M., Prigge, S.T., Caridha, D. and Chiang, P.K. (2003). Structure, evolution, and inhibitor interaction of S-adenosyl-L-homocysteine hydrolase from *Plasmodium falciparum. Proteins: Structure, Function, and Bioinformatics*, 52 (4), pp.624-632.

Bull, P.C. and Cox, D.W. (1994). Wilson disease and Menkes disease: new handles on heavy-metal transport. *Trends in Genetics*, 10 (7), pp.246-252.

Burkitt, M.J. (2001). A critical overview of the chemistry of copper-dependent low-density lipoprotein oxidation: roles of lipid hydroperoxides, α-tocopherol, thiols, and ceruloplasmin. *Archives of Biochemistry and Biophysics*, 394 (1), pp.117-135.

Burns, A.L., Dans, M.G., Balbin, J.M., de Koning-Ward, T.F., Gilson, P.R., Beeson, J.G., Boyle, M.J. and Wilson, D.W. (2019). Targeting malaria parasite invasion of red blood cells as an antimalarial strategy. *FEMS microbiology reviews*, 43 (3), pp.223-238.

Byass, P., Collinson, M.A., Kabudula, C., Gómez-Olivé, F.X., Wagner, R.G., Ngobeni, S., Silaule, B., Mee, P., Coetzee, M., Twine, W. and Tollman, S.M. (2017). The long road to elimination: malaria mortality in a South African population cohort over 21 years. *Global Health, Epidemiology and Genomics*, *2*, p.11.

Cai, B. and Jiang, X. (2016). Computational methods for ubiquitination site prediction using physicochemical properties of protein sequences. *BMC Bioinformatics*, 17, pp.1-12.

Calderaro, A., Piccolo, G. and Chezzi, C. (2024). The laboratory diagnosis of malaria: a focus on the diagnostic assays in non-endemic areas. *International Journal of Molecular Sciences*, 25 (2), p.695.

Cankorur-Cetinkaya, A., Eraslan, S. and Kirdar, B. (2016). Transcriptomic response of yeast cells to Atx1 deletion under different copper levels. *BMC Genomics*, 17, pp.1-14.

Caracausi, M., Ramacieri, G., Catapano, F., Cicilloni, M., Lajin, B., Pelleri, M.C., Piovesan, A., Vitale, L., Locatelli, C., Pirazzoli, G.L. and Strippoli, P. (2024). The functional roles of S-adenosyl-methionine and S-adenosyl-homocysteine and their involvement in trisomy 21. *BioFactors,* pp 1-16

Caron-Godon, C.A., Collington, E., Wolf, J.L., Coletta, G. and Glerum, D.M. (2024). More than Just Bread and Wine: Using Yeast to Understand Inherited Cytochrome Oxidase Deficiencies in Humans. *International Journal of Molecular Sciences*, 25 (7), p.3814.

Carr, H.S., George, G.N. and Winge, D.R. (2002). Yeast Cox11, a protein essential for cytochrome *c* oxidase assembly, is a Cu (I)-binding protein. *Journal of Biological Chemistry*, 277 (34), pp.31237-31242.

Carroll, M.C., Girouard, J.B., Ulloa, J.L., Subramaniam, J.R., Wong, P.C., Valentine, J.S. and Culotta, V.C. (2004). Mechanisms for activating Cu-and Zn-containing superoxide dismutase in the absence of the CCS Cu chaperone. *Proceedings of the National Academy of Sciences*, 101 (16), pp.5964-5969.

Carruth, Gorton, Ehrlich, Eugene. (2002) "Bond Energies." Volume Library. Ed. Carruth, Gorton. Vol 1. Tennessee: Southwestern.

Casteleijn, M.G., Urtti, A. and Sarkhel, S. (2013). Expression without boundaries: cell-free protein synthesis in pharmaceutical research. *International Journal of Pharmaceutics*, 440 (1), pp.39-47.

Cater, M.A., Materia, S., Xiao, Z., Wolyniec, K., Ackland, S.M., Yap, Y.W., Cheung, N.S. and La Fontaine, S. (2014). Glutaredoxin1 protects neuronal cells from copper-induced toxicity. *Biometals*, 27, pp.661-672.

Centers for Disease Control and Prevention. (2023). “Choosing a drug to prevent malaria,”, https://www.cdc.gov/ malaria/travelers/drugs.html

Chai, Y.C. and Mieyal, J.J. (2023). Glutathione and glutaredoxin—key players in cellular redox homeostasis and signaling. *Antioxidants*, 12 (8), p.1553.

Chang, A.Y., Chau, V., Landas, J.A. and Pang, Y. (2017). Preparation of calcium-competent *Escherichia coli* and heat-shock transformation. *JEMI methods*, 1 pp 22-25

Changela, A., Chen, K., Xue, Y., Holschen, J., Outten, C.E., O'Halloran, T.V. and Mondragón, A. (2003). Molecular basis of metal-ion selectivity and zeptomolar sensitivity by CueR. *Science*, 301 (5638), pp.1383-1387.

Chauhan, N., Kumar, R., Badhai, J., Preet, A. and Yadava, P.K. (2005). Immunogenicity of cholera toxin B epitope inserted in *Salmonella flagellin* expressed on bacteria and administered as DNA vaccine. *Molecular and Cellular Biochemistry*, 276, pp.1-6.

Chen, C.C., Hwang, J.K. and Yang, J.M. (2009). 2-v2: template-based protein structure prediction server. *Bmc Bioinformatics*, 10, pp.1-13.

Chen, J., Jiang, Y., Shi, H., Peng, Y., Fan, X. and Li, C. (2020). The molecular mechanisms of copper metabolism and its roles in human diseases. *Pflügers Archiv-European Journal of Physiology*, 472, pp.1415-1429.

Chen, R., Mintseris, J., Janin, J. and Weng, Z. (2003). A protein-protein docking benchmark. *Proteins: Structure, Function, and Bioinformatics*, 52 (1), pp.88-91.

Chen, S.J., Kuo, C.C., Pan, H.Y., Tsou, T.C., Yeh, S.C. and Chang, J.Y. (2015). The mechanistic basis of a combination of D-penicillamine and platinum drugs synergistically inhibits tumor growth in oxaliplatin-resistant human cervical cancer cells *in vitro* and *in vivo*. *Biochemical Pharmacology*, 95 (1), pp.28-37.

Chen, X., Li, K., Xiao, Y., Wu, W., Lin, H., Qing, X., Tian, S., Liu, S., Feng, S., Wang, B. and Shao, Z. (2024). SP1/CTR1-mediated oxidative stress-induced cuproptosis in intervertebral disc degeneration. *BioFactors*, pp 1-15.

Chen, X., Qiu, J.D., Shi, S.P., Suo, S.B., Huang, S.Y. and Liang, R.P. (2013). Incorporating key position and amino acid residue features to identify general and species-specific Ubiquitin conjugation sites. *Bioinformatics*, 29 (13), pp.1614-1622.

Cheuka, P.M., Njaria, P., Mayoka, G. and Funjika, E. (2024). Emerging drug targets for antimalarial drug discovery: validation and insights into molecular mechanisms of function. *Journal of Medicinal Chemistry*, 67 (2), pp.838-863.

Chhonker, Y.S., Bhosale, V.V., Sonkar, S.K., Chandasana, H., Kumar, D., Vaish, S., Choudhary, S.C., Bhadhuria, S., Sharma, S., Singh, R.K. and Jain, G.K. (2017). Assessment of clinical pharmacokinetic drug-drug interaction of antimalarial drugs α/β-arteether and sulfadoxine-pyrimethamine. *Antimicrobial Agents and Chemotherapy*, 61 (9), pp.10-1128.

Chidambaram, M.V., Barnes, G. and Frieden, E. (1984). Inhibition of ceruloplasmin and other copper oxidases by thiomolybdate. *Journal of Inorganic Biochemistry*, 22 (4), pp.231-239.

Chisholm, C.L., Wang, H., Wong, A.H.H., Vazquez-Ortiz, G., Chen, W., Xu, X. and Deng, C.X. (2016). Ammonium tetrathiomolybdate treatment targets the copper transporter ATP7A and enhances sensitivity of breast cancer to cisplatin. *Oncotarget*, 7 (51), p.84439.

Chonn, A., Semple, S.C. and Cullis, P.R. (1991). Separation of large unilamellar liposomes from blood components by a spin column procedure: towards identifying plasma proteins which mediate liposome clearance in vivo. *Biochimica Et Biophysica Acta (BBA)-Biomembranes*, 1070 (1), pp.215-222.

Choveaux, D.L. (2011). Recombinant expression and initial characterization of two *Plasmodium falciparum* copper-binding proteins. University of KwaZulu-Natal.

Choveaux, D.L., Krause, R.G., Przyborski, J.M. and Goldring, J.D. (2015). Identification and initial characterization of a *Plasmodium falciparum* Cox17 copper metallochaperone. *Experimental Parasitology*, 148, pp.30-39.

Choveaux, D.L., Przyborski, J.M. and Goldring, J.D. (2012). A *Plasmodium falciparum* copper-binding membrane protein with copper transport motifs. *Malaria Journal*, 11, pp.1-15.

Ciechanover, A. and Schwartz, A.L. (2004). The ubiquitin system: pathogenesis of human diseases and drug targeting. *Biochimica et Biophysica Acta (BBA)-Molecular Cell Research*, 1695 (1-3), pp.3-17.

Cleland, W.W. (1964). Dithiothreitol, a new protective reagent for SH groups. *Biochemistry*, 3 (4), pp.480-482.

Cobine, P.A., George, G.N., Jones, C.E., Wickramasinghe, W.A., Solioz, M. and Dameron, C.T. (2002). Copper transfer from the Cu (I) chaperone, CopZ, to the repressor, Zn (II) CopY: metal coordination environments and protein interactions. *Biochemistry*, 41 (18), pp.5822-5829.

Cobine, P.A., Moore, S.A. and Leary, S.C. (2021). Getting out what you put in: Copper in mitochondria and its impacts on human disease. *Biochimica Et Biophysica Acta (BBA)-Molecular Cell Research*, 1868 (1), p.118867.

Cobine, P.A., Ojeda, L.D., Rigby, K.M. and Winge, D.R. (2004). Yeast contain a non-proteinaceous pool of copper in the mitochondrial matrix. *Journal of Biological Chemistry*, 279 (14), pp.14447-14455.

Cobine, P.A., Pierrel, F. and Winge, D.R. (2006). Copper trafficking to the mitochondrion and assembly of copper metalloenzymes. *Biochimica et Biophysica Acta (BBA)-Molecular Cell Research*, 1763 (7), pp.759-772.

Coetzee, M., Kruger, P., Hunt, R.H., Durrheim, D.N., Urbach, J. and Hansford, C.F. (2013). Malaria in South Africa: 110 years of learning to control the disease. *South African Medical Journal*, 103 (10), pp.770-778.

Coleman, R.E., Sattabongkot, J., Promstaporm, S., Maneechai, N., Tippayachai, B., Kengluecha, A., Rachapaew, N., Zollner, G., Miller, R.S., Vaughan, J.A. and Thimasarn, K. (2006). Comparison of PCR and microscopy for the detection of asymptomatic malaria in a *Plasmodium falciparum*/*vivax* endemic area in Thailand. *Malaria Journal*, *5*, pp.1-7.

Collins, W.E. and Barnwell, J.W. (2009). *Plasmodium knowlesi*: finally, being recognized. *The Journal of Infectious Diseases*, 199 (8), pp.1107-1108.

Collinson, E.J., Wheeler, G.L., Garrido, E.O., Avery, A.M., Avery, S.V. and Grant, C.M. (2002). The yeast glutaredoxins are active as glutathione peroxidases. *Journal of Biological Chemistry*, 277 (19), pp.16712-16717.

Colovos, C. and Yeates, T.O. (1993). Verification of protein structures: patterns of nonbonded atomic interactions. *Protein Science*, 2 (9), pp.1511-1519.

Comeau, S.R., Gatchell, D.W., Vajda, S. and Camacho, C.J. (2004). ClusPro: an automated docking and discrimination method for the prediction of protein complexes. *Bioinformatics*, 20 (1), pp.45-50.

Comini, M.A., Rettig, J., Dirdjaja, N., Hanschmann, E.M., Berndt, C., and Krauth-Siegel, R.L. (2008). Monothiol glutaredoxin-1 is an essential iron-sulfur protein in the mitochondrion of African trypanosomes. *Journal of Biological Chemistry*, 283 (41), pp.27785-27798.

Conrad, M.D., Asua, V., Garg, S., Giesbrecht, D., Niaré, K., Smith, S., Namuganga, J.F., Katairo, T., Legac, J., Crudale, R.M. and Tumwebaze, P.K. (2023). Evolution of partial resistance to artemisinins in malaria parasites in Uganda. *New England Journal of Medicine*, 389 (8), pp.722-732.

Consalvi, S., Tammaro, C., Appetecchia, F., Biava, M. and Poce, G. (2022). Malaria transmission-blocking compounds: a patent review. *Expert Opinion on Therapeutic Patents*, 32 (6), pp.649-666.

Cook, J., Aydin-Schmidt, B., González, I.J., Bell, D., Edlund, E., Nassor, M.H., Msellem, M., Ali, A., Abass, A.K., Mårtensson, A. and Björkman, A. (2015). Loop-mediated isothermal amplification (LAMP) for point-of-care detection of asymptomatic low-density malaria parasite carriers in Zanzibar. *Malaria journal*, 14, pp.1-6.

Corrales, R.M., Leiba, J., Cohen-Gonsaud, M., Molle, V. and Kremer, L. (2013). Mycobacterium tuberculosis S-adenosyl-l-homocysteine hydrolase is negatively regulated by Ser/Thr phosphorylation. *Biochemical and biophysical research communications*, 430 (2), pp.858-864.

Coudert, E., Gehant, S., de Castro, E., Pozzato, M., Baratin, D., Neto, T., Sigrist, C.J., Redaschi, N. and Bridge, A. (2023). Annotation of biologically relevant ligands in UniProtKB using ChEBI. *Bioinformatics*, 39 (1), p.793.

Coulter-Karis, D.E. and Hershfield, M.S. (1989). Sequence of full-length cDNA for human S-adenosylhomocysteine hydrolase. *Annals of Human Genetics*, 53 (2), pp.169-175.

Couturier, J., Jacquot, J.P. and Rouhier, N. (2009). Evolution and diversity of glutaredoxins in photosynthetic organisms. *Cellular and Molecular Life Sciences*, 66, pp.2539-2557.

Couturier, J., Jacquot, J.P. and Rouhier, N. (2013). Toward a refined classification of class I dithiol glutaredoxins from poplar: biochemical basis for the definition of two subclasses. *Frontiers in Plant Science*, 4, p.518.

Cowman, A.F., Healer, J., Marapana, D. and Marsh, K. (2016). Malaria: Biology And Disease. *Cell*, 167 (3), pp.610-624.

Cox, B.A., Henningsen, R.A., Spanoyannis, A., Neve, R.L. and Neve, K.A. (1992). Contributions of conserved serine residues to the interactions of ligands with dopamine D2 receptors. *Journal of Neurochemistry*, 59 (2), pp.627-635.

Creedon, K.A., Rathod, P.K. and Wellems, T.E. (1994). *Plasmodium falciparum* S-adenosylhomocysteine hydrolase. cDNA identification, predicted protein sequence, and expression in *Escherichia coli*. *Journal of Biological Chemistry*, 269 (23), pp.16364-16370.

Crichton, R.R., Wilmet, S., Legssyer, R. and Ward, R.J. (2002). Molecular and cellular mechanisms of iron homeostasis and toxicity in mammalian cells. *Journal of Inorganic Biochemistry*, 91 (1), pp.9-18.

Crider, S.E., Holbrook, R.J., and Franz, K.J. (2010). Coordination of platinum therapeutic agents to met-rich motifs of human copper transport protein1. *Metallomics*, 2 (1), pp.74-83.

Croft, A.M. (2014). Malaria: prevention in travelers (non-drug interventions). *BMJ Clinical Evidence*, pp 1-21

Cueto, R., Shen, W., Liu, L., Wang, X., Wu, S., Mohsin, S., Yang, L., Khan, M., Hu, W., Snyder, N. and Wu, Q. (2024). SAH is a major metabolic sensor mediating worsening metabolic crosstalk in metabolic syndrome. *Redox Biology*, 73, p.103139.

Cui, H., Zhang, A.J., McKeage, M.J., Nott, L.M., Geraghty, D., Guven, N., and Liu, J.J. (2017). Copper transporter 1 in human colorectal cancer cell lines: Effects of endogenous and modified expression on oxaliplatin cytotoxicity. *Journal of Inorganic Biochemistry*, 177, pp.249-258.

Cui, L., Mharakurwa, S., Ndiaye, D., Rathod, P.K. and Rosenthal, P.J. (2015). Antimalarial drug resistance: literature review and activities and findings of the ICEMR network. *The American Journal of Tropical Medicine and Hygiene*, 93 (3 Suppl), p.57.

Dagert, M. and Ehrlich, S.D. (1979). Prolonged incubation in calcium chloride improves the competence of *Escherichia coli* cells. *Gene*, 6 (1), pp.23-28.

Dai, X., Liu, S., Cheng, L., Huang, T., Guo, H., Wang, D., Xia, M., Ling, W. and Xiao, Y. (2022b). Epigenetic upregulation of H19 and AMPK inhibition concurrently contribute to S-adenosylhomocysteine hydrolase deficiency-promoted atherosclerotic calcification. *Circulation Research*, 130 (10), pp.1565-1582.

Dai, X., Liu, S., Cheng, L., Huang, T., Guo, H., Wang, D., Xia, M., Ling, W. and Xiao, Y. (2022a). Betaine supplementation attenuates S-adenosylhomocysteine hydrolase-deficiency-accelerated atherosclerosis in apolipoprotein E-deficient mice. *Nutrients*, 14 (3), p.718.

Dancis, A., Haile, D., Yuan, D.S. and Klausner, R.D. (1994). The *Saccharomyces cerevisiae* copper transport protein (Ctr1p). Biochemical characterization, regulation by copper, and physiologic role in copper uptake. *Journal of Biological Chemistry*, 269 (41), pp.25660-25667.

Davis, A.V. and O'Halloran, T.V. (2008). A place for thioether chemistry in cellular copper ion recognition and trafficking. *Nature Chemical Biology*, 4 (3), pp.148-151.

De Benedetto, M.L., Capo, C.R., Ferri, A., Valle, C., Polimanti, R., Carrì, M.T. and Rossi, L. (2014). Glutaredoxin 1 is a major player in copper metabolism in neuroblastoma cells. *Biochimica Et Biophysica Acta (BBA)-General Subjects*, 1840 (1), pp.255-261.

De Castro, I.F., Sanz-Sánchez, L. and Risco, C. (2014). Metallothioneins for correlative light and electron microscopy. *Methods in Cell Biology*, 124, pp.55-70.

De Feo, C.J., Aller, S.G., Siluvai, G.S., Blackburn, N.J. and Unger, V.M. (2009). Three-dimensional structure of the human copper transporter *h*Ctr1. *Proceedings of the National Academy of Sciences*, 106 (11), pp.4237-4242.

De Groot, N.S. and Ventura, S. (2006). Effect of temperature on protein quality in bacterial inclusion bodies. *FEBS letters*, 580 (27), pp.6471-6476.

De Rienzo, F., Gabdoulline, R.R., Menziani, M.C. and Wade, R.C. (2000). Blue copper proteins: a comparative analysis of their molecular interaction properties. *Protein Science*, 9 (8), pp.1439-1454.

Debeljak, N., Feldman, L., Davis, K.L., Komel, R. and Sytkowski, A.J. (2006). Variability in the immunodetection of His-tagged recombinant proteins. *Analytical biochemistry*, 359 (2), pp.216-223.

DeLano, W.L. (2002). Pymol: An open-source molecular graphics tool. *CCP4 Newsl. Protein Crystallogr*, 40 (1), pp.82-92.

Delves, M., Plouffe, D., Scheurer, C., Meister, S., Wittlin, S., Winzeler, E.A., Sinden, R.E. and Leroy, D. (2012). The activities of current antimalarial drugs on the life cycle stages of Plasmodium: a comparative study with human and rodent parasites. *PLoS Medicine*, 9 (2), p.1001169.

Deng, R., Zhu, L., Jiang, J., Chen, J. and Li, H. (2024). Cuproptosis-related gene LIPT1 as a prognostic indicator in non-small cell lung cancer: Functional involvement and regulation of Atox1 expression. *Biomolecules and Biomedicine* 24 (3), p.647

Deng, W., Wang, C., Zhang, Y., Xu, Y., Zhang, S., Liu, Z. and Xue, Y. (2016). GPS-PAIL: prediction of lysine acetyltransferase-specific modification sites from protein sequences. *Scientific Reports*, 6 (1), p.39787.

Denomme, G.A., Rios, M. and Reid, M.E. (2000). *Molecular protocols in transfusion medicine*. Elsevier.

Desta, I.T., Porter, K.A., Xia, B., Kozakov, D. and Vajda, S. (2020). Performance and its limits in rigid-body protein-protein docking. *Structure*, 28 (9), pp.1071-1081.

Diallo, A.O., Banek, K., Kashamuka, M.M., Bala, J.A.M., Nkalani, M., Kihuma, G., Nseka, T.M., Atibu, J.L., Mahilu, G.E., McCormick, L. and White, S.J. (2023). Impact of malaria diagnostic choice on monitoring of *Plasmodium falciparum* prevalence estimates in the Democratic Republic of the Congo and relevance to control programs in high-burden countries. *PLOS Global Public Health*, 3 (7), p.e0001375.

Dierick, H.A., Adam, A.N., Escara-Wilke, J.F. and Glover, T.W. (1997). Immunocytochemical localization of the Menkes copper transport protein (ATP7A) to the trans-Golgi network. *Human molecular genetics*, 6 (3), pp.409-416.

Ding, C., Festa, R.A., Sun, T.S. and Wang, Z.Y. (2014). Iron and copper as virulence modulators in human fungal pathogens. *Molecular Microbiology*, 93 (1), pp.10-23.

Ding, X., Xie, H. and Kang, Y.J. (2011). The significance of copper chelators in clinical and experimental application. *The Journal of Nutritional Biochemistry*, 22 (4), pp.301-310.

Djimdé, A., Doumbo, O.K., Cortese, J.F., Kayentao, K., Doumbo, S., Diourté, Y., Coulibaly, D., Dicko, A., Su, X.Z., Nomura, T. and Fidock, D.A. (2001). A molecular marker for chloroquine-resistant falciparum malaria. *New England Journal of Medicine*, 344 (4), pp.257-263.

Djimde, A.A., Fofana, B., Sagara, I., Sidibe, B., Toure, S., Dembele, D., Dama, S., Ouologuem, D., Dicko, A. and Doumbo, O.K. (2008). Efficacy, safety, and selection of molecular markers of drug resistance by two ACTs in Mali. *American Journal of Tropical Medicine and Hygiene*, 78 (3), pp.455-461.

Djuika, C.F., Fiedler, S., Schnölzer, M., Sanchez, C., Lanzer, M. and Deponte, M. (2013). Plasmodium falciparum antioxidant protein as a model enzyme for a special class of glutaredoxin/glutathione-dependent peroxiredoxins. *Biochimica et Biophysica Acta (BBA)-General Subjects*, 1830 (8), pp.4073-4090.

Docampo, R. (2024). Advances in the cellular biology, biochemistry, and molecular biology of acidocalcisomes. *Microbiology and Molecular Biology Reviews*, 88 (1), pp.e00042-23.

Doe, K.A., Gryzbac, M. and Schumacher, H.R. (1988). A new modified rapid noncarcinogenic myeloperoxidase staining technique using 4-chloro-1-naphthol. *Laboratory Medicine*, 19 (6), pp.374-375.

Dolgova, N.V., Nokhrin, S., Yu, C.H., George, G.N. and Dmitriev, O.Y. (2013). Copper chaperone Atox1 interacts with the metal-binding domain of Wilson's disease protein in cisplatin detoxification. *Biochemical Journal*, 454 (1), pp.147-156.

Dondorp, A.M., Nosten, F., Yi, P., Das, D., Phyo, A.P., Tarning, J., Lwin, K.M., Ariey, F., Hanpithakpong, W., Lee, S.J. and Ringwald, P. (2009). Artemisinin resistance in *Plasmodium falciparum* malaria. *New England Journal of Medicine*, 361 (5), pp.455-467.

Dong, L., Li, W., Xu, Q., Gu, J., Kang, Z., Chen, J., Xu, X., Zhang, X., Zhang, X., Jiang, H. and Guan, M. (2023). A rapid multiplex assay of human malaria parasites by digital PCR. *Clinica Chimica Acta*, 539, pp.70-78.

Douradinha, B., Augustijn, K.D., Moore, S.G., Ramesar, J., Mota, M.M., Waters, A.P., Janse, C.J. and Thompson, J. (2011). Plasmodium Cysteine Repeat Modular Proteins 3 and 4 are essential for malaria parasite transmission from the mosquito to the host. *Malaria Journal*, 10, pp.1-9.

Dudzik, C.G., Walter, E.D., Abrams, B.S., Jurica, M.S. and Millhauser, G.L. (2013). Coordination of copper to the membrane-bound form of α-synuclein. *Biochemistry*, 52 (1), pp.53-60.

Duffy, P.E. (2022). Current approaches to malaria vaccines. *Current Opinion in Microbiology*, 70, p.102227.

Dvorin, J.D. and Goldberg, D.E. (2022). Plasmodium egress across the parasite life cycle. *Annual Review of Microbiology*, 76 (1), pp.67-90.

Dym, O., Eisenberg, D. and Yeates, T.O. (2006). VERIFY3D.

Edgar, R.C. and Batzoglou, S. (2006). Multiple sequence alignment. *Current opinion in structural biology*, 16 (3), pp.368-373.

Ehrlich, H.Y., Jones, J. and Parikh, S. (2020). Molecular surveillance of antimalarial partner drug resistance in sub-Saharan Africa: a spatial-temporal evidence mapping study. *The Lancet Microbe*, 1 (5), pp.e209-e217.

Eisenberg, D., Lüthy, R. and Bowie, J.U. (1997). VERIFY3D: assessment of protein models with three-dimensional profiles. *Methods in enzymology* 277, pp. 396-404.

Eisses, J.F. and Kaplan, J.H. (2005). The mechanism of copper uptake mediated by human Ctr1: a mutational analysis. *Journal of Biological Chemistry*, 280 (44), pp.37159-37168.

El Khoury, G., Azzam, W. and Rebehmed, J. (2023). PyProtif: a PyMol plugin to retrieve and visualize protein motifs for structural studies. *Amino Acids*, 55 (10), pp.1429-1436.

Elad, N., Bellapadrona, G., Houben, L., Sagi, I. and Elbaum, M. (2017). Detection of isolated protein-bound metal ions by single-particle cryo-STEM. *Proceedings of the National Academy of Sciences*, 114 (42), pp.11139-11144.

Elko, E.A., Cunniff, B., Seward, D.J., Chia, S.B., Aboushousha, R., van de Wetering, C., van der Velden, J., Manuel, A., Shukla, A., Heintz, N.H. and Anathy, V. (2019). Peroxiredoxins and beyond; redox systems regulating lung physiology and disease. *Antioxidants & Redox Signaling*, 31 (14), pp.1070-1091.

Fairfield, A.S., Eaton, J.W. and Meshnick, S.R. (1986). Superoxide dismutase and catalase in murine malaria, *Plasmodium berghei*: content and subcellular distribution. *Archives of Biochemistry and Biophysics*, 250 (2), pp.526-529.

Fairfield, A.S., Meshnick, S.R. and Eaton, J.W. (1983). Malaria parasites adopt host cell superoxide dismutase. *Science*, 221 (4612), pp.764-766.

Fan, S.H., Chang, Y., Xiong, X.Y., Xiang, M., Yuan, W.L., Yang, X.Q., Wei, W.H., Chen, L., Cheng, M.N., Zhu, F.H. and He, S.J. (2024). Reversible SAHH inhibitor ameliorates MIA-induced osteoarthritis of rats through suppressing MEK/ERK pathway. *Biomedicine & Pharmacotherapy*, 170, p.115975.

Faure, G., Joseph, A.P., Craveur, P., Narwani, T.J., Srinivasan, N., Gelly, J.C., Rebehmed, J. and de Brevern, A.G. (2019). iPBAvizu: a PyMOL plugin for an efficient 3D protein structure superimposition approach. *Source Code for Biology and Medicine*, 14, pp.1-5.

Feitosa, L.M., Franca, R.R.F., Maria de Lourdes, G.F., Aguiar, A.C., de Souza, G.E., Maluf, S.E.C., de Souza, J.O., Zapata, L., Duarte, D., Morais, I. and Nogueira, F. 2024. Discovery of new piperaquine hybrid analogs linked by triazolopyrimidine and pyrazolopyrimidine scaffolds with antiplasmodial and transmission-blocking activities. *European Journal of Medicinal Chemistry*, 267, p.116163.

Fetherolf, M. (2017). Oxygen-dependent activation of Cu, Zn-superoxide dismutase-1. Metallomics 9: 1047–1059.

Field, L.S., Furukawa, Y., O'Halloran, T.V. and Culotta, V.C. (2003). Factors controlling the uptake of yeast copper/zinc superoxide dismutase into mitochondria. *Journal of Biological Chemistry*, 278 (30), pp.28052-28059.

Fishov, I., Zaritsky, A. and Grover, N.B. (1995). On microbial states of growth. *Molecular Microbiology*, 15 (5), pp.789-794.

Flannery, E.L., Chatterjee, A.K. and Winzeler, E.A. (2013). Antimalarial drug discovery—approaches and progress towards new medicines. *Nature Reviews Microbiology*, 11 (12), pp.849-862.

Flores, A. G., and Unger, V.M. (2013). Atox1 contains positive residues that mediate membrane association and aid subsequent copper loading. *The Journal of Membrane Biology*, 246, pp.903-913.

Fontanesi, F. and Barrientos, A. (2013). Mitochondrial cytochrome c oxidase assembly in health and human diseases. *Mitochondrial Disorders Caused by Nuclear Genes*, pp.239-259.

Foster, A.W., Osman, D. and Robinson, N.J. (2014). Metal preferences and metallation. *Journal of Biological Chemistry*, 289 (41), pp.28095-28103.

Frédérich, M., Dogné, J.M., Angenot, L. and Mol, P.D. (2002). New trends in anti-malarial agents. *Current medicinal chemistry*, 9 (15), pp.1435-1456.

Freedman, D.O. (2019). Tafenoquine: integrating a new drug for malaria prophylaxis into travel medicine practice. *Journal of Travel Medicine*, 26 (4), p.tay140.

Frischknecht, F. and Matuschewski, K. (2017). Plasmodium sporozoite biology. *Cold Spring Harbor Perspectives in Medicine*, 7 (5), p.a025478.

Fung, K.L., Tepede, A.K., Pluchino, K.M., Pouliot, L.M., Pixley, J.N., Hall, M.D. and Gottesman, M.M. (2014). Uptake of compounds that selectively kill multidrug-resistant cells: the copper transporter SLC31A1 (Ctr1) increases the cellular accumulation of the thiosemicarbazone NSC73306. *Molecular Pharmaceutics*, 11 (8), pp.2692-2702.

Furukawa, Y., Torres, A.S. and O'Halloran, T.V. (2004). Oxygen-induced maturation of SOD1: a key role for disulfide formation by the copper chaperone CCS. *The EMBO Journal*, 23 (14), pp.2872-2881.

G Postema, P. and AM Wilde, A. (2014). The measurement of the QT interval. *Current cardiology reviews*, 10 (3), pp.287-294.

Gaballa, A. and Helmann, J.D. (2003). *Bacillus subtilis* CPx-type ATPases: characterization of Cd, Zn, Co, and Cu efflux systems. *Biometals*, 16, pp.497-505.

Gadalla, N.B., Abdallah, T.M., Atwal, S., Sutherland, C.J. and Adam, I. (2013). Selection of *Pf*dhfr/*Pf*dhps alleles and declining artesunate/sulphadoxine-pyrimethamine efficacy against *Plasmodium falciparum* eight years after deployment in eastern Sudan. *Malaria Journal*, 12, pp.1-8.

Gadalla, N.B., Adam, I., Elzaki, S.E., Bashir, S., Mukhtar, I., Oguike, M., Gadalla, A., Mansour, F., Warhurst, D., El-Sayed, B.B. and Sutherland, C.J. (2011). Increased pfmdr1 copy number and sequence polymorphisms in *Plasmodium falciparum* isolates from Sudanese malaria patients treated with artemether-lumefantrine. *Antimicrobial Agents and Chemotherapy*, 55 (11), pp.5408-5411.

Gaetke, L.M., Chow-Johnson, H.S. and Chow, C.K. (2014). Copper: toxicological relevance and mechanisms. *Archives of Toxicology*, 88, pp.1929-1938.

Gale, J. and Aizenman, E. (2024). The physiological and pathophysiological roles of copper in the nervous system. *European Journal of Neuroscience* 60, pp.3505-3543

Galinski, M.R., Dluzewski, A.R. and Barnwell, J.W. (2005). A mechanistic approach to merozoite invasion of red blood cells: merozoite biogenesis, rupture, and invasion of erythrocytes. *Molecular Approaches to Malaria*, pp.111-168.

Gamo, F.J., Sanz, L.M., Vidal, J., De Cozar, C., Alvarez, E., Lavandera, J.L., Vanderwall, D.E., Green, D.V., Kumar, V., Hasan, S. and Brown, J.R. (2010). Thousands of chemical starting points for antimalarial lead identification. *Nature*, 465 (7296), pp.305-310.

Gardner, M.J., Hall, N., Fung, E., White, O., Berriman, M., Hyman, R.W., Carlton, J.M., Pain, A., Nelson, K.E., Bowman, S., and Paulsen, I.T. (2002). Genome sequence of the human malaria parasite *Plasmodium falciparum*. *Nature*, 419 (6906), pp.498-511.

Garg, N., Taylor, A.J., Pastorelli, F., Flannery, S.E., Jackson, P.J., Johnson, M.P. and Kelly, D.J. (2021). Genes linking copper trafficking and homeostasis to the biogenesis and activity of the cbb 3-Type cytochrome *c* oxidase in the enteric pathogen *Campylobacter jejuni*. *Frontiers in Microbiology*, 12, p.683260.

Georgatsou, E., Mavrogiannis, L.A., Fragiadakis, G.S. and Alexandraki, D. (1997). The yeast Fre1p/Fre2p cupric reductases facilitate copper uptake and are regulated by the copper-modulated Mac1p activator. *Journal of Biological Chemistry*, 272 (21), pp.13786-13792.

Gerald, N., Mahajan, B. and Kumar, S. (2011). Mitosis in the human malaria parasite *Plasmodium falciparum*. *Eukaryotic cell*, 10 (4), pp.474-482.

Ghosh, A., Trivedi, P.P., Timbalia, S.A., Griffin, A.T., Rahn, J.J., Chan, S.S. and Gohil, V.M. (2014). Copper supplementation restores cytochrome *c* oxidase assembly defect in a mitochondrial disease model of Coa6 deficiency. *Human Molecular Genetics*, 23 (13), pp.3596-3606.

Gill, R.T., Valdes, J.J. and Bentley, W.E. (2000). A comparative study of global stress gene regulation in response to overexpression of recombinant proteins in *Escherichia coli*. *Metabolic engineering*, 2 (3), pp.178-189.

Gilles, H.M. and Warrell, D.A. eds. (2002). *Essential Malariology*. Arnold.

Glerum, D.M., Shtanko, A. and Tzagoloff, A., (1996). Characterization of Cox17, a yeast gene involved in copper metabolism and assembly of cytochrome *c* oxidase. *Journal of Biological Chemistry*, 271 (24), pp.14504-14509.

Glick, B.R. (1995). Metabolic load and heterologous gene expression. *Biotechnology advances*, 13 (2), pp.247-261.

Golassa, L., Kamugisha, E., Ishengoma, D.S., Baraka, V., Shayo, A., Baliraine, F.N., Enweji, N., Erko, B., Aseffa, A., Choy, A. and Swedberg, G. (2015). Identification of large variation in *pfcrt, pfmdr-1,* and *pfubp-1* markers in *Plasmodium falciparum* isolates from Ethiopia and Tanzania. *Malaria Journal*, 14, pp.1-9.

Goldberg, M.E. Rudolph, R. and Jaenicke, R. (1991). A kinetic study of the competition between renaturation and aggregation during the refolding of denatured-reduced egg white lysozyme. *Biochemistry*, 30 (11), pp.2790-2797.

Goldring, J.D. (2015). Spectrophotometric methods to determine protein concentration. *Western Blotting: Methods and Protocols*, pp.41-47.

Goldring, J.P.D. (2021). The multiple facets of three-phase partitioning in the purification, concentration, yield, and activity of enzymes and proteins. In *Three Phase Partitioning:* Elsevier pp. 59-78.

Gomi, T., Date, T., Ogawa, H., Fujioka, M., Aksamit, R.R., Backlund Jr, P.S. and Cantoni, G.L. (1989). Expression of rat liver S-adenosylhomocysteinase cDNA in *Escherichia coli* and mutagenesis at the putative NAD binding site. *Journal of Biological Chemistry*, 26 (27), pp.16138-16142.

Gonzales, J.M. (2008a). Genetic analysis of gene expression and the underlying polymorphisms in *Plasmodium falciparum*. University of Notre Dame.

Gonzales, J.M., Patel, J.J., Ponmee, N., Jiang, L., Tan, A., Maher, S.P., Wuchty, S., Rathod, P.K. and Ferdig, M.T. (2008b). Regulatory hotspots in the malaria parasite genome dictate transcriptional variation. *PLoS Biology*, 6 (9), p.e238.

González-Guerrero, M. and Argüello, J.M. (2008a). Mechanism of Cu+-transporting ATPases: soluble Cu+ chaperones directly transfer Cu+ to transmembrane transport sites. *Proceedings of the National Academy of Sciences*, 105 (16), pp.5992-5997.

Gonzalez-Guerrero, M., Eren, E., Rawat, S., Stemmler, T.L. and Argüello, J.M. (2008b). Structure of the two transmembrane Cu+ transport sites of the Cu+-ATPases. *Journal of Biological Chemistry*, 283 (44), pp.29753-29759.

González-Guerrero, M., Hong, D. and Argüello, J.M. (2009). Chaperone-mediated Cu+ delivery to Cu+ transport ATPases: requirement of nucleotide binding. *Journal of Biological Chemistry*, 284 (31), pp.20804-20811.

Grechnikova, M., Füssy, Z. and Sutak, R. (2023). Copper in parasitic protists–a hitherto neglected virulence factor. *Trends in Parasitology*.

Greenwood, B. (2017). Elimination of malaria: halfway there. *Transactions of the Royal Society of Tropical Medicine and Hygiene*, 111 (1), pp.1-2.

Gul, A., Haq, N. and Rafique, K. (2022). The Copper Transport Mechanism in Plants. *Plant Metal and Metalloid Transporters* pp. 275-287.

Günther, S., Matuschewski, K. and Müller, S. (2009). Knockout studies reveal an important role of Plasmodium lipoic acid protein ligase A1 for asexual blood stage parasite survival. *PLoS One*, 4 (5), p.e5510.

Guo, H.J. and Tadi, P. (2020). Biochemistry, ubiquitination. StatPearls Publishing, Treasure Island (FL); 2023. PMID: 32310512.

Guo, X., Chen, K., Ji, L., Wang, S., Ye, X., Xu, L. and Feng, L. (2024). Ultrasound-targeted microbubble technology facilitates SAHH gene delivery to treat diabetic cardiomyopathy by activating the AMPK pathway. *Science*, 27 (2).

Guo, Y., Smith, K. and Petris, M.J. (2004). Cisplatin stabilizes a multimeric complex of the human Ctr1 copper transporter: requirement for the extracellular methionine-rich clusters. *Journal of Biological Chemistry*, 279 (45), pp.46393-46399.

Gupta, A. and Lutsenko, S. (2009). Human copper transporters: mechanism, role in human diseases and therapeutic potential. *Future Medicinal Chemistry*, 1 (6), pp.1125-1142.

Gupta, H., Galatas, B., Chidimatembue, A., Huijben, S., Cisteró, P., Matambisso, G., Nhamussua, L., Simone, W., Bassat, Q., Ménard, D. and Ringwald, P. (2020). Effect of mass dihydroartemisinin–piperaquine administration in southern Mozambique on the carriage of molecular markers of antimalarial resistance. *PLoS One*, 15 (10), p.e0240174.

Gustafsson, C., Govindarajan, S. and Minshull, J. (2004). Codon bias and heterologous protein expression. *Trends in Biotechnology*, 22 (7), pp.346-353.

Gutman, J.R., Stephens, D.K., Tiendrebeogo, J., Badolo, O., Dodo, M., Burke, D., Williamson, J., Vibbert, K., Youll, S.J., Savadogo, Y. and Brieger, W.R. (2020). A cluster randomized trial of delivery of intermittent preventive treatment of malaria in pregnancy at the community level in Burkina Faso. *Malaria Journal*, 19, pp.1-11.

Haas, K.L., Putterman, A.B., White, D.R., Thiele, D.J. and Franz, K.J. (2011). Model peptides provide new insights into the role of histidine residues as potential ligands in human cellular copper acquisition via Ctr1. *Journal of the American Chemical Society*, 133 (12), pp.4427-4437.

Haddadin, F.A.T. and Harcum, S.W. (2005). Transcriptome profiles for high-cell-density recombinant and wild-type Escherichia coli. *Biotechnology and Bioengineering*, 90 (2), pp.127-153

Haider, S.R., Reid, H.J. and Sharp, B.L. (2019). Tricine-SDS-PAGE. *Electrophoretic Separation of Proteins: Methods and Protocols*, pp.151-160.

Haiyambo, D.H., Uusiku, P., Mumbengegwi, D., Pernica, J.M., Bock, R., Malleret, B., Renia, L., Greco, B. and Quaye, I.K. (2019). Molecular detection of P. vivax and P. ovale foci of infection in asymptomatic and symptomatic children in Northern Namibia. *PLoS Neglected Tropical Diseases*, 13 (5), p.e0007290.

Haldar, K., Bhattacharjee, S. and Safeukui, I. (2018). Drug resistance in Plasmodium. *Nature Reviews Microbiology*, 16 (3), pp.156-170.

Hall, N., Pain, A., Berriman, M., Churcher, C., Harris, B., Harris, D., Mungall, K., Bowman, S., Atkin, R., Baker, S. and Barron, A. (2002). Sequence of *Plasmodium falciparum* chromosomes 1, 3–9 and 13. *Nature*, 419 (6906), pp.527-531.

Halliwell, B. and Gutteridge, J. (1984). Oxygen toxicity, oxygen radicals, transition metals, and disease. *Biochemical Journal*, 219 (1), p.1.

Hamza, I. and Gitlin, J.D. (2002). Copper chaperones for cytochrome *c* oxidase and human disease. *Journal of Bioenergetics and Biomembranes*, 34, pp.381-388.

Hansen, K.S., Grieve, E., Mikhail, A., Mayan, I., Mohammed, N., Anwar, M., Baktash, S.H., Drake, T.L., Whitty, C.J., Rowland, M.W. and Leslie, T.J. (2015). Cost-effectiveness of malaria diagnosis using rapid diagnostic tests compared to microscopy or clinical symptoms alone in Afghanistan. *Malaria Journal*, 14, pp.1-15.

Happi, C.T., Gbotosho, G.O., Folarin, O.A., Sowunmi, A., Hudson, T., O'Neil, M., Milhous, W., Wirth, D.F. and Oduola, A.M.J. (2009). Selection of *Plasmodium falciparum* multidrug resistance gene 1 allele in asexual stages and gametocytes by artemether-lumefantrine in Nigerian children with uncomplicated *falciparum* malaria. *Antimicrobial Agents and Chemotherapy*, 53 (3), pp.888-895.

Harcum, S.W., Ramirez, D.M. and Bentley, W.E. (1992). Optimal nutrient feed policies for heterologous protein production. *Applied Biochemistry and Biotechnology*, 34, pp.161-173.

Harris, E.D. (2000). Cellular copper transport and metabolism. *Annual review of nutrition*, 20 (1), pp.291-310.

Harrison, M.D., Jones, C.E., Solioz, M. and Dameron, C.T. (2000). Intracellular copper routing: the role of copper chaperones. *Trends in Biochemical Sciences*, 25 (1), pp.29-32.

Hasan, N.M. and Lutsenko, S. (2012). Regulation of copper transporters in human cells. *Current Topics in Membranes*, 69, pp.137-161.

Hassan, A.O., Oso, O.V., Obeagu, E.I. and Adeyemo, A.T. (2022). Malaria vaccine: prospects and challenges. *Madonna University Journal of Medicine and Health Sciences ISSN: 2814-3035*, 2 (2), pp.22-40.

Hastings, I.M., Watkins, W.M. and White, N.J. (2002). The evolution of drug-resistant malaria: the role of drug elimination half-life. *Philosophical Transactions of the Royal Society of London. Series B: Biological Sciences*, 357 (1420), pp.505-519.

Hatori, Y. and Lutsenko, S. (2013). An expanding range of functions for the copper chaperone/antioxidant protein Atox1. *Antioxidants & Redox Signaling*, 19 (9), pp.945-957.

Hatori, Y. and Lutsenko, S. (2016). The role of copper chaperone Atox1 in coupling redox homeostasis to intracellular copper distribution. *Antioxidants*, 5 (3), p.25.

Hatori, Y., Clasen, S., Hasan, N.M., Barry, A.N. and Lutsenko, S. (2012). Functional partnership of the copper export machinery and glutathione balance in human cells. *Journal of Biological Chemistry*, 287 (32), pp.26678-26687.

Heaton, D., Nittis, T., Srinivasan, C. and Winge, D.R. (2000). Mutational analysis of the mitochondrial copper metallochaperone Cox17. *Journal of Biological Chemistry*, 275 (48), pp.37582-37587.

Heaton, D.N., George, G.N., Garrison, G. and Winge, D.R. (2001). The mitochondrial copper metallochaperone Cox17 exists as an oligomeric, polycopper complex. *Biochemistry*, 40 (3), pp.743-751.

Hekkelman, M.L., de Vries, I., Joosten, R.P. and Perrakis, A. (2023). AlphaFill: enriching AlphaFold models with ligands and cofactors. *Nature Methods*, 20 (2), pp.205-213.

Hermann, R., Walther, P. and Müller, M. (1996). Immunogold labeling in scanning electron microscopy. *Histochemistry and cell Biology*, 106 (1), pp.31-39.

Hia, F. and Takeuchi, O. (2021). The effects of codon bias and optimality on mRNA and protein regulation. *Cellular and Molecular Life Sciences*, *78*, pp.1909-1928.

Hien, T.T., White, N.J., Thuy-Nhien, N.T., Hoa, N.T., Thuan, P.D., Tarning, J., Nosten, F., Magnusson, B., Jain, J.P. and Hamed, K. (2017). Estimation of the *in vivo* MIC of cipargamin in uncomplicated *Plasmodium falciparum* malaria. *Antimicrobial Agents and Chemotherapy*, 61 (2), pp.10-1128.

Himelblau, E., Mira, H., Lin, S.J., Cizewski Culotta, V., Penarrubia, L. and Amasino, R.M. (1998). Identification of a functional homolog of the yeast copper homeostasis gene Atx1 from Arabidopsis. *Plant Physiology*, 117 (4), pp.1227-1234.

Hirayama, T., Kieber, J.J., Hirayama, N., Kogan, M., Guzman, P. Nourizadeh, S., Alonso, J.M., Dailey, W.P., Dancis, A. and Ecker, J.R. (1999). Responsive-To-Antagonist1, a Menkes/Wilson disease-related copper transporter, is required for ethylene signaling in *Arabidopsis*. *Cell*, 97 (3), pp.383-393.

Holzer, A.K., Manorek, G.H. and Howell, S.B. (2006). Contribution of the major copper influx transporter Ctr1 to the cellular accumulation of cisplatin, carboplatin, and oxaliplatin. *Molecular Pharmacology*, 70 (4), pp.1390-1394.

Honig, B.H. and Hubbell, W.L. (1984). Stability of" salt bridges" in membrane proteins. *Proceedings of the National Academy of Sciences*, 81 (17), pp.5412-5416.

Hool, K. and Nieman, T.A. (1988). Immobilized luminol chemiluminescence reagent system for hydrogen peroxide determinations in flowing streams. *Analytical Chemistry*, 60 (9), pp.834-837.

Hopkins, H., Kambale, W., Kamya, M.R., Staedke, S.G., Dorsey, G. and Rosenthal, P.J. (2007). Comparison of HRP2-and pLDH-based rapid diagnostic tests for malaria with longitudinal follow-up in Kampala, Uganda. *The American Journal of Tropical Medicine and Hygiene*, 76 (6), pp.1092-1097.

Horn, D. and Barrientos, A. (2008). Mitochondrial copper metabolism and delivery to cytochrome *c* oxidase. *IUBMB life*, 60 (7), pp.421-429.

Horng, Y.C., Cobine, P.A., Maxfield, A.B., Carr, H.S. and Winge, D.R. (2004). Specific copper transfer from the Cox17 metallochaperone to both Sco1 and Cox11 in the assembly of yeast cytochrome *c* oxidase. *Journal of Biological Chemistry*, 279 (34), pp.35334-35340.

Howard, R.J., Uni, S., Aikawa, M., Aley, S.B., Leech, J.H., Lew, A.M., Wellems, T.E., Rener, J. and Taylor, D.W. (1986). Secretion of a malarial histidine-rich protein (Pf HRP II) from *Plasmodium falciparum*-infected erythrocytes. *The Journal of Cell Biology*, 103 (4), pp.1269-1277.

Howell, S.B., Safaei, R., Larson, C.A., and Sailor, M.J. (2010). Copper transporters and the cellular pharmacology of the platinum-containing cancer drugs. *Molecular Pharmacology*, 77 (6), pp.887-894.

Hsu, M.T. and Berg, P. (1978). Altering the specificity of restriction endonuclease: effect of replacing Mg^{2+} with Mn^{2+}. *Biochemistry*, 17 (1), pp.131-138.

Huffman, D.L. and O'Halloran, T.V. (2000). Energetics of copper trafficking between the Atx1 metallochaperone and the intracellular copper transporter, Ccc2. *Journal of Biological Chemistry*, 275 (25), pp.18611-18614.

Huffman, D.L., Huyett, J., Outten, F.W., Doan, P.E., Finney, L.A., Hoffman, B.M. and O'Halloran, T.V. (2002). Spectroscopy of Cu (II)-PcoC and the multicopper oxidase function of PcoA, two essential components of *Escherichia coli* pco copper resistance operon. *Biochemistry*, 41 (31), pp.10046-10055.

Hughes, D. and Andersson, D.I. (2015). Evolutionary consequences of drug resistance: shared principles across diverse targets and organisms. *Nature Reviews Genetics*, 16 (8), pp.459-471.

Hung, I.H., Suzuki, M., Yamaguchi, Y., Yuan, D.S., Klausner, R.D. and Gitlin, J.D. (1997). Biochemical characterization of the Wilson disease protein and functional expression in the yeast *Saccharomyces cerevisiae*. *Journal of Biological Chemistry*, 272 (34), pp.21461-21466.

Huppke, P., Brendel, C., Korenke, G.C., Marquardt, I., Donsante, A., Yi, L., Hicks, J.D., Steinbach, P.J., Wilson, C., Elpeleg, O. and Møller, L.B. (2012). Molecular and biochemical characterization of a unique mutation in CCS, the human copper chaperone to superoxide dismutase. *Human mutation*, 33 (8), pp.1207-1215.

Hurdayal, R., Achilonu, I., Choveaux, D., Coetzer, T.H. and Goldring, J.D. (2010). Anti-peptide antibodies differentiate between Plasmodial lactate dehydrogenases. *Peptides*, 31 (4), pp.525-532.

Ikeda, M., Kaneko, M., Tachibana, S.I., Balikagala, B., Sakurai-Yatsushiro, M., Yatsushiro, S., Takahashi, N., Yamauchi, M., Sekihara, M., Hashimoto, M. and Katuro, O.T. (2018). Artemisinin-resistant *Plasmodium falciparum* with high survival rates, Uganda, 2014–2016. *Emerging Infectious Diseases*, 24 (4), p.718.

Iqbal, J., Hira, P.R., Sher, A. and Al-Enezi, A.A. (2001). Diagnosis of imported malaria by Plasmodium lactate dehydrogenase (pLDH) and histidine-rich protein 2 (*Pf*HRP-2)-based immunocapture assays. *The American Journal of Tropical Medicine and Hygiene*, 64 (1), pp.20-23.

Isah, M.B., Goldring, J.D. and Coetzer, T.H. (2020). Expression and copper binding properties of the N-terminal domain of copper P-type ATPases of African trypanosomes. *Molecular and Biochemical Parasitology*, 235, p.111245.

Islam, M.N., Rauf, A., Fahad, F.I., Emran, T.B., Mitra, S., Olatunde, A., Shariati, M.A., Rebezov, M., Rengasamy, K.R. and Mubarak, M.S. (2022). Superoxide dismutase: an updated review on its health benefits and industrial applications. *Critical Reviews in Food Science and Nutrition*, 62 (26), pp.7282-7300.

Ito, H., Monobe, K., Okubo, S. and Aoki, S. (2024). Identification of Novel Antimicrobial Compounds Targeting *Mycobacterium Tuberculosis* S-Adenosyl-L-Homocysteine Hydrolase Using Dual Hierarchical *in-Silico* Structure-Based Drug Screening. *Molecules*, 29 (6), p.1303.

Jang, I.K., Tyler, A., Lyman, C., Rek, J.C., Arinaitwe, E., Adrama, H., Murphy, M., Imwong, M., Proux, S., Haohankhunnatham, W. and Barney, R. (2020). Multiplex human malaria array: quantifying antigens for malaria rapid diagnostics. *The American Journal of Tropical Medicine and Hygiene*, 102 (6), p.1366.

Jensen, L.T. and Culotta, V.C. (2005). Activation of Cu/Zn superoxide dismutases from *Caenorhabditis elegans* does not require the copper chaperone CCS. *Journal of Biological Chemistry*, 280 (50), pp.41373-41379.

Jiang, J., Nadas, I.A., Kim, M.A., and Franz, K.J. (2005). A Mets motif peptide found in copper transport proteins selectively binds Cu (I) with methionine-only coordination. *Inorganic Chemistry*, 44 (26), pp.9787-9794.

JMOL development team. 2016. *Jmol*, Available at: (http://jmol.sourceforge.net/).

Jones, C.E., Daly, N.L., Cobine, P.A., Craik, D.J. and Dameron, C.T. (2003). Structure and metal binding studies of the second copper-binding domain of the Menkes ATPase. *Journal of Structural Biology*, 143 (3), pp.209-218.

Jortzik, E. and Becker, K. (2012). Thioredoxin and glutathione systems in Plasmodium falciparum. *International Journal of Medical Microbiology*, 302 (4-5), pp.187-194.

Josling, G.A. and Llinás, M. (2015). Sexual development in Plasmodium parasites: knowing when it's time to commit. *Nature Reviews Microbiology*, 13 (9), pp.573-587.

Joubert, F., Harrison, C.M., Koegelenberg, R.J., Odendaal, C.J. and de Beer, T.A. (2009). Discovery: an interactive resource for the rational selection and comparison of putative drug target proteins in malaria. *Malaria Journal*, *8*, pp.1-8.

Kadioglu, O., Serly, J., Seo, E.J., Vincze, I., Somlai, C., Saeed, M.E., Molnar, J. and Efferth, T. (2015). Molecular docking analysis of steroid-based copper transporter 1 inhibitors. *Anticancer Research*, 35 (12), pp.6505-6508.

Kahsay, R.Y., Gao, G. and Liao, L. (2005). An improved hidden Markov model for transmembrane protein detection and topology prediction and its applications to complete genomes. *Bioinformatics*, 21 (9), pp.1853-1858.

Kajubi, R., Ochieng, T., Kakuru, A., Jagannathan, P., Nakalembe, M., Ruel, T., Opira, B., Ochokoru, H., Ategeka, J., Nayebare, P. and Clark, T.D. (2019). Monthly sulfadoxine-pyrimethamine versus dihydroartemisinin–piperaquine for intermittent preventive treatment of malaria in pregnancy: a double-blind, randomized, controlled, superiority trial. *The Lancet*, 393 (10179), pp.1428-1439.

Kakolwa, M.A., Mahende, M.K., Ishengoma, D.S., Mandara, C.I., Ngasala, B., Kamugisha, E., Kataraihya, J.B., Mandike, R., Mkude, S., Chacky, F. and Njau, R. (2018). Efficacy and safety of artemisinin-based combination therapy, and molecular markers for artemisinin and piperaquine resistance in Mainland Tanzania. *Malaria Journal*, 17, pp.1-10.

Kamau, E., Campino, S., Amenga-Etego, L., Drury, E., Ishengoma, D., Johnson, K., Mumba, D., Kekre, M., Yavo, W., Mead, D. and Bouyou-Akotet, M. (2015). K13-propeller polymorphisms in Plasmodium falciparum parasites from sub-Saharan Africa. *The Journal of Infectious Diseases*, 211 (8), pp.1352-1355.

Kanatani, S., Stiffler, D., Bousema, T., Yenokyan, G. and Sinnis, P. (2024). Revisiting the Plasmodium sporozoite inoculum and elucidating the efficiency with which malaria parasites progress through the mosquito. *Nature Communications*, 15 (1), p.748.

Kangueane, P., Nilofer, C., Kangueane, P. and Nilofer, C. (2018). (Protein-protein docking): Methods and tools. *Protein-protein and domain-domain interactions*, pp.161-168.

Kapiya, G., Sialubanje, C. and Nawa, M. (2024). The Effects of Indoor Residual Spraying on Prevalence of Malaria among Under-five Children in Zambia; A Retrospective Cohort Study. *MedRxiv*, pp.2024-05.

Kaplan, J.H. and Lutsenko, S. (2009). Copper transport in mammalian cells: special care for a metal with special needs. *Journal of Biological Chemistry*, 284 (38), pp.25461-25465.

Kaplan, J.H. and Maryon, E.B. (2016). How mammalian cells acquire copper: an essential but potentially toxic metal. *Biophysical Journal*, 110 (1), pp.7-13.

Kardos, J., Héja, L., Simon, Á., Jablonkai, I., Kovács, R. and Jemnitz, K. (2018). Copper signaling causes and consequences. *Cell Communication and Signaling*, 16, pp.1-22.

Karema, C., Imwong, M., Fanello, C.I., Stepniewska, K., Uwimana, A., Nakeesathit, S., Dondorp, A., Day, N.P. and White, N.J. (2010). Molecular correlates of high-level antifolate resistance in Rwandan children with Plasmodium falciparum malaria. *Antimicrobial Agents and Chemotherapy*, 54 (1), pp.477-483.

Karplus, M. and Petsko, G.A. (1990). Molecular dynamics simulations in biology. *Nature*, 347 (6294), pp.631-639.

Kay, K.L., Zhou, L., Tenori, L., Bradley, J.M., Singleton, C., Kihlken, M.A., Ciofi-Baffoni, S. and Le Brun, N.E. (2017). Kinetic analysis of copper transfer from a chaperone to its target protein mediated by complex formation. *Chemical Communications*, 53 (8), pp.1397-1400.

Kehr, S., Sturm, N., Rahlfs, S., Przyborski, J.M. and Becker, K. (2010). Compartmentation of redox metabolism in malaria parasites. *PLoS Pathogens*, 6 (12), p.e1001242.

Kenthirapalan, S., Waters, A.P., Matuschewski, K. and Kooij, T.W. (2014). Copper-transporting ATPase is important for malaria parasite fertility. *Molecular Microbiology*, 91 (2), pp.315-325.

Kenthirapalan, S., Waters, A.P., Matuschewski, K. and Kooij, T.W. (2016). Functional profiles of orphan membrane transporters in the life cycle of the malaria parasite. *Nature Communications*, 7 (1), pp.1-10.

Kersting, S., Rausch, V., Bier, F.F. and von Nickisch-Rosenegk, M. (2014). Rapid detection of *Plasmodium falciparum* with isothermal recombinase polymerase amplification and lateral flow analysis. *Malaria Journal*, 13, pp.1-9.

Khow, O. and Suntrarachun, S. (2012). Strategies for production of active eukaryotic proteins in bacterial expression system. *Asian Pacific Journal of Tropical Biomedicine*, 2 (2), pp.159-162.

Kiaco, K., Teixeira, J., Machado, M., do Rosário, V. and Lopes, D. (2015). Evaluation of artemether-lumefantrine efficacy in the treatment of uncomplicated malaria and its association with *Pf*mdr1, *Pf*atpase6, and K13-propeller polymorphisms in Luanda, Angola. *Malaria Journal*, 14, pp.1-10.

Kilejian, A. (1979). Characterization of a protein correlated with the production of knob-like protrusions on membranes of erythrocytes infected with *Plasmodium falciparum*. *Proceedings of the National Academy of Sciences*, 76 (9), pp.4650-4653.

Kim, B.E., Nevitt, T. and Thiele, D.J. (2008. Mechanisms for copper acquisition, distribution, and regulation. *Nature Chemical Biology*, 4 (3), pp.176-185.

Kimple, M.E., Brill, A.L. and Pasker, R.L. (2013). Overview of affinity tags for protein purification. *Current protocols in protein science*, *73* (1), pp.9-9.

Kimura, M., Kaneko, O., Liu, Q., Zhou, M., Kawamoto, F., Wataya, Y., Otani, S., Yamaguchi, Y. and Tanabe, K. (1997). Identification of the four species of human malaria parasites by nested PCR that targets variant sequences in the small subunit rRNA gene. *Parasitology International*, 46 (2), pp.91-95.

Kipruto, E.K., Ochieng, A.O., Anyona, D.N., Mbalanya, M., Mutua, E.N., Onguru, D., Nyamongo, I.K. and Estambale, B.B. (2017). Effect of climatic variability on malaria trends in Baringo County, Kenya. *Malaria Journal*, 16, pp.1-11.

Kirsipuu, T., Zadorožnaja, A., Smirnova, J., Friedemann, M., Plitz, T., Tõugu, V. and Palumaa, P. (2020). Copper (II)-binding equilibria in human blood. *Scientific Reports*, 10 (1), p.5686.

Kita, K., Watanabe, Y.I., Takeo, S., Mineki, S., Hirawake, H., Amino, H., Aso, E., Watanabe, J. and Kojima, S. (1998). Mitochondrial respiratory chain of malaria parasite. *Tokai Journal of Experimental and Clinical Medicine*, 23, pp.89-90.

Klatt, P. and Lamas, S. (2000). Regulation of protein function by S-glutathiolation in response to oxidative and nitrosative stress. *European Journal of Biochemistry*, 267 (16), pp.4928-4944.

Klomp, L.W., Lin, S.J., Yuan, D.S., Klausner, R.D., Culotta, V.C. and Gitlin, J.D. (1997). Identification and functional expression of HAH1, a novel human gene involved in copper homeostasis. *Journal of Biological Chemistry*, 272 (14), pp.9221-9226.

Ko, J., Park, H., Heo, L. and Seok, C. (2012). GalaxyWEB server for protein structure prediction and refinement. *Nucleic Acids Research*, 40 (1), pp.294-297. Available at: (http://www.galux.co.kr/)

Koay, M., Zhang, L., Yang, B., Maher, M.J., Xiao, Z. and Wedd, A.G. (2005). CopC protein from *Pseudomonas s yringae*: Intermolecular Transfer of Copper from Both the Copper (I) and Copper (II) Sites. *Inorganic Chemistry*, 44 (15), pp.5203-5205.

Kobayashi, R. and Tashima, Y. (1989). Visualization of antigen on a nitrocellulose membrane by the oxidative coupling reaction of N, N′-dimethyl-p-phenylendiamine, and 4-Chloro-1-naphthol. *Analytical Biochemistry*, 183 (1), pp.9-12.

Koeppl, L.H., Popadić, D., Saleem-Batcha, R., Germer, P. and Andexer, J.N. (2024). Structure, function, and substrate preferences of archaeal S-adenosyl-l-homocysteine hydrolases. *Communications Biology*, 7 (1), p.380.

Kommuguri, U.N., Bodiga, S., Sankuru, S. and Bodiga, V.L. (2012). Copper deprivation modulates CTR1 and CUP1 expression and enhances cisplatin cytotoxicity in Saccharomyces cerevisiae. *Journal of Trace Elements in Medicine and Biology*, 26 (1), pp.13-19.

Kongsaeree, P., Khongsuk, P., Leartsakulpanich, U., Chitnumsub, P., Tarnchompoo, B., Walkinshaw, M.D. and Yuthavong, Y. (2005). Crystal structure of dihydrofolate reductase from *Plasmodium vivax*: pyrimethamine displacement linked with mutation-induced resistance. *Proceedings of the National Academy of Sciences*, 102 (37), pp.13046-13051.

Korsinczky, M., Chen, N., Kotecka, B., Saul, A., Rieckmann, K. and Cheng, Q. (2000). Mutations in *Plasmodium falciparum* cytochrome *b* that are associated with atovaquone resistance are located at a putative drug-binding site. *Antimicrobial Agents and Chemotherapy*, 44 (8), pp.2100-2108.

Kozakov, D., Beglov, D., Bohnuud, T., Mottarella, S.E., Xia, B., Hall, D.R. and Vajda, S. (2013). How good is automated protein docking? *Proteins: Structure, Function, and Bioinformatics*, 81 (12), pp.2159-2166.

Kozakov, D., Brenke, R., Comeau, S.R. and Vajda, S. (2006). PIPER: an FFT-based protein docking program with pairwise potentials. *Proteins: Structure, Function, and Bioinformatics*, 65 (2), pp.392-406.

Kozakov, D., Clodfelter, K.H., Vajda, S. and Camacho, C.J. (2005). Optimal clustering for detecting near-native conformations in protein docking. *Biophysical Journal*, 89 (2), pp.867-875.

Kozakov, D., Hall, D.R., Beglov, D., Brenke, R., Comeau, S.R., Shen, Y., Li, K., Zheng, J., Vakili, P., Paschalidis, I.C. and Vajda, S. (2010). Achieving reliability and high accuracy in automated protein docking: ClusPro, PIPER, SDU, and stability analysis in CAPRI rounds 13–19. *Proteins: Structure, Function, and Bioinformatics*, 78 (15), pp.3124-3130.

Kozakov, D., Hall, D.R., Xia, B., Porter, K.A., Padhorny, D., Yueh, C., Beglov, D. and Vajda, S. (2017). The ClusPro web server for protein-protein docking. *Nature Protocols*, 12 (2), pp.255-278.

Krause, R.G. and Goldring, J.D. (2018). Phosphoethanolamine-N-methyltransferase is a potential biomarker for the diagnosis of *P. knowlesi* and *P. falciparum* malaria. *PLoS One*, 13 (3), p.0193833.

Krause, R.G., Hurdayal, R., Choveaux, D., Przyborski, J.M., Coetzer, T.H. and Goldring, J.D. (2017). Plasmodium glyceraldehyde-3-phosphate dehydrogenase: a potential malaria diagnostic target. *Experimental Parasitology*, 179, pp.7-19.

Kremsner, P.G. and Krishna, S. (2004). Antimalarial combinations. *The Lancet*, 364 (9430), pp.285-294.

Kricka, L.J. and Thorpe, G.H. (1983). Chemiluminescent and bioluminescent methods in analytical chemistry. A Review. *Analyst*, 108 (1292), pp.1274-1296.

Krnajski, Z., Gilberger, T.W., Walter, R.D. and Müller, S. (2001). The malaria parasite *Plasmodium falciparum* possesses a functional thioredoxin system. *Molecular and Biochemical Parasitology*, 112 (2), pp.219-228.

Krupanidhi, S., Sreekumar, A., and Sanjeevi, C.B. (2008). Copper & biological health. *Indian Journal of Medical Research*, 128 (4), pp.448-461.

Kufareva, I. and Abagyan, R. (2012). Methods of protein structure comparison. *Homology modeling: Methods and Protocols*, pp.231-257.

Kulinska, K.I., Białas, P., Dera-Szymanowska, A., Billert, M., Kotwicka, M., Szymanowski, K. and Wołun-Cholewa, M. (2023). The role of phoenixin in the proliferation and migration of ectopic epithelial cells *in vitro*. *Biochemical and Biophysical Research Communications*, 646, pp.44-49.

Kuo, M.T., Huang, Y.F., Chou, C.Y. and Chen, H.H., (2021). Targeting the copper transport system to improve treatment efficacies of platinum-containing drugs in cancer chemotherapy. *Pharmaceuticals*, 14 (6), p.549.

Kurien, B.T. and Scofield, R.H. (2006). Western blotting. *Methods*, 38 (4), pp.283-293.

Kurland, C. and Gallant, J. (1996). Errors of heterologous protein expression. *Current Opinion in Biotechnology*, 7 (5), pp.489-493.

Kusakabe, Y., Ishihara, M., Umeda, T., Kuroda, D., Nakanishi, M., Kitade, Y., Gouda, H., Nakamura, K.T. and Tanaka, N. (2015). Structural insights into the reaction mechanism of S-adenosyl-L-homocysteine hydrolase. *Scientific reports*, 5 (1), p.16641.

Kyomuhangi, I., Andrada, A., Mao, Z., Pollard, D., Riley, C., Bennett, A., Hamainza, B., Slater, H., Millar, J., Miller, J.M. and Eisele, T.P. (2023). Assessing national vector control micro-planning in Zambia using the 2021 malaria indicator survey. *Malaria Journal*, 22 (1), p.365.

La Fontaine, S. and Mercer, J.F. (2007). Trafficking of the copper-ATPases, ATP7A and ATP7B: role in copper homeostasis. *Archives of Biochemistry and Biophysics*, 463 (2), pp.149-167.

Laemmli, U.K. (1970). Cleavage of structural proteins during the assembly of the head of bacteriophage T4. *Nature*, 227 (5259), pp.680-685.

Lalloo, D.G. and Hill, D.R. (2008). Preventing malaria in travelers. *British Medical Journal*, 336 (7657), pp.1362-1366.

Lamola, M.T., Musekiwa, A., de Voux, A., Reddy, C., Morifi, M. and Mutevedzi, P.C. (2024). The prevalence of malaria in the five districts of Limpopo Province, South Africa, 2015-2017. *South African Medical Journal*, 114 (5), pp.48-55.

Larson, C.A., Adams, P.L., Jandial, D.D., Blair, B.G., Safaei, R., and Howell, S.B. (2010). The role of the N-terminus of mammalian copper transporter 1 in the cellular accumulation of cisplatin. *Biochemical pharmacology*, 80 (4), pp.448-454.

Larson, C.A., Blair, B.G., Safaei, R., and Howell, S.B. (2009). The role of the mammalian copper transporter 1 in the cellular accumulation of platinum-based drugs. *Molecular pharmacology*, 75 (2), pp.324-330.

Laskowski, P.R., Pfreundschuh, M., Stauffer, M., Ucurum, Z., Fotiadis, D. and Müller, D.J. (2017). High-resolution imaging and multiparametric characterization of native membranes by combining confocal microscopy and an atomic force microscopy-based toolbox. *ACS nano*, 11 (8), pp.8292-8301.

Laskowski, R.A. (2001). PDBsum: summaries and analyses of PDB structures. *Nucleic acids research*, 29 (1), pp.221-222.

Law, A.J. and Leaver, J. (2000). Effect of pH on the thermal denaturation of whey proteins in milk. *Journal of Agricultural and Food Chemistry*, 48 (3), pp.672-679.

Le Roch, K.G., Zhou, Y., Blair, P.L., Grainger, M., Moch, J.K., Haynes, J.D., De la Vega, P., Holder, A.A., Batalov, S., Carucci, D.J. and Winzeler, E.A. (2003). Discovery of gene function by expression profiling of the malaria parasite life cycle. *Science*, 301 (5639), pp.1503-1508.

Leary, S.C., Cobine, P.A., Nishimura, T., Verdijk, R.M., de Krijger, R., de Coo, R., Tarnopolsky, M.A., Winge, D.R. and Shoubridge, E.A. (2013). Cox19 mediates the transduction of a mitochondrial redox signal from Sco1 that regulates ATP7A-mediated cellular copper efflux. *Molecular biology of the cell*, 24 (6), pp.683-691.

Leary, S.C., Kaufman, B.A., Pellecchia, G., Guercin, G.H., Mattman, A., Jaksch, M. and Shoubridge, E.A. (2004). Human Sco1 and Sco2 have independent, cooperative functions in copper delivery to cytochrome *c* oxidase. *Human molecular genetics*, 13 (17), pp.1839-1848.

Lee, J., Peña, M.M.O., Nose, Y. and Thiele, D.J. (2002). Biochemical characterization of the human copper transporter Ctr1. *Journal of Biological Chemistry*, 277 (6), pp.4380-4387.

Lee, J., Prohaska, J.R., Dagenais, S.L., Glover, T.W. and Thiele, D.J. (2000). Isolation of a murine copper transporter gene, tissue-specific expression, and functional complementation of a yeast copper transport mutant. *Gene*, 254 (1-2), pp.87-96.

Lee, P.Y., Costumbrado, J., Hsu, C.Y. and Kim, Y.H. (2012. Agarose gel electrophoresis for the separation of DNA fragments. *Journal of Visualized Experiments*, 62, p.e3923.

Leitch, J.M., Jensen, L.T., Bouldin, S.D., Outten, C.E., Hart, P.J. and Culotta, V.C. (2009). Activation of Cu, Zn-superoxide dismutase in the absence of oxygen and the copper chaperone CCS. *Journal of Biological Chemistry*, 284 (33), pp.21863-21871.

Lemaire, S.D., Guillon, B., Le Maréchal, P., Keryer, E., Miginiac-Maslow, M. and Decottignies, P. (2004). New thioredoxin targets in the unicellular photosynthetic eukaryote *Chlamydomonas reinhardtii*. *Proceedings of the National Academy of Sciences*, 101 (19), pp.7475-7480.

Letunic, I., Copley, R.R., Schmidt, S., Ciccarelli, F.D., Doerks, T., Schultz, J., Ponting, C.P. and Bork, P. (2004). SMART 4.0: towards genomic data integration. *Nucleic acids research*, 32 (suppl_1), pp. D142-D144.

Letunic, I., Doerks, T. and Bork, P. (2012). SMART 7: recent updates to the protein domain annotation resource. *Nucleic Acids Research*, 40 (D1), pp.D302-D305.

Liang, Z.D., Long, Y., Chen, H.H., Savaraj, N. and Kuo, M.T. (2014). Regulation of the high-affinity copper transporter *(h*Ctr1) expression by cisplatin and heavy metals. *JBIC Journal of Biological Inorganic Chemistry*, 19, pp.17-27.

Liao, B.C., Hsieh, C.W., Lin, Y.C. and Wung, B.S. (2010). The glutaredoxin/glutathione system modulates NF-κB activity by glutathionylation of p65 in cinnamaldehyde-treated endothelial cells. *Toxicological Sciences*, 116 (1), pp.151-163.

Liedgens, L., Zimmermann, J., Wäschenbach, L., Geissel, F., Laporte, H., Gohlke, H., Morgan, B. and Deponte, M. (2020). Quantitative assessment of the determinant structural differences between redox-active and inactive glutaredoxins. *Nature Communications*, 11 (1), p.1725.

Lim, C.M., Cater, M.A., Mercer, J.F. and La Fontaine, S. (2006). Copper-dependent interaction of glutaredoxin with the N termini of the copper-ATPases (ATP7A and ATP7B) defective in Menkes and Wilson diseases. *Biochemical and Biophysical Research Communications*, 348 (2), pp.428-436.

Lin, S.J. and Culotta, V.C. (1995). The Atx1 gene of Saccharomyces cerevisiae encodes a small metal homeostasis factor that protects cells against reactive oxygen toxicity. *Proceedings of the National Academy of Sciences*, 92 (9), pp.3784-3788.

Lin, S.J., Pufahl, R.A., Dancis, A., O'Halloran, T.V. and Culotta, V.C. (1997). A role for the *Saccharomyces cerevisiae* Atx1 gene in copper trafficking and iron transport. *Journal of Biological Chemistry*, 272 (14), pp.9215-9220.

Lin, Y.F., Cheng, C.W., Shih, C.S., Hwang, J.K., Yu, C.S. and Lu, C.H. (2016). MIB: metal ion-binding site prediction and docking server. *Journal of Chemical Information and Modeling*, 56 (12), pp.2287-2291.

Lindahl, M. and Florencio, F.J. (2003). Thioredoxin-linked processes in cyanobacteria are as numerous as in chloroplasts, but targets are different. *Proceedings of the National Academy of Sciences*, 100 (26), pp.16107-16112.

Linder, M.C. and Hazegh-Azam, M. (1996). Copper biochemistry and molecular biology. *The American Journal of Clinical Nutrition*, 63 (5), pp.797S-811S.

Linder, M.C., Ricarte, A., Kidane, T.Z., Corona, L., Azenon, J. and Jaime, A. (2020). Non-CTR1 mechanisms of intestinal copper absorption determined with the Caco2 cell culture model. *The FASEB Journal*, 34 (S1), pp.1-1.

Liu, P.C., Koeller, D.M. and Kaler, S.G. (2003). Genomic organization of Atox1, a human copper chaperone. *BMC Genetics*, 4, pp.1-4.

Liu, X., Jann, J., Xavier, C. and Wu, H. (2015). Glutaredoxin 1 (Grx1) protects human retinal pigment epithelial cells from oxidative damage by preventing AKT glutathionylation. *Investigative Ophthalmology & Visual Science*, 56 (5), pp.2821-2832.

Ljolje, D., Abdallah, R. and Lucchi, N.W. (2021). Detection of malaria parasites in samples from returning US travelers using the Alethia® Malaria Plus LAMP assay. *BMC Research Notes*, 14, pp.1-5.

Llases, M.E., Morgada, M.N. and Vila, A.J. (2019). Biochemistry of copper site assembly in heme-copper oxidases: a theme with variations. *International Journal of Molecular Sciences*, 20 (15), p.3830.

López-Barragán, M.J., Lemieux, J., Quiñones, M., Williamson, K.C., Molina-Cruz, A., Cui, K., Barillas-Mury, C., Zhao, K. and Su, X.Z. (2011). Directional gene expression and antisense transcripts in sexual and asexual stages of *Plasmodium falciparum*. *BMC Genomics*, 12, pp.1-13.

Loveridge, K.M. and Sigala, P.A. (2024). Identification of a divalent metal transporter required for cellular iron metabolism in malaria parasites. *BioRxiv*, pp.2024-05.

Lu, C.H., Chen, C.C., Yu, C.S., Liu, Y.Y., Liu, J.J., Wei, S.T., and Lin, Y.F. (2022). MIB2: metal ion-binding site prediction and modeling server. *Bioinformatics*, 38 (18), pp.4428-4429.

Lu, C.H., Lin, Y.F., Lin, J.J. and Yu, C.S. (2012). Prediction of metal ion–binding sites in proteins using the fragment transformation method. *PLoS One*, 7 (6), p.39252.

Lu, C.H., Lin, Y.S., Chen, Y.C., Yu, C.S., Chang, S.Y. and Hwang, J.K. (2006). The fragment transformation method to detect the protein structural motifs. *Proteins: Structure, Function, and Bioinformatics*, 63 (3), pp.636-643.

Lu, Z.H. and Solioz, M. (2002). Bacterial copper transport. *Advances in Protein Chemistry*, 60, pp.93-121.

Luo, A.P., Giannangelo, C., Siddiqui, G. and Creek, D.J. (2023). Promising antimalarial hits from phenotypic screens: a review of recently described multi-stage actives and their modes of action. *Frontiers in Cellular and Infection Microbiology*, 13, p.1308193.

Lutsenko, S. (2010). Human copper homeostasis: a network of interconnected pathways. *Current Opinion in Chemical Biology*, 14 (2), pp.211-217.

Lutsenko, S. (2021). Dynamic and cell-specific transport networks for intracellular copper ions. *Journal of Cell Science*, 134 (21), p.240523.

Lutsenko, S. 2016. Copper trafficking to the secretory pathway. *Metallomics*, 8 (9), pp.840-852.

Lutsenko, S., Barnes, N.L., Bartee, M.Y. and Dmitriev, O.Y. (2007). Function and regulation of human copper-transporting ATPases. *Physiological Reviews*, 87 (3), pp.1011-1046.

Lutsenko, S., Petrukhin, K., Cooper, M.J., Gilliam, C.T. and Kaplan, J.H. (1997). N-terminal domains of human copper-transporting adenosine triphosphatases (the Wilson's and Menkes disease proteins) bind copper selectively in vivo and in vitro with the stoichiometry of one copper per metal-binding repeat. *Journal of Biological Chemistry*, 272 (30), pp.18939-18944.

Ma, Z., Cowart, D.M., Scott, R.A. and Giedroc, D.P. (2009). Molecular insights into the metal selectivity of the copper (I)-sensing repressor CsoR from Bacillus subtilis. *Biochemistry*, 48 (15), pp.3325-3334.

Maciel-Flores, C.E., Lozano-Alvarez, J.A., and Bivián-Castro, E.Y. (2024). Recently Reported Biological Activities and Action Targets of Pt (II)-and Cu (II)-Based Complexes. *Molecules*, 29 (5), p.1066.

Madamet, M., Amalvict, R., Benoit, N., French National Reference Centre for Imported Malaria Study Group and Pradines, B. (2022). Assessment of a commercial real-time PCR assay (Vitassay qPCR malaria 5 test) to detect human malaria infection in travelers returning to France. *Diagnostics*, 12 (11), p.2747.

Maghool, S., Fontaine, S.L., Roberts, B.R., Kwan, A.H., and Maher, M.J. (2020). Human glutaredoxin-1 can transfer copper to isolated metal binding domains of the P1B-type ATPase, ATP7B. *Scientific Reports*, 10 (1), p.4157.

Maharaj, R., Raman, J., Morris, N., Moonasar, D., Durrheim, D.N., Seocharan, I., Kruger, P., Shandukani, B. and Kleinschmidt, I. (2013). Epidemiology of malaria in South Africa: From control to elimination. *South African Medical Journal*, 103 (10), pp.779-783.

Makrides, S.C. (1996) Strategies for achieving high-level expression of genes in *Escherichia coli*. *Microbiological Reviews*, 60 (3), pp.512-538.

Makrides, S.C. (1996). Strategies for achieving high-level expression of genes in *Escherichia coli*. *Microbiological Reviews*, 60 (3), pp.512-538.

Maksum, I.P., Latifah, F.P.U., Nabiel, A., Sriwidodo, S., Lestari, N.F., Azizah, M.I. and Utami, D.F. (2023). An Overview of Culture Conditions for Recombinant Protein Expression in *Escherichia coli*. *Journal of Applied Biotechnology Reports*, 10 (1), pp.864-875.

Malhotra, A. (2009). Tagging for protein expression. *Methods in enzymology*, 463, pp.239-258.

Mandal, A.K., Yang, Y., Kertesz, T.M. and Argüello, J.M. (2004). Identification of the transmembrane metal binding site in Cu+-transporting PIB-type ATPases. *Journal of Biological Chemistry*, 279 (52), pp.54802-54807.

Mandel, M. and Higa, A. (1970). Calcium-dependent bacteriophage DNA infection. *Journal of Molecular Biology*, 53 (1), pp.159-162.

Mann, J.R., Camakaris, J., Danks, D.M. and Walliczek, E.G. (1979). Copper metabolism in mottled mouse mutants: copper therapy of brindled (Mobr) mice. *Biochemical Journal*, 180 (3), pp.605-612.

Markus, M.B. (2018). New evidence for hypnozoite-independent *Plasmodium vivax* malarial recurrences. *Trends in Parasitology*, 34 (12), pp.1015-1016.

Markus, M.B. (2021). Safety and efficacy of tafenoquine for *Plasmodium vivax* malaria prophylaxis and radical cure: Overview and perspectives. *Therapeutics and Clinical Risk Management*, pp.989-999.

Markus, M.B. (2023). Putative contribution of 8-aminoquinolines to preventing recrudescence of malaria. *Tropical Medicine and Infectious Disease*, 8 (5), p.278.

Marsh, K., Akl, E., Achan, J., Alzahrani, M., Baird, J.K., Bousema, T., Gamboa, D., Lacerda, M., Mendis, K., Penny, M. and Schapira, A. (2024). Development of WHO recommendations for the final phase of elimination and prevention of re-establishment of malaria. *The American Journal of Tropical Medicine and Hygiene*, 110, p.3.

Martin, R.E. (2020). The transportome of the malaria parasite. *Biological Reviews*, 95 (2), pp.305-332.

Martin, R.E., Ginsburg, H. and Kirk, K. (2009a). Membrane transport proteins of the malaria parasite. *Molecular microbiology*, 74 (3), pp.519-528.

Martin, R.E., Henry, R.I., Abbey, J.L., Clements, J.D. and Kirk, K. (2005). The'permeome'of the malaria parasite: an overview of the membrane transport proteins of Plasmodium falciparum. *Genome Biology*, 6, pp.1-22.

Martin, R.E., Marchetti, R.V., Cowan, A.I., Howitt, S.M., Bröer, S. and Kirk, K. (2009b). Chloroquine transport via the malaria parasite's chloroquine resistance transporter. *Science*, 325 (5948), pp.1680-1682.

Martínez-Ruiz, A., García-Ortega, L., Kao, R., Oñaderra, M., Mancheño, J.M., Davies, J., Martínez del Pozo, Á. and Gavilanes, J.G. (2000). Ribonuclease U2: cloning, production in *Pichia pastoris*, and affinity chromatography purification of the active recombinant protein. *FEMS Microbiology Letters*, 189 (2), pp.165-169.

Marva, E., Cohen, A., Saltman, P., Chevion, M. and Golenser, J. (1989). Deleterious synergistic effects of ascorbate and copper on the development of *Plasmodium falciparum*: an *in vitro* study in normal and in G6PD-deficient erythrocytes. *International journal for parasitology*, 19 (7), pp.779-785.

Maryon, E.B., Molloy, S.A. and Kaplan, J.H. (2013b). Cellular glutathione plays a key role in copper uptake mediated by human copper transporter 1. *American Journal of Physiology-Cell Physiology*, 304 (8), pp.768-779.

Maryon, E.B., Molloy, S.A., Ivy, K., Yu, H., and Kaplan, J.H. (2013a). Rate and regulation of copper transport by human copper transporter 1 (*h*Ctr1). *Journal of Biological Chemistry*, 288 (25), pp.18035-18046.

Masuoka, J. and Saltman, P. (1994). Zinc (II) and copper (II) binding to serum albumin. A comparative study of dog, bovine, and human albumin. *Journal of Biological Chemistry*, 269 (41), pp.25557-25561.

Maurya, R. and Namdeo, M. (2022). Superoxide Dismutase: A key Enzyme for the survival of intracellular pathogens in the host. *Reactive Oxygen Species*, p.49.

Maxfield, A.B., Heaton, D.N. and Winge, D.R. (2004). Cox17 is functional when tethered to the mitochondrial inner membrane. *Journal of Biological Chemistry*, 279 (7), pp.5072-5080.

Maya-Maldonado, K., Cardoso-Jaime, V., González-Olvera, G., Osorio, B., Recio-Tótoro, B., Manrique-Saide, P., Rodríguez-Sánchez, I.P., Lanz-Mendoza, H., Missirlis, F. and Hernández-Hernández, F.D.L.C. (2021). Mosquito metallomics reveals copper and iron as critical factors for Plasmodium infection. *PLoS Neglected Tropical Diseases*, 15 (6), p.e0009509.

Mayxay, M., Pukrittayakamee, S., Newton, P.N. and White, N.J. (2004). Mixed-species malaria infections in humans. *Trends in Parasitology*, 20 (5), pp.233-240.

Mbanefo, A. and Kumar, N. (2020). Evaluation of malaria diagnostic methods as a key for successful control and elimination programs. *Tropical Medicine and Infectious Disease*, 5 (2), p.102.

Mboma, Z.M., Festo, C., Lorenz, L.M., Massue, D.J., Kisinza, W.N., Bradley, J., Moore, J.D., Mandike, R., Akim, I., Lines, J. and Overgaard, H.J. (2021). The consequences of declining population access to insecticide-treated nets (ITNs) on net use patterns and physical degradation of nets after 22 months of ownership. *Malaria Journal*, 20, pp.1-13.

McConville, R., Krol, J.M., Steel, R.W., O'Neill, M.T., Davey, B.K., Hodder, A.N., Nebl, T., Cowman, A.F., Kneteman, N. and Boddey, J.A. (2024). Flp/FRT-mediated disruption of ptex150 and exp2 in *Plasmodium falciparum* sporozoites inhibits liver-stage development. *Proceedings of the National Academy of Sciences*, 121 (28), p.e2403442121.

McNamara, C.W., Lee, M.C., Lim, C.S., Lim, S.H., Roland, J., Nagle, A., Simon, O., Yeung, B.K., Chatterjee, A.K., McCormack, S.L. and Manary, M.J. (2013). Targeting Plasmodium PI (4) K to eliminate malaria. *Nature*, 504 (7479), pp.248-253.

Mehlin, C., Boni, E., Buckner, F.S., Engel, L., Feist, T., Gelb, M.H., Haji, L., Kim, D., Liu, C., Mueller, N. and Myler, P.J. (2006). Heterologous expression of proteins from *Plasmodium falciparum*: results from 1000 genes. *Molecular and Biochemical Parasitology*, 148 (2), pp.144-160.

Meltzer, E., Rahav, G. and Schwartz, E. (2018). Vivax malaria chemoprophylaxis: the role of atovaquone-proguanil compared to other options. *Clinical Infectious Diseases*, 66 (11), pp.1751-1755.

Menard, D. and Dondorp, A. (2017). Antimalarial drug resistance: a threat to malaria elimination. *Cold Spring Harbor Perspectives in Medicine*, 7 (7), p.a025619.

Ménard, D., Khim, N., Beghain, J., Adegnika, A.A., Shafiul-Alam, M., Amodu, O., Rahim-Awab, G., Barnadas, C., Berry, A., Boum, Y. and Bustos, M.D. (2016). A worldwide map of *Plasmodium falciparum* K13-propeller polymorphisms. *New England Journal of Medicine*, 374 (25), pp.2453-2464.

Mercer, S.W. and Burke, R. (2016). Evidence for a role for the putative *Drosophila h*GRX1 orthologue in copper homeostasis. *Biometals*, 29, pp.705-713.

Mering, C.V., Huynen, M., Jaeggi, D., Schmidt, S., Bork, P. and Snel, B. (2003). STRING: a database of predicted functional associations between proteins. *Nucleic Acids Research*, 31 (1), pp.258-261.

Meshnick, S.R., Scott, M.D., Lubin, B., Ranz, A. and Eaton, J.W. (1990). Antimalarial activity of diethyldithiocarbamate: potentiation by copper. *Biochemical Pharmacology*, 40 (2), pp.213-216.

Messaoudi, A., Belguith, H. and Ben Hamida, J. (2013). Homology modeling and virtual screening approaches to identify potent inhibitors of VEB-1 β-lactamase. *Theoretical Biology and Medical Modelling*, 10, pp.1-10.

Meyer, Y., Siala, W., Bashandy, T., Riondet, C., Vignols, F. and Reichheld, J.P. (2008). Glutaredoxins and thioredoxins in plants. *Biochimica Et Biophysica Acta (BBA)-Molecular Cell Research*, 1783 (4), pp.589-600.

Michelet, L., Zaffagnini, M., Massot, V., Keryer, E., Vanacker, H., Miginiac-Maslow, M., Issakidis-Bourguet, E. and Lemaire, S.D. (2006). Thioredoxins, glutaredoxins, and glutathionylation: new crosstalks to explore. *Photosynthesis Research*, 89 (2), pp.225-245.

Migocka, M. and Malas, K. (2018). Plant responses to copper: molecular and regulatory mechanisms of copper uptake, distribution, and accumulation in plants. *Plant Micronutrient Use Efficiency* pp. 71-86.

Ministry of Health, **Zambia.** Malaria Indicator Survey 2021., (2021). [Available at: https://www.nmec.org.zm/publications]

Miyayama, T., Ishizuka, Y., Iijima, T., Hiraoka, D. and Ogra, Y. (2011). Roles of copper chaperone for superoxide dismutase 1 and metallothionein in copper homeostasis. *Metallomics*, 3 (7), pp.693-701.

MMV. MMV's Pipeline of Antimalarial Drugs. (2023) https://www.mmv.org/research-development/ mmvs-pipeline-antimalarial-drugs.

Montenegro, L.M., Montenegro, R.A., Lima, A.S., Carvalho, A.B., Schindler, H.C. and Abath, F.G. (2004)**.** Development of a single tube hemi-nested PCR for genus-specific detection of Plasmodium in oligoparasitemic patients. *Transactions of the Royal Society of Tropical Medicine and Hygiene*, 98 (10), pp.619-625.

Morgada, M.N., Abriata, L.A., Cefaro, C., Gajda, K., Banci, L. and Vila, A.J. (2015). Loop recognition and copper-mediated disulfide reduction underpin metal site assembly of CuA in human cytochrome oxidase. *Proceedings of the National Academy of Sciences*, 112 (38), pp.11771-11776.

Morris, N., Frean, J., Baker, L., Ukpe, I.S., Barnes, K.I., Kruger, P., Mabuza, A., Raswiswi, E., Maharaj, R., Blumberg, L. and Moonasar, D. (2013). Re-defining the extent of malaria transmission in South Africa: implications for chemoprophylaxis. *South African Medical Journal*, 103 (11), pp.861-864.

Müller, S. (2015). Role and regulation of glutathione metabolism in *Plasmodium falciparum*. *Molecules*, 20 (6), pp.10511-10534.

Multhaup, G., Strausak, D., Bissig, K.D. and Solioz, M. (2001). Interaction of the CopZ copper chaperone with the CopA copper ATPase of *Enterococcus hirae* assessed by surface plasmon resonance. *Biochemical and Biophysical Research Communications*, 288 (1), pp.172-177.

Munsami, J. (2022). Recombinant expression and initial characterization of *Plasmodium falciparum* copper-binding protein Synthesis of cytochrome *c* oxidase 1 (Sco1). University of KwaZulu-Natal.

Murray, V., Campbell, H.M. and Gero, A.M. (2011). *Plasmodium falciparum*: DNA sequence specificity of cisplatin and cisplatin analogues. *Experimental parasitology*, 128 (4), pp.396-400.

Nair, L. And Bhasin, V.K. (1994). Cure with cisplatin (II) of murine malaria infection and *in vitro* inhibition of a chloroquine-resistant *Plasmodium falciparum* isolate. *Japanese Journal of Medical Science and Biology*, 47 (5-6), pp.241-252.

Nakanishi, M. (2007). S-adenosyl-L-homocysteine hydrolase as an attractive target for antimicrobial drugs. *Yakugaku Zasshi: Journal of the Pharmaceutical Society of Japan*, 127 (6), pp.977-982.

Nakanishi, M., Iwata, A., Yatome, C. and Kitade, Y. (2001). Purification and properties of recombinant *Plasmodium falciparum* S-adenosyl-L-homocysteine hydrolase. *The Journal of Biochemistry*, 129 (1), pp.101-105.

Nakanishi, M., Yabe, S., Tanaka, N., Ito, Y., Nakamura, K.T. and Kitade, Y. (2005). Mutational analyses of *Plasmodium falciparum* and human S-adenosylhomocysteine hydrolases. *Molecular and Biochemical Parasitology*, 143 (2), pp.146-151.

Namuganga, J.F., Epstein, A., Nankabirwa, J.I., Mpimbaza, A., Kiggundu, M., Sserwanga, A., Kapisi, J., Arinaitwe, E., Gonahasa, S., Opigo, J. and Ebong, C. (2021). The impact of stopping and starting indoor residual spraying on malaria burden in Uganda. *Nature communications*, 12 (1), p.2635.

Narayanan, G., Vuyyuru, H., Muthuvel, B. and Konerirajapuram Natrajan, S. (2013). CTR1 silencing inhibits angiogenesis by limiting copper entry into endothelial cells. *PLoS One*, 8 (9), p.71982.

Nath, S., Brahma, A. and Bhattacharyya, D. (2003). Extended application of gel-permeation chromatography by spin column. *Analytical Biochemistry*, 320 (2), pp.199-206.

Nayeri, N., Li, P., Górecki, K., Lindkvist-Petersson, K. and Gourdon, P. (2023). Principles to recover copper-conducting Ctr proteins for the purpose of structural and functional studies. *Protein Expression and Purification*, 203, p.106213.

Nevitt, T., Öhrvik, H. and Thiele, D.J. (2012). Charting the travels of copper in eukaryotes from yeast to mammals. *Biochimica Et Biophysica Acta (BBA)-Molecular Cell Research*, 1823 (9), pp.1580-1593.

Ngasala, B.E., Malmberg, M., Carlsson, A.M., Ferreira, P.E., Petzold, M.G., Blessborn, D., Bergqvist, Y., Gil, J.P., Premji, Z. and Mårtensson, A. (2011). Effectiveness of artemether-lumefantrine provided by community health workers in under-five children with uncomplicated malaria in rural Tanzania: an open-label prospective study. *Malaria Journal*, 10, pp.1-10.

Njumkeng, C., Apinjoh, T.O., Anchang-Kimbi, J.K., Amin, E.T., Tanue, E.A., Njua-Yafi, C. and Achidi, E.A. (2019). Coverage and usage of insecticide-treated nets (ITNs) within households: associated factors and effect on the prevalence of malaria parasitemia in the Mount Cameroon area. *BMC Public Health*, 19, pp.1-11.

Nobrega, M.P., Bandeira, S.C., Beers, J. and Tzagoloff, A. (2002). Characterization of Cox19, a widely distributed gene required for expression of mitochondrial cytochrome oxidase. *Journal of Biological Chemistry*, 277 (43), pp.40206-40211.

Noedl, H., Se, Y., Schaecher, K., Smith, B.L., Socheat, D. and Fukuda, M.M. (2008). Evidence of artemisinin-resistant malaria in western Cambodia. *New England Journal of Medicine*, 359 (24), pp.2619-2620.

Nývltová, E., Dietz, J.V., Seravalli, J., Khalimonchuk, O. and Barrientos, A. (2022). Coordination of metal center biogenesis in human cytochrome *c* oxidase. *Nature communications*, 13 (1), p.3615.

Obeagu, E.I., Chijioke, U.O. and Ekelozie, I.S. (2018). Malaria rapid diagnostic test (RDTs). *Annals of Clinical and Laboratory Research*, 6 (4), p.275.

Ocan, M., Akena, D., Nsobya, S., Kamya, M.R., Senono, R., Kinengyere, A.A. and Obuku, E. (2019). K13-propeller gene polymorphisms in *Plasmodium falciparum* parasite population in malaria-affected countries: a systematic review of prevalence and risk factors. *Malaria Journal*, 18, pp.1-17.

Ogata, F.T., Branco, V., Vale, F.F. and Coppo, L. (2021). Glutaredoxin: Discovery, redox defence, and much more. *Redox Biology*, 43, p.101975.

O'Halloran, T.V. and Culotta, V.C. (2000). Metallochaperones, an intracellular shuttle service for metal ions. *Journal of Biological Chemistry*, 275 (33), pp.25057-25060.

Öhrvik, H. and Thiele, D.J. (2014). How copper traverses cellular membranes through the mammalian copper transporter 1, Ctr1. *Annals of the New York Academy of Sciences*, 1314 (1), pp.32-41.

Öhrvik, H., Aaseth, J. and Horn, N. (2017). Orchestration of dynamic copper navigation–new and missing pieces. *Metallomics*, 9 (9), pp.1204-1229.

Ohse, V.A., Klotz, L.O. and Priebs, J. (2024). Copper Homeostasis in the Model Organism *C. elegans*. *Cells*, 13 (9), p.727.

Okafor, P.E., Osuji, C.F., and Ekwezuo, C.M. (2024). Investigation of the role of copper ion in biological systems and its implications on diseases: a review. *Journal of Health, Metabolism and Nutrition Studies*.

Okombo, J. and Chibale, K. (2018). Recent updates in the discovery and development of novel antimalarial drug candidates. *Medicinal Chemistry Communications*, 9 (3), pp.437-453.

Okombo, J., and Fidock, D.A. (2024). Towards next-generation treatment options to combat Plasmodium falciparum malaria. *Nature Reviews Microbiology*, pp.1-14.

Okwu, D.G., Manego, R.Z., Duparc, S., Kremsner, P.G., Ramharter, M. and Mombo-Ngoma, G. (2025). The non-artemisinin antimalarial drugs under development: a review. *Clinical Microbiology and Infection*.

Olliaro, P.L. and Goldberg, D.E. (1995). The Plasmodium digestive vacuole: metabolic headquarters and choice drug target. *Parasitology Today*, 11 (8), pp.294-297.

Österberg, R. (1974). Models for copper-protein interaction based on solution and crystal structure studies. *Coordination Chemistry Reviews*, 12 (4), pp.309-347.

Oswald, C., Krause-Buchholz, U. and Rödel, G. (2009). Knockdown of human Cox17 affects the assembly and supramolecular organization of cytochrome *c* oxidase. *Journal of Molecular Biology*, 389 (3), pp.470-479.

Ouji, M., Augereau, J.M., Paloque, L. and Benoit-Vical, F. (2018). *Plasmodium falciparum* resistance to artemisinin-based combination therapies: A sword of Damocles in the path toward malaria elimination. *Parasite*, 25.

Ouyang, Y., Peng, Y., Li, J., Holmgren, A. and Lu, J. (2018). Modulation of thiol-dependent redox system by metal ions via thioredoxin and glutaredoxin systems. *Metallomics*, 10 (2), pp.218-228.

Padley, D., Moody, A.H., Chiodini, P.L. and Saldanha, J. (2003). Use of a rapid, single-round, multiplex PCR to detect malarial parasites and identify the species present. *Annals of Tropical Medicine & Parasitology*, 97 (2), pp.131-137.

Painter, H.J., Morrisey, J.M., Mather, M.W. and Vaidya, A.B. (2007). Specific role of mitochondrial electron transport in blood-stage *Plasmodium falciparum*. *Nature*, 446 (7131), pp.88-91.

Pais, F.S.M., Ruy, P.D.C., Oliveira, G., and Coimbra, R.S. (2014). Assessing the efficiency of multiple sequence alignment programs. *Algorithms for Molecular Biology*, 9, pp.1-8.

Palani, B. (2018). Quantification of histidine-rich protein 3 of *Plasmodium falciparum*. *Monoclonal Antibodies in Immunodiagnosis and Immunotherapy*, 37 (2), pp.87-90.

Palmgren, M. (2023). P-type ATPases: Many more enigmas left to solve. *Journal of Biological Chemistry*, 299 (11).

Palumaa, P., Kangur, L., Voronova, A. and Sillard, R. (2004). Metal-binding mechanism of Cox17, a copper chaperone for cytochrome *c* oxidase. *Biochemical Journal*, 382 (1), pp.307-314.

Papaneophytou, C.P. and Kontopidis, G. (2014). Statistical approaches to maximize recombinant protein expression in *Escherichia coli*: a general review. *Protein Expression and Purification*, 94, pp.22-32.

Patzewitz, E.M., Wong, E.H. and Müller, S. (2012). Dissecting the role of glutathione biosynthesis in *Plasmodium falciparum*. *Molecular microbiology*, 83 (2), pp.304-318.

Pavelková, M., Vysloužil, J., Kubová, K. and Vetchý, D. (2018). Biological role of copper as an essential trace element in the human organism. *Farm*, 67 (4), pp.143-153.

Pebay-Peyroula, E., Dahout-Gonzalez, C., Kahn, R., Trézéguet, V., Lauquin, G.J.M. and Brandolin, G. (2003). Structure of mitochondrial ADP/ATP carrier in complex with carboxyatractyloside. *Nature*, 426 (6962), pp.39-44.

Peersen, O.B. (2019). A comprehensive superposition of viral polymerase structures. *Viruses*, 11 (8), p.745.

Perkins, S.L. (2014). Malaria's many mates: past, present, and future of the systematics of the order H*aemosporida*. *Journal of Parasitology*, 100 (1), pp.11-25.

Pessentheiner, A.R., Pelzmann, H.J., Walenta, E., Schweiger, M., Groschner, L.N., Graier, W.F., Kolb, D., Uno, K., Miyazaki, T., Nitta, A. and Rieder, D. (2013). NAT8L (N-acetyltransferase 8-like) accelerates lipid turnover and increases energy expenditure in brown adipocytes. *Journal of Biological Chemistry*, 288 (50), pp.36040-36051.

Peters, T. and Blumenstock, F.A. (1967). Copper-binding properties of bovine serum albumin and its amino-terminal peptide fragment. *Journal of Biological Chemistry*, 242 (7), pp.1574-1578.

Petković Ramadža, D., Kuhtić, I., Žarković, K., Lochmüller, H., Čavka, M., Kovač, I., Barić, I. and Prutki, M. (2022). Case Report: Advanced Skeletal Muscle Imaging in S-Adenosylhomocysteine Hydrolase Deficiency and Further Insight into Muscle Pathology. *Frontiers in Pediatrics*, 10, p.847445.

Petris, M.J., Mercer, J.F., Culvenor, J.G., Lockhart, P., Gleeson, P.A. and Camakaris, J. (1996). Ligand-regulated transport of the Menkes copper P-type ATPase efflux pump from the Golgi apparatus to the plasma membrane: a novel mechanism of regulated trafficking. *The EMBO Journal*, 15 (22), pp.6084-6095.

Petrucci, Ralph H., Harwood, William S., Herring, F. G., and Madura Jeffrey D. (2007). General Chemistry: Principles and Modern Applications. 9th ed. Upper Saddle River: Pearson Education, Inc.

Petzoldt, S., Kahra, D., Kovermann, M., Dingeldein, A.P., Niemiec, M.S., Ådén, J. and Wittung-Stafshede, P. (2015). Human cytoplasmic copper chaperones Atox1 and CCS exchange copper ions *in vitro*. *Biometals*, 28, pp.577-585.

Phyo, A.P., Jittamala, P., Nosten, F.H., Pukrittayakamee, S., Imwong, M., White, N.J., Duparc, S., Macintyre, F., Baker, M. and Möhrle, J.J. (2016). Antimalarial activity of artefenomel (OZ439), a novel synthetic antimalarial endoperoxide, in patients with *Plasmodium falciparum* and *Plasmodium vivax* malaria: an open-label phase 2 trial. *The Lancet Infectious Diseases*, 16 (1), pp.61-69.

Piacenza, L., Alvarez, M.N., Peluffo, G. and Radi, R. (2009). Fighting the oxidative assault: the *Trypanosoma cruzii* journey to infection. *Current Opinion in Microbiology*, 12 (4), pp.415-421.

Picciocchi, A., Saguez, C., Boussac, A., Cassier-Chauvat, C. and Chauvat, F. (2007). CGFS-type monothiol glutaredoxins from the cyanobacterium Synechocystis PCC6803 and other evolutionary distant model organisms possess a glutathione-ligated [2Fe-2S] cluster. *Biochemistry*, 46 (51), pp.15018-15026.

Pickard, A.L., Wongsrichanalai, C., Purfield, A., Kamwendo, D., Emery, K., Zalewski, C., Kawamoto, F., Miller, R.S. and Meshnick, S.R. (2003). Resistance to antimalarials in Southeast Asia and genetic polymorphisms in pfmdr1. *Antimicrobial Agents and Chemotherapy*, 47 (8), pp.2418-2423.

Pickart, C.M. (2001). Mechanisms underlying ubiquitination. *Annual review of Biochemistry*, 70 (1), pp.503-533.

Picot, S., Cucherat, M. and Bienvenu, A.L. (2020). Systematic review and meta-analysis of diagnostic accuracy of loop-mediated isothermal amplification (LAMP) methods compared with microscopy, polymerase chain reaction, and rapid diagnostic tests for malaria diagnosis. *International Journal of Infectious Diseases*, 98, pp.408-419.

Pillay, E., Khodaiji, S., Bezuidenhout, B.C., Litshie, M. and Coetzer, T.L. (2019). Evaluation of automated malaria diagnosis using the Sysmex XN-30 analyzer in a clinical setting. *Malaria Journal*, 18, pp.1-14.

Pimentel, D., Haeussler, D.J., Matsui, R., Burgoyne, J.R., Cohen, R.A. and Bachschmid, M.M. (2012). Regulation of cell physiology and pathology by protein S-glutathionylation: lessons learned from the cardiovascular system. *Antioxidants & Redox Signaling*, 16 (6), pp.524-542.

Platon, L. and Ménard, D. (2024). *Plasmodium falciparum* ring-stage plasticity and drug resistance. *Trends in Parasitology*.

Plouffe, D.M., Wree, M., Du, A.Y., Meister, S., Li, F., Patra, K., Lubar, A., Okitsu, S.L., Flannery, E.L., Kato, N. and Tanaseichuk, O. (2016). High-throughput assay and discovery of small molecules that interrupt malaria transmission. *Cell Host & Microbe*, 19 (1), pp.114-126.

Plucinski, M.M., Dimbu, P.R., Fortes, F., Murphy, S.C., Smith, N.T., Cruz, K.R., Seilie, A.M., Halsey, E.S., Aidoo, M. and Rogier, E. (2019). Malaria parasite density in individuals with different rapid diagnostic test results and concentrations of HRP2 antigen. *The American Journal of Tropical Medicine and Hygiene*, 100 (5), p.1202.

Plucinski, M.M., Dimbu, P.R., Macaia, A.P., Ferreira, C.M., Samutondo, C., Quivinja, J., Afonso, M., Kiniffo, R., Mbounga, E., Kelley, J.S. and Patel, D.S. (2017). Efficacy of artemether-lumefantrine, artesunate-amodiaquine, and dihydroartemisinin-piperaquine for treatment of uncomplicated *Plasmodium falciparum* malaria in Angola, 2015. *Malaria Journal*, 16, pp.1-10.

Polishchuk, R. and Lutsenko, S. (2013). Golgi in copper homeostasis: a view from the membrane trafficking field. *Histochemistry and Cell Biology*, 140, pp.285-295.

Polisky, B., Greene, P., Garfin, D.E., McCarthy, B.J., Goodman, H.M., and Boyer, H.W. (1975). Specificity of substrate recognition by the EcoRI restriction endonuclease. *Proceedings of the National Academy of Sciences*, 72 (9), pp.3310-3314.

Pope, C.R., Flores, A.G., Kaplan, J.H. and Unger, V.M. (2012). Structure and function of copper uptake transporters. *Current Topics in Membranes* 69, pp. 97-112).

Porollo, A. and Meller, J. (2007). Versatile annotation and publication quality visualization of protein complexes using Polyview-3d. *BMC Bioinformatics*, 8, pp.1-8.

Povea-Cabello, S., Brischigliaro, M. and Fernández-Vizarra, E. (2024). Emerging mechanisms in the redox regulation of mitochondrial cytochrome *c* oxidase assembly and function. *Biochemical Society Transactions*, 52 (2), pp.873-885.

Prohaska, J.R. and Gybina, A.A. (2004). Intracellular copper transport in mammals. *The Journal of Nutrition*, 134 (5), pp.1003-1006.

Pronobis, M.I., Deuitch, N. and Peifer, M. (2016). The Miraprep: A protocol that uses a Miniprep kit and provides Maxiprep yields. *PLoS One*, 11 (8), p.e0160509.

Prudêncio, M., Rodriguez, A. and Mota, M.M. (2006). The silent path to thousands of merozoites: the Plasmodium liver stage. *Nature Reviews Microbiology*, 4 (11), pp.849-856.

Pufahl, R.A., Singer, C.P., Peariso, K.L., Lin, S.J., Schmidt, P.J., Fahrni, C.J., Culotta, V.C., Penner-Hahn, J.E. and O'halloran, T.V. 1997. Metal ion chaperone function of the soluble Cu (I) receptor Atx1. *Science*, 278 (5339), pp.853-856.

Puig, S., Lee, J., Lau, M. and Thiele, D.J. (2002). Biochemical and genetic analyses of yeast and human high-affinity copper transporters suggest a conserved mechanism for copper uptake. *Journal of Biological Chemistry*, 277 (29), pp.26021-26030.

Punter, F.A. and Glerum, D.M. (2003). Mutagenesis reveals a specific role for Cox17p in copper transport to cytochrome *c* oxidase. *Journal of Biological Chemistry*, 278 (33), pp.30875-30880.

Qureshi, M.A. and Javed, S. (2022). Investigating binding dynamics of trans-resveratrol to HSA for an efficient displacement of aflatoxin B1 using spectroscopy and molecular simulation. *Scientific Reports*, 12 (1), p.2400.

Rabenau, K.E., Sohrabi, A., Tripathy, A., Reitter, C., Ajioka, J.W., Tomley, F.M. and Carruthers, V.B. (2001). TgM2AP participates in *Toxoplasma gondii* invasion of host cells and is tightly associated with the adhesive protein TgMIC2. *Molecular microbiology*, 41 (3), pp.537-547.

Radivojac, P., Vacic, V., Haynes, C., Cocklin, R.R., Mohan, A., Heyen, J.W., Goebl, M.G. and Iakoucheva, L.M. (2010). Identification, analysis, and prediction of protein ubiquitination sites. *Proteins: Structure, Function, and Bioinformatics*, 78 (2), pp.365-380.

Rae, T.D., Schmidt, P.J., Pufahl, R.A., Culotta, V.C. and V. O'Halloran, T. (1999). Undetectable intracellular free copper: the requirement of a copper chaperone for superoxide dismutase. *Science*, 284 (5415), pp.805-808.

Rahlfs, S. and Becker, K. (2006). Interference with redox-active enzymes as a basis for the design of antimalarial drugs. *Mini-Reviews in Medicinal Chemistry*, 6 (2), pp.163-176.

Rahlfs, S., Fischer, M. and Becker, K. (2001). *Plasmodium falciparum* possesses a classical glutaredoxin and a second, glutaredoxin-like protein with a PICOT homology domain. *Journal of Biological Chemistry*, 276 (40), pp.37133-37140.

Rai, D.K. and Rieder, E. (2012). Homology modeling and analysis of structure predictions of the bovine rhinitis B virus RNA dependent RNA polymerase (RdRp). *International Journal of Molecular Sciences*, 13 (7), pp.8998-9013.

Raman, J., Kagoro, F.M., Mabuza, A., Malatje, G., Reid, A., Frean, J. and Barnes, K.I. (2019). Absence of kelch13 artemisinin resistance markers but strong selection for lumefantrine-tolerance molecular markers following 18 years of artemisinin-based combination therapy use in Mpumalanga Province, South Africa (2001–2018). *Malaria Journal*, 18, pp.1-12.

Ramirez OT, Zamora R, Espinosa G, Merino E, Bolivar F, Quintero R. (1994) Kinetic study of penicillin acylase production by recombinant *E. coli* in batch cultures. Process Biochemistry, 29 (3):197-206.

Ramos, D., Mar, D., Ishida, M., Vargas, R., Gaite, M., Montgomery, A. and Linder, M.C. (2016). Mechanism of copper uptake from blood plasma ceruloplasmin by mammalian cells. *PLoS One*, 11 (3), p.e0149516.

Ramos-Zúñiga, J., Bruna, N. and Pérez-Donoso, J.M. (2023). Toxicity mechanisms of copper nanoparticles and copper surfaces on bacterial cells and viruses. *International Journal of Molecular Sciences*, 24 (13), p.10503.

Rasoloson, D., Shi, L., Chong, C.R., Kafsack, B.F. and Sullivan Jr, D.J. (2004). Copper pathways in *Plasmodium falciparum*-infected erythrocytes indicate an efflux role for the copper P-ATPase. *Biochemical Journal*, 381 (3), pp.803-811.

Recht, J., Siqueira, A.M., Monteiro, W.M., Herrera, S.M., Herrera, S. and Lacerda, M.V. (2017). Malaria in Brazil, Colombia, Peru, and Venezuela: current challenges in malaria control and elimination. *Malaria Journal*, 16, pp.1-18.

Reddy, M.C., Kuppan, G., Shetty, N.D., Owen, J.L., Ioerger, T.R. and Sacchettini, J.C. (2008). Crystal structures of *Mycobacterium tuberculosis* S-adenosyl-L-homocysteine hydrolase in ternary complex with substrate and inhibitors. *Protein Science*, 17 (12), pp.2134-2144.

Reiner, R.C., Geary, M., Atkinson, P.M., Smith, D.L. and Gething, P.W. (2015). Seasonality of *Plasmodium falciparum* transmission: a systematic review. *Malaria Journal*, 14, pp.1-14.

Rensing, C., and McDevitt, S.F. (2013). The copper metallome in prokaryotic cells. *Metallomics and the Cell*, pp.417-450.

Rentzsch, A., Krummeck-Weiß, G., Hofer, A., Bartuschka, A., Ostermann, K. and Rödel, G. (1999). Mitochondrial copper metabolism in yeast: mutational analysis of Sco1p involved in the biogenesis of cytochrome *c* oxidase. *Current genetics*, 35, pp.103-108.

Ridley, R.G. (2002). Medical need, scientific opportunity, and the drive for antimalarial drugs. *Nature*, 415 (6872), pp.686-693.

Rigby, K., Zhang, L., Cobine, P.A., George, G.N. and Winge, D.R. (2007). Characterization of the cytochrome *c* oxidase assembly factor Cox19 of *Saccharomyces cerevisiae*. *Journal of Biological Chemistry*, 282 (14), pp.10233-10242.

Robinson, A.J., Overy, C. and Kunji, E.R. (2008). The mechanism of transport by mitochondrial carriers is based on the analysis of symmetry. *Proceedings of the National Academy of Sciences*, 105 (46), pp.17766-17771.

Robinson, L.J., Wampfler, R., Betuela, I., Karl, S., White, M.T., Li Wai Suen, C.S., Hofmann, N.E., Kinboro, B., Waltmann, A., Brewster, J. and Lorry, L. (2015). Strategies for understanding and reducing the *Plasmodium vivax* and *Plasmodium ovale* hypnozoite reservoir in Papua New Guinean children: a randomized placebo-controlled trial and mathematical model. *PLoS medicine*, 12 (10), p.e1001891.

Robinson, N.J. and Winge, D.R. (2010). Copper metallochaperones. *Annual Review of Biochemistry*, 79 (1), pp.537-562.

Rosenthal, P.J. (2003). Antimalarial drug discovery: old and new approaches. *Journal of Experimental Biology*, 206 (21), pp.3735-3744.

Rosenthal, P.J. (2012). How do we best diagnose malaria in Africa? *The American Journal of Tropical Medicine and Hygiene*, 86 (2), p.192.

Rosenthal, P.J., Asua, V. and Conrad, M.D. (2024b). Emergence, transmission dynamics and mechanisms of artemisinin partial resistance in malaria parasites in Africa. *Nature Reviews Microbiology*, pp.1-12.

Rosenthal, P.J., Asua, V., Bailey, J.A., Conrad, M.D., Ishengoma, D.S., Kamya, M.R., Rasmussen, C., Tadesse, F.G., Uwimana, A. and Fidock, D.A. (2024a). The emergence of artemisinin partial resistance in Africa: how do we respond? *The Lancet Infectious Diseases* pp.1-12

Rosenzweig, A.C. (2002). Metallochaperones: bind and deliver. *Chemistry & Biology*, 9 (6), pp.673-677.

Rouhier, N. and Jacquot, J.P. (2002). Plant peroxiredoxins: alternative hydroperoxide scavenging enzymes. *Photosynthesis Research*, 74, pp.259-268.

Rout, S. and Mahapatra, R.K. (2019). *In silico* study of M18 aspartyl amino peptidase (M18AAP) of *Plasmodium vivax* as an antimalarial drug target. *Bioorganic & Medicinal Chemistry*, 27 (12), pp.2553-2571.

Ruiz, L.M., Libedinsky, A. and Elorza, A.A. (2021). Role of copper on mitochondrial function and metabolism. *Frontiers in Molecular Biosciences*, 8, p.711227.

Ruprecht, J.J., Hellawell, A.M., Harding, M., Crichton, P.G., McCoy, A.J. and Kunji, E.R. (2014). Structures of yeast mitochondrial ADP/ATP carriers support a domain-based alternating-access transport mechanism. *Proceedings of the National Academy of Sciences*, 111 (4), pp.426-E434.

Ryan, S.J., Lippi, C.A. and Zermoglio, F. (2020). Shifting transmission risk for malaria in Africa with climate change: a framework for planning and intervention. *Malaria Journal*, 19, pp.1-14.

Saaranen, M.J., Salo, K.E., Latva-Ranta, M.K., Kinnula, V.L. and Ruddock, L.W. (2009). The C-terminal active site cysteine of *Escherichia coli* glutaredoxin 1 determines the glutathione specificity of the second step of peptide deglutathionylation. *Antioxidants & Redox Signaling*, 11 (8), pp.1819-1828.

Sailer, J., Nagel, J., Akdogan, B., Jauch, A.T., Engler, J., Knolle, P.A. and Zischka, H. (2024). Deadly excess copper. *Redox Biology*, p.103256.

Salman, A.A. (2019). Recombinant expression and initial characterization of two *Plasmodium falciparum* copper binding proteins: Cox11 and Cox19. University of KwaZulu-Natal.

Salman, A.A. and Goldring, J.D. (2022). Expression and copper binding characteristics of *Plasmodium falciparum* cytochrome *c* oxidase assembly factor 11, Cox11. *Malaria Journal*, 21 (1), p.173.

Salman, A.A. and Goldring, J.D. (2023). Expression and copper binding studies of a *Plasmodium falciparum* protein with Cox19 copper-binding motifs. *Experimental Parasitology*, 251, p.108572.

Sambrook, J. and Russell, D.W. (2001). *Molecular Cloning: Ch. 8. In Vitro amplification of DNA by the polymerase chain reaction*. *Cold Spring Harbor* Laboratory Press, 2.

Sambrook, J. and Russell, D.W. (2006). Preparation and transformation of competent *E. coli* using calcium chloride. *Cold Spring Harbor Protocols*, 1, pp.39-32.

Sánchez-Riego, A.M., López-Maury, L., and Florencio, F.J. (2013). Glutaredoxins are essential for stress adaptation in the cyanobacterium Synechocystis sp. PCC 6803. *Frontiers in Plant Science*, 4, p.63520.

Sandalio, L.M., López-Huertas, E., Bueno, P. and Del Río, L.A. (1997). Immunocytochemical localization of copper, zinc superoxide dismutase in peroxisomes from Watermelon (Citrullus vulgaris Schrad.) cotyledons. *Free Radical Research*, 26 (3), pp.187-194.

Sandén, A.M., Prytz, I., Tubulekas, I., Förberg, C., Le, H., Hektor, A., Neubauer, P., Pragai, Z., Harwood, C., Ward, A. and Picon, A. (2003). Limiting factors in *Escherichia coli* fed-batch production of recombinant proteins. *Biotechnology and Bioengineering*, 81 (2), pp.158-166.

Saporito-Magriñá, C.M., Musacco-Sebio, R.N., Andrieux, G., Kook, L., Orrego, M.T., Tuttolomondo, M.V., Desimone, M.F., Boerries, M., Borner, C. and Repetto, M.G. (2018). Copper-induced cell death and the protective role of glutathione: the implication of impaired protein folding rather than oxidative stress. *Metallomics*, 10 (12), pp.1743-1754.

Sato, S. (2021). Plasmodium—a brief introduction to the parasites causing human malaria and their basic biology. *Journal of Physiological Anthropology*, 40 (1), p.1.

Schägger, H. (2006). Tricine–sds-page. *Nature Protocols*, 1 (1), pp.16-22.

Schägger, H. and Von Jagow, G. (1987). Tricine-sodium dodecyl sulfate-polyacrylamide gel electrophoresis for the separation of proteins in the range from 1 to 100 kDa. *Analytical Biochemistry*, 166 (2), pp.368-379.

Scheiber, I., Dringen, R. and Mercer, J.F. (2013). Copper: effects of deficiency and overload. *Interrelations Between Essential Metal Ions and Human Diseases*, pp.359-387.

Scheiber, I.F., Mercer, J.F. and Dringen, R. (2014). Metabolism and functions of copper in the brain. *Progress in Neurobiology*, 116, pp.33-57.

Scheich, C., Sievert, V. and Büssow, K. (2003). An automated method for high-throughput protein purification applied to a comparison of His-tag and GST-tag affinity chromatography. *BMC Biotechnology*, 3, pp.1-8.

Schirmer, R.H., Müller, J.G. and Krauth-Siegel, R.L. (1995). Disulfide-reductase inhibitors as chemotherapeutic agents: the design of drugs for trypanosomiasis and malaria. *Angewandte Chemie International Edition in English*, *34* (2), pp.141-154.

Schlagenhauf, P. and Petersen, E. (2008). Malaria chemoprophylaxis: strategies for risk groups. *Clinical Microbiology Reviews*, 21 (3), pp.466-472.

Schlecht, U., Suresh, S., Xu, W., Aparicio, A.M., Chu, A., Proctor, M.J., Davis, R.W., Scharfe, C. and St Onge, R.P. (2014). A functional screen for copper homeostasis genes identifies a pharmacologically tractable cellular system. *BMC Genomics*, 15, pp.1-14.

Schrödinger, L. & DeLano, W. (2020). PyMOL, Available at: http://www.pymol.org/pymol.

Schwarzer, E., Kuehn, H. and Arese, P. (2003). The hidden faces of hemozoin and its dangerous midwives. *Trends in Parasitology*, 19 (5), pp.197-198.

Schwarzer, E., Kühn, H., Valente, E. and Arese, P. (2003). Malaria-parasitized erythrocytes and hemozoin nonenzymatically generate large amounts of hydroxy fatty acids that inhibit monocyte functions. *Blood, The Journal of the American Society of Hematology*, 101 (2), pp.722-728.

Scolari Grotto, F. and Glaser, V. (2024). Are high copper levels related to Alzheimer's and Parkinson's diseases? A systematic review and meta-analysis of articles published between 2011 and 2022. *Biometals*, 37 (1), pp.3-22.

Sehnal, D. (2009). Superimposing Multiple Structures and Exploring Protein Binding Sites. Masaryk University Faculty of Informatics.

Senior, W., de La Cruz, R. and Troccoli, L. (2020). Copper: essential and noxious to aquatic organisms. *Coastal and Deep Ocean Pollution,* pp. 107-152. CRC Press.

Seo, H.C. and Ettinger, M.J. (1993). Identification and purification of a self-associating copper-binding protein from mouse hepatic cytosols. *Journal of Biological Chemistry*, 268 (2), pp.1151-1159.

Serly, J., Vincze, I., Somlai, C., Hodoniczki, L. and Molnar, J. (2011). Synthesis and comparison of the antitumor activities of steroids on ABCB1-transfected mouse lymphoma and human ovary carcinoma. *Letters in Drug Design & Discovery*, 8 (2), pp.138-147.

Severe Malaria Observatory. Severe Malaria Criteria Features and Definition (2022) [Available at: https://www.severemalaria.org/severe-malaria/severe-malaria-criteria-featuresdefinition].

Sharma, S.S., Blattner, F.R. and Harcum, S.W. (2007). Recombinant protein production in an *Escherichia coli* reduced genome strain. *Metabolic engineering*, 9 (2), pp.133-141.

Shen, J., Griffiths, P.T., Campbell, S.J., Utinger, B., Kalberer, M. and Paulson, S.E. (2021). Ascorbate oxidation by iron, copper and reactive oxygen species: Review, model development, and derivation of key rate constants. *Scientific reports*, 11 (1), p.7417.

Shenberger, Y., Marciano, O., Gottlieb, H.E. and Ruthstein, S. (2018). Insights into the N-terminal Cu (II) and Cu (I) binding sites of the human copper transporter Ctr1. *Journal of Coordination Chemistry*, 71 (11-13), pp.1985-2002.

Shepard, E.M., Heggem, H., Juda, G.A. and Dooley, D.M. (2003). Inhibition of six copper-containing amine oxidases by the antidepressant drug tranylcypromine. *Biochimica et Biophysica Acta (BBA)-Proteins and Proteomics*, 1647 (1-2), pp.252-259.

Shokoples, S.E., Ndao, M., Kowalewska-Grochowska, K. and Yanow, S.K. (2009). Multiplexed real-time PCR assay for discrimination of Plasmodium species with improved sensitivity for mixed infections. *Journal of Clinical Microbiology*, 47 (4), pp.975-980.

Shretta, R., Liu, J., Cotter, C., Cohen, J., Dolenz, C., Makomva, K., Newby, G., Ménard, D., Phillips, A., Tatarsky, A. and Gosling, R. (2018). Malaria elimination and eradication. PMID: 30212099

Siciliano, G., Costa, G., Suárez-Cortés, P., Valleriani, A., Alano, P. and Levashina, E.A. (2020). Critical steps of *Plasmodium falciparum* ookinete maturation. *Frontiers in Microbiology*, 11, p.513816.

Sidhu, A.B.S., Verdier-Pinard, D. and Fidock, D.A. (2002). Chloroquine resistance in *Plasmodium falciparum* malaria parasites conferred by *Pf*crt mutations. *Science*, 298 (5591), pp.210-213.

Sikaala, C.H., Dlamini, B., Lungu, A., Fakudze, P., Chisenga, M., Siame, C.L., Mwendera, N., Shaba, D., Chimumbwa, J.M. and Kleinschmidt, I. (2024). Malaria elimination and the need for intensive inter-country cooperation: a critical evaluation of regional technical co-operation in Southern Africa. *Malaria Journal*, 23 (1), p.62.

Simon, I., Schaefer, M., Reichert, J. and Stremmel, W. (2008). Analysis of the human Atox 1 homolog in Wilson patients. *World Journal of Gastroenterology: WJG*, 14 (15), p.2383.

Sinaga, H., Bansal, N. and Bhandari, B. (2017). Effects of milk pH alteration on casein micelle size and gelation properties of milk. *International Journal of Food Properties*, 20 (1), pp.179-197.

Sinden, R.E. and Hartley, R.H. (1985). Identification of the meiotic division of malarial parasites. *The Journal of Protozoology*, 32 (4), pp.742-744.

Singh, B. and Daneshvar, C. (2013). Human infections and detection of *Plasmodium knowlesi*. *Clinical Microbiology Reviews*, 26 (2), pp.165-184.

Singh, B., McCaffery, J.N., Kong, A., Ah, Y., Wilson, S., Chatterjee, S., Tomar, D., Aidoo, M., Udhayakumar, V. and Rogier, E. (2021). Purification of native histidine-rich protein 2 (nHRP2) from Plasmodium falciparum culture supernatant, infected RBCs, and parasite lysate. *Malaria Journal*, 20, pp.1-13.

Singh, B., Sung, L.K., Matusop, A., Radhakrishnan, A., Shamsul, S.S., Cox-Singh, J., Thomas, A. and Conway, D.J. (2004). A large focus of naturally acquired *Plasmodium knowlesi* infections in human beings. *The Lancet*, 363 (9414), pp.1017-1024.

Singh, D.B. and Dwivedi, S. (2016). Structural insight into the binding mode of inhibitor with SAHH of Plasmodium and human: interaction of curcumin with anti-malarial drug targets. *Journal of Chemical Biology*, 9, pp.107-120.

Singh, S.P., Khan, F., and Mishra, B.N. (2010). Computational characterization of *Plasmodium falciparum* proteomic data for screening of potential vaccine candidates. *Human Immunology*, 71 (2), pp.136-143.

Singleton, W.C., McInnes, K.T., Cater, M.A., Winnall, W.R., McKirdy, R., Yu, Y., Taylor, P.E., Ke, B.X., Richardson, D.R., Mercer, J.F. and La Fontaine, S. (2010). Role of glutaredoxin1 and glutathione in regulating the activity of the copper-transporting P-type ATPases, ATP7A and ATP7B. *Journal of Biological Chemistry*, 285 (35), pp.27111-27121.

Siqueira-Neto, J.L., Wicht, K.J., Chibale, K., Burrows, J.N., Fidock, D.A. and Winzeler, E.A. (2023). Antimalarial drug discovery: progress and approaches. *Nature Reviews Drug Discovery*, 22 (10), pp.807-826.

Sirangelo, I. and Iannuzzi, C. (2017). The role of metal binding in the amyotrophic lateral sclerosis-related aggregation of copper-zinc superoxide dismutase. *Molecules*, 22 (9), p.1429.

Slater, H.C., Griffin, J.T., Ghani, A.C. and Okell, L.C. (2016). Assessing the potential impact of artemisinin and partner drug resistance in sub-Saharan Africa. *Malaria journal*, 15, pp.1-11.

Smith, A.D., Logeman, B.L. and Thiele, D.J. (2017). Copper acquisition and utilization in fungi. *Annual Review of Microbiology*, 71, pp.597-623.

Smith, R.C. and Jacobs-Lorena, M. (2010). Plasmodium–mosquito interactions: a tale of roadblocks and detours. *Advances in Insect Physiology*, 39, pp. 119-149.

Spriestersbach, A., Kubicek, J., Schäfer, F., Block, H. and Maertens, B. (2015). Purification of his-tagged proteins. In *Methods in Enzymology* 559, pp. 1-15.

Springer, C., Humayun, D. and Skouta, R. (2024). Cuproptosis: Unraveling the Mechanisms of Copper-Induced Cell Death and Its Implication in Cancer Therapy. *Cancers*, 16 (3), p.647.

Stahl, H.D., Kemp, D.J., Crewther, P.E., Scanlon, D.B., Woodrow, G., Brown, G.V., Bianco, A.E., Anders, R.F. and Coppel, R.L. (1985). The sequence of a cDNA encoding a small polymorphic histidine-and alanine-rich protein from *Plasmodium falciparum*. *Nucleic Acids Research*, 13 (21), pp.7837-7846.

Staines, H.M., Derbyshire, E.T., Slavic, K., Tattersall, A., Vial, H. and Krishna, S. (2010). Exploiting the therapeutic potential of *Plasmodium falciparum* solute transporters. *Trends in Parasitology*, 26 (6), pp.284-296.

Stanley, B.A., Sivakumaran, V., Shi, S., McDonald, I., Lloyd, D., Watson, W.H., Aon, M.A. and Paolocci, N. (2011). Thioredoxin reductase-2 is essential for keeping low levels of H_2O_2 emission from isolated heart mitochondria. *Journal of Biological Chemistry*, 286 (38), pp.33669-33677.

Stiburek, L., Vesela, K., Hansikova, H., Hulkova, H. and Zeman, J. (2009). Loss of function of Sco1 and its interaction with cytochrome *c* oxidase. *American Journal of Physiology-Cell Physiology*, 296 (5), pp.1218-1226.

Strader, C.D., Candelore, M.R., Hill, W.S., Sigal, I.S. and Dixon, R.A. (1989). Identification of two serine residues involved in agonist activation of the β-adrenergic receptor. *Journal of Biological Chemistry*, 264 (23), pp.13572-13578.

Straimer, J., Gnädig, N.F., Witkowski, B., Amaratunga, C., Duru, V., Ramadani, A.P., Dacheux, M., Khim, N., Zhang, L., Lam, S. and Gregory, P.D. (2015). K13-propeller mutations confer artemisinin resistance in *Plasmodium falciparum* clinical isolates. *Science*, 347 (6220), pp.428-431.

Strausak, D., Howie, M.K., Firth, S.D., Schlicksupp, A., Pipkorn, R., Multhaup, G. and Mercer, J.F. (2003). Kinetic analysis of the interaction of the copper chaperone Atox1 with the metal binding sites of the Menkes protein. *Journal of Biological Chemistry*, 278 (23), pp.20821-20827.

Stroeher, E. and Millar, A.H. (2012). The biological roles of glutaredoxins. *Biochemical Journal*, 446 (3), pp.333-348.

Sturm, A., Amino, R., Van de Sand, C., Regen, T., Retzlaff, S., Rennenberg, A., Krueger, A., Pollok, J.M., Menard, R. and Heussler, V.T. (2006). Manipulation of host hepatocytes by the malaria parasite for delivery into liver sinusoids. *Science*, 313 (5791), pp.1287-1290.

Sturm, N., Jortzik, E., Mailu, B.M., Koncarevic, S., Deponte, M., Forchhammer, K., Rahlfs, S. and Becker, K. (2009). Identification of proteins targeted by the thioredoxin superfamily in *Plasmodium falciparum*. *PLoS Pathogens*, 5 (4), p.e1000383.

Sun, C., Berardi, M.J. and Bushweller, J.H. (1998). The NMR solution structure of human glutaredoxin in the fully reduced form. *Journal of Molecular Biology*, 280 (4), pp.687-701.

Supan, C., Mombo-Ngoma, G., Kombila, M., Salazar, C.L.O., Held, J., Lell, B., Cantalloube, C., Djeriou, E., Ogutu, B., Waitumbi, J. and Otsula, N. (2017). Phase 2a, open-label, 4-escalating-dose, randomized multicenter study evaluating the safety and activity of ferroquine (SSR97193) plus artesunate, versus amodiaquine plus artesunate, in African adult men with uncomplicated Plasmodium falciparum malaria. *The American Journal of Tropical Medicine and Hygiene*, 97 (2), p.514.

Sutherland, C.J. (2016). Persistent parasitism: the adaptive biology of malariae and ovale malaria. *Trends in Parasitology*, 32 (10), pp.808-819.

Suzuki, K.T., Karasawa, A. and Yamanaka, K. (1989). Binding of copper to albumin and participation of cysteine in vivo and in vitro. *Archives of Biochemistry and Biophysics*, 273 (2), pp.572-577.

Szklarczyk D., Kirsch R., Koutrouli M., Nastou K., Mehryary F., Hachilif R., Gable AL., Fang T., Doncheva NT., Pyysalo S., Bork P., Jensen LJ., von Mering C. (2023). The STRING database in 2023: protein-protein association networks and functional enrichment analyses for any sequenced genome of interest. *Nucleic Acids Research,* p.51, Available at: (https://string-db.org/)

Tadele, G., Jawara, A., Oboh, M., Oriero, E., Dugassa, S., Amambua-Ngwa, A. and Golassa, L. (2023). Clinical isolates of uncomplicated falciparum malaria from high and low malaria transmission areas show distinct pfcrt and pfmdr1 polymorphisms in western Ethiopia. *Malaria Journal*, 22 (1), p.171.

Takahashi, Y., Kako, K., Kashiwabara, S.I., Takehara, A., Inada, Y., Arai, H., Nakada, K., Kodama, H., Hayashi, J.I., Baba, T. and Munekata, E. (2002). Mammalian copper chaperone Cox17p has an essential role in the activation of cytochrome *c* oxidase and embryonic development. *Molecular And Cellular Biology*, 22 (21), pp. 7614-7121.

Tamayo, E., Knight, S.A., Valderas, A., Dancis, A. and Ferrol, N. (2018). The arbuscular mycorrhizal fungus *Rhizophagus irregularis* uses a reductive iron assimilation pathway for high-affinity iron uptake. *Environmental microbiology*, 20 (5), pp.1857-1872.

Tamber, S., and Hancock, R.E. (2001). Electrophoresis and Blotting of DNA. Nature *Encyclopedia of Life Sciences,* pp.1-6.

Tanaka, N., Nakanishi, M., Kusakabe, Y., Shiraiwa, K., Yabe, S., Ito, Y., Kitade, Y. and Nakamura, K.T. (2004). Crystal structure of S-adenosyl-L-homocysteine hydrolase from the human malaria parasite *Plasmodium falciparum*. *Journal of molecular biology*, 343 (4), pp.1007-1017.

Tanaka, N., Nakanishi, M., Kusakabe, Y., Shiraiwa, K., Yabe, S., Ito, Y., Kitade, Y. and Nakamura, K.T. (2004). Three-dimensional structure of S-adenosyl-L-homocysteine hydrolase from *Plasmodium falciparum*. In *Nucleic Acids Symposium Series*, 48 (1), pp. 281-282. Oxford University Press.

Tang, D., Kang, R., Berghe, T.V., Vandenabeele, P. and Kroemer, G. (2019). The molecular machinery of regulated cell death. *Cell research*, 29 (5), pp.347-364.

Tapiero, H., Townsend, D.Á. and Tew, K.D. (2003). Trace elements in human physiology and pathology. Copper. *Biomedicine & Pharmacotherapy*, 57 (9), pp.386-398.

Tchekounou, C., Zida, A., Zongo, C., Soulama, I., Sawadogo, P.M., Guiguemde, K.T., Sangaré, I., Guiguemde, R.T. and Traore, Y. (2022). Antimalarial drugs resistance genes of *Plasmodium falciparum*: a review. *Annals of Parasitology*, 68 (2).

Ter Kuile, F.O., Luxemburger, C., Nosten, F., Thwai, K.L., Chongsuphajaisiddhi, T. and White, N.J. (1995). Predictors of mefloquine treatment failure: a prospective study of 1590 patients with uncomplicated *falciparum* malaria. *Transactions of the Royal Society of Tropical Medicine and Hygiene*, 89 (6), pp.660-664.

The Plasmodium Genome Consortium. (2001) PlasmoDB: an integrative database of the *Plasmodium falciparum* genome, Available at: https://plasmodb.org/plasmo/app

Thermofisher Scientific™ GeneRuler™ DNA ladders. (2018). Available at: (http://thermofisher.com/generuler)

Thompson, A.K., Gray, J., Liu, A. and Hosler, J.P. (2012). The roles of Rhodobacter sphaeroides copper chaperones PCuAC and Sco (PrrC) in the assembly of the copper centers of the aa3-type and the cbb3-type cytochrome *c* oxidases. *Biochimica et Biophysica Acta (BBA)-Bioenergetics*, 1817 (6), pp.955-964.

Thompson, A.K., Smith, D., Gray, J., Carr, H.S., Liu, A., Winge, D.R. and Hosler, J.P. (2010). Mutagenic analysis of Cox11 of *Rhodobacter sphaeroides*: insights into the assembly of CuB of cytochrome *c* oxidase. *Biochemistry*, 49 (27), pp.5651-5661.

Thompson, J.D., Gibson, T.J. and Higgins, D.G. (2003). Multiple sequence alignment using ClustalW and ClustalX. *Current protocols in Bioinformatics*, (1), pp.2-3.

Thompson, J.D., Higgins, D.G. and Gibson, T.J. (1994). CLUSTAL W: improving the sensitivity of progressive multiple sequence alignment through sequence weighting, position-specific gap penalties, and weight matrix choice. *Nucleic Acids Research*, 22 (22), pp.4673-4680.

Thorpe, G.H., Kricka, L.J., Moseley, S.B. and Whitehead, T.P. (1985). Phenols as enhancers of the chemiluminescent horseradish peroxidase-luminol-hydrogen peroxide reaction: application in luminescence-monitored enzyme immunoassays. *Clinical Chemistry*, 31 (8), pp.1335-1341.

Tiwari, S., Sharma, N., Sharma, G.P. and Mishra, N. (2021). Redox interactome in malaria parasite *Plasmodium falciparum*. *Parasitology Research*, 120 (2), pp.423-434.

Tottey, S., Harvie, D.R. and Robinson, N.J. (2005). Understanding how cells allocate metals using metal sensors and metallochaperones. *Accounts of Chemical Research*, 38 (10), pp.775-783.

Towbin, H., Staehelin, T. and Gordon, J. (1979). Electrophoretic transfer of proteins from polyacrylamide gels to nitrocellulose sheets: procedure and some applications. *Proceedings of the National Academy of Sciences*, 76 (9), pp.4350-4354.

Toye, P., Nyanjui, J., Goddeeris, B. and Musoke, A.J. (1996). Identification of neutralization and diagnostic epitopes on PIM, the polymorphic immunodominant molecule of Theileria parva. *Infection and immunity*, 64 (5), pp.1832-1838.

Tripathi, A.K., Sha, W., Shulaev, V., Stins, M.F. and Sullivan Jr, D.J. (2009). *Plasmodium falciparum*-infected erythrocytes induce NF-κB regulated inflammatory pathways in human cerebral endothelium. *Blood, The Journal of the American Society of Hematology*, 114 (19), pp.4243-4252.

Trnka, D., Engelke, A.D., Gellert, M., Moseler, A., Hossain, M.F., Lindenberg, T.T., Pedroletti, L., Odermatt, B., de Souza, J.V., Bronowska, A.K. and Dick, T.P. (2020). Molecular basis for the distinct functions of redox-active and FeS-transferring glutaredoxins. *Nature Communications*, 11 (1), p.3445.

Tuteja, R. (2007) Malaria - an overview. *The FEBS Journal*; 274, 4670-9

Ugarte, N., Petropoulos, I. and Friguet, B. (2010). Oxidized mitochondrial protein degradation and repair in aging and oxidative stress. *Antioxidants & redox signaling*, 13 (4), pp.539-549.

UniProt Consortium. (2015). UniProt: a hub for protein information. *Nucleic Acids Research*, 43 (1), pp.204-212. Available at: (http://www.uniprot.org/)

Vaidya, A.B. and Mather, M.W. (2009). Mitochondrial evolution and functions in malaria parasites. *Annual Review of Microbiology*, 63 (1), pp.249-267.

Vajda, S., Yueh, C., Beglov, D., Bohnuud, T., Mottarella, S.E., Xia, B., Hall, D.R. and Kozakov, D. (2017). New additions to the CLusPro server motivated by CAPRI. *Proteins: Structure, Function, and Bioinformatics*, 85 (3), pp.435-444.

Valentine, J.S. and Gralla, E.B. (1997). Delivering copper inside yeast and human cells. *Science*, 278 (5339), pp.817-818.

Valko, M., Jomova, K., Rhodes, C.J., Kuča, K. and Musílek, K. (2016). Redox-and non-redox-metal-induced formation of free radicals and their role in human disease. *Archives of Toxicology*, 90, pp.1-37.

Van den Berghe, P.V., Folmer, D.E., Malingré, H.E., Van Beurden, E., Klomp, A.E., Van de Sluis, B., Merkx, M., Berger, R. and Klomp, L.W. (2007). Human copper transporter 2 is localized in late endosomes and lysosomes and facilitates cellular copper uptake. *Biochemical Journal*, 407 (1), pp.49-59.

Van Schaijk, B.C., Kumar, T.S., Vos, M.W., Richman, A., van Gemert, G.J., Li, T., Eappen, A.G., Williamson, K.C., Morahan, B.J., Fishbaugher, M. and Kennedy, M. (2014). Type II fatty acid biosynthesis is essential for *Plasmodium falciparum* sporozoite development in the midgut of Anopheles mosquitoes. *Eukaryotic Cell*, 13 (5), pp.550-559.

Varadi, M., Anyango, S., Deshpande, M., Nair, S., Natassia, C., Yordanova, G., Vaughan, J.A. (2007). Population dynamics of Plasmodium sporogony. *Trends in Parasitology*, 23 (2), pp.63-70.

Varadi, M., Anyango, S., Deshpande, M., Nair, S., Natassia, C., Yordanova, G., Yuan, D., Stroe, O., Wood, G., Laydon, A. and Žídek, A. (2022). AlphaFold Protein Structure Database: massively expanding the structural coverage of protein-sequence space with high-accuracy models. *Nucleic Acids Research*, 50 (1), pp.439-444.

Varadi, M., Bertoni, D., Magana, P., Paramval, U., Pidruchna, I., Radhakrishnan, M., Tsenkov, M., Nair, S., Mirdita, M., Yeo, J. and Kovalevskiy, O. (2024). AlphaFold Protein Structure Database in 2024: providing structure coverage for over 214 million protein sequences. *Nucleic acids research*, 52 (1), pp.368-375.

Vaughan, J.A. (2007). Population dynamics of Plasmodium sporogony. *Trends in Parasitology*, 23 (2), pp.63-70.

Vedadi, M., Lew, J., Artz, J., Amani, M., Zhao, Y., Dong, A., Wasney, G.A., Gao, M., Hills, T., Brokx, S. and Qiu, W. (2007). Genome-scale protein expression and structural biology of *Plasmodium falciparum* and related Apicomplexan organisms. *Molecular and Biochemical Parasitology*, 151 (1), pp.100-110.

Venkatesan, P. (2024). The 2023 WHO World Malaria Report. *The Lancet Microbe*, 5, p.214

Verma, R. (2024). Antimalarial Drugs and Drug Resistance. In *Drug Targets for Plasmodium Falciparum: Historic to Future Perspectives* (pp. 41-55).

Vest, K.E., Leary, S.C., Winge, D.R. and Cobine, P.A. (2013). Copper import into the mitochondrial matrix in *Saccharomyces cerevisiae* is mediated by Pic2, a mitochondrial carrier family protein. *Journal of Biological Chemistry*, 288 (33), pp.23884-23892.

Vest, K.E., Wang, J., Gammon, M.G., Maynard, M.K., White, O.L., Cobine, J.A., Mahone, W.K. and Cobine, P.A. (2016). Overlap of copper and iron uptake systems in mitochondria in *Saccharomyces cerevisiae*. *Open Biology*, 6 (1), p.150223.

Vest, K.E., Zhu, X. and Cobine, P.A. (2019). Copper disposition in yeast. In *Clinical and Translational Perspectives on Wilson Disease*, pp. 115-126

Vita, N., Landolfi, G., Baslé, A., Platsaki, S., Lee, J., Waldron, K.J. and Dennison, C. (2016). Bacterial cytosolic proteins with a high capacity for Cu (I) that protect against copper toxicity. *Scientific Reports*, 6 (1), p.39065.

Voorberg-van der Wel, A., Roma, G., Gupta, D.K., Schuierer, S., Nigsch, F., Carbone, W., Zeeman, A.M., Lee, B.H., Hofman, S.O., Faber, B.W. and Knehr, J. (2017). A comparative transcriptomic analysis of replicating and dormant liver stages of the relapsing malaria parasite *Plasmodium cynomolgi*. *Elife*, 6, p.e29605.

Votýpka, J., Modrý, D., Oborník, M., Šlapeta, J. and Lukeš, J. (2016). Apicomplexa. *Handbook of the Protists*, pp.1-58.

Waalkes, M.P., Fox, D.A., States, J.C., Patierno, S.R. and McCabe Jr, M.J. (2000). Metals and disorders of cell accumulation: modulation of apoptosis and cell proliferation. *Toxicological Sciences*, 56 (2), pp.255-261.

Walke, G., Aupič, J., Kashoua, H., Janoš, P., Meron, S., Shenberger, Y., Qasem, Z., Gevorkyan-Airapetov, L., Magistrato, A. and Ruthstein, S. (2022). Dynamical interplay between the human high-affinity copper transporter *h*Ctr1 and its cognate metal ion. *Biophysical Journal*, 121 (7), pp.1194-1204.

Wang, J., Luo, C., Shan, C., You, Q., Lu, J., Elf, S., Zhou, Y., Wen, Y. Vinkenborg, J.L., Fan, J. and Kang, H. (2015). Inhibition of human copper trafficking by a small molecule significantly attenuates cancer cell proliferation. *Nature Chemistry*, 7 (12), pp.968-979.

Wang, Y., Hodgkinson, V., Zhu, S., Weisman, G.A. and Petris, M.J. (2011). Advances in the understanding of mammalian copper transporters. *Advances in Nutrition*, 2 (2), pp.129-137.

Warrell, D.A. and Gilles, H.M. (2017). Rationale and technique of Malaria control. *Essential malariology*, pp. 107-190

Watson, S.A. and McStay, G.P. (2020). Functions of cytochrome *c* oxidase assembly factors. *International Journal of Molecular Sciences*, 21 (19), p.7254.

Wee, N.K., Weinstein, D.C., Fraser, S.T. and Assinder, S.J. (2013). The mammalian copper transporters Ctr1 and Ctr2 and their roles in development and disease. *The International Journal of Biochemistry & Cell Biology*, 45 (5), pp.960-963.

Weiner, J. and Kooij, T.W. (2016). Phylogenetic profiles of all membrane transport proteins of the malaria parasite highlight new drug targets. *Microbial Cell*, 3 (10), p.511.

Weiss, G. and Carver, P.L. (2018). Role of divalent metals in infectious disease susceptibility and outcome. *Clinical Microbiology and Infection*, 24 (1), pp.16-23.

Whaun, J.M., Miura, G.A., Brown, N.D., Gordon, R.K. and Chiang, P.K. (1986). Antimalarial activity of neplanocin A with perturbations in the metabolism of purines, polyamines and S-adenosylmethionine. *The Journal of Pharmacology and Experimental Therapeutics*, 236 (1), pp.277-283.

White, N.J. (2004). Antimalarial drug resistance. *The Journal of Clinical Investigation*, 113 (8), pp.1084-1092.

White, N.J. (2008). *Plasmodium knowlesi*: the fifth human malaria parasite. *Clinical infectious diseases*, 46 (2), pp.172-173.

White, N.J. and Olliaro, P.L. (1996). Strategies for the prevention of antimalarial drug resistance: rationale for combination chemotherapy for malaria. *Parasitology Today*, 12 (10), pp.399-401.

Wichers, J.S., Scholz, J.A., Strauss, J., Witt, S., Lill, A., Ehnold, L.I., Neupert, N., Liffner, B., Lühken, R., Petter, M. and Lorenzen, S. (2019). Dissecting the gene expression, localization, membrane topology, and function of the *Plasmodium falciparum* STEVOR protein family. *MBio*, 10 (4), pp.10-1128.

Winograd, E., Prudhomme, J.G. and Sherman, I.W. (2005). Band 3 clustering promotes the exposure of neoantigens in *Plasmodium falciparum*-infected erythrocytes. *Molecular and biochemical parasitology*, 142 (1), pp.98-105.

Wong, P.C., Waggoner, D., Subramaniam, J.R., Tessarollo, L., Bartnikas, T.B., Culotta, V.C., Price, D.L., Rothstein, J. and Gitlin, J.D. (2000). Copper chaperone for superoxide dismutase is essential to activate mammalian Cu/Zn superoxide dismutase. *Proceedings of the National Academy of Sciences*, 97 (6), pp.2886-2891.

World Health Organization. (1967). Chemotherapy of malaria: report of a WHO scientific group [meeting held in Geneva from 25 April to 1 May 1967].

World Health Organization. (2012). WHO policy recommendation: intermittent preventive treatment of malaria in pregnancy using sulfadoxine-pyrimethamine (IPTp-SP). World Health Organization.

World Health Organization. (2014). *WHO policy brief for the implementation of intermittent preventive treatment of malaria in pregnancy using sulfadoxine-pyrimethamine (IPTp-SP)* (No. WHO/HTM/GMP/2014.4). World Health Organization.

World Health Organization. (2015). *Guidelines for the treatment of malaria*. World Health Organization.

World Health Organization. (2017). World Malaria Report 2017. World Health Organization.

World Health Organization. (2018). World Malaria Report 2018. World Health Organisation.

World Health Organization. (2021). Full evidence reports on the RTS, S/AS01 malaria vaccine.

World Health Organization. (2023). World Malaria Report *2023*. World Health Organization.

World Health Organization. (2019). World Malaria Report 2019. World Health Organization.

World Health Organization. (2020). World malaria report 2020: 20 years of global progress and challenges. World Health Organization.

Xi, Z., Guo, W., Tian, C., Wang, F. and Liu, Y. (2014). Copper binding modulates the platination of human copper chaperone Atox1 by antitumor trans-platinum complexes. *Metallomics*, 6 (3), pp.491-497.

Xi, Z., Shi, C., Tian, C. and Liu, Y. (2013). Conserved residue modulates copper-binding properties through structural dynamics in human copper chaperone Atox1. *Metallomics*, 5 (11), pp.1566-1573.

Xia, X. (2017). Bioinformatics and drug discovery. *Current Topics in Medicinal Chemistry*, 17 (15), pp.1709-1726.

Xia, Y., Pei, T., Zhao, J., Wang, Z., Shen, Y., Yang, Y. and Liang, J. (2024). Long noncoding RNA H19: functions and mechanisms in regulating programmed cell death in cancer. *Cell Death Discovery*, 10 (1), p.76.

Xiao, Z., Brose, J., Schimo, S., Ackland, S.M., La Fontaine, S. and Wedd, A.G. (2011). Unification of the copper (I) binding affinities of the metallo-chaperones Atx1, Atox1, and related proteins: detection probes and affinity standards. *Journal of Biological Chemistry*, 286 (13), pp.11047-11055.

Xiao, Z., La Fontaine, S., Bush, A.I. and Wedd, A.G. (2019). Molecular mechanisms of glutaredoxin enzymes: versatile hubs for thiol-disulfide exchange between protein thiols and glutathione. *Journal of Molecular Biology*, 431 (2), pp.158-177.

Xu, D., Tsai, C.J. and Nussinov, R. (1997). Hydrogen bonds and salt bridges across protein-protein interfaces. *Protein engineering*, 10 (9), pp.999-1012.

Xu, E.W., Kearney, P. and Brown, D.G. (2006). The use of functional domains to improve transmembrane protein topology prediction. *Journal of Bioinformatics and Computational Biology*, 4 (01), pp.109-123.

Yamada, T., Takata, Y., Komoto, J., Gomi, T., Ogawa, H., Fujioka, M. and Takusagawa, F. (2005). Catalytic mechanism of S-adenosylhomocysteine hydrolase: roles of His 54, Asp130, Glu155, Lys185, and Aspl89. *The International Journal of Biochemistry & Cell Biology*, 37 (11), pp.2417-2435.

Yamaguchi, Y., Heiny, M.E., Suzuki, M. and Gitlin, J.D. (1996). Biochemical characterization and intracellular localization of the Menkes disease protein. *Proceedings of the National Academy of Sciences*, 93 (24), pp.14030-14035.

Yang, C.R., Tongyoo, P., Emamian, M., Sandoval, P.C., Raghuram, V. and Knepper, M.A. (2015). Deep proteomic profiling of vasopressin-sensitive collecting duct cells. I. Virtual Western blots and molecular weight distributions. *American Journal of Physiology-Cell Physiology*, 309 (12), pp.785-C798.

Yang, X., Hu, Y., Yin, D.H., Turner, M.A., Wang, M., Borchardt, R.T., Howell, P.L., Kuczera, K. and Schowen, R.L. (2003). Catalytic strategy of S-adenosyl-L-homocysteine hydrolase: transition-state stabilization and the avoidance of abortive reactions. *Biochemistry*, 42 (7), pp.1900-1909.

Yang, Y., Peng, X., Ying, P., Tian, J., Li, J., Ke, J., Zhu, Y., Gong, Y., Zou, D., Yang, N. and Wang, X. (2019). AWESOME: a database of SNPs that affect protein post-translational modifications. *Nucleic Acids Research*, 47, pp.874-D880.

Yang, Y., Yin, J., Liu, J., Xu, Q., Lan, T., Ren, F. and Hao, Y. (2017). The copper homeostasis transcription factor CopR is involved in H2O2 stress in Lactobacillus plantarum CAUH2. *Frontiers in Microbiology*, 8, p.282678.

Yao, F., He, J., Li, X., Zou, H. and Yuan, Z. (2012). Studies of the interaction of copper and zinc ions with Alzheimer's Aβ (1–16) using surface plasmon resonance spectrometer. *Sensors and Actuators B: Chemical*, 161 (1), pp.886-891.

Yogavel, M., Tripathi, T., Gupta, A., Banday, M.M., Rahlfs, S., Becker, K., Belrhali, H. and Sharma, A. (2014). Atomic resolution crystal structure of glutaredoxin 1 from *Plasmodium falciparum* and comparison with other glutaredoxins. *Acta Crystallographica Section D: Biological Crystallography*, 70 (1), pp.91-100.

Yu Gorobets, N., V Sedash, Y., K Singh, B., and Rathi, B. (2017). An overview of currently available antimalarials. *Current topics in Medicinal Chemistry*, 17 (19), pp.2143-2157.

Yu, K., Zhang, Q., Liu, Z., Du, Y., Gao, X., Zhao, Q., Cheng, H., Li, X. and Liu, Z.X. (2020). Deep learning-based prediction of reversible HAT/HDAC-specific lysine acetylation. *Briefings in Bioinformatics*, 21 (5), pp.1798-1805.

Yuan, C.S., Saso, Y., Lazarides, E., Borchardt, R.T. and Robins, M.J. (1999). Recent advances in S-adenosyl-L-homocysteine hydrolase inhibitors and their potential clinical applications. *Expert Opinion on Therapeutic Patents*, 9 (9), pp.1197-1206.

Yuan, D., Stroe, O., Wood, G., Laydon, A. and Žídek, A. (2022). AlphaFold Protein Structure Database: massively expanding the structural coverage of protein-sequence space with high-accuracy models. *Nucleic Acids Research*, 50, pp.439-D444.

Yuan, D.S., Dancis, A. and Klausner, R.D. (1997). Restriction of copper export in *Saccharomyces cerevisiae* to a late Golgi or post-Golgi compartment in the secretory pathway. *Journal of Biological Chemistry*, 272 (41), pp.25787-25793.

Yuan, D.S., Stearman, R., Dancis, A., Dunn, T., Beeler, T. and Klausner, R.D. (1995). The Menkes/Wilson disease gene homologue in yeast provides copper to a ceruloplasmin-like oxidase required for iron uptake. *Proceedings of the National Academy of Sciences*, 92 (7), pp.2632-2636.

Yuan, S., Chan, H.S. and Hu, Z. (2017). Using PyMOL as a platform for computational drug design. *Wiley Interdisciplinary Reviews: Computational Molecular Science*, 7 (2), p.e1298.

Zaffagnini, M., Michelet, L., Massot, V., Trost, P. and Lemaire, S.D. (2008). Biochemical characterization of glutaredoxins from *Chlamydomonas reinhardtii* reveals the unique properties of a chloroplastic CGFS-type glutaredoxin. *Journal of Biological Chemistry*, 283 (14), pp.8868-8876.

Zanatta, Â., Cecatto, C., Ribeiro, R.T., Amaral, A.U., Wyse, A.T., Leipnitz, G. and Wajner, M. (2018). S-adenosylmethionine promotes oxidative stress and decreases Na+, K+-ATPase activity in cerebral cortex supernatants of adolescent rats: implications for the pathogenesis of S-adenosylhomocysteine hydrolase deficiency. *Molecular Neurobiology*, 55, pp.5868-5878.

Zhalsanova, I.Z., Fonova, E.A., Zhigalina, D.I. and Skryabin, N.A. (2023). The ATOX1 gene's role in copper metabolism and the pathogenesis of copper-induced diseases. *Russian Journal of Genetics*, 59 (3), pp.242-250.

Zhang, M., Wang, C., Otto, T.D., Oberstaller, J., Liao, X., Adapa, S.R., Udenze, K., Bronner, I.F., Casandra, D., Mayho, M. and Brown, J. (2018). Uncovering the essential genes of the human malaria parasite *Plasmodium falciparum* by saturation mutagenesis. *Science*, 360 (6388), p.eaap7847.

Zhang, Z., Wu, Y., Wang, S., Wang, G., Zhang, H., Yang, X., Liu, G. and Huang, S. (2024). Copper-related cell death and the role of copper in head and neck squamous cell Carcinoma and therapeutic strategies. *Advanced Therapeutics*, 7 (5), p.2300198.

Zhao, X., Li, J., Wang, R., He, F., Yue, L. and Yin, M. (2018). General and species-specific lysine acetylation site prediction using a bi-modal deep architecture. *IEEE Access*, 6, pp.63560-63569.

Zhao, Y., Liu, Z., Soe, M.T., Wang, L., Soe, T.N., Wei, H., Than, A., Aung, P.L., Li, Y., Zhang, X. and Hu, Y. (2019). Genetic variations associated with drug resistance markers in asymptomatic *Plasmodium falciparum* infections in Myanmar. *Genes*, 10 (9), p.692.

Zhou, X. (1998). Regulation of S-Adenosylhomocysteine hydrolase levels by copper, growth, and during development. State University of New York at Buffalo.

Zhu, X., Boulet, A., Buckley, K.M., Phillips, C.B., Gammon, M.G., Oldfather, L.E., Moore, S.A., Leary, S.C. and Cobine, P.A. (2021). Mitochondrial copper and phosphate transporter specificity was defined early in the evolution of eukaryotes. *Elife*, 10, p.e64690.

Additional information

Table A1 Cluster scores for *Pf*Ctr1_*Pf*Grx1 complex

Cluster	Members	Representative	Weighted Score
0	124	Center	-927.1
		Lowest Energy	-1030.5
1	112	Center	-915.3
		Lowest Energy	-945.7
2	75	Center	-840.3
		Lowest Energy	-1006.2
3	66	Center	-808.6
		Lowest Energy	-964.7
4	50	Center	-965.3
		Lowest Energy	-965.3
5	42	Center	-900.7
		Lowest Energy	-900.7
6	34	Center	-933.3
		Lowest Energy	-1027.9
7	29	Center	-968.4
		Lowest Energy	-1041.6
8	29	Center	-813.1
		Lowest Energy	-959.1
9	28	Center	-823.6
		Lowest Energy	-939.7
10	26	Center	-794.0
		Lowest Energy	-956.0

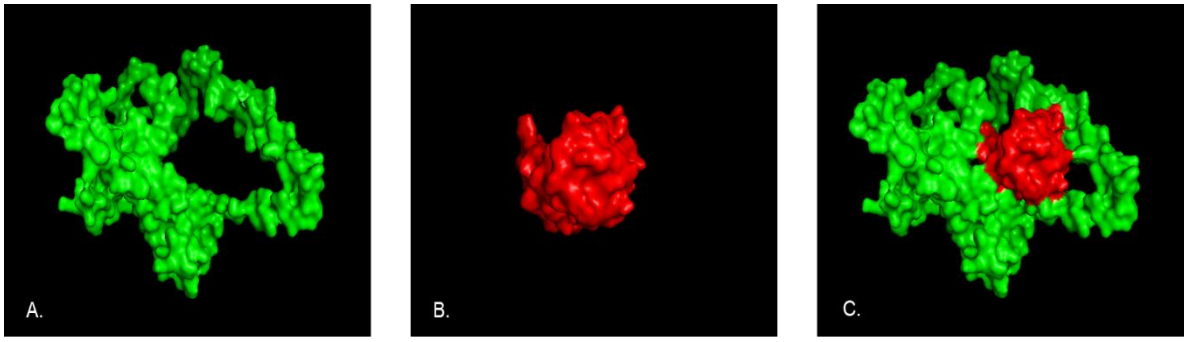

Fig A1 Interaction between *Pf*Ctr1 and *Hs*Grx1 using ClusPro. A. AlphaFold *Pf*Ctr1 structure **B.** *Hs*Grx1 crystal structure **C.** Complex formed between *Pf*Ctr1 and *P*fGrx1 in ClusPro and visualized in PyMOL.

A.

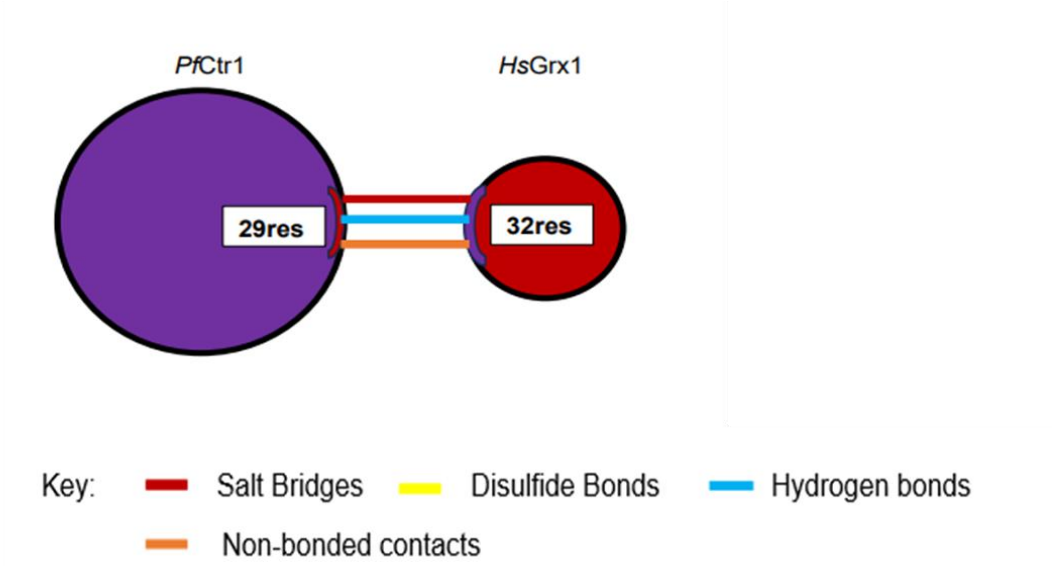

B.

Interface statistics						
Protein name	No. of interface residues	Interface area (Å^2)	No. of salt bridges	No. of disulfide bonds	No. of hydrogen bonds	No. of non-bonded contacts
*Pf*Ctr1	29	1629	3	-	6	203
*Hs*Grx1	32	1703				

Fig A2 Schematic diagram of the interaction between *Pf*Ctr1 and *Hs*Grx1 of the PDBSum generated complex. A. Interacting chains are joined by colored lines, each representing a different type of interaction, as shown in the key above. The area of each circle is proportional to the surface area of the corresponding protein chain. The extent of the interface region on each chain is represented by the wedge (red and purple) showing the interface surface area. **B.** Indicates the interface statistics concerning the number of residues involved in the interface of each chain, interface area, number of salt bridges, number of disulfide bonds, and number of non-bonded contacts.

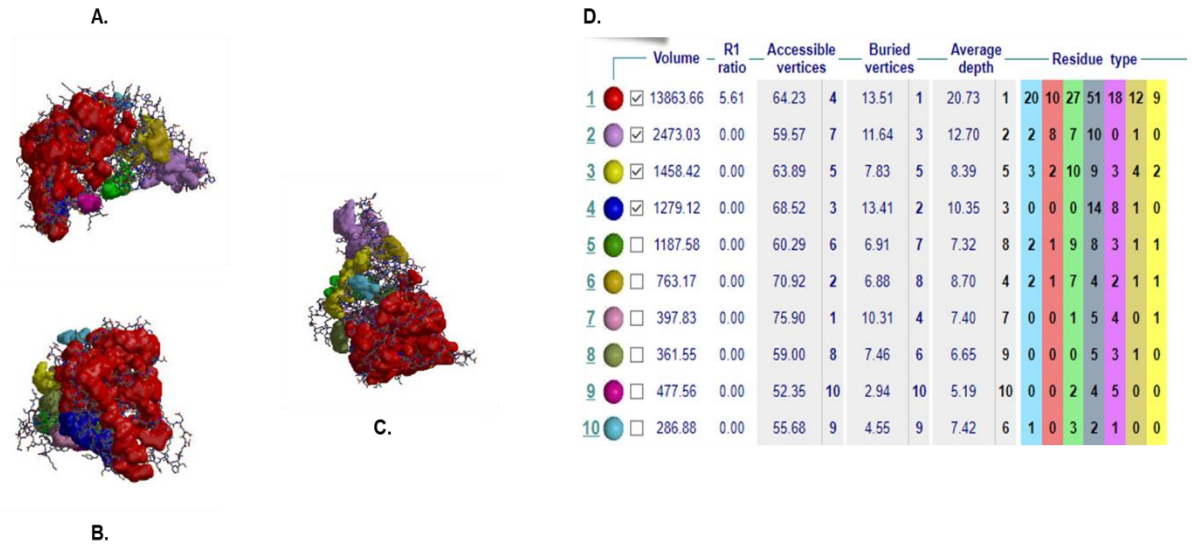

	Volume	R1 ratio	Accessible vertices		Buried vertices		Average depth		Residue type						
1	13863.66	5.61	64.23	4	13.51	1	20.73	1	20	10	27	51	18	12	9
2	2473.03	0.00	59.57	7	11.64	3	12.70	2	2	8	7	10	0	1	0
3	1458.42	0.00	63.89	5	7.83	5	8.39	5	3	2	10	9	3	4	2
4	1279.12	0.00	68.52	3	13.41	2	10.35	3	0	0	0	14	8	1	0
5	1187.58	0.00	60.29	6	6.91	7	7.32	8	2	1	9	8	3	1	1
6	763.17	0.00	70.92	2	6.88	8	8.70	4	2	1	7	4	2	1	1
7	397.83	0.00	75.90	1	10.31	4	7.40	7	0	0	1	5	4	0	1
8	361.55	0.00	59.00	8	7.46	6	6.65	9	0	0	0	5	3	1	0
9	477.56	0.00	52.35	10	2.94	10	5.19	10	0	0	2	4	5	0	0
10	286.88	0.00	55.68	9	4.55	9	7.42	6	1	0	3	2	1	0	0

Fig A3 Clefts on the protein AlphaFold surface structure of *Pf*Ctr1. Three orientations (**A**, **B**, and **C**) of protein structure with highlighted clefts (marked in various colors that correspond to those in Table **D**) are illustrated for the protein. A table is included with details on the pocket's volume, R1 ratio, depth, and residue type are visible on the right; the coloring of the residues involved is below the table. Data is generated from PDBsum.

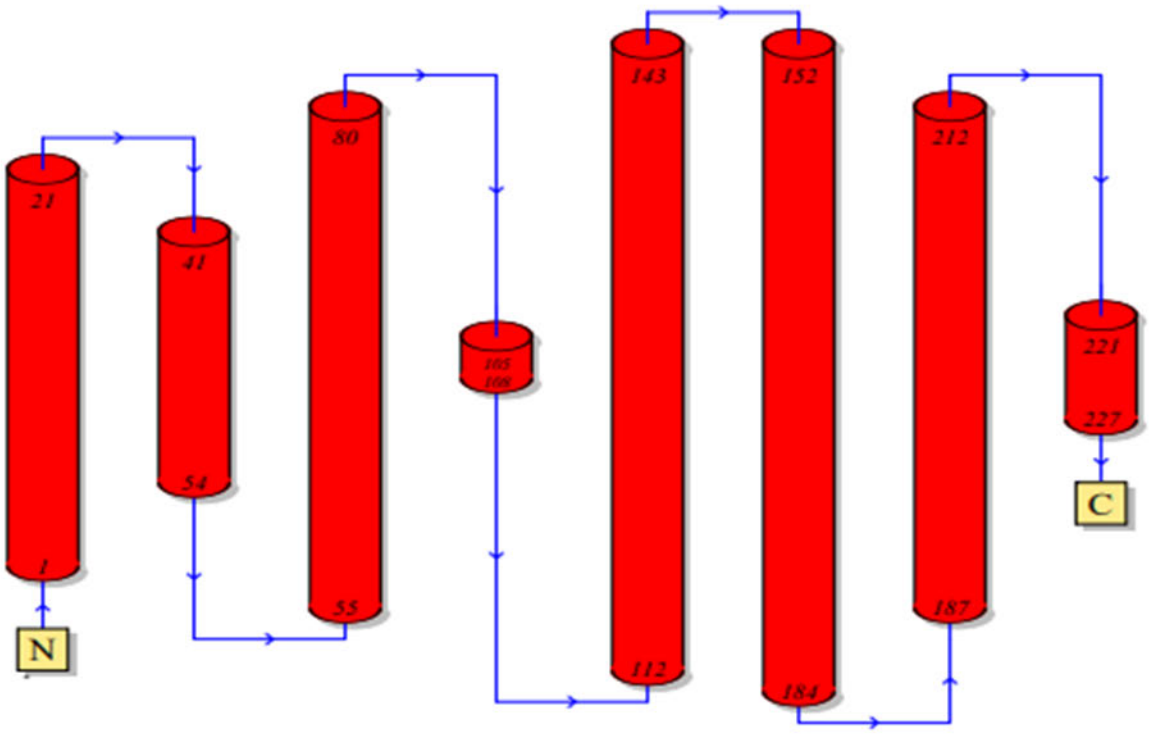

Fig A4 *Pf*Ctr1 topology as generated by PDBSum program.

Table A2 Cluster scores for *Pf*Ctr1_*Hs*Grx1 complex

Cluster	Members	Representative	Weighted Score
0	118	Center	-1029.6
		Lowest Energy	-1059.0
1	111	Center	-925.8
		Lowest Energy	-1115.4
2	110	Center	-1027.9
		Lowest Energy	-1194.5
3	64	Center	-938.8
		Lowest Energy	-1151.4
4	59	Center	-916.9
		Lowest Energy	-1006.7
5	59	Center	-1004.2
		Lowest Energy	-1023.4
6	57	Center	-961.1
		Lowest Energy	-1017.4
7	55	Center	-940.5
		Lowest Energy	-1047.7
8	51	Center	-995.8
		Lowest Energy	-995.8
9	44	Center	-983.8
		Lowest Energy	-1056.5
10	38	Center	-934.6
		Lowest Energy	-1087.3

A.

i.

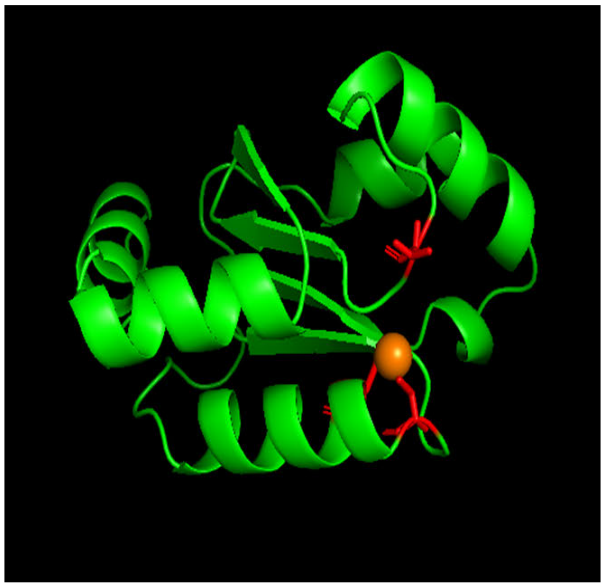

ii.

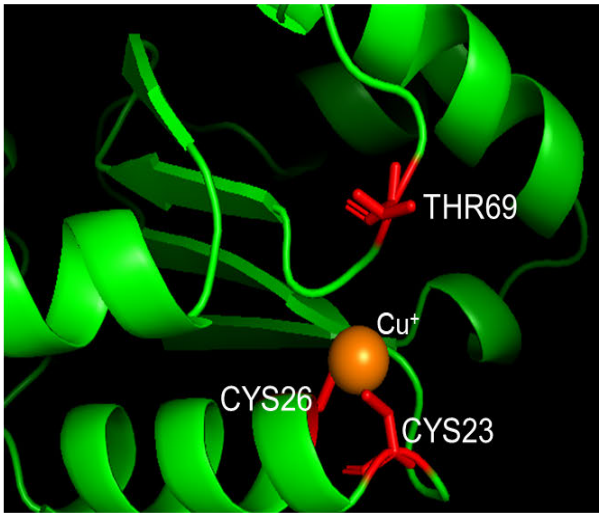

iii.

No.	Binding Residues	Template	Score
1	23C , 26C , 69T	6n5uA0	4.510
2	23C , 26C , 70V	1rjuV5	3.536
3	23C , 26C , 70V , 83C	5arnA6	2.272
4	23C , 26C , 70V	5arnA1	2.184

Fig A5 Docking of copper (I) with Human Red Blood cell Grx1 (*Hs*Grx1). A, I. The *Hs*Grx1 crystal structure with copper (I) bound. **II**. *Hs*Grx1_Cu complex (binding score of 5.906) with lysine and cysteine at 19 and 22, respectively, as copper-binding sites. **III.** Table indicating other *Hs*Grx1_Cu complexes with binding scores.

Note: Copper binds to two (2) cysteines that are part of the **CXXC** motif, data that shows a similar pattern with *Pf*Grx1 that has been shown to bind copper in a similar region.

Table B1 Cluster scores for *Pf*CuATPase_*Pf*Grx1 complex

Cluster	Members	Representative	Weighted Score
0	107	Center	-846.3
		Lowest Energy	-1029.2
1	78	Center	-1217.0
		Lowest Energy	-1217.0
2	78	Center	-922.7
		Lowest Energy	-965.1
3	65	Center	-833.4
		Lowest Energy	-946.7
4	60	Center	-806.9
		Lowest Energy	-970.7
5	48	Center	-973.0
		Lowest Energy	-973.0
6	41	Center	-830.5
		Lowest Energy	-1001.1
7	41	Center	-806.0
		Lowest Energy	-1044.0
8	34	Center	-847.5
		Lowest Energy	-923.6
9	28	Center	-846.9
		Lowest Energy	-884.3
10	23	Center	-878.7
		Lowest Energy	-878.7

Table C1 Cluster scores for *Pf*Cox17_*Pf*Grx1 complex

Cluster	Members	Representative	Weighted Score
0	97	Center	-355.3
		Lowest Energy	-489.7
1	94	Center	-373.1
		Lowest Energy	-441.0
2	76	Center	-374.7
		Lowest Energy	-400.7
3	71	Center	-391.6
		Lowest Energy	-459.7
4	70	Center	-347.7
		Lowest Energy	-422.2
5	69	Center	-383.3
		Lowest Energy	-415.4
6	44	Center	-372.1
		Lowest Energy	-500.8
7	41	Center	-348.7
		Lowest Energy	-425.4
8	40	Center	-382.1
		Lowest Energy	-497.1
9	33	Center	-387.1
		Lowest Energy	-421.6
10	33	Center	-373.7
		Lowest Energy	-408.3

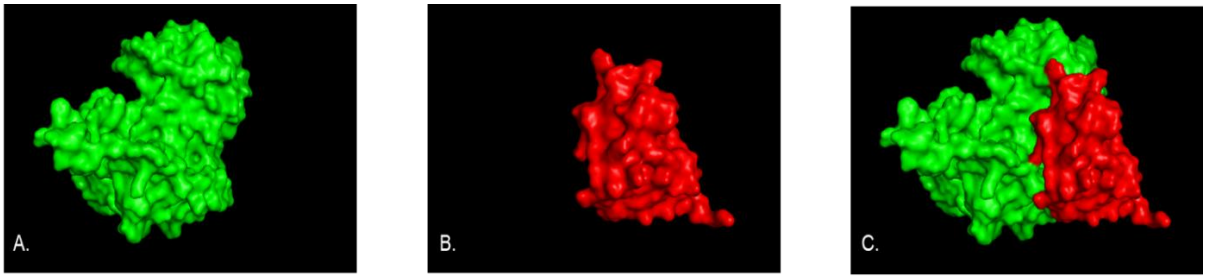

Fig A6 Interaction between *Pf*SAHH and *Pf*Grx1 using ClusPro. A. *Pf*SAHH crystal structure **B.** *Pf*Grx1 crystal structure **C.** Complex formed between *Pf*SAHH and *Pf*Grx1 in ClusPro and visualized in PyMOL.

A.

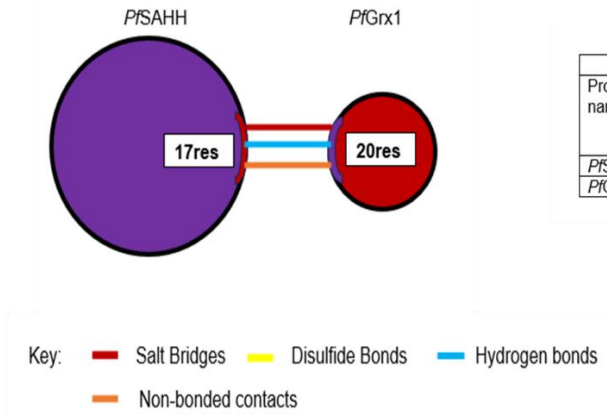

B.

Interface statistics						
Protein name	No. of interface residues	Interface area (Å²)	No. of salt bridges	No. of disulfide bonds	No. of hydrogen bonds	No. of non-bonded contacts
*Pf*SAHH	17	955	5	-	13	138
*Pf*Grx1	20	902				

Fig A7 Schematic diagram of the interaction between *Pf*SAHH and *Pf*Grx1 of the PDBSum generated complex. A. Colored lines join interacting chains, each representing a different type of interaction, as shown in the key above. The area of each circle is proportional to the surface area of the corresponding protein chain. The extent of the interface region on each chain is represented by the wedge (red and purple) showing the interface surface area. **B.** Indicates the interface statistics concerning the number of residues involved in the interface of each chain, interface area, number of salt bridges, number of disulfide bonds, and number of non-bonded contacts.

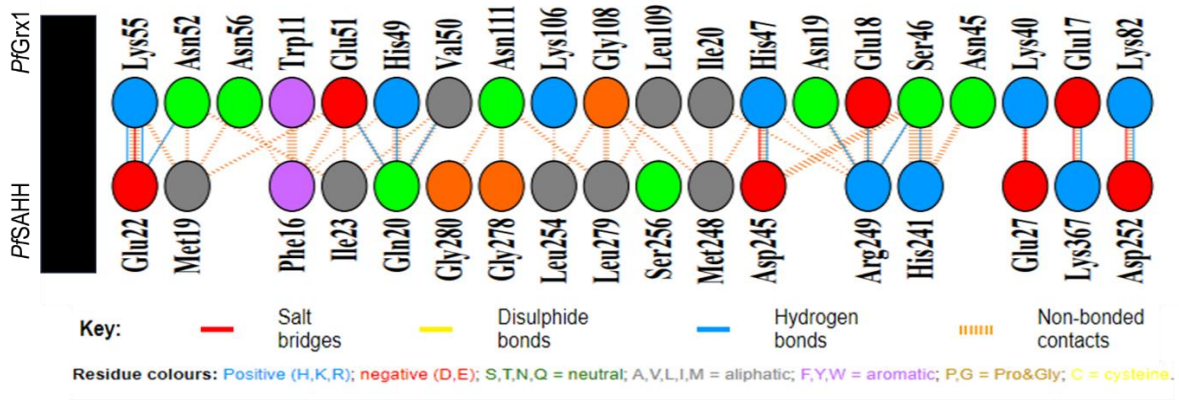

Fig A8 PDBsum interaction plots for the interface between the *Pf*SAHH and *Pf*Grx1. A plot of hydrogen bonds (blue lines), nonbonded contacts (orange tick-marks), and salt bridges (red lines) between residues on either side of the protein-protein interface are shown on the diagram

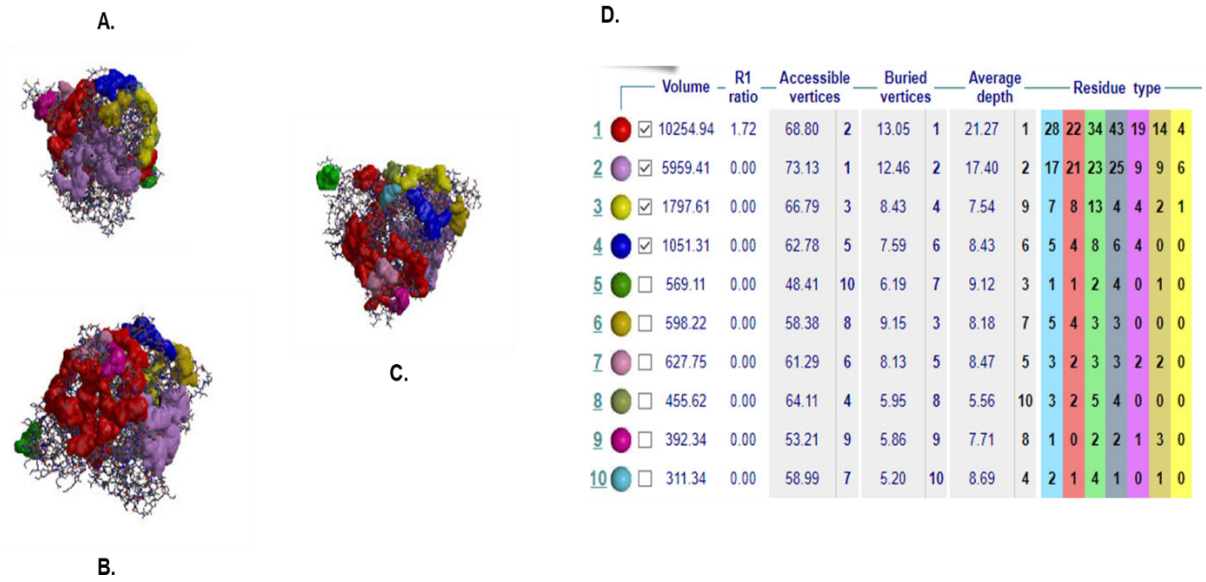

Fig A9 Clefts on the protein AlphaFold surface structure of *Pf*SAHH. Three orientations (**A**, **B,** and **C**) of protein structure with highlighted clefts (marked in various colors that correspond to those in Table **D**) are illustrated for the protein. A table is included with details on the pocket's volume, R1 ratio, depth, and residue type are visible on the right; the coloring of the residues involved is below the table. Data is generated from PDBsum.

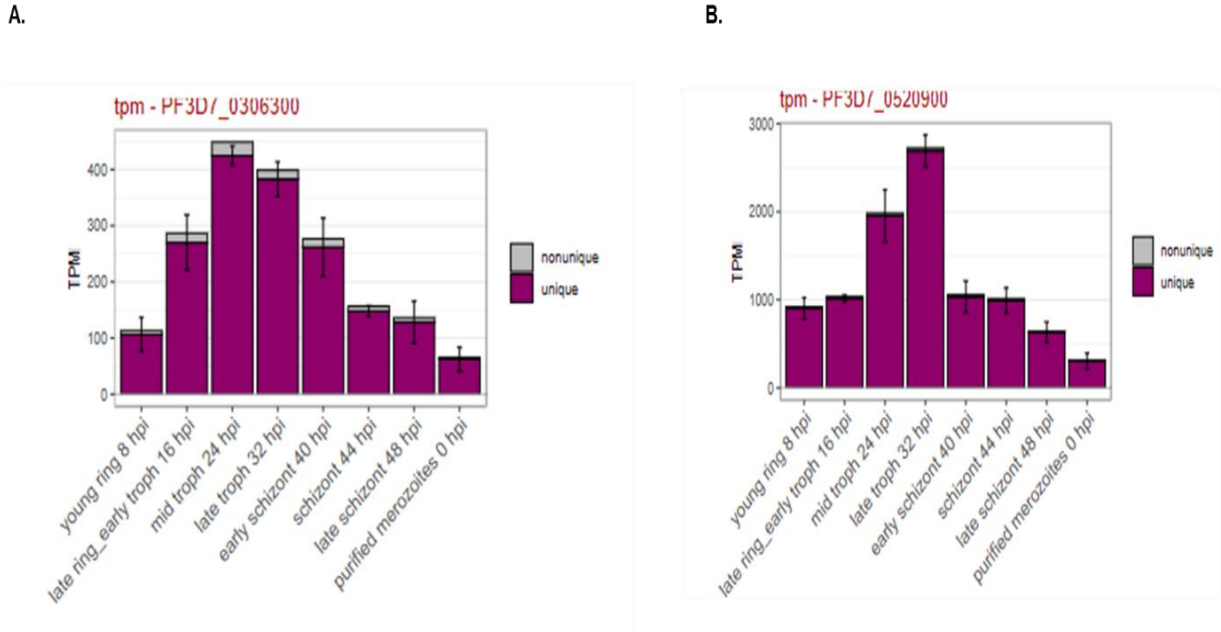

Fig A10 Relative expression of *P. falciparum* Glutaredoxin1 and S-adenosylhomocysteine hydrolase during the erythrocytic stage. Blood-stage *Plasmodium falciparum* transcriptome determined by RNA-Seq analysis at 8 developmental stages including young ring stage (8 hpi), late ring stage/early trophozoite (16 hpi), mid-age trophozoite (24 hpi), late trophozoite (32 hpi), early schizont (40 hpi), schizont (44 hpi), late schizont (48 hpi) and purified merozoites (0 hpi). (paired end, unstranded Illumina HiSeq 4000), **A.** *Pf*Grx1 (PF3D7_0306300) **B.** *Pf*SAHH (PF3D7_0520900)

A.

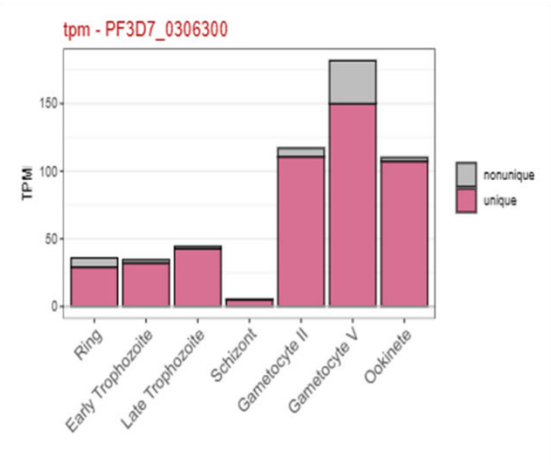

B.

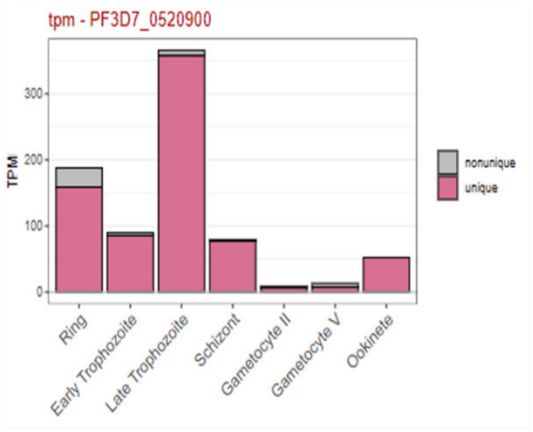

Fig A11 Relative expression of *P. falciparum* Glutaredoxin1 and S-adenosylhomocysteine hydrolase in gametocyte stage. Illumina-based sequencing of *P. falciparum* 3D7 mRNA from two gametocyte stages (II and V), ookinete, and four-time points of erythrocytic stages representing ring, early trophozoite, late trophozoite, and schizont. **A.** *Pf*Grx1 (PF3D7_0306300) **B.** *Pf*SAHH (PF3D7_0520900)

Table C2 Cluster scores for *Pf*Grx1_*Pf*SAHH complex

Cluster	Members	Representative	Weighted Score
0	145	Center	-532.1
		Lowest Energy	-643.6
1	73	Center	-668.2
		Lowest Energy	-668.2
2	51	Center	-626.6
		Lowest Energy	-644.5
3	49	Center	-578.2
		Lowest Energy	-673.0
4	46	Center	-523.2
		Lowest Energy	-610.0
5	45	Center	-534.6
		Lowest Energy	-664.6
6	41	Center	-583.7
		Lowest Energy	-583.7
7	40	Center	-585.3
		Lowest Energy	-585.3
8	39	Center	-500.3
		Lowest Energy	-579.1
9	37	Center	-568.7
		Lowest Energy	-568.7
10	37	Center	-511.7
		Lowest Energy	-602.4

Table C3 Bond energy involved in the formation of protein-to-protein complexes

Proteins involved in the interaction	Number and type of Bonds in the interaction		Energy in the Bond (kJ/mol)		Total Bond energy (kJ/mol)
	Salt Bridges	Hydrogen Bond	Salt Bridges	Hydrogen Bond	
*Pf*Ctr1_*Pf*Grx1	4	13	12	13	217
*Pf*CuATPase_*Pf*Grx1	-	2			26
*Pf*Grx1_*Pf*Cox17	6	9			189
*Pf*Grx1_*Pf*SAHH	5	13			229

Fig D1 Summary of the protein-to-protein interaction analyses using various bioinformatic tools.

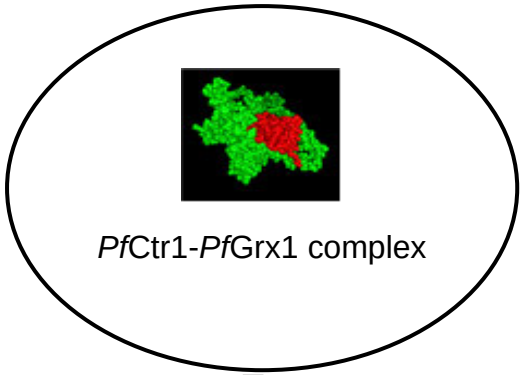

*Pf*Ctr1-*Pf*Grx1 complex

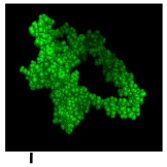

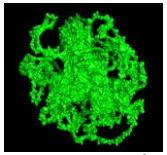

Protein-to-protein interaction using ClusPro 2.0 server.

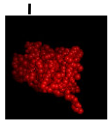

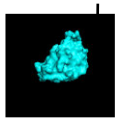

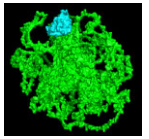

*Pf*CuATPase-*Pf*Grx1 complex

Analysis of *Pf*Ctr1-*Pf*Grx1 complex in PDBSum

Analysis of *Pf*CuATPase-*Pf*Grx1 complex in PDBSum

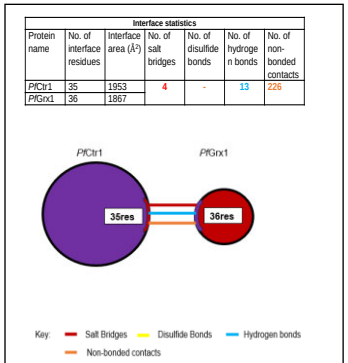

Interface statistics						
Protein name	No. of interface residues	Interface area (Å²)	No. of salt bridges	No. of disulfide bonds	No. of hydrogen bonds	No. of non-bonded contacts
*Pf*Ctr1	35	1953	4	-	13	226
*Pf*Grx1	36	1867				

Type and number of bonds involved in the interaction.

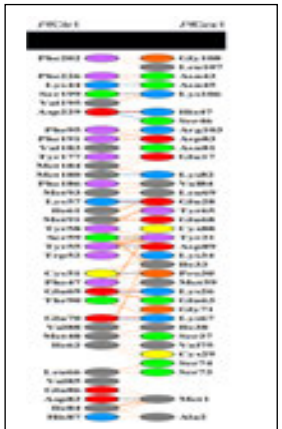

Amino acids involved in the interaction.

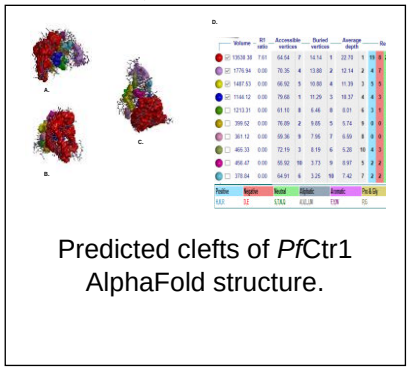

Predicted clefts of *Pf*Ctr1 AlphaFold structure.

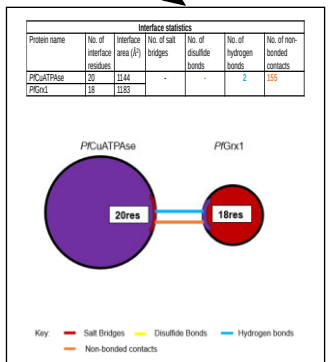

Interface statistics						
Protein name	No. of interface residues	Interface area (Å²)	No. of salt bridges	No. of disulfide bonds	No. of hydrogen bonds	No. of non-bonded contacts
*Pf*CuATPase	20	1144	-	-	2	153
*Pf*Grx1	18	1183				

Type and number of bonds involved in the interaction.

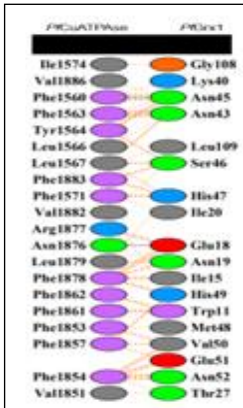

Amino acids involved in the interaction

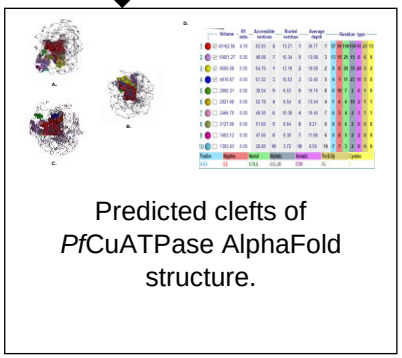

Predicted clefts of *Pf*CuATPase AlphaFold structure.